



UNIVERSITY OF
BIRMINGHAM

North Atlantic Winter Wind Storm Variability across different Time Scales

Simon Wild

A thesis submitted to the University of Birmingham for the degree
of DOCTOR OF PHILOSOPHY.

School of Geography, Earth and Environmental Sciences
College of Life and Environmental Sciences
University of Birmingham
March 2018

UNIVERSITY OF
BIRMINGHAM

University of Birmingham Research Archive

e-theses repository

This unpublished thesis/dissertation is copyright of the author and/or third parties. The intellectual property rights of the author or third parties in respect of this work are as defined by The Copyright Designs and Patents Act 1988 or as modified by any successor legislation.

Any use made of information contained in this thesis/dissertation must be in accordance with that legislation and must be properly acknowledged. Further distribution or reproduction in any format is prohibited without the permission of the copyright holder.

ABSTRACT

In this thesis atmospheric and oceanic conditions important for the development of wind storms on different time scales are analysed. The potential usefulness and limitations of seasonal prediction models and long-term reanalyses with respect to wind storm frequency is investigated and sources of potential seasonal predictability of wind storm frequency are discussed.

On the synoptic scale tropospheric growth conditions such as baroclinicity, latent heat and upper level divergence show greater magnitudes of one standard deviation on average compared to all extra-tropical cyclones. Mid-latitude Rossby waves show generally greater amplitudes for different wave numbers during wind storm events. Greater amplitudes are also found in wave numbers not typically associated with storm track activity.

The analysis of extra-tropical cyclones and wind storms on the seasonal scale reveal positive, significant skill for some European regions in state-of-the-art seasonal prediction models. North Atlantic sea surface temperatures (SST) are shown to be a source of seasonal predictability and a potential reason for the achieved skill for wind storm frequency predictions in reanalysis and AMIP-type sensitivity experiments. The role of tropical Pacific and Atlantic SST for the record number of wind storms over the UK in winter 2013/14 is discussed.

AUTHOR'S DECLARATION

Individual contributions for each main chapter of this thesis are detailed below:

Chapter 3

Concept: Simon Wild (SW) and Gregor C. Leckebusch (GCL)

Method Development: SW, Daniel J. Befort (DJB), and GCL

Analyses: SW

Figures: SW

Text: SW

Chapter 4

Concept: SW and GCL

Method Development: SW and Ian Simmonds

Analyses: SW

Figures: SW

Text: SW

Chapter 5

Concept: SW, DJB and GCL

Method Development: SW, DJB and GCL

Analyses: SW and DJB

Figures: SW and DJB

Text: SW (First Draft), DJB, and GCL

Comments and Editing: Jeff R. Knight, Julia F. Lockwood, Hazel E. Thornton, Philip E. Bett, and Antje Weisheimer

This chapter has been submitted to the *Quarterly Journal of the Royal Meteorological Society* and is currently under review

Chapter 6

Concept: SW, DJB, Dominik Renggli (DR) and GCL

Method Development: SW, DJB, DR, and GCL

Analyses: SW and DJB

Figures: SW

Text: SW

Chapter 7

Concept: SW and GCL

Method Development: SW

Analyses: SW

Figures: SW

Text: SW

Comments and Editing: DJB and GCL

This chapter is published in the *Bulletin of the American Meteorological Society*.

Appendix

Concept: DJB

Method Development: SW, DJB, Tim Kruschke (TK), and GCL

Analyses: SW and DJB

Figures: DJB

Text: DJB

Comments and Editing: SW, TK, and GCL

This chapter is published in *Atmospheric Science Letters*.

ACKNOWLEDGMENTS

First and foremost I would like to thank Gregor Leckebusch for giving me this *Philosophiae Doctor* opportunity, for his supervision, support, general advice, trust, and the fact of bringing me to Birmingham. I thoroughly enjoyed very many lengthy discussions about obviously wind storms, but also about the UK, football, the French Revolution, and current politics.

I would further like to thank Ian Simmonds who provided some very useful scientific guidance during my stay at the University of Melbourne. It was a great pleasure to be surrounded by his seemingly infinite knowledge. I am also very grateful to Len Shaffrey and Xiaoming Cai for agreeing to be my examiners and therefore be part of the lucky few to actually having to completely read this piece of work. I did the best I could to make it worth it!

Further thanks goes to Daniel Befort for countless discussions, support, ideas, and critical reviews of scientific practices (not mine). I would also like to thank my office colleagues and team mates from B* Abrantas: Michael, Colin, Vasileios, Clemens, Jim, Tasos, Ian, Joss, and Sam, who made work and life certainly more enjoyable. The biggest thank you goes to Kaat for her endless patience and for simply being part of my life.

CONTENTS

Abstract	i
Author’s Declaration	ii
Acknowledgements	iv
Contents	v
List of Figures	vii
List of Tables	ix
List of Acronyms	x
Preface	xiii
1 General Introduction	1
1.1 Why Wind Storms?	1
1.2 North Atlantic Winter Wind Storms in the Recent Climate	2
1.3 Variability of Winter Wind Storms...	5
1.3.1 ...on the Synoptic Time Scale	5
1.3.2 ...on Seasonal to Interannual Time Scales	8
1.3.3 ...on Decadal to Centenary Time Scales	10
1.4 Research Gaps	12
1.5 Objectives of Thesis	14
1.6 Structure of Thesis	16
2 Data, Methods and Key Variables	18
2.1 Data	18
2.1.1 ERA Interim	18
2.1.2 Other Data Sets	19
2.2 Methods	20
2.2.1 Algorithm for the Identification and Tracking of Extra-tropical Cyclones and Wind Storms	20
2.2.2 Matching Algorithm for the Association of a Wind Storm to an Extra-tropical Cyclone	23
2.2.3 Storm Severity Index	23
2.2.4 Normalisation of Analysed Variables	25
2.2.5 Correlation Analyses	26
2.2.6 Composite Analysis	26
2.2.7 Principle Component Analysis	27
2.3 Atmospheric Growth Factors	29

2.3.1	Equivalent Potential Temperature	29
2.3.2	Maximum Eady Growth Rate	30
2.3.3	Upper-tropospheric Divergence and Jet Stream	31
3	Tropospheric Growth Factors	33
3.1	Introduction	33
3.2	Wind Storms in Specific Months	35
3.3	Composites for ETCs and Wind Storms	41
3.3.1	Different Composite Sets	41
3.3.2	Composites for All Cyclones	44
3.3.3	Comparison of different Composite Sets	50
3.4	Event to Event Variability	55
3.5	Principle Component Selection	59
3.6	Summary and Discussion	62
4	Waves and Storms	68
4.1	Introduction	68
4.2	FFT for a single storm	71
4.3	Results	76
4.3.1	From Storms to Wave Anomalies	76
4.3.2	From Wave Anomalies to Storms	82
4.4	Summary and Discussion	85
5	Seasonal Skill in ETCs and Wind Storms	91
5.1	Introduction	92
5.2	Data	94
5.3	Identification and Tracking Algorithms	94
5.4	Cyclones and Wind Storms in the NH	97
5.5	Forecasted Cyclones and Wind Storms - Direct Method	101
5.5.1	Temporal Variability	101
5.5.2	Spatial Variability	103
5.6	Forecasted Cyclones and Wind Storms - Indirect Method	105
5.7	Summary and Discussion	109
6	Sea Surface Temperatures in Relation to Storms	114
6.1	Potential Predictability on Seasonal Scale	114
6.2	NAH and Wind Storm in ERA-I	117
6.2.1	Definition of the Horseshoe-Index	117
6.2.2	Relation of HSI and Wind Storms	119
6.2.3	HSI and Growth Factors in ERA-I	121
6.2.4	Summary of HSI results in ERA-I	126
6.3	NAH and Wind Storms in ECHAM5	129
6.3.1	Set-Up of ECHAM5 Simulations	129
6.3.2	HSI and Growth Factors in ECHAM5	131
6.3.3	Summary of HSI results in ECHAM5	136
6.4	Discussion	137

7	Conditions in Winter 2013/14	140
7.1	Introduction	140
7.2	Data and Methods	141
7.3	Results	144
7.3.1	The winter 2013/14 over the British Isles and upstream conditions	144
7.3.2	The Role of the PNA	147
7.4	Discussion and Attribution to Climate Change	147
8	Synthesis	151
8.1	Summary and Discussion	151
8.2	Outlook	157
	Bibliography	159
	APPENDIX: Different trends in ERA-20C and NOAA-20CR	185
9.1	Introduction	186
9.2	Data and Methods	188
9.3	Results	190
9.3.1	Northern Hemisphere	190
9.3.1.1	All cyclone events	190
9.3.1.2	Extreme Cyclone Events	193
9.3.1.3	Wind Storm Events	195
9.3.2	Southern Hemisphere	195
9.3.2.1	All Cyclone Events	195
9.3.2.2	Extreme Cyclone Events	197
9.3.2.3	Wind Storm Events	198
9.4	Discussion and Conclusion	198

LIST OF FIGURES

1	Begrüßung (Greeting) by Paul Klee, 1922	xiii
1.1	Track density and Frequency of Wind Storms between 1979 and 2013	4
3.1	Cyclone-, Wind Storm Tracks and Growth Factors in January 2007	38
3.2	Cyclone-, Wind Storm Tracks and Growth Factors in February 2008	39
3.3	Cyclone-, Wind Storm Tracks and Growth Factors in January 2009	40
3.4	Composites for Θ_E at 850hPa for ETCs with $p < 1000hPa$	45
3.5	Composites for σ_{BI} at 775hPa for ETCs with $p < 1000hPa$	46
3.6	Composites for σ_{BI} at 400hPa for ETCs with $p < 1000hPa$	47
3.7	Composites for UTD for ETCs with $p < 1000hPa$	48
3.8	Composites for Θ_E at 850hPa for all Event Sets	51
3.9	Composites for σ_{BI} at 775hPa for other Event Sets	52
3.10	Composites for σ_{BI} at 400hPa for other Event Sets	53
3.11	Composites for σ_{BI} at 400hPa for other Event Sets	54
3.12	EOF Loadings for Θ_E at 850hPa Composites	57
3.13	EOF Loadings for σ_{BI} at 775hPa Composites	57
3.14	EOF Loadings for σ_{BI} at 400hPa Composites	58
3.15	EOF Loadings for upper tropospheric divergence Composites	58
3.16	Box-Whisker Diagram for Principal Component Selection	61
4.1	FFT Decomposition for Storm <i>Christian</i>	74
4.2	GPH500 Field during Wind Storm <i>Christian</i>	75
4.3	Amplitudes for FFT over NH	77
4.4	Wave Position for FFT over NH	80
4.5	Amplitudes for FFT over North Atlantic Sector	81
4.6	Distribution of wave location for FFT over North Atlantic Sector	81
4.7	Sampling Probability for Storms when GPH Amplitude is high	84
4.8	Sampling Probability for Storms when GPH Amplitude is low	84
4.9	GPH500 and Great Storm of 1987	88
5.1	Track density of all cyclones	97
5.2	Track density of extreme cyclones	99
5.3	Track density of wind storms	100
5.4	Skill for all cyclones	101
5.5	Skill for extreme cyclones	102
5.6	Skill for wind storms	102
5.7	Anomaly Correlation Coefficient	104
5.8	Regression Wind Storms vs. NAO	106
5.9	Skill Comparison - Direct vs. Indirect Method	108
6.1	Correlation of SST in ASO with Storms in DJF in ERA-40	118
6.2	Correlation between SST and Number of Storms	119

6.3	Lead-lag correlations between HSI and Number of Storms	120
6.4	Time series of HSI and NAO and their correlation	122
6.5	HSI Composite Difference for Jet in 200hPa	123
6.6	HSI Composite Difference for Θ_e in 850hPa	123
6.7	HSI Composite Difference for Eady Growth Rates	124
6.8	Geopotential Wave Amplitude Anomalies in HSI Years	126
6.9	ECHAM5 - Prescribed SST Anomalies	130
6.10	Track densities in ECHAM5 Sensitivity Experiments	132
6.11	HSI Composite Difference for Jet in 200hPa in ECHAM5	132
6.12	HSI Composite Difference for Θ_e in 850hPa in ECHAM5	133
6.13	HSI Composite Difference for Eady Growth Rates in ECHAM5	134
6.14	Geopotential Wave Amplitude in +2K and -2K Experiments	135
7.1	Conditions in DJF 2013/2014	143
7.2	OLR Anomaly in DJF 2013/14	145
7.3	Correlation between PNA and Cyclone Events / OLR	146
7.4	Correlation between PNA Wind Storms	146
7.5	SST in DJF 2013-14 & Correlation Gradient Index and Wind Storms	149
9.1	NH Track Densities for All Cyclones in ERA-20C and NOAA-20CR	191
9.2	NH Time Series for All Cyclones in ERA-20C and NOAA-20CR . .	192
9.3	NH Time Series for Extreme Cyclones in ERA-20C and NOAA-20CR	194
9.4	SH Track Densities for All Cyclones in ERA-20C and NOAA-20CR	196
9.5	SH Time Series for Extreme Cyclones in ERA-20C and NOAA-20CR	197

LIST OF TABLES

4.1	Changes in GPH Amplitude during Storm Occurrence	86
6.1	Horseshoe composite differences for zonal wind in 200hPa	123
6.2	Horseshoe composite differences for Θ_e in 850hPa	124
6.3	Horseshoe composite differences for Eady Growth Rates	125
6.4	HSI composite differences for zonal wind in 200hPa in ECHAM5 . .	133
6.5	Horseshoe composite differences for Θ_e in 850hPa in ECHAM5 . . .	134
6.6	Horseshoe composite differences for Eady Growth Rates in ECHAM5	135
7.1	Correlation Matrix for Winter 2013/14 Study	146

LIST OF ACRONYMS

ACC	Anomaly Correlation Coefficient
AGCM	Atmospheric General Circulation Model
AMJ	April, May, and June
AMIP	Atmospheric Model Intercomparison Project
AMOC	Atlantic Meridional Overturning Circulation
AOGCM	Atmosphere-Ocean General Circulation Model
ASO	August, September, and October
BeNeLux	Belgium, Netherlands, and Luxembourg
CMIP	Coupled Model Intercomparison Project
CPC	Climate Prediction Center
DJF	December, January, and February
doF	Degrees of Freedom
ECHAM	EC from ECMWF, HAM from Hamburg
ECMWF	European Centre for Medium-Range Weather Forecasts
ENSO	El Niño Southern Oscillation
EOF	Empirical Orthogonal Function
ERSST	Extended Reconstructed Sea Surface Temperature
ETC	Extra-tropical Cyclone
FFT	Fast Fourier Transform
FMA	February, March, and April
GCM	General Circulation Model
GPH	Geopotential Height
gpm	geopotential metres
HadGEM	Hadley Centre Global Environmental Model
HFV	High Frequency Variability
HSI	Horseshoe Index
JAS	July, August, and September
JFM	January, February, and March
JJA	June, July, and August
LFV	Low Frequency Variability
MAM	March, April, and May
MJJ	May, June, and July
MSLP	Mean Sea Level Pressure

NAO	North Atlantic Oscillation
NAt	North Atlantic
NCAR	National Center for Atmospheric Research
NCEP	National Centers for Environmental Prediction
NCL	NCAR Command Language
NEP	North East Pacific
NDJ	November, December, and January
NH	Northern Hemisphere
NOAA	National Oceanic and Atmospheric Association
OND	October, November, and December
OLR	Outgoing Longwave Radiation
PCA	Principal Component Analysis
PNA	Pacific / North America Pattern
PV	Potential Vorticity
sd	Standard Deviation
SON	September, October, and November
SSI	Storm Severity Index
SST	Sea Surface Temperature
UTC	Coordinated Universal Time
UTD	Upper-tropospheric Divergence

PREFACE

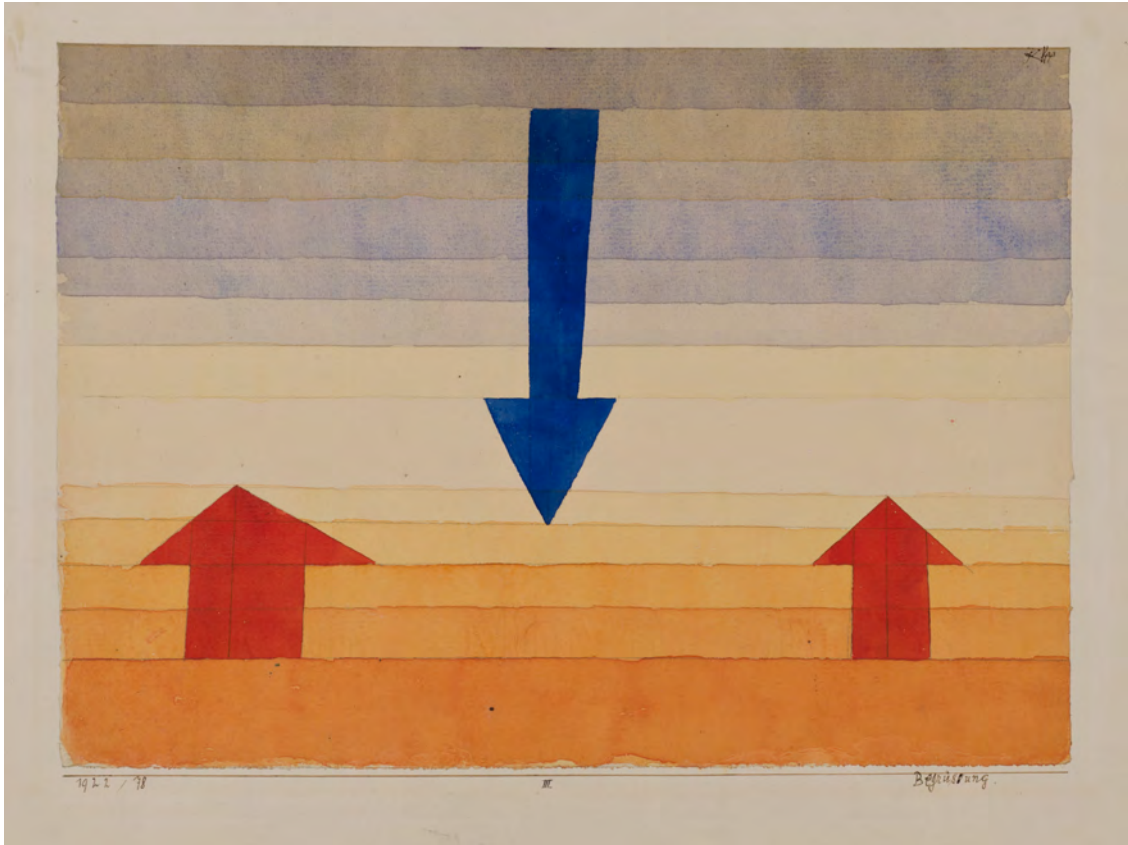


Figure 1: Paul Klee; Swiss, 1879-1940; **Begrüßung (Greeting)**; Watercolor, pen and brown ink on paper, 8 15/16 x 12 15/16 in.; Wadsworth Atheneum Museum of Art, Hartford, CT; The Ella Gallup Sumner and Mary Catlin Sumner Collection Fund. Endowed in memory of father, Gilbert Heublein, 1953.209. The rights to reproduce this image have been granted by the Wadsworth Atheneum Museum of Art.

Begrüßung – is the title of Paul Klee’s painting from 1922. *Greeting* – is its English name. Starting any piece of writing with a greeting can hardly be wrong. I find this specific ‘Greeting’ to be very fitting for the beginning of this present piece of written work. It shows in a quite simplistic way the transition from bluish to orange and reddish (or the other way round) parallel stripes with three prominent opposing arrows – two red, one blue – perpendicular to the underlying colours. With only schoolboy experience of water colours and no real arts education I do not dare to propose an interpretation for the actual meaning of the painting or the reason for its name. A short survey amongst family members revealed that one might see the sun rise or simply stripes and arrows. A Guardian review¹ about an exhibition featuring this painting suggested an imminent piquant encounter while a scientist from the Met Office² -I am apparently not the only meteorologist to have discovered the painting - speculates it to show a vertical temperature profile with the arrows representing incoming shortwave and upwelling longwave radiation. The sun appears to be the one that is ‘greeting’. This includes my interpretation. I had to immediately think about the word ‘baroclinicity’ when I first saw it. For me the painting shows a horizontal temperature distribution between the equator and the Arctic. In my interpretation the arrows represent the atmosphere’s tendency to counter balance the insolation induced energy imbalance. Without that differential insolation there would be no meridional temperature gradient, therefore no baroclinicity and no extra-tropical cyclones or wind storms - hence the connection in my mind.

Dear reader, whatever you might see in the painting or whether you do not really care that much, feel ‘greeted’ – either by the sun or this preface. I hope reading this thesis is about as enjoyable as it was to write these lines.

Simon Wild in February 2018

¹<https://www.theguardian.com/artanddesign/2013/oct/20/paul-klee-making-visible-review>

²<https://markringer.net/2014/02/23/paul-klee-the-earths-radiation-budget/>

GENERAL INTRODUCTION

1.1 Why Wind Storms?

“Extra-tropical cyclones and their associated heavy precipitation and wind storms can have major socio-economic impacts.” This inflationary used statement or a variation of it (definitely containing the expression “socio-economic impact”) is very likely to appear in any publication dealing with Northern Atlantic extra-tropical cyclones. Reading it (again) as a meteorologist, climatologist or suchlike might appear unnecessary or even boring on the quest to find the main scientific outcome of a paper. Next to all the personal joy or potential academic success wind storm research might provide, this very statement is however a gentle reminder why researching extra-tropical cyclones actually matters. Lack of scientific knowledge can cause failure of forecasting storms correctly as the example of the (in-)famous prediction with all its consequences of the *Great Storm of October 1987* in the UK has shown (Burt and Mansfield, 1988; Houghton, 1988). Therefore:

Extra-tropical cyclones and their associated wind storms can have major socio-economic impacts!

Storms are worldwide the most costly natural catastrophe with a share of 42% of economic losses and 71% of insured losses (Munich RE Group, 2016). These numbers include tropical storms, extra-tropical storms and thunderstorms. Nine North Atlantic winter wind storms appear in the list of the 40 costliest natural catastrophes and man-made disasters between 1970 and 2010 surpassed only by the

number of hurricanes hitting neighbouring countries of the Caribbean Sea and the Gulf of Mexico (Swiss Re, 2011).

The basic motivation of this thesis is to increase our knowledge about wind storms, which atmospheric and oceanic conditions on different time scales favour their development and how they are represented in seasonal forecast models and reanalyses data sets.

1.2 North Atlantic Winter Wind Storms in the Recent Climate

Extra-tropical cyclones are a very common weather phenomenon in the mid-latitudes. About 50 to 100 cyclone systems can pass the most frequented regions over the North Atlantic during one extended winter season from October to March depending on the identification method (Neu et al., 2012) or data set and resolution (Hodges et al., 2011). The regions over the North Atlantic and Pacific with highest cyclone activity are usually referred to as “storm tracks” (Blackmon et al., 1977), see also next section 1.3. A small relative amount of extra-tropical cyclones can be classified as wind storms.

Extra-tropical cyclones are synoptic scale phenomem characterised or defined over their lower than average pressure in their centre. The classical view or evolution of extra-tropical cyclones goes back the Norwegian model of Bjerknes and Solber (1922) and has been refined and updated by Shapiro and Keyser (1990). Wind storms as used in this thesis are defined over their meteorological impact, meaning strong winds and the potetential damage they can cause. The definition goes back to Klawa and Ulbrich (2003) that the upper 2% of the local climatological wind speeds are likely to cause damage. Wind storms *are* extra-tropical cyclones, but with extreme wind speeds over a certain period, usually one day (Leckebusch

et al., 2008). The main differences between an average extra-tropical cyclone and a wind storm are therefore the frequency and the impact.

Extra-tropical cyclones that can also be classified as wind storms undergo a strong intensification period associated with a fall in core pressure, and therefore greater pressure gradients and higher wind speeds. A list of the strongest and most damaging wind storms over the last 30 to 40 years can be found in Hewson and Neu (2015) or Pirret et al. (2017). A very recent example is storm *Friederike* on 18th January 2018 which caused damages and major disruptions mainly in the Netherlands, Germany and Poland (Haeseler et al., 2018). The storm occurred to the day 11 years after storm *Kyrrill* that affected a very similar region (Fink et al., 2012).

An interesting recent example that hit the UK and also Ireland is ex-hurricane *Ophelia* in October 2017. It was the farthest east a major Atlantic hurricane has ever travelled¹ before it underwent the transition to become an extra-tropical storm. This storm hit the UK to the day 30 years after storm *Tosca* better known as the *Great Storm of 1987* (Burt and Mansfield, 1988). The most damage storms have caused in the UK in recent years was primarily through heavy precipitation events. In the winter 2013/14 a record number of wind storms reached the UK that eventually caused wide spread flooding (Huntingford et al., 2014) even though the individual storms were not comparable in strength with the previous examples (see also figure 1.1b).

Winter seasons or shorter periods with a series of wind storms are often referred to as wind storm or cyclone clustering (Priestley et al., 2017a; Mailier et al., 2006; Pinto et al., 2014; Hanley and Caballero, 2012). Besides the mentioned winter 2013/14, other periods include January / February 1990 (McCallum and Norris, 1990), December 1999 (Ulbrich et al., 2001; Wernli et al., 2002) and January 2007 (Pinto et al., 2014). The general spatial pattern of wind storm frequency over the North

¹Phil Klotzbach, Colorado State University, on Twitter 14th October 2017

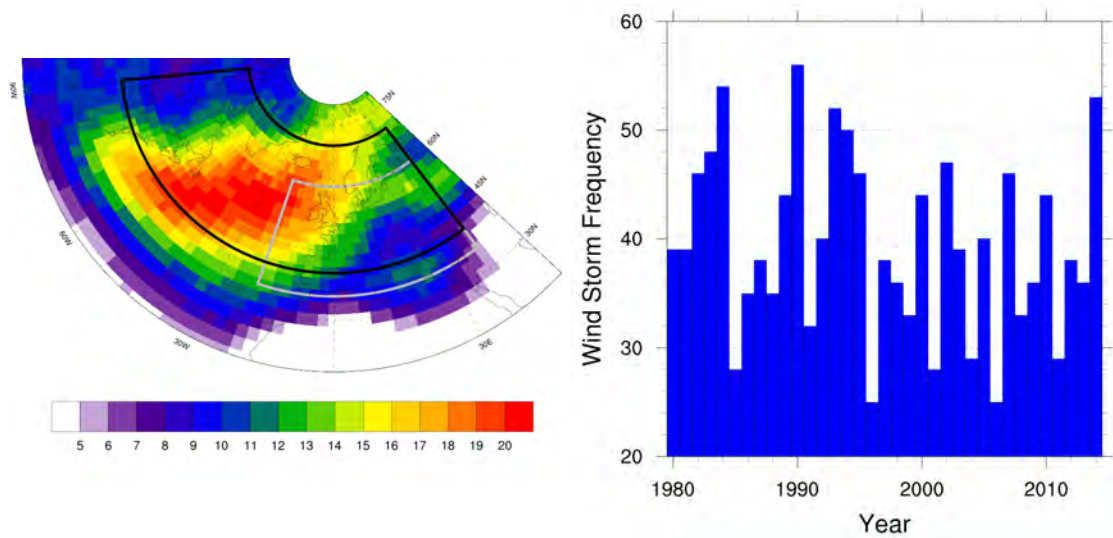


Figure 1.1: Mean Track density per Winter from 1980-2014 (a) and Winter Wind Storm Frequency (b). Frequency is number of individual storms that cross black box in (a) and are added from October to March. 1980 refers to winter 1979/80.

Atlantic, here shown as wind storm track density (Neu et al., 2012), resembles the spatial pattern of the stormtracks (Hodges et al., 2011) with a southward and slight downstream shift (see figure 1.1a). The maximum region with over 20 wind storms per season reaches from about 60°W and 45°N to 15°W and 55°N with a slight northeastward tilt of the spatial distribution. The latitudinal shift is due to the definition of cyclone track and wind storm track (centres). The cyclone centre is usually defined as minimum in mean sea level pressure or a maximum in relative vorticity in the lower troposphere (Neu et al., 2012), while wind storm “centroids” are defined as the centre of a region with strong wind speeds (Leckebusch et al., 2008). The strongest wind speeds occur in most cases in the frontal regions of the cyclone (Hewson and Neu, 2015) located south of the cyclone centre on the northern hemisphere. The British Isles and western Scandinavia are affected the most in Europe with about 15 wind storm events per extended winter season.

The wind storm frequency over the North Atlantic varies from about 25 to 55 wind storm events per season (see figure 1.1b). Note the winters with wind storm clustering 1989/90 or 2013/14 with generally a great number of wind storms over

the North Atlantic. Some winters with high wind storm frequency like 1983/84 did however not lead to any major events affecting Europe. The number of storms appears to have decreased on average somewhat in the second period of the here shown ERA Interim period from 1979/80 to 2013/14 in line with a decrease of insured losses (Dawkins et al., 2016).

1.3 Variability of Winter Wind Storms...

...on the Synoptic Time Scale

The North Atlantic stormtrack is a region of high synoptic activity (Hoskins and Valdes, 1990). Blackmon (1976) defined it as the fluctuations of a “regime” with medium scale waves of planetary (Rossby) wave numbers 7 to 12 of mid-tropospheric geopotential height. The waves have a frequency of 2.5 to 6 days and a wavelength of around 2,000km to 4,000km which is usually referred to as the **synoptic scale**. Following this definition stormtracks are usually identified by bandpass-filtering geopotential height fields in 500hPa to retain only the synoptic scale activity (Ulbrich et al., 2008; Zappa, Shaffrey and Hodges, 2013). The areas with a high standard deviation then define the stormtracks.

In the northern hemisphere two regions show high fluctuations or variability over the North Atlantic and North Pacific and are usually referred to as the northern hemisphere stormtracks. Despite the suggestion of the name these regions are *a priori* not related to either storms or individual tracks of storms. The stormtracks are however the regions where extra-tropical cyclone frequency including those that reach wind storm strength is highest.

The stormtracks owe their existence first and foremost to the differential solar radiation reaching the earth leading to a meridional temperature gradient. This temperature gradient is the reason for baroclinic instability or also often referred

to as baroclinicity (Woollings, 2010). Baroclinic conditions are given when in contrast to barotropic conditions isotherms and isobars are not aligned, meaning a temperature gradient exists along a surface of constant pressure. From a more observational perspective there is a phase shift between the temperature and the geopotential wave in the lower and middle troposphere. This leads to horizontal temperature advection and with vertical temperature fluxes to increased energy, i.e. amplitudes for the wave. The phase shift is associated with a vertical tilt of the wave axis and thus a vertical wind shear. This wind shear can be referred to as the thermal wind or thermal wind balance.

The theory of baroclinic instability identifies the development of synoptic activity with the intensification or growth of “baroclinic waves”. The waves can grow if they are superimposed to a baroclinic mean zonal flow, that is horizontally homogeneous and stationary (Sogalla, 1996). There are several concepts or models to quantify this intensification or wave growth, either through growth rates (Eady, 1949; Lindzen and Farrell, 1980), through the ratio of scale heights between baroclinic waves and the atmosphere in general (Charney, 1947; Held, 1978) and through the instability criterion of Phillips (1951). The latter can be used to define a minimum or critical wave length that has to be exceeded for a wave to grow due to baroclinic instability. This minimum wave length is independent of the vertical wind shear but depends on other assumption such as the static stability. Values are in the range of 2,500km (Sogalla, 1996) or 3,000km (Kurz, 1990). Diabatic processes, that may or may not be taken into account for its estimation, reduce the critical wave length. The upper limit for the wave length increases with greater vertical wind shear.

The amplitude of the waves grow until the wave turns into cyclonic or anticyclonic eddies (Kurz, 1990), the meridional temperature gradient is reduced and so is baroclinicity (Novak et al., 2014). Associated with a reduction in baroclinic instability is further energy dissipation through friction at the boundary layer and an alignment of the vertical axis of the waves to eventually barotropic conditions

with no vertical wind shear (Sogalla, 1996). Through diabatic processes, especially the release of latent heat, the baroclinic instability can be sustained longer (Hoskins and Valdes, 1990).

The meridional temperature gradient is greater in the winter season and therefore also baroclinicity. This is the also the reason why there are substantially more extra-tropical cyclones and wind storms in the winter months over the North Atlantic. The two main storm track regions differ slightly as there is a so-called midwinter suppression of baroclinic wave activity over the Pacific (Nakamura, 1992). On the one hand baroclinic instability leads to cyclogenesis especially in the western North Atlantic when small wave perturbations grow because of orographic forcing or disturbances related to (decaying) tropical cyclones for example. The cyclogenesis becomes more likely when a positive potential vorticity (PV) anomaly is present at upper levels (Hoskins et al., 1985). On the other hand baroclinicity has been shown to be crucial in the intensification of extra-tropical development of surface wind storms (Ulbrich et al., 2001; Pinto et al., 2009; Fink et al., 2012; Nissen et al., 2014; Renggli et al., 2011).

The development of strong extra-tropical cyclones are intensified if an anomaly of potential vorticity As mentioned above diabatic processes can have an influence on the wave length minimum of a wave undergoing baroclinic growth and on the time period a wave or extra-tropical cyclone can grow due to baroclinic instability. In the baroclinic instability theory diabatic process are generally not represented (Hoffmann, 1999). Diabatic process are not primarily associated with cyclogenesis but can play a major role for the intensification of cyclones (Catto, 2016). The release of latent heat can generate positive PV anomalies in the lower troposphere and thus increasing the temperature advection ahead of the cyclone (Grams et al., 2011) which in turn can amplify the wave. Above the heating level negative or anticyclonic PV anomalies are associated with latent heating (Hoskins et al., 1985). These negative anomalies can slow down the propagation

of the upper level wave and thus maintain the tilted structure and the cyclone can further intensify. Next to the strength of the diabatic heating but also its position with respect to the cyclone is therefore important (Hawcroft et al., 2017). A substantial amount of studies have linked diabatic heating to the intensification of extra-tropical cyclones and associated wind storms (Wernli et al., 2002; Ulbrich et al., 2001; Pirret et al., 2017; Pinto et al., 2009; Ludwig et al., 2014).

As mentioned the characteristics of atmospheric geopotential waves are crucial for the whole life cycle of extra-tropical cyclones. The trajectory of extra-tropical cyclones has long been linked to the breaking of atmospheric waves, usually termed Rossby wave breaking (Nakamura and Plumb, 1994; McIntyre and Palmer, 1983). In practise a wave is said to break when the potential temperature gradient on the 2 potential vorticity unit surface is reversed (Masato et al., 2013). Several studies associate Rossby wave breaking with the occurrence of extreme extra-tropical cyclones and wind storms (Hanley and Caballero, 2012; Gómara, Pinto, Woollings, Masato, Zurita-Gotor and Rodríguez-Fonseca, 2014) and additionally the relation to the clustering of such events (Priestley et al., 2017a; Pinto et al., 2014). Rossby wave breaking is also associated with “blocking” events, a stationary anomaly blocking the general westerly flow over the North Atlantic (e.g. Franzke and Woollings, 2011). Blocking events usually persist for a couple of days and either prevent extra-tropical cyclones completely to progress further east or deflect their path depending of the location of the block (Woollings, 2010).

...on Seasonal to Interannual Time Scales

The North Atlantic Oscillation (NAO) is the most prominent variability mode of northern hemispheric winter climate (Wanner et al., 2001). The pattern is characterised by two variability centres located over Iceland and the Azores and accounts for about 40% of surface pressure variability (Hurrell et al., 2003)

and about 30% of temperature variability in the winter season (Hurrell, 1996). The NAO is most dominant on interannual to (multi-)decadal time scales (see therefore also section 1.3.3 below), but weather and climate variability can be explained to some extent using the NAO on time scales ranging from days to centuries (Wanner et al., 2001; Pinto and Raible, 2012). The NAO has thus also been linked to the occurrence and intensity of North Atlantic / European wind storms or storminess (Pinto and Raible, 2012; Economou et al., 2014; Dawkins et al., 2016; Ulbrich and Christoph, 1999; Pinto et al., 2009; Donat, Leckebusch, Pinto and Ulbrich, 2010; Scaife et al., 2014).

A positive phase of the NAO is thereby usually related to an increased pressure difference between Iceland and the Azores, enhanced westerlies and more and more intense extra-tropical cyclones and wind storms that reach western and northern Europe. These systems also lead to relatively warmer and wetter conditions in northern and drier conditions in southern Europe. The negative phase of the NAO is characterised by a weaker pressure gradient over the North Atlantic. The extra-tropical cyclone frequency is higher and the precipitation increased over southern Europe while northern Europe is usually drier.

Most of the previously mentioned studies remark however a non-linearity of the link between NAO and wind storms, especially for wind storm intensity (Della-Marta et al., 2010; Renggli et al., 2011). For a critical review of the relation of NAO and wind speeds see also Burningham and French (2013). Depending on the investigated European region other teleconnection patterns such as the East Atlantic or the Scandinavian Pattern might play an even more important role on the interannual variability of wind storm frequency (Walz, Donat and Leckebusch, 2018).

Due to its general importance for European winter climate several studies have investigated the seasonal predictability and prediction skill of the NAO (Müller et al., 2005; Müller et al., 2008; Renggli et al., 2011; Scaife et al., 2014; Hansen et al., 2017; Athanasiadis et al., 2017; Scaife et al., 2016). It is primarily the

existence of relatively slow and predictable variations of boundary conditions that make a seasonal prediction of the NAO possible. Various boundary conditions have been linked or shown to have some or significant influence on the winter mean phase of the NAO. These drivers include:

- sea surface temperature (SST) anomalies over the North Atlantic (Rodwell and Folland, 2002; Czaja and Frankignoul, 1999; Czaja and Frankignoul, 2002; García-Serrano et al., 2008; Gastineau and Frankignoul, 2014)
- SST anomalies over the tropical Pacific (Greatbatch and Jung, 2007; Ineson and Scaife, 2008; Bell et al., 2009)
- snow cover over the Eurasian continent (Cohen and Entekhabi, 1999)
- Arctic sea ice extent (Wu and Zhang, 2010)
- soil moisture content (Douville, 2010)
- stratospheric variability (Scaife et al., 2016; Hansen et al., 2017)

Given the link of NAO and wind storms, all the above boundary conditions could potentially also influence wind storm frequency. Renggli (2011) as the only study investigating some of these drivers in seasonal prediction models has shown that North Atlantic SST appear to be a good source of seasonal predictability while snow cover and sea ice are not.

...on Decadal to Centenary Time Scales

Focussing on decadal and longer-scale variability, the objective of most studies is the question *what is?* rather than *what drives?* decadal variability and/or long-term trends of extra-tropical cyclones and wind storms over Europe either in the past or in the future. The observational record is of sufficient quality and length to analyse wind storm frequency and intensity and thus provides also the

possibility to investigate their drivers. That is arguably somewhat more difficult for the assessment of decadal variability of extra-tropical cyclones and wind storms. The availability and subsequent evaluation of the NOAA 20th Century Reanalysis (hereafter 20CR, Compo et al. (2011)) with respect to storminess triggered a controversial discussion in recent years. Donat et al. (2011) found an increasing trend of winter storminess for large parts of northern Europe in 20CR which is in some regions and for some periods in agreement with Broennimann et al. (2012) and Wang et al. (2011). The trend results do however not agree with works from Hanna et al. (2008) or Wang et al. (2009). Studies from Krueger et al. (2013,2014) point out potential inconsistencies in 20CR and conclude therefore that the trend in storminess is an artefact of the data set. This has in turn been challenged by Wang et al. (2014).

Despite the controversy all of the above studies agree that European storminess shows decadal variability, with periods of high wind storm activity roughly around the 1940s and 1990s in northern Europe. This also agrees with a study by Welker and Martius (2014) that finds high wind speeds to vary on a decadal scale with periods of approximately 36-47 years.

The sources of decadal variability for extra-tropical cyclones include the NAO (Hurrell and VanLoon, 1997; Matulla et al., 2008; Luo et al., 2014), sea surface temperatures (Rodwell et al., 1999), the Atlantic meridional overturning circulation (Nissen et al., 2014), a variable link between the Pacific/North America Pattern (PNA) and the NAO (Pinto et al., 2011), and potentially Arctic sea ice extent (Hoskins and Woollings, 2015; Cohen et al., 2014).

Decadal variability and especially long-term trends are of further importance when considering extra-tropical cyclone and wind storm frequency in a future climate (Zappa, Shaffrey, Hodges, Sansom and Stephenson, 2013; Harvey et al., 2012; Harvey et al., 2014). Climate models ought to be capable of capturing natural (multi-) decadal variability and long term trends to a sufficient extent otherwise

the interpretation whether a potential change is driven by an increase in greenhouse gases and thus of anthropogenic origin could be flawed (Solomon et al., 2011).

1.4 Research Gaps

Following on from the factors governing wind storm variability on the synoptic scale, such as baroclinic instability or diabatic heating, all of the above studies suggest the possibly obvious result: the greater the magnitude of the growth factor, the greater the likelihood of an intense extra-tropical cyclone. Pinto et al. (2009) showed for example that the growth factors baroclinic instability, latent heat release, upper-tropospheric divergence, and jet stream strength, are generally greater in magnitude for extreme extra-tropical cyclones than for all cyclones. Ulbrich et al. (2001) showed however that the development with respect to baroclinic instability, latent heat release and upper-tropospheric divergence for three storms in 1999 was “rather different”. Also Fink et al. (2012) point out that some storms have a strong diabatic contributions while others do not. This follows the earlier findings from Zillman and Price (1972) that stated: “no two vortices are the same”. This storm to storm variability with respect to growth factors has so far only been assessed systematically by Pirret et al. (2017) for a set number of 58 events. In their discussion they suggest further studies to increase the sample size.

Another method to investigate growth factors associated with extra-tropical cyclones are composite analyses. They allow generally the spatial distribution of physical characteristics around an extra-tropical cyclone revealing the typical structure of an (intense) extra-tropical cyclones (Dacre et al., 2012; Rudeva and Gulev, 2010; Hawcroft et al., 2017; Catto et al., 2009). Pinto et al. (2009) is so far the only study to have used this method for extreme strong extra-tropical cyclones. Their results exclude however a event to event variability with respect to cyclone growth factors.

The combination of investigating the storm to storm variability using composite analyses is thus missing in the current literature. There has also not been a study using composite analysis for extra-tropical cyclones with associated wind storm.

The Eady growth rate, a measure for baroclinic instability, has been shown to be a factor for the intensification of an extra-tropical cyclone (Ulbrich et al., 2001; Pinto et al., 2009; Nissen et al., 2014; Renggli et al., 2011) and is thus also analysed in chapter 3. The term *growth rate* relates thereby to an increasing amplitude of atmospheric waves. While in recent years many studies have shown a link between the amplitude of mid-latitude geopotential (Rossby) waves and meteorological extreme events such an analysis for strong wind events or wind storms in the mid-latitudes is still missing.

Several studies have shown a link between extreme extra-tropical cyclones and Rossby wave breaking (Pinto et al., 2014; Gómara, Pinto, Woollings, Masato, Zurita-Gotor and Rodríguez-Fonseca, 2014; Priestley et al., 2017a; Hanley and Caballero, 2012). Under the assumption that a wave has to grow in amplitude first, before it can break the analysis of the actual wave amplitude in relation to extreme extra-tropical cyclones and wind storms seems logical. The mentioned studies do not, however, focus at all on wave amplitudes.

Moving on to the seasonal scale, a possible break-through study of Scaife et al. (2014) showed relatively high prediction skill for the interannual variability of the North Atlantic Oscillation compared to previous studies. Renggli (2011a) has shown that the prediction of wind storms has some skill on the seasonal time scale. With the increased prediction skill for the NAO in improved seasonal models compared to the study of Renggli (2011), the seasonal prediction skill is likely to improve too. Renggli (2011a) has shown a systematic link between North Atlantic SST in late summer/early autumn and wind storm frequency in the subsequent winter but pointed out that for the understanding of the physical mechanism additional analysis would be needed to answer some of the following questions: How does a

SST anomaly affect the synoptic scale growth factors, given that concurrent SST anomaly patterns and wind storm frequency show no correlation? Does the SST anomaly potentially persist through anomalies in the upper ocean layers? Could such a mechanism if captured well by seasonal prediction models be the reason for predictive skill?

Seasonal prediction skill for the NAO has been linked to tropical convection that trigger stationary Rossby waves and thus provide a potential predictability (Trenberth and Fasullo, 2012; Trenberth et al., 2014; Scaife et al., 2017; Hansen et al., 2017). The very stormy winter 2013/14 has been linked to SST anomalies over the tropical Pacific (Huntingford et al., 2014; Slingo, J. et al. (Met Office and Centre for Ecology and Hydrology)., 2014; Kendon and McCarthy, 2015). All of these three studies do however not systematically show a link between tropical SST and wind storm frequency and only hypothesise, that such a link exists and was responsible for the very high number of storms that hit the British Isles in this specific winter. The validation of the hypothesis is still missing.

The decadal variability and long-term trends of wind storm frequency or storminess over Europe in general has been discussed extensively with different outcomes depending on the used method since the release of the 20CR reanalysis data set covering the years 1871 to 2011. The newly available ERA-20C reanalysis data starting at the year 1900 provides an excellent opportunity to further analyse decadal variability and potentially support the results of studies using 20CR.

1.5 Objectives of Thesis

The overarching objective of this thesis is investigation of reasons for changes in wind storm frequency on different time scales. What and/or where are the difference between an average extra-tropical cyclone and one that leads to strong wind speeds. It would be enormously overambitious to assume that one thesis could cover the

whole range of possible reasons for wind storm frequency variability but some are here investigated in more detail. The aim is thereby also to potentially link time scales, for example, how does the interannual variability of sea surface temperatures affect latent heat availability on the synoptic time scale? The main objectives for each individual chapter are the following:

Chapter 3: What are the synoptic scale differences of tropospheric growth factors between average extra-tropical cyclones and wind storms?

This research question is similar to Pirret et al. (2017) but the applied composite analysis comprises of a larger event set than their 58 storms. The emphasis of chapter 3 is especially on the wind storm event to event variability with respect to growth factors. Different composite sets further allow to investigate whether there are differences between extreme extra-tropical cyclone (defined by mean sea level pressure) and wind storms (defined by surface wind speeds).

Chapter 4: How do mid-latitude, mid-tropospheric geopotential wave characteristic differ during wind storm occurrence?

This chapter investigates whether the documented link between Rossby wave breaking and strong wind events can also be identified by purely analysing the geopotential wave characteristics. The chapter also extends recent research about geopotential wave amplitudes in relation to mid-latitude extreme events by strong wind events.

Chapter 5: How well do state-of-the art seasonal forecast models predict extra-tropical cyclones and wind storms?

Small but positive skill has been shown for the prediction of winter storms in previous seasonal forecast models (Renggli et al., 2011). Does this skill improve given the apparent recent success in some seasonal models to forecast mid-latitude variability patterns (Scaife et al., 2014)?

Chapter 6: Are North Atlantic sea surface temperatures a source of potential seasonal predictability of European wind storm frequency on a seasonal scale?

A well described link between Atlantic sea surface temperatures in late summer / early autumn and the

NAO (Czaja and Frankignoul, 1999; Czaja and Frankignoul, 2002; García-Serrano et al., 2008; Rodwell and Folland, 2002; Gastineau and Frankignoul, 2014) could potentially increase the seasonal predictability of wind storm frequency. Results from Renggli (2011) suggest such a link. Sensitivity experiments using ECHAM5 allow for further investigation of that link and could reveal the potential physical mechanism. **Chapter 7: Was the extreme storm season over the North Atlantic and the UK in winter 2013/14 triggered by changes in the West Pacific Warm Pool?** The link between the Pacific and increased extra-tropical cyclone (wind storm) frequency has been suggested shortly after the record number of storms over the UK in this winter (Huntingford et al., 2014). Given the low skill for seasonal predictions of extreme events in the mid-latitudes, is there really such a straightforward link?

1.6 Structure of Thesis

The thesis is structured as follows:

After this introduction an overview is given about the used data, applied methods and calculation of analysed variables in this thesis. The following six chapters 3 to 7 make up the main body of this thesis. Each chapter includes an introduction and conclusion so that they could be read independently of each other. Chapter 3 and 4 cover the **synoptic scale**, chapters 5 to 7 the **seasonal to interannual scale** and the appendix the **decadal to centennial scale**.

In chapter 3 atmospheric growth factors important for the development of strong extra-tropical cyclones and wind storms are analysed using mainly composite analysis. The data base is ERA Interim. This chapter has not been published but is currently prepared for publication in a shorter version

Chapter 4 deals with mid tropospheric waves in relation to extra-tropical cyclones and wind storms. Wave amplitudes and phase shifts are calculated using wave

frequency analysis. The data base is ERA Interim. This chapter has not been published.

In chapter 5 seasonal forecast model suites are analysed with respect to their capability of successfully predicting extra-tropical cyclone and wind storm frequency. Three data sets are analysed, namely the ECMWF-System 3 and 4 and the Met Office GloSea5. This chapter is identical to the manuscript submitted to the *Quarterly Journal of the Royal Meteorological Society*.

In chapter 6 a potential mechanism for seasonal forecast skill is analysed. The influence of North Atlantic sea surface temperatures in late summer on wind storm frequency in winter. ERA Interim and the sensitivity simulations with the AGCM ECHAM5 are used in this chapter. After the additional analysis the proposed mechanism in a seasonal forecast model this chapter will be prepared for publication.

In chapter 7 the possibility of an influence from the West Pacific Warm Pool on the wind storm frequency over the East Atlantic and Europe is investigated with an emphasis on the stormy winter 2013/14 in the UK. The analysed data is ERA Interim and two additional observational data sets. This chapter is published in the *Bulletin of the American Meteorological Society*.

The appendix deals with differences in decadal variations and long-term trends of extra-tropical cyclones and wind storms in two century long reanalyses: ERA-20C and NOAA-20CR. This chapter has been published in *Atmospheric Science Letters*.

The thesis finishes with a chapter incorporating the results of all previous chapters and discusses them with respect to the outlined objectives in section 1.5 followed by a short outlook of potential future research.

DATA, METHODS AND KEY VARIABLES

2.1 Data

ERA Interim

The data set primarily used in this thesis is the ERA Interim reanalysis (Dee et al., 2011). Reanalyses are based on a finite set of historical observations which are irregularly distributed over space and time. The observations are assimilated onto a gridded data set which is regularly distributed and complete over space and time using a Numerical Weather Prediction model. Observations include satellites, radiosondes, aircraft, ships, buoys, land stations etc. and number in the order of 10^6 at around 1990 and in the order of 10^7 around 2010 in ERA Interim. ERA Interim is the latest complete reanalysis version of the European Center for Medium-Range Weather Forecast (ECMWF), following on from ERA 40 (Uppala et al., 2005) and soon to be replaced by ERA 5 (Hersbach and Dee, 2016). ERA-Interim is a global atmospheric reanalysis starting in 1979 and is continuously updated. The period used in this thesis spans from 1979 to 2014, only considering the extended winter season from October to March. The spatial resolution of ERA Interim is T255 (spectral) corresponding to roughly $0.75^\circ \times 0.75^\circ$ or $80\text{km} \times 80\text{km}$ on 60 vertical levels from the surface up to 0.1hPa. The temporal resolution is 6 hourly which is also used here.

The data assimilation system used to produce ERA Interim is based on the IFS

release Cy31r2 from 2006 used in operational forecasting at the ECMWF in 2006 and 2007. The data assimilation is carried out with a 4D-Var scheme using a 12 hour window of observations (Dee et al., 2011).

Despite that a model component with all its constraints, such as resolution physical parametrisations, forecast error etc., reanalyses are often regarded as “historical reality”. They certainly provide historical data in the most convenient way to study weather and climate in the past on a large scale.

In a study about extra-tropical cyclone representation in reanalyses Hodges et al. (2011) found ERA Interim to compare well with other reanalysis data sets in terms of frequency and spatial distribution of cyclones. The intensities of extra-tropical cyclones compare less well across the reanalyses. Outliers are thereby however primarily older reanalyses.

It is here assumed that all the described processes in the introduction are well represented in the ERA Interim data set. While in the North Atlantic / European region with a dense observation network the difference between reality and reanalyses might be sufficiently small for the analyses performed in this thesis, model deficiencies have to be kept in mind. ERA Interim compares well with observations for large storm systems, like *Kyrrill*, but differences arise for smaller systems (Hewson and Neu, 2015). ERA Interim systematically underestimates depth, gradients and wind speeds. This is likely due to its insufficient spatial resolution which is not high enough to realistically represent small scale features like for example sting jets (Hewson and Neu, 2015).

Other Data Sets

Other data sets and models used in this thesis are briefly outlined in the individual chapters. These data sets include seasonal forecast model systems ECMWF-System 3 (Anderson et al., 2007), ECMWF-System 4 (Molteni et al., 2011), and Met Office

GloSea 5 (MacLachlan et al., 2015) in chapter 5, The AGCM ECHAM5 is used for AMIP-type sensitivity experiments in chapter 6. NOAA/NCAR outgoing longwave radiation and (Liebmann and Smith, 1996) and sea surface temperatures from the 4th version of the ERSST data set (Huang et al., 2014) are used in chapter 7. In appendix A the two reanalyses ERA-20C (Poli et al., 2016) and NOAA-20CR (Compo et al., 2011) are compared.

Monthly mean time series for large scale variability patterns, such as the NAO, are taken from the NOAA Climate Prediction Center (Barnston and Livezey, 1987).

2.2 Methods

In this section some methods are described which are used throughout this thesis. With the exception of the somewhat lengthy explanation of the PCA procedure, all methods that are only applied in a specific chapter are explained within that respective chapter.

Algorithm for the Identification and Tracking of Extra-tropical Cyclones and Wind Storms

Extra-tropical Cyclone Events

For the identification and tracking of extra-tropical cyclones an algorithm originally developed by Murray and Simmonds (1991a) is used. Further specifications for the algorithm can be found in Simmonds and Murray (1999) and Simmonds et al. (1999).

If not otherwise indicated the input field is 6 hourly MSLP data. Irrespective of the resolution the input data is firstly smoothed and then interpolated onto

polar stereographic grid using a bicubic spline. The Laplacian of the MSLP $\nabla^2 p$ is calculated on the new grid that is proportional to the quasi-geostrophic relative vorticity. Local minima of the MSLP in the vicinity of the maximum values are identified as cyclone centres. If a minimum with a closed isobar can be identified within a 1,200km radius, the minimum determines the location of a closed system. Otherwise, meaning there are no closed isobars within the search radius, the minimum determines the location of an open depression. In a next step a subsequent position of each cyclone is predicted and compared to newly identified cyclone centres. The identified tracks are then filtered according to the criteria

- Lifetime at least 24 hours, i.e. five 6-hour time steps
- At least once strong and closed in its lifetime ($\nabla^2 p > 0.7\text{hPa } ^\circ\text{lat}^{-2}$)

These criteria have been found useful in previous studies using the same algorithm (Grieger et al., 2014; Leckebusch and Ulbrich, 2004). This cyclone identification and tracking algorithm has been used by numerous times in the past (Pinto et al., 2009; Kruschke et al., 2014; Nissen et al., 2014; Gómara, Rodriguez-Fonseca, Zurita-Gotor and Pinto, 2014; Nissen et al., 2013) and is part of Intercomparison of Mid-Latitude Storm Diagnostics Initiative, *IMILAST* (Neu et al., 2012; Ulbrich et al., 2013). The cyclone tracking scheme is applied for the northern hemisphere north of 20°N.

Wind Storm Events

For the identification and tracking of wind storm events an algorithm originally developed Leckebusch et al. (2008) is used. A detailed overview for the algorithm can be found in Renggli (2011) and Kruschke (2015).

The development of the algorithm was motivated through the the socio-economic impact of wind storms. Following the study of Klawns and Ulbrich (2003) in line with results of Palutikof and Skellern (1991), the local climatological 98th percentile of near-surface wind speeds constitutes a threshold for (potential) wind damage. The basic settings for the algorithm require a gridded data set with a data point of at

least 6 hours. If not otherwise indicated this is the case for the data analysed in this thesis.

Coherent fields (i.e. grid cells) are identified as wind storm clusters where the 98th percentile threshold is exceeded and the overall affected area is greater than $150,000\text{km}^2$. The position of the storm is then calculated as a weighted average over all wind storm grid cells of these clusters. The weights are calculated according to the Storm Severity Index (SSI, see below in 2.2.3) as the cubic exceedance of the 98th percentile. This identified “centroid” of the storm can be outside the coherent cluster. This happens frequently as strong wind speeds often occur along the fronts of an extra-tropical cyclone, which is usually crescent-shaped. The clusters are subsequently connected in time with a nearest-neighbour approach, with two restrictions: the maximum distance of 720km (equivalent to a translational velocity of $120\text{km}/\text{h}$) between centroids cannot be exceeded and 30% of the grid boxes of the neighbouring clusters between two time steps have to overlap. The life time of the identified wind storms has to be at least 18 hours (i.e. 4 time steps) otherwise it is filtered out in a final step.

The wind tracking scheme is also applied to the northern hemisphere north of 20°N .

Track Density Calculation for Cyclone and Wind Events

The climatologies for extra-tropical cyclone and wind storm frequency follow the track density definition of Neu et al.(2012). A track density is thereby the number of systems that passes a grid cell with each event only counted once. If not otherwise indicated, passing a grid cell, means here that the cyclone or wind storm track is within a great circle distance, often referred to as the “search radius” of 700km of the centre of a grid cell. The grid is hereby independent of the used data set as the longitude and latitude information of the events are points and not grids. If not otherwise indicated a grid of $2.5^\circ \times 2.5^\circ$ is used. The track between two time steps or event track points is assumed to be a great circle segment.

Matching Algorithm for the Association of a Wind Storm to an Extra-tropical Cyclone

Each wind storm as identified by the wind storm tracking algorithm is associated with an extra-tropical cyclone. The wind tracks are therefore linked to the cyclone tracks using a method following Nissen et al. (2010). In this study a three step iteration procedure is described of which only the first two steps are used here. In the first step tracks are matched if all of the wind track time steps coexist with a cyclone track and the average distance of cyclone centre and wind storm cluster centroid is less than $800km$. If two cyclone tracks are found, the strongest one with respect to $\nabla^2 p$ is taken. These criteria are sufficient for about three quarters of the wind tracks to be associated with a cyclone track.

If no cyclone is found in the first step, the closest cyclone with a mean distance of less than $1200km$ is chosen. The threshold of $1,200km$ maximum distance between wind track cluster centroid and cyclone centre corresponds to the search radius for the cyclone centre in the vicinity of a $\nabla^2 p$ maximum in the cyclone identification algorithm.

More than one wind track can be associated with a cyclone track. In ERA-Interim over 94% of wind tracks can be matched. The remaining 6% consist to a large extent of short wind tracks at the southern edge of the considered area.

Storm Severity Index

Based on the assumption that the strongest 2% of wind events at a given location can cause damage to insured values such as infrastructure or buildings, Klawa and Ulbrich (2003) developed a model for the estimation of potential wind storm losses. The cubic relative exceedance of the local climatological 98th percentile was thereby found to be a suitable measure for real loss data. Leckebusch et al., (2008) defined

the *Storm Severity Index* - SSI based on these findings:

$$SSI(t, k) = \sum_t^T \sum_k^K (\max(0, \frac{v(k, t)}{v_{98}(k)} - 1)^3) \cdot A_k \quad (2.1)$$

with t the time step, k the grid cell, v the near-surface horizontal wind speed, v_{98} the climatological 98th percentile and A the real area of the grid cell k . The unit of the *SSI* is *area* as the sum of the area where a wind speed threshold is exceeded, also taking into account the life time of a system. It is therefore rather a practical, simple, integrated measure over space and time than an actual physical quantity. The original work by Klawns and Ulbrich is based on gust wind speeds from observations in relation to insurance data for Germany. This is different to the 6-hourly wind speed reanalysis data which is used in this thesis for the whole North Atlantic and European region. The percentile approach together with cubic wind speed exceedances has however been applied in many studies (Nissen et al., 2013; Pirret et al., 2017; Pinto et al., 2012; Donat, Leckebusch, Wild and Ulbrich, 2010; Donat et al., 2011; Cusack, 2013). These studies predominantly also use 6-hourly reanalysis data for the whole of Europe or European regions.

Leckebusch et al. (2008) differentiate between an *Area SSI* (equation 2.2) and an *Event SSI* (equation 2.1). The former refers to one time step (i.e. $t = T = 1$) in a given area with potentially several events contributing to the total SSI. The latter refers to one single event, i.e. A_k is a coherent region. Only the *Event-SSI* is used in this thesis. The *Area SSI* for a pre-defined region simplifies equation 2.1 into:

$$SSI(k) = \sum_k^K (\max(0, \frac{v(k, t)}{v_{98}(k)} - 1)^3) \cdot A_k \quad (2.2)$$

The grid cells k with a wind speed exceedance *do not* have to be adjacent. The wind speed exceedances *do not* have to be from the same event. In case of the *Event SSI*, that is calculated using equation 2.1, the grid cells k with a wind speed exceedance *do* have to be adjacent and it is thereby assumed that the wind speed exceedance

do belong to the same event. In chapter 4 the time of strongest intensity of a storm refers to the greatest single time step SSI.

In a further refinement of the SSI, Walz et al. (2017) defined the distribution independent SSI or *DI-SSI*. This index takes into account the tail of the local wind speed distribution. *Event-SSI* values of different wind storms can sometimes not be compared if the events occurred in different areas, for example in the main storm track region and an area where wind storms are rare.

Normalisation of Analysed Variables

In many parts of this thesis the investigated variable or quantity is normalised at each time step (see equation 2.3). This normalisation or in fact standardisation is often referred to as standard score or z-score.

$$z(lon, lat, t, y) = \frac{x(lon, lat, t, y) - \overline{x(lon, lat, y)}}{\sigma(x(lon, lat, y))} \quad (2.3)$$

with the mean \bar{x} and the standard deviation $\sigma(x)$ of one given date y during the year (e.g. 1st January 00:00UTC) for one grid cell with longitude lon and latitude lat . The mean and standard deviation are thus specific for each point of time in the year and each grid cell. The intent is to minimise temporal and spatial variability for a better comparison between different quantities such as the maximum Eady growth rate (see section 2.3 below) in for example the composite analysis in chapter 3. This procedure will remove seasonality in the data but keep long term trends if not otherwise removed. The analysed quantities do however not show any significant trend different from zero.

Correlation Analyses

Three correlation coefficients are used in this thesis: the often used *Pearson Correlation Coefficient* (Pearson, 1901) and *Spearman Rank Correlation Coefficient* (Spearman, 1904) but also the less frequently used *Kendall Rank Correlation Coefficient* (Kendall and Dickinson, 1990). The latter allows in its so called *b-version* or τ_b for ties in either of the sample sizes to be correlated and is therefore in the case of wind storm frequency more appropriate than the other two. Especially in regions with few wind storms per year, the number of ties cannot be neglected when for example the interannual correlation coefficient is calculated. It is worth mentioning that all correlation results throughout this thesis are calculated for all three coefficients are agree very well especially in regions with high and significant correlation.

Composite Analysis

A very common procedure in atmospheric sciences is the use of composites. It is essentially the temporal mean of spatial patterns for selected dates depending on some condition or threshold. Composites can be especially useful when there is a non-linear relation between two quantities. Correlation coefficients would show a low or no relation or dependency in these cases.

$$c = \left\{ \frac{1}{N} \sum_{n=1}^N x_n(y) \mid y \in S \right\} \quad (2.4)$$

Equation 2.4 can be read as the composite c is sum over all x_n , which are dependant on y , which has to be a subset of S . For example, x could be the equivalent potential temperature, y the time, and S the days with strong storms. Composites are used in two different ways in this thesis. Firstly to analyse the average signal of a

quantity given a certain condition as in equation 2.3. Secondly, composites are used in form of composite differences. This is a composite as in the first case with a certain condition A minus the a composite with condition A^* . A and A^* are usually opposites, for example A could be a positive SST anomaly of one standard deviation above some mean and A^* would then be a negative SST anomaly of one standard deviation below that mean. The composite signal is thus amplified.

Principle Component Analysis

In chapter 3, section 3.4 a principle component analysis (PCA) is carried out using the eigenanalysis of the covariance matrix. The eigenvectors, empirical orthogonal functions (EOF) or loadings represent the main variability patterns around the cyclone centre while each element in the principle component (PC) represents one cyclone event. PCA is widely used and became popular in atmospheric science after the study of Lorenz (1965). PCA reduces the number of variables of a data set to a smaller number of variables. The new variables are a linear combination of the old ones (Wilks, 1995). At first anomalies are calculated for the normalised fields \mathbf{X} with K entries 2.5.

$$\mathbf{X}' = \mathbf{X} - \bar{\mathbf{X}} \quad (2.5)$$

Any symmetric matrix \mathbf{C} can be decomposed in the following way through a diagonalisation, or eigenanalysis:

$$\begin{aligned} \mathbf{C}e_i &= \lambda_i e_i \\ \mathbf{C}\mathbf{E} &= \mathbf{E}\mathbf{\Lambda} \end{aligned} \quad (2.6)$$

\mathbf{C} is here the correlation matrix. The PCA is then carried out with Equation 2.7

$$\mathbf{Z} = \mathbf{E}^T \mathbf{X}' \quad (2.7)$$

with \mathbf{Z} containing the PCs z_i and \mathbf{E} contains the eigenvectors e_i or EOFs. Λ is the matrix containing the eigenvalues λ_i , that correspond to the explained variance of an EOF. The original variables or in this case anomalies of the composite fields can be re-calculated out of the EOFs and PCs with the synthesis equation 2.8.

$$\mathbf{X}' = \mathbf{E} \mathbf{Z}$$

$$x'_k = \sum_{i=1}^M e_{ki} z_i, \quad k = 1, \dots, K \quad (2.8)$$

M is the number of EOFs and equals K . Usually only a few EOFs are retained corresponding the EOFs with the largest eigenvalues. That makes M a lot smaller than K . The values of the EOF and PC are difficult to interpret as the amplitudes of EOFs and PCs respectively can only be compared to each other but not to the original normalised fields that go into the PCA. In order to include some information about the amplitudes an adapted approach by Dennis Hartmann, University of Washington is followed ¹:

At first the PCs are normalised by dividing through their standard deviation that can be expressed using the eigenvalues (Equation 2.9).

$$\tilde{\mathbf{Z}} = \Lambda^{-1/2} \mathbf{Z}, \quad (2.9)$$

The normalised PCs in $\tilde{\mathbf{Z}}$ are then projected onto the original normalised anomaly field \mathbf{X}' (Equation 2.10).

$$\tilde{\mathbf{E}} = \mathbf{X}' \tilde{\mathbf{Z}}^T / K \quad (2.10)$$

The so obtained maps $\tilde{\mathbf{E}}$ contains now new EOFs with the same spatial structure than the previous EOFs \mathbf{E} , but with the amplitude and sign representing the original data, here composite fields with unit standard deviation. The eigenvalues or the explained variance of each EOF remains the same as after the PCA. Each EOF in

¹https://atmos.washington.edu/~dennis/552_Notes ftp.html

$\tilde{\mathbf{E}}$ gives the amplitudes in the original normalised field (in standard deviation units) associated with a one standard deviation variation in the principle component time series.

If adjacent EOFs are too close together with respect to their eigenvalue or explained variance, they are called *degenerated*. It is then unlikely that their structures are particularly significant. North et al. (1982) suggested that the true eigenvalue of a PCA should lie within the standard error

$$\Delta\lambda = \lambda\sqrt{2/doF} \quad (2.11)$$

with doF is the number of degrees of freedom. In practise this means, if the error bars of two adjacent eigenvalues overlap, the EOFs become indistinguishable.

2.3 Atmospheric Growth Factors

In several studies analysing wind storms different atmospheric conditions were favourable for the intensification of an extra-tropical cyclone. These growth factors include enhanced baroclinicity, latent heat release and upper-tropospheric divergence (Ulbrich et al., 2001; Pinto et al., 2009). The following section gives an overview of how these growth factors are quantified in this thesis.

Equivalent Potential Temperature

Diabetic processes can play an important role in the intensification of cyclones. While not all wind storms have a strong diabetic influence on their intensification, others have diabetic contributions of more than 60% (Fink et al., 2012). The equivalent potential temperature is commonly used as a measure of latent heat or potential latent heating. It takes into account the energy stored in moist air and

although its unit is Kelvin it is considered a humidity measure. It is here calculated as recommended by Bolton (1980) :

$$\Theta_E = T_K \left(\frac{1000}{p} \right)^{0.2854 \cdot (1 - 0.28 \cdot 10^{-3} r)} \exp \left[\left(\frac{3.376}{T_L} - 0.00254 \right) r (1 + 0.81 \cdot 10^{-3} r) \right] \quad (2.12)$$

with T_K , p , r the absolute temperature, pressure and mixing ratio at 850hPa (see also equation 2.13) and T_L is the absolute temperature at the lifting condensation level (see equation 2.14).

$$r = \frac{sh}{1 - sh} \quad \text{with } sh \text{ the specific humidity} \quad (2.13)$$

$$T_L = \frac{2840}{3.5 \ln(T_K) - 5.805} + 55 \quad (2.14)$$

Maximum Eady Growth Rate

It could be shown by Lindzen and Farrel (1980) that the maximum Eady growth rate is a suitable measure for baroclinic instability and can be expressed as given in equation 2.15. It is based on the works of Charney (1947) and Eady (1949).

$$\sigma_{BI} = 0.3125 \frac{f}{N} \frac{d\bar{u}}{dz} \Big|_{z=0} \quad (2.15)$$

with f the Coriolis parameter N the Brunt-Väisälä-Frequency and $\frac{d\bar{u}}{dz}$ the vertical shear of the mean zonal wind. baroclinicity is thus influenced by the static stability and vertical wind shear. Hoskins and Valdes (1990) reformulated Lindzen and Farrel's equation slightly into:

$$\sigma_{BI} = 0.31 \frac{f}{N} \left| \frac{\partial v}{\partial z} \right| \quad (2.16)$$

with $|\frac{\partial v}{\partial z}|$ the absolute vertical shear of the horizontal wind. This equation 2.16 has since been used in several studies (Ulbrich et al., 2001; Nissen et al., 2013; Lehmann et al., 2014; Seiler and Zwiers, 2015*a*; Seiler and Zwiers, 2015*b*), while in some of these studies only the zonal wind is used (Novak et al., 2014; Gastineau and Frankignoul, 2014).

Equation 2.16 is used in this thesis as a measure of lower and upper baroclinicity. It is calculated for both cases between two p-levels: in the lower troposphere between 850hPa and 700hPa (sometimes referred to as “in 775hPa”) as in e.g. Hoskins and Valdes (1990) and in the upper troposphere between 500hPa and 300hPa (referred to as “in 400hPa”) as e.g. in Pinto et al. (2009). The two lower troposphere levels as used here can be associated to the steering level (Beare et al., 2003) of an extra-tropical cyclone. The flow in this level has the largest influence on propagation and speed of the extra-tropical cyclone. In the original Eady model the steering level is defined at 500hPa (Eady, 1949). With the maximum Eady growth rate it is possible to quantify the large-scale conditions for the potential growth of a wave disturbance. This means, that an extra-tropical cyclone only *potentially* grows, i.e. deepens when large maximum Eady growth rate values exist.

Upper-tropospheric Divergence and Jet Stream

Upper tropospheric divergence at the left jet exit region has also been associated with the intensification of extra-tropical cyclones (Uccellini et al., 1987; Fink et al., 2012; Pirret et al., 2017). It is here directly taken from ERA Interim and summed up over five pressure levels from 500hPa to 200hPa (including 400hPa, 300hPa and 250hPa).

$$UTD = \sum_{500}^{200} \nabla \cdot \mathbf{v} \quad (2.17)$$

The maximum in the extra-tropics is associated with the jet stream. The eddy driven jet is usually deeper than the subtropical jet and can therefore also be identified in lower levels (Woollings et al., 2010). Following Pinto et. al (2009) or Renggli (2011), upper-level zonal wind in 200hPa is taken here.

**INFLUENCE OF MAGNITUDE AND
LOCATION OF TROPOSPHERIC GROWTH
FACTORS FOR THE TRANSFORMATION OF
CYCLONES TO SEVERE STORMS OVER
THE NORTH ATLANTIC**

3.1 Introduction

In a study about three severe winter wind storms in December 1999 Ulbrich et al. (2001) found enhanced baroclinicity played a crucial role in their development and intensification. In this study the maximum Eady growth rate σ_{BI} (see 2.3.2) is used as a measure of baroclinicity. In several other more recent studies σ_{BI} was also used as a general measure of storm track activity (Novak et al., 2014; Gastineau and Frankignoul, 2014; Lehmann et al., 2014; Seiler and Zwiers, 2015*a*; Seiler and Zwiers, 2015*b*). Fewer studies followed Ulbrich et al. (2001) and used σ_{BI} in direct relation to wind storms (Pinto et al., 2009; Nissen et al., 2014; Renggli et al., 2011). All studies agree that higher baroclinicity leads to increased storm track activity and therefore also to more and/or stronger wind storms.

Equivalent potential temperature or Θ_E (see 2.3.1) as a quantity combining the effect of latent and sensible heat on extra-tropical cyclones is the other analysed quantity in Ulbrich et al. (2001). The influence of diabatic processes, including

latent heat, on the development and structure of extra-tropical cyclones and wind storms has found a lot of attention recently (Pirret et al., 2017; Hawcroft et al., 2017; Binder et al., 2016; Catto et al., 2015; Ludwig et al., 2014). The availability of latent heat can play an important role for the intensification of ETCs (Hoskins et al., 1985; Hawcroft et al., 2017; Pinto et al., 2009) but this does not mean that the availability of latent heat is always necessary for the formation of a strong extra-tropical cyclone (Catto, 2016). While the spatial distribution of quantities such as for example latent heat in the lower troposphere in relation to ETCs is well established from a climatological perspective (e.g. Dacre and Gray, (2012)), it remains unclear whether this relation differs systematically in magnitude or location for an ETC with an associated wind storm. Fink et al., (2012) found that synoptic scale conditions in the vicinity of wind storms can differ substantially. They looked mainly at five different wind storms in recent years and found that some have diabatic contributions of above 60% while others are more baroclinically driven and have diabatic contributions of below 30%.

Positive anomalies in upper-tropospheric divergence can further substantially influence the development and deepening of an extra-tropical cyclone (Fink et al., 2009; Liberato et al., 2011; Liberato, 2014; Pinto et al., 2009). The anomalies of divergence are closely related to the position of the jet stream and are a smaller in spatial scale than the σ and Θ_E (Fink et al., 2009). In this chapter these three atmospheric growth factors on the **synoptic scale** important for the development but especially for the intensification of ETCs are analysed.

Previous work about differences between average extra-tropical cyclones and strong extra-tropical cyclones and / or wind storms is predominantly focussed on case studies. This chapter therefore aims to answer the question whether there are fundamental differences not only in magnitude but also in spatial structure of atmospheric growth factors for the development of a strong extra-tropical cyclone or a wind storm in comparison to the climatology of extra-tropical cyclones.

In the next section 3.2 of this chapter some case studies of strong winter storms and their relation to the three growth factors are discussed. Composite analyses for ETCs, strong ETCs, and wind storms are carried out in section 3.3. This is followed by a principle component analysis over these composites in sections 3.4 and 3.5. The chapter finishes with a summary and discussion of the results. 6 hourly ERA-Interim reanalysis from 1979 to 2013 (Dee et al., 2011) is used throughout this chapter (see 2.1.1).

3.2 Wind Storms and Tropospheric Growth Factors in Specific Months

Some case studies of well known wind storms in the recent past are discussed in this section. The focus hereby is on the magnitude and location of the growth conditions relative to the cyclone or wind storm that ultimately led to (or did not lead to) the development of a specific event. All investigated growth factors are normalised according to 2.2.4. For the Hovmoeller plots in figure 3.1, 3.2 and 3.3 the growth factors are further averaged from 40° to 60°N. The first example is the storm “Kyrill” hitting Europe between the 17th and 19th January 2007. In figure 3.1a it shows as the storm with the highest SSI values (red colour) crossing central Europe. The centre of highest wind speeds associated with Kyrill is located around northern France, southern UK and the BeNeLux countries for more than 24 hours, that is why the wind storm track “zick-zacks” in this area before it continues further east across Germany and the Czech Republic. The cyclone track for Kyrill starts at around 80°W on the 15th January. The tracking algorithm scheme (see 2.2.1) identifies it as two different systems which is in accordance with (Fink et al., 2009) describing the cyclone as two different systems named Kyrill I and Kyrill II. The wind storm is associated with Kyrill II. Note here that with the same cyclone

tracking algorithm (Murray and Simmonds, 1991) and different data sets and/or different settings, Kyrill is identified as one or two systems (Fink et al., 2009, using NCEP1: one system; Pinto et al., 2014, using ERA-Interim: one system; Befort et al., 2016, using ERA-20C: two systems; Befort et al., 2016, using NOAA-20CR: one system). Kyrill I developed in a region with enhanced baroclinicity in the upper and especially the lower troposphere between 10th and 15th January around the east coast of the US (Figs. 3.1b and c). Baroclinicity shows consistently positive anomalies just prior to the arrival of the cyclone throughout Kyrill's passage across the Atlantic. The maximum Eady growth rate shows strong positive anomalies just *after* Kyrill II, providing suitable conditions for the next storm *Lancelot* only two days later. There is higher availability of latent heat in the eastern part just before and around the arrival of Kyrill. East of the Greenwich Meridian latent heat shows positive anomalies since the beginning of the month. Upper tropospheric divergence has a strong maximum around the 30°W on 15th January.

In agreement with Fink et al. (2012) enhanced baroclinicity played a major role for the initial development of Kyrill I and was also important to maintain its strength until it reached Europe. While the configuration of upper-tropospheric waves and wave breaking played a role during Kyrill's intensification (Fink et al., 2009; Pinto et al., 2014), latent heat availability and upper-tropospheric divergence were crucial to maintain the strength of Kyrill II (Fink et al., 2009). In short: baroclinicity was needed for Kyrill's (the cyclone) development and latent heat and upper-tropospheric divergence were needed for its intensification and transformation into a severe wind storm.

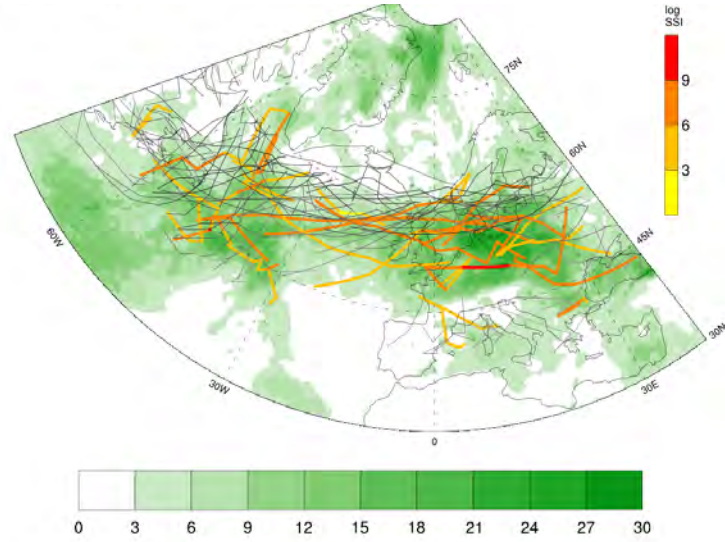
The Hovmoeller diagrams show also a period at the beginning of January 2007 with enhanced latent heat availability especially in the western but also in the eastern part of the Atlantic. Baroclinicity in the lower troposphere and upper-tropospheric divergence show however negative or no anomalies, which made the development of a wind storm or even cyclone more difficult. This can be seen

even more pronounced in February 2008 3.2. Very stable conditions in association with an atmospheric blocking (Woollings, 2010) also visible as negative anomalies in baroclinicity throughout the entire troposphere and neither con- nor divergence in the upper troposphere led to a cyclone and wind storm free period of about two weeks in mid February 2008. Latent heat shows however positive anomalies for most parts of that month over the eastern Atlantic, suggesting that purely the presence of positive latent heat anomalies are not sufficient for the development or intensification of a wind storm.

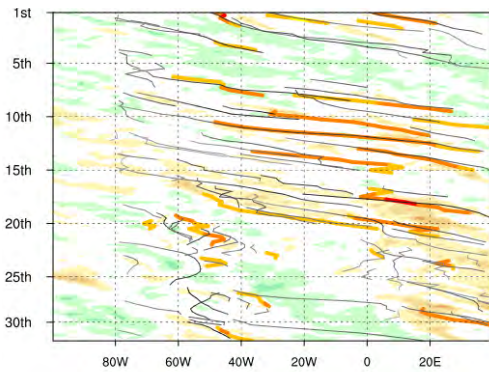
The next case study includes the winter storm *Klaus* hitting mainly southern France and the Iberian Peninsula (Liberato et al., 2011) on 23rd and 24th January 2009. The storm intensified quickly with high SSI values already around 30°W in the central North Atlantic and remained strong until it reached the Western Mediterranean around the Balearic Islands (Fig. 3.3a, mainly red SSI values). The only other identified wind storm progressing into south-western Europe in this month is *Joris*. It reached France only one day prior to Klaus. Klaus can be regarded as a textbook case: baroclinicity is enhanced in the upper and lower troposphere and latent heat availability and upper-tropospheric divergence show strong positive anomalies just prior to the event (Figs. 3.3b-e). The consequence is a wind storm. The same is however true for *Joris*, which is also classified as a wind storm but is not comparable with respect to wind speeds and socio-economic impact. This raises the question about their main differences in growth conditions. It appears that not only the location of the various growth conditions but also its location with respect to the cyclone or wind storm is of crucial importance.

January 2007

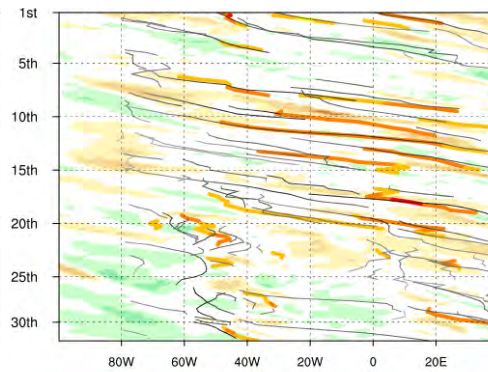
(a) Exceedances of 98th percentile in 10m wind speeds



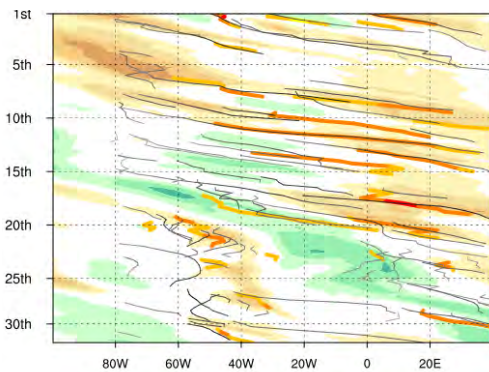
(b) Eady Growth Rate between 850hPa and 700hPa



(c) Eady Growth Rate between 500hPa and 200hPa



(d) Equivalent Potential Temperature in 850hPa



(e) Divergence from 500hPa to 200hPa

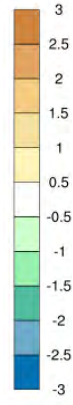
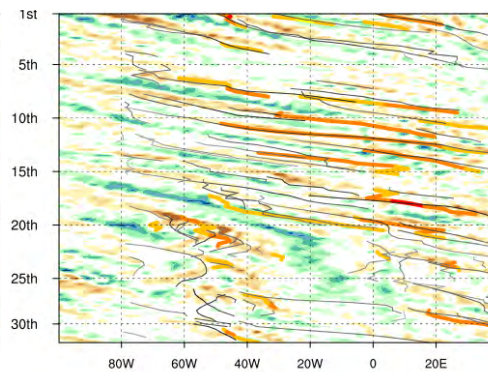
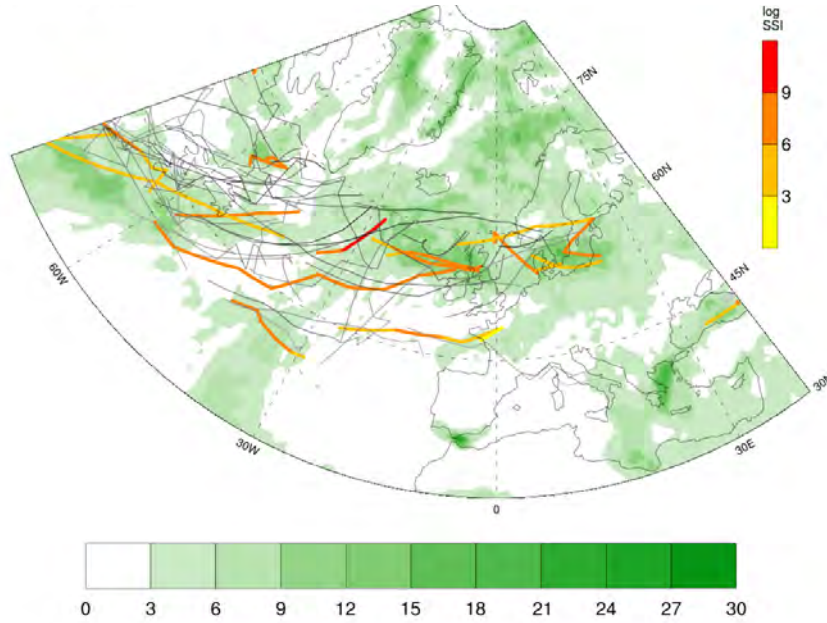


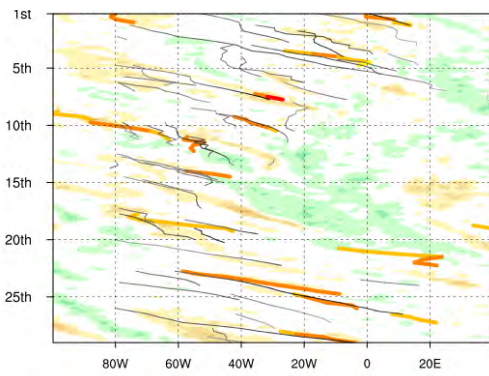
Figure 3.1: Cyclone (black line) and wind storm tracks (coloured line) in January 2007 (a-e). The darker the colour the lower the pressure for cyclone tracks. Colours in top right colour bar indicate severity of storm according to the SSI. (a) Monthly sum of exceedances of 98th percentile of 10m wind speed in green. (b-e) Hovmoeller diagrams for meridional mean (40° to 60° N) of normalised tropospheric growth factors (in standard deviations). Time dimension from top to bottom.

February 2008

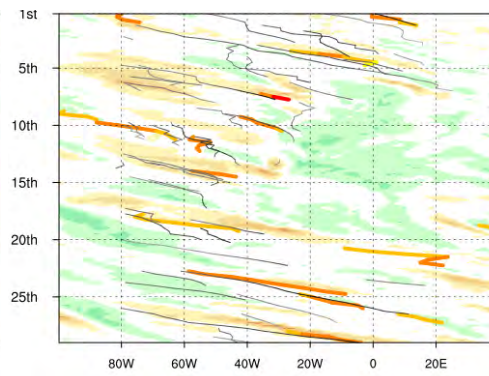
(a) Exceedances of 98th percentile in 10m wind speeds



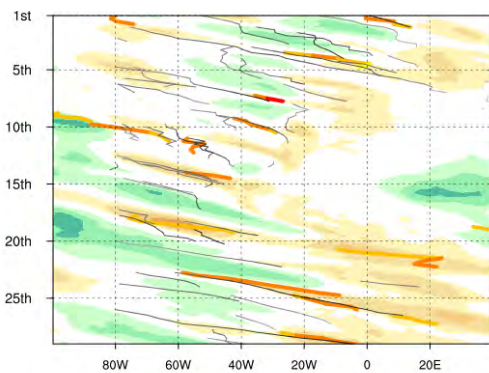
(b) Eady Growth Rate between 850hPa and 700hPa



(c) Eady Growth Rate between 500hPa and 200hPa



(d) Equivalent Potential Temperature in 850hPa



(e) Divergence from 500hPa to 200hPa

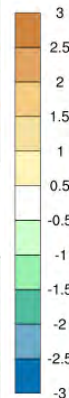
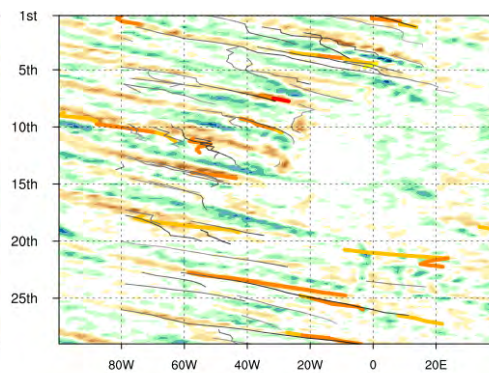
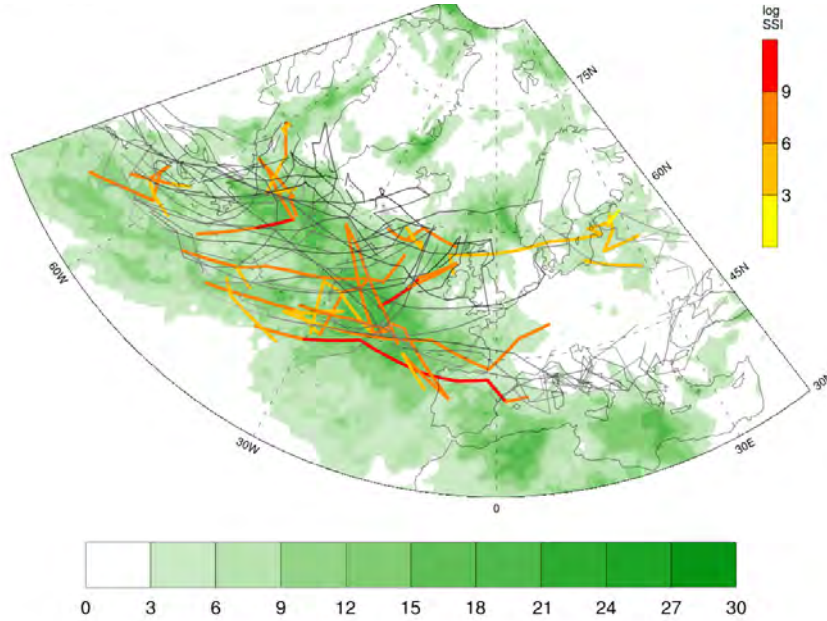


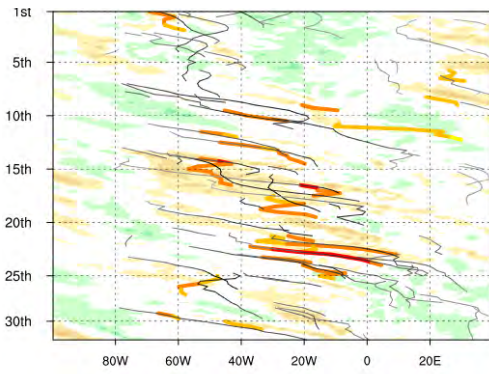
Figure 3.2: same as Figure 3.1 for February 2008

January 2009

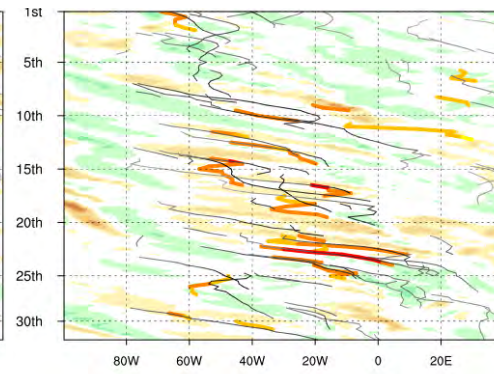
(a) Exceedances of 98th percentile in 10m wind speeds



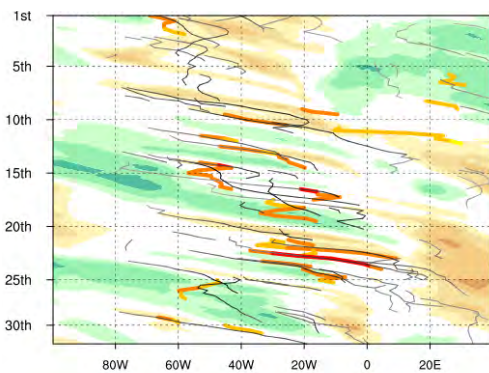
(b) Eady Growth Rate between 850hPa and 700hPa



(c) Eady Growth Rate between 500hPa and 200hPa



(d) Equivalent Potential Temperature in 850hPa



(e) Divergence from 500hPa to 200hPa

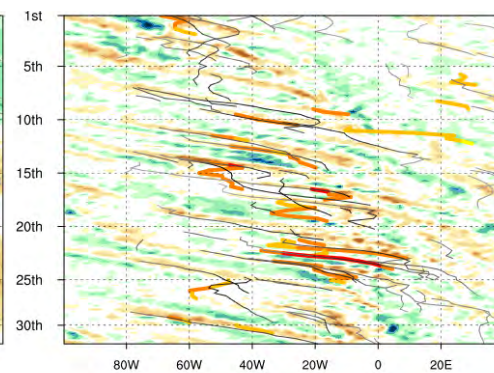


Figure 3.3: same as Figure 3.1 for January 2009

3.3 Composite Analyses for Extra-tropical Cyclones and Wind Storms

Different Composite Sets

The aim of the following part of this chapter is a systematic analysis of the synoptic scale differences of tropospheric growth factors for extra-tropical cyclones as discussed above (see also 2.3) with a composite analysis. The previous section showed that the magnitude but also the location of growth factors appear to be important. Different to previous studies with similar approaches (Dacre et al., 2012; Rudeva and Gulev, 2010; Hawcroft et al., 2017; Catto et al., 2009) the emphasis here is on **the difference of these growth factors between extra-tropical cyclones in general and those that can be classified as wind storms.**

Previous studies have either only looked at smaller subsets of cyclones defined by region or intensity or have not compared different sets of composites depending of the intensity of the extra-tropical cyclones. Additionally, the connection of extra-tropical cyclones to objectively defined wind storms has not been investigated with such a composite analysis. All investigated growth factors are again normalised according to 2.2.4.

Composites are created according to β_{comp} with respect to their time of strongest intensification, i.e. fall in pressure. $t = 0h$ is referred to in the following as the time with maximum intensification which means that the fall in pressure was greatest between $t = 0h$ and $t = 6h$. To be considered for the composites the cyclones have to further fulfil the following criteria:

- Track Point after greatest reduction in core pressure in extended winter season from October until March
- Lifetime at least 24 hours before and after time of strongest intensification
- Pressure at least once below 1000hPa
- Track point after greatest reduction in core pressure over the North Atlantic / European region (90°W-40°E; 40-70°N)
- Tracks with track points *only* in the Mediterranean region are excluded (0°-40°W; 45°N)
- Each cyclone is only selected once

The selected region corresponds in longitudinal extent to the region in which the NAO is usually defined (Hurrell, 1995). With these criteria about 3610 cyclone events are selected corresponding to just over 100 events per winter. The actual number of cyclones in the outlined region totals to more than twice as many without the temporal selection criteria. This apparently harsh criterion remains however justified in order to investigate the temporal behaviour before and after the point of greatest reduction in pressure. As outlined, temporally, the composites are performed with respect to the point of greatest reduction in pressure. Spatially, the composites are centred on the location of the surface pressure minimum of the cyclone. The 2D surface fields of the investigated variables on Gaussian grids have to be transformed otherwise distortions or spatial biases would be introduced when averaging the fields (Bengtsson et al., 2007; Bengtsson et al., 2009; Catto et al., 2009). In regional climate modelling it is a common procedure to rotate spherical coordinates (Kotlarski et al., 2014). This method is also applied here for the composite analysis. The new centre of each cyclone is then located at 0°N; 0°E. Similar to (Bengtsson et al., 2007), this newly obtained grid, centred at 0°N; 0°E, is subsequently bilinearly interpolated onto a regular, equidistant longitude

– latitude grid with 0.75° spatial resolution. Unlike (Bengtsson et al., 2007; Catto et al., 2009; Dacre et al., 2012; Rudeva and Gulev, 2010) the fields are NOT rotated according to direction of travel of the ETC. The composites are calculated with equal weights. The analyses are carried out for four different composite event sets:

- All cyclones, 3610 events, $p > 1000\text{hPa}$
- Strong cyclones, 489 events $p < 960\text{hPa}$
- All cyclones with matching wind storm, 1115 events, $\text{SSI} > 0$
- Strongest wind storms, 52 events, $\text{SSI} > 30$

The strong cyclone group is defined with respect to the minimum core pressure in the cyclone’s lifetime and represents about 5% of all cyclones in the outlined North Atlantic/European region. The threshold of 960hPa is chosen as it is close to the exact value of 958.9hPa for the top 5% with respect to core pressure and has been used in previous studies (see appendix or Befort et al., 2016, respectively). The association of ETC and wind storm follows 2.2.2. The overlap of strong cyclones and wind storms is quite high with 411 of the 489 strong cyclone events are also wind storm events. However of the strongest wind storms only 20 out of the 52 have a core pressure below 960hPa. The choice of grouping the strongest 52 wind storm events results out of a compromise between having enough events for the following statistical analyses, a round SSI threshold and only selecting the high-impact, socio-economically relevant wind storms.

Composites for All Cyclones

The composite analysis corroborate results from previous composite studies (e.g. Dacre et al., 2012) but extends them by the addition of the baroclinicity composites and a cyclone intensity differentiation. The composites here are centred around the time of the maximum intensification which leads to a time shift of about 12h when compared to composites of previous studies centred around the time of maximum intensity. All of the following analyses were also carried out for composites centred around the time of maximum intensity but besides the mentioned 12h shift the differences are only marginal and therefore not shown here. Note that the composites show not the entire life cycle of extra-tropical cyclones as they only span 48h. Some main features during the development of extra-tropical cyclones become however obvious. For the interpretation of these composites it is worth keeping in mind that Northern Atlantic cyclones propagate in a north-easterly direction on average. At 24h before the time of maximum intensification the former diminutive wave and then frontal wave has already developed into a frontal wave cyclone (see Hewson and Titley, (2010) for life cycle stages of extra-tropical cyclones). During the course of the shown 48h the composites show the transformation into a mature cyclone and early signs of cyclone decay.

Lower Troposphere:

In the Θ_E composites the lower-level temperature wave becomes obvious as it divides the composite in a north-western part with negative anomalies and south-eastern part with positive anomalies (Fig. 3.4). These positive anomalies form the warm sector with the warm and cold front on either end. This wave and the fronts are also apparent in the composite for σ_{BI} between 850 and 700hPa with a bean shaped maximum just north of the cyclone centre (Fig. 3.5). As the cyclone develops the surface wave becomes more prominent and the warm sector reduces in size as the

Equivalent Potential Temperature in 850hPa

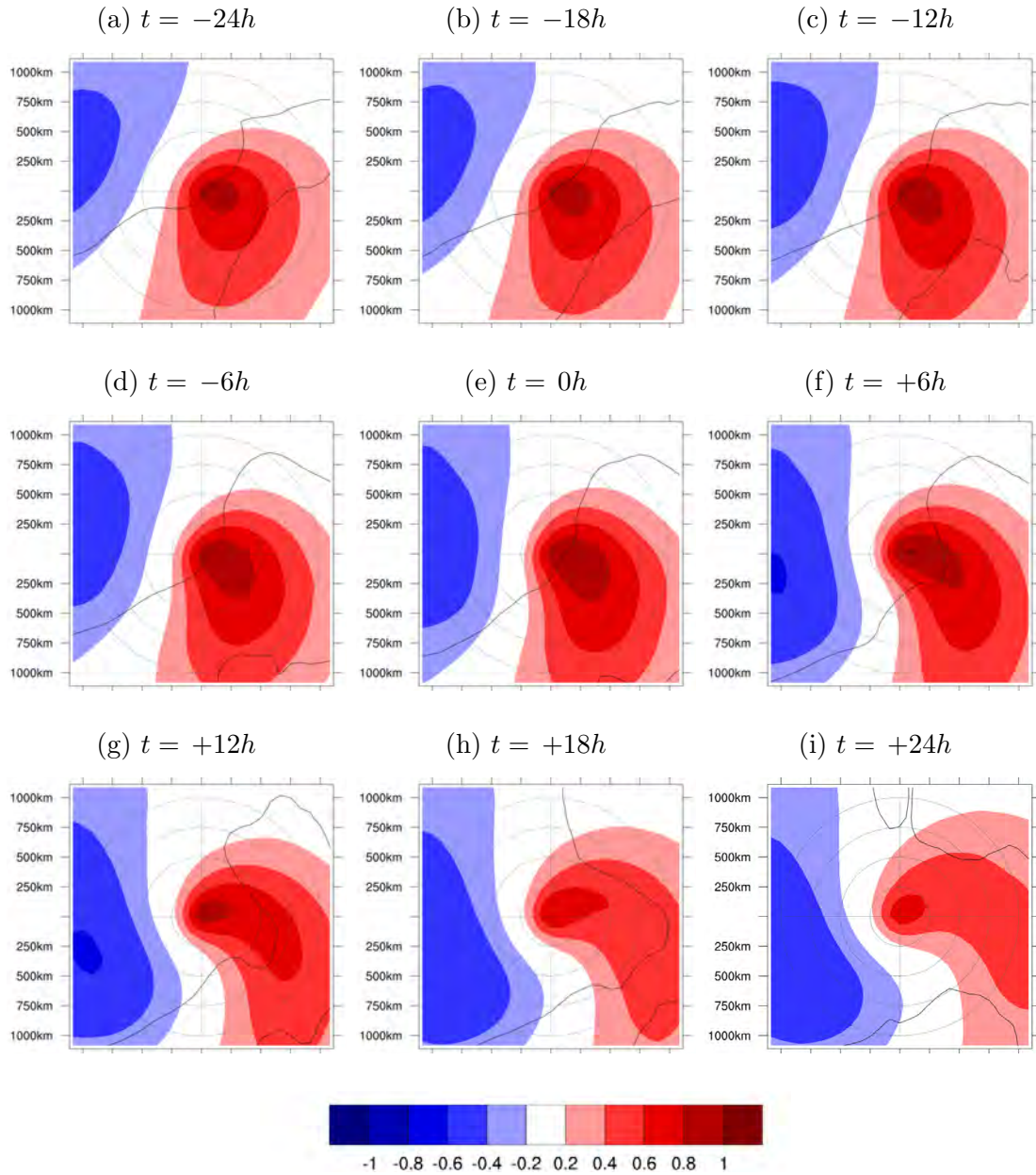


Figure 3.4: Composites for Equivalent Potential Temperature (Θ_E) in 850hPa for all Northern Atlantic cyclones with core pressure below 1000hPa in interannual standard deviation units. Composites are built with respect to strongest pressure fall of the cyclone ($t=0h$). Black lines denote standard deviation across composite (most prominent line: $sd=1$; increment:0.2).

Maximum Eady growth rate between 850 and 700hPa

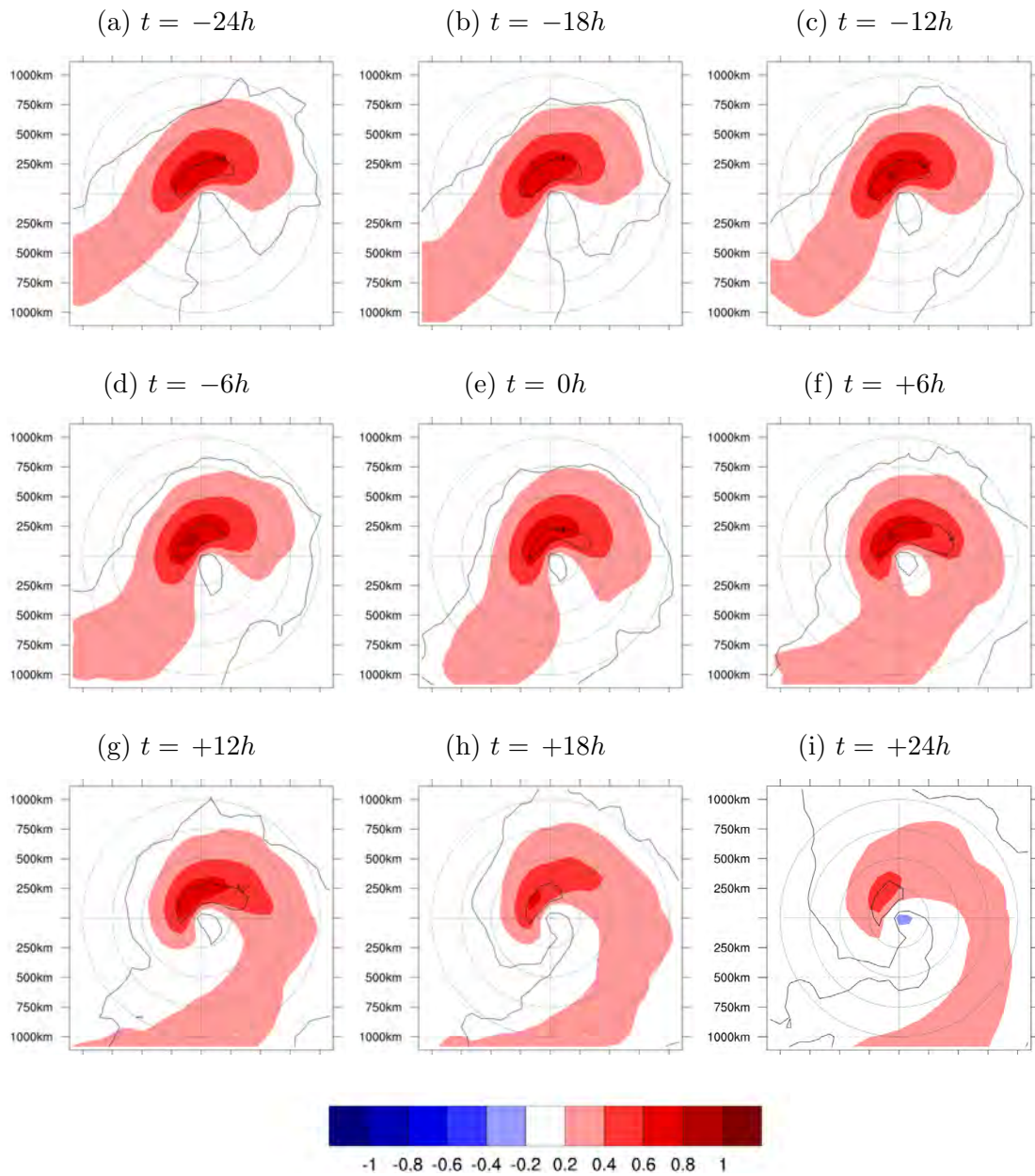


Figure 3.5: Composites for maximum Eady growth rate (σ_{BI}) in lower troposphere for all Northern Atlantic cyclones with core pressure below 1000hPa in interannual standard deviation units. Composites are built with respect to strongest pressure fall of the cyclone ($t=0h$). Black lines denote standard deviation across composite (most prominent line: $sd=1$; increment:0.2).

Maximum Eady growth rate between 500 and 300hPa

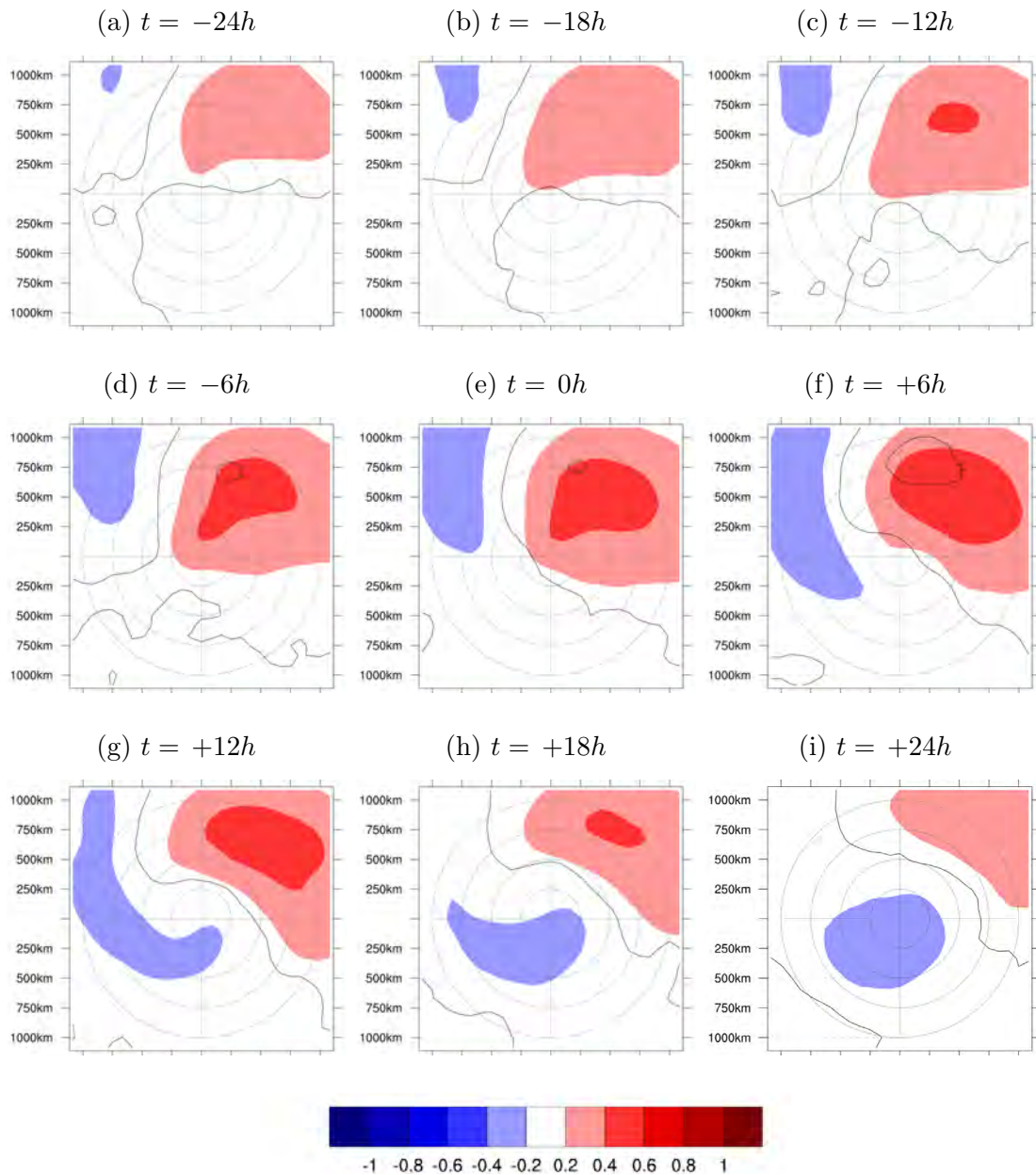


Figure 3.6: Composites for maximum Eady growth rate (σ_{BI}) in upper troposphere for all Northern Atlantic cyclones with core pressure below 1000hPa in interannual standard deviation units. Composites are built with respect to strongest pressure fall of the cyclone ($t=0h$). Black lines denote standard deviation across composite (most prominent line: $sd=1$; increment: 0.2).

Divergence between 500 and 200hPa

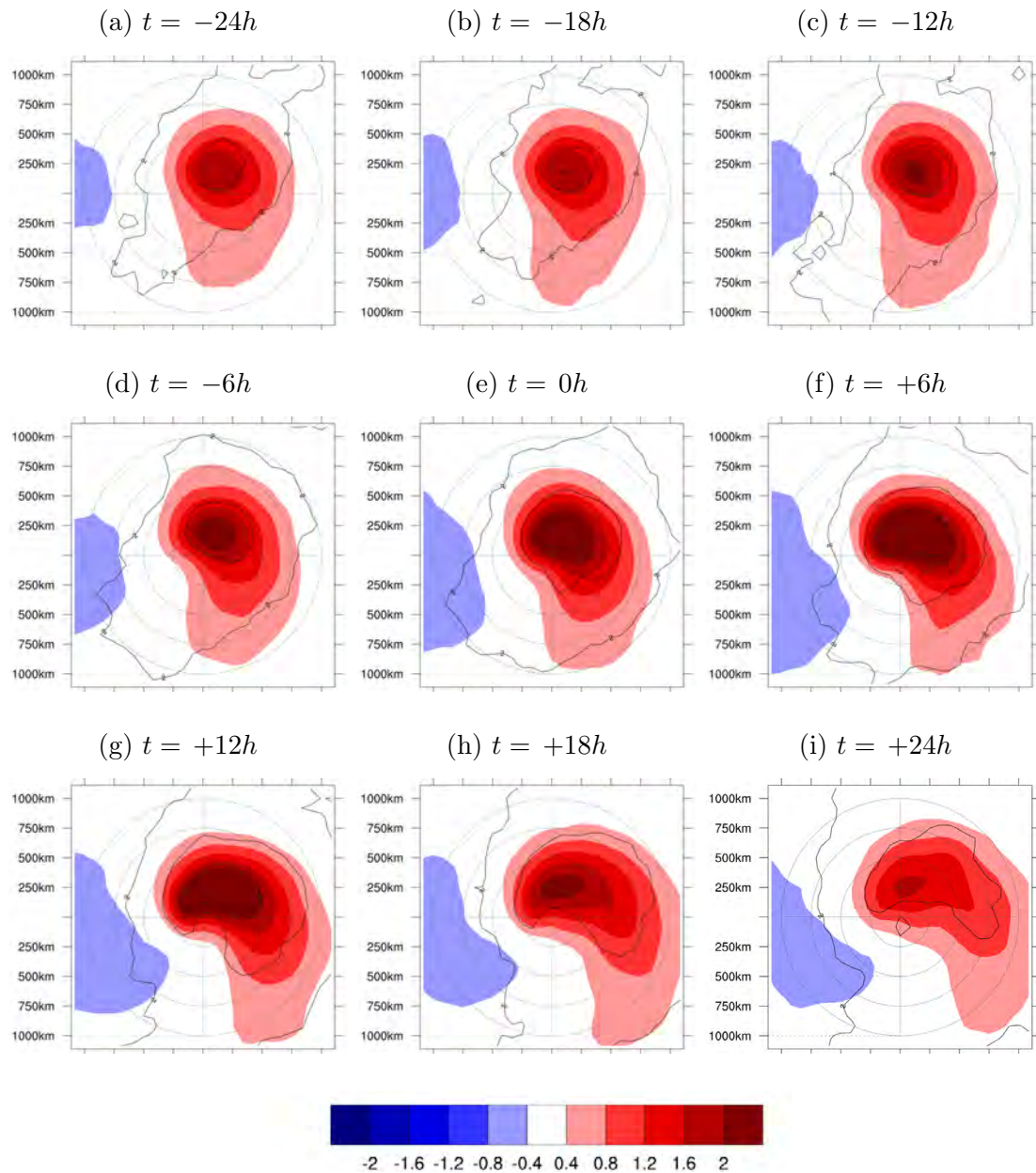


Figure 3.7: Composites for Divergence between 500hPa and 200hPa for all Northern Atlantic cyclones with core pressure below 1000hPa in interannual standard deviation units. Composites are built with respect to strongest pressure fall of the cyclone ($t=0h$). Black lines denote standard deviation across composite (most prominent line: $sd=2$; increment: 0.4).

cold front catches up with the warm front. The average magnitude of Θ_E and low-level baroclinicity remains similar during the shown 48h of the cyclone life cycle while the maximum for Θ_E is reached just after - for σ_{BI} just before the time of maximum intensification. The uncertainty of the composites is however high as the magnitude of the standard deviation across all events is in the order or greater than the mean. This remains true for basically all composites. The low-level composites also illustrate the anti-clockwise rotation of the cyclone.

Upper Troposphere:

In the upper troposphere the baroclinicity appears to be highest slightly upstream of the surface pressure minimum. The cyclone centre, or the area with a pressure minimum, is tilted with height towards the west (Kurz, 1990), this maximum of baroclinicity is therefore clearly upstream of the cyclone centre. During the cyclone development the upper-level baroclinicity intensifies with the maximum around the time of maximum cyclone intensification (Fig. 3.6). After this stage the upper-level baroclinicity weakens until the cyclone enters its barotropic phase, indicated by the negative anomalies that start to appear around 6h after the time of maximum intensification. (Fig. 3.6). Upper tropospheric divergence shows the strongest anomalies of the four analysed quantities (Fig. 3.7). Highest positive anomalies could be described as hook-shaped and are located in a similar area as upper tropospheric baroclinicity anomalies. In this area the warm conveyor belt, slightly upstream of the centre of the surface cyclone, changes direction from a more south-north propagation to either an east- or westward direction. The strongest anomalies in divergence also occur just after the time of maximum intensification. Behind the cyclone centre is a region of negative anomalies (i.e. convergence) that moves more and more over the area of the surface cyclone centre during the course of the shown 48h.

Comparison of different Composite Sets

The comparison of the **spatial distribution** across the different sets of composites reveals only minor structural differences between all cyclones, strong cyclones and all wind storms for all analysed variables (compare Figs. 3.6 to 3.7 with Figs. 3.10 to 3.11). There is an indication in the Θ_E and the upper tropospheric divergence composites of greater anti-clockwise rotation around the cyclone centre.

The patterns change somewhat when only the strongest storms are considered. Due to the decreased sample size the spatial distribution is noisier and the standard deviation across the events is higher. In the lower troposphere there is no qualitative difference in distribution when comparing composite sets. For the two upper-tropospheric variables the centre of highest activity is moved slightly westwards and located directly north of the cyclone centre.

The comparison of the **intensity** across the different composite sets shows however clear differences. All variables show an increase of positive anomalies when all cyclones are compared to the strongest 5% cyclones and wind storms. In the lower troposphere Θ_E increases of up to 50% in the area of maximum intensity when compared to strong cyclones or all wind storms (compare Fig. 3.4 and Fig. 3.8). This number increases to around 100% for the strongest wind storms. The greatest increase occurs at the time of maximum intensification of the cyclone and shortly after. The negative anomalies west of the cyclone centre for Θ_E decrease but not as strong in magnitude.

The differences in baroclinicity, both in the upper and lower troposphere and upper tropospheric divergence are even greater. There is an increase of about 100% primarily before the time of maximum intensification (compare e.g. Fig. 3.6 and Fig. 3.10). This difference becomes already obvious 24 hours before the maximum intensification. The strongest storms show an even greater increase when compared to all cyclones also for baroclinicity and upper-tropospheric divergence, albeit to

Equivalent Potential Temperature in 850hPa

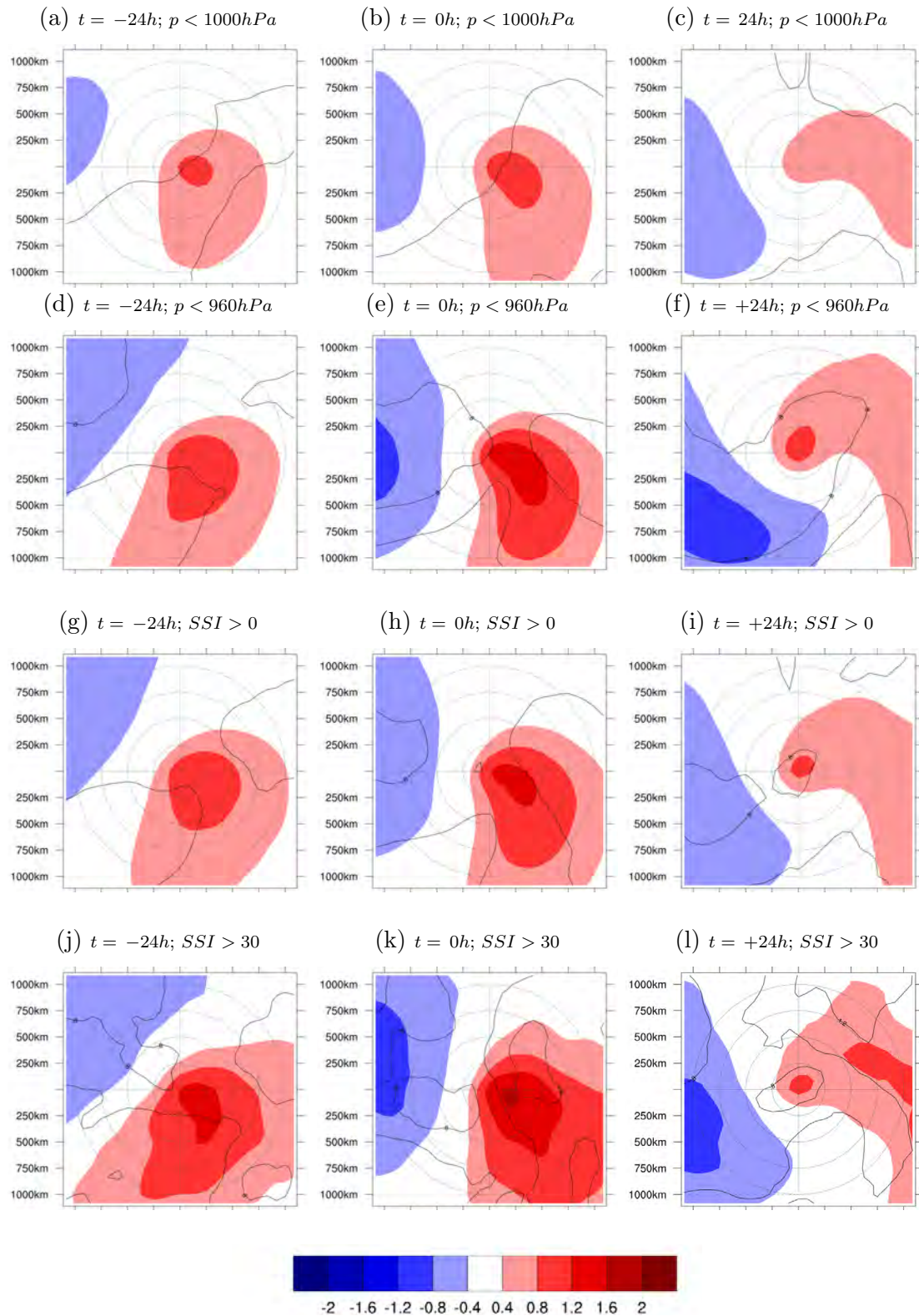


Figure 3.8: as figure 3.4 for all four composite sets.

Maximum Eady growth rate between 850 and 700hPa

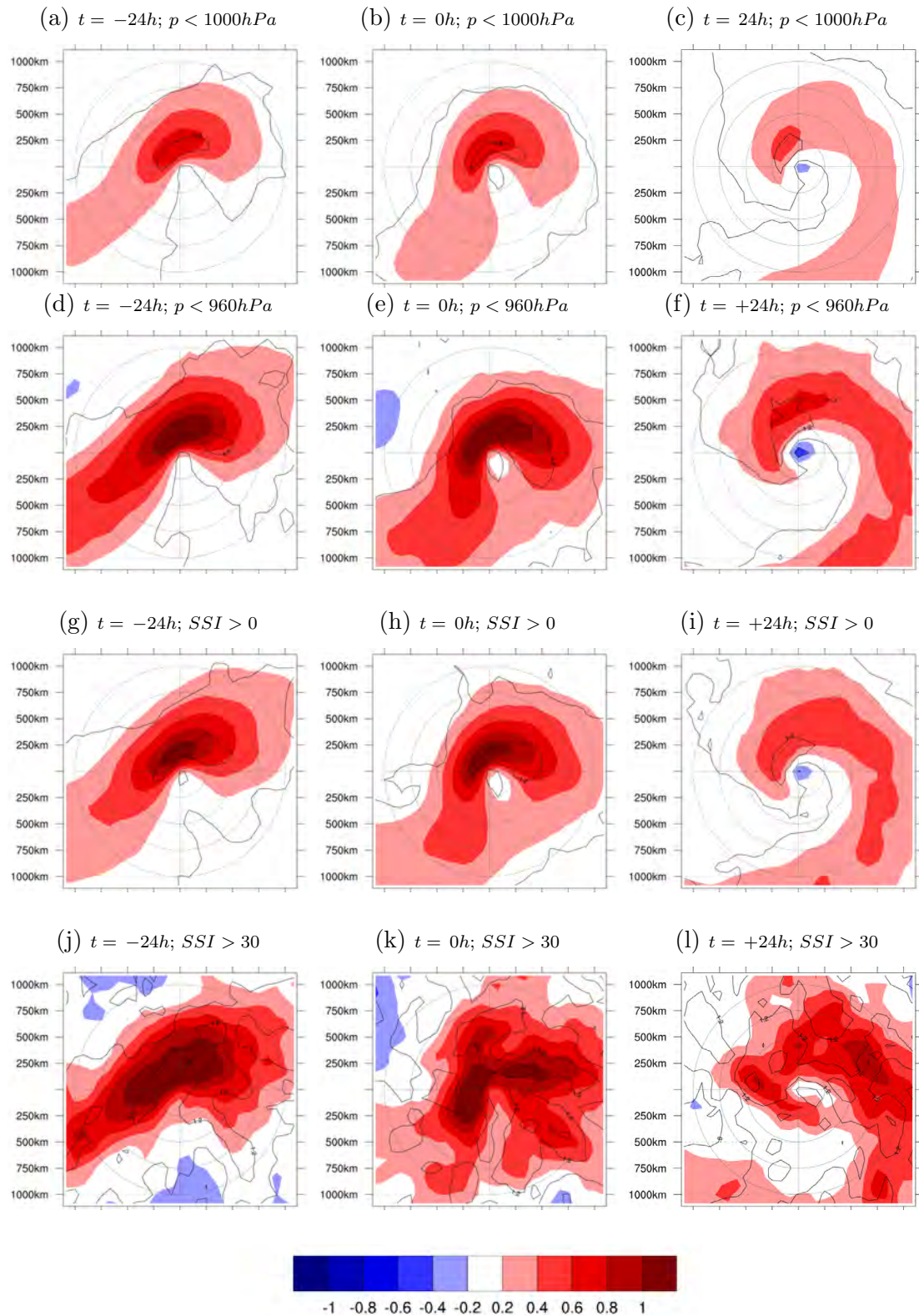


Figure 3.9: as figure 3.5 for all four composite sets.

Maximum Eady growth rate between 500 and 300hPa

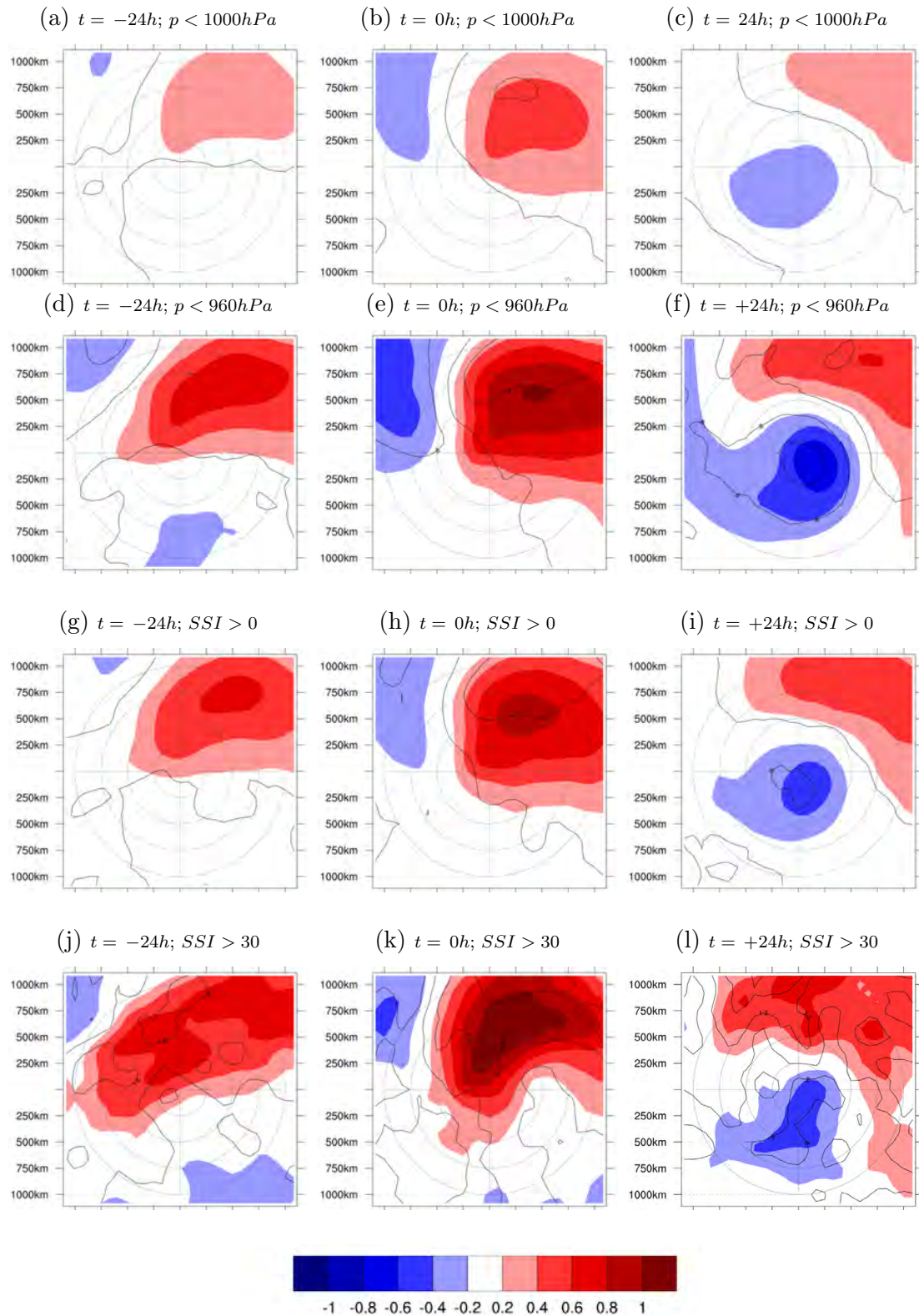


Figure 3.10: as figure 3.6 for all four composite sets.

Divergence between 500 and 200hPa

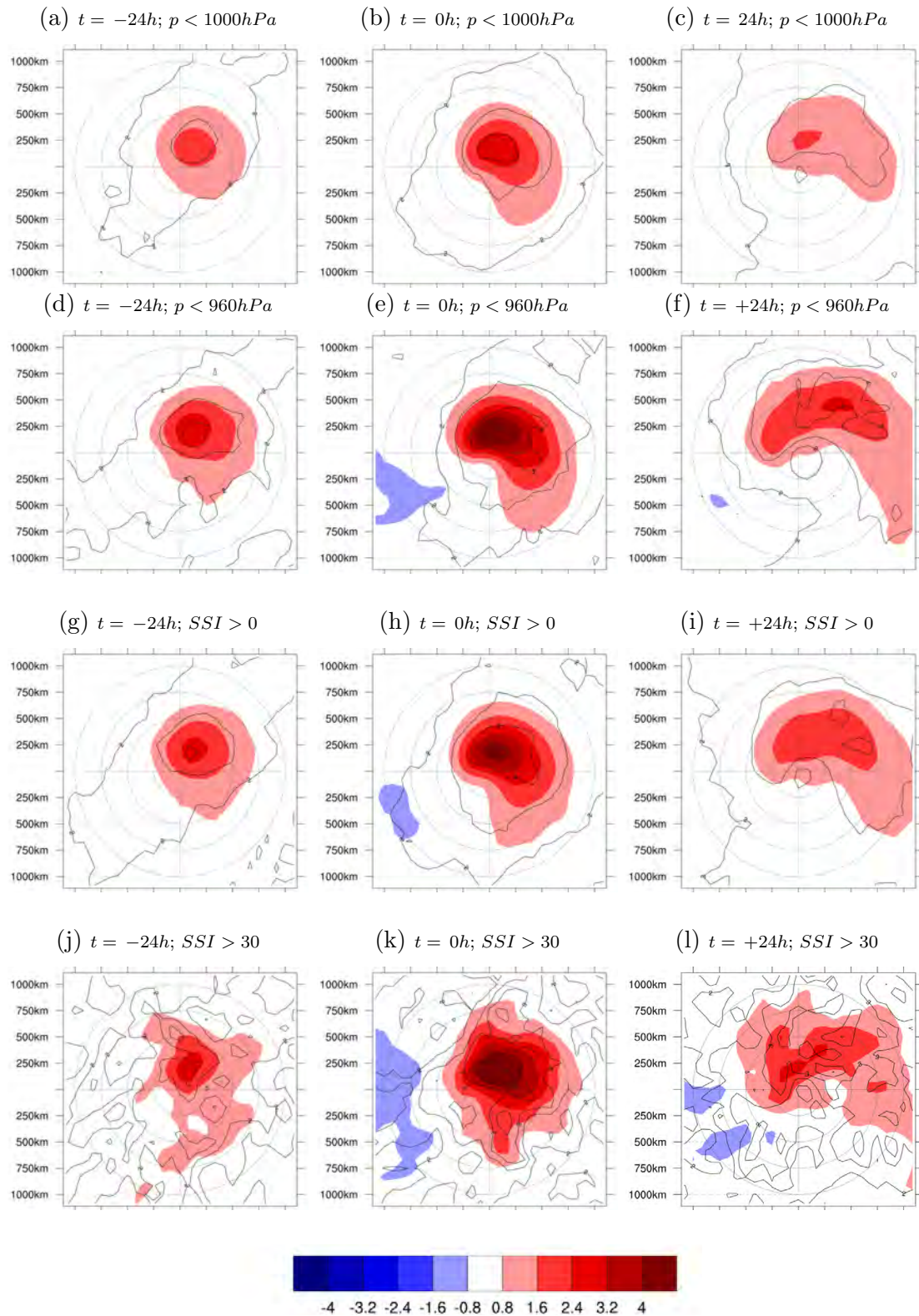


Figure 3.11: as figure 3.7 for all four composite sets.

only a relatively small region around the cyclone centre.

The composites of the strongest 5% cyclones and all wind storms generally agree to a large extent both in magnitude and spatial distributions.

3.4 Event to Event Variability

The primary goal of such composite analyses is to group events or entities to find general characteristics of the event set. Previous studies (Catto et al., 2009; Dacre et al., 2012; Rudeva and Gulev, 2010) about the characteristics of extra-tropical cyclones and/or wind storms operate along these lines by investigating the average and possibly its range for different variables associated with the selected events. The previous paragraph outlines some similarities and differences of mean cyclone characteristics between the chosen event sets. Following one overarching goal of the thesis (see section 1.5) the reasons for differences (or lack thereof) in the composites need to be looked at in more detail. It is therefore the variability of composites that is also investigated here. There has so far not been a study about the temporal or spatial variability of composites of extra-tropical cyclones. For each of the event sets a principle component analysis is carried out as described in 2.2.7. The structures in each EOF give the amplitudes of the original normalised fields in standard deviation units. Each principle component represents one cyclone or wind event. The EOF loadings for this PCA are shown in figures 3.12 to 3.15 for the time of maximum cyclone intensification. There is no substantial difference in EOF loadings between the three different points in time of the cyclone life cycle, that is why only on one of them is shown here.

The first EOF over the Θ_E composites represents the large scale conditions, as to whether latent heat is generally available or not. With a relative high explained variability of above 30% this shows that ETCs with associated wind storms can develop either with or without latent heat (release). The 2nd and 3rd Θ_E EOF

represent the synoptic scale. The highest variability in the 2nd EOF is associated with the cold front and in the 3rd EOF with the warm front at the surface. As Θ_E is general highest in between the fronts in the warm air sector, the position of the fronts determines where high or low Θ_E values are located with respect to the cyclone centre.

The EOF analysis for the other growth factors does not reveal such a variability of the large scale conditions between events. The most dominant variability pattern, i.e. EOF1, generally resembles the composite. This means that variability scales with magnitude which the standard deviation in the composites also suggests. The total explained variability for the first three EOFs for baroclinicity in the upper and lower troposphere, and for upper-tropospheric divergence is also significantly reduced when compared to Θ_E . EOF 2 and 3 for upper-tropospheric divergence are even degenerated (North et al., 1982) which disallows any interpretation (see 2.2.7).

With these potential caveats in mind, the EOFs still reveal some interesting insights into the variation of wind storm events. The 2nd EOF for σ_{BI} in the lower troposphere is very similar in shape to the 1st EOF for σ_{BI} in the upper troposphere but with different explained variability. This means that while upper level baroclinicity is linked to lower level baroclinicity, a variation in the one is not necessarily associated with a variation in the other. The 2nd EOF in upper level baroclinicity shows some event to event variations to the east of the cyclone centre. Upper-tropospheric divergence shows the greatest variability in magnitude between events.

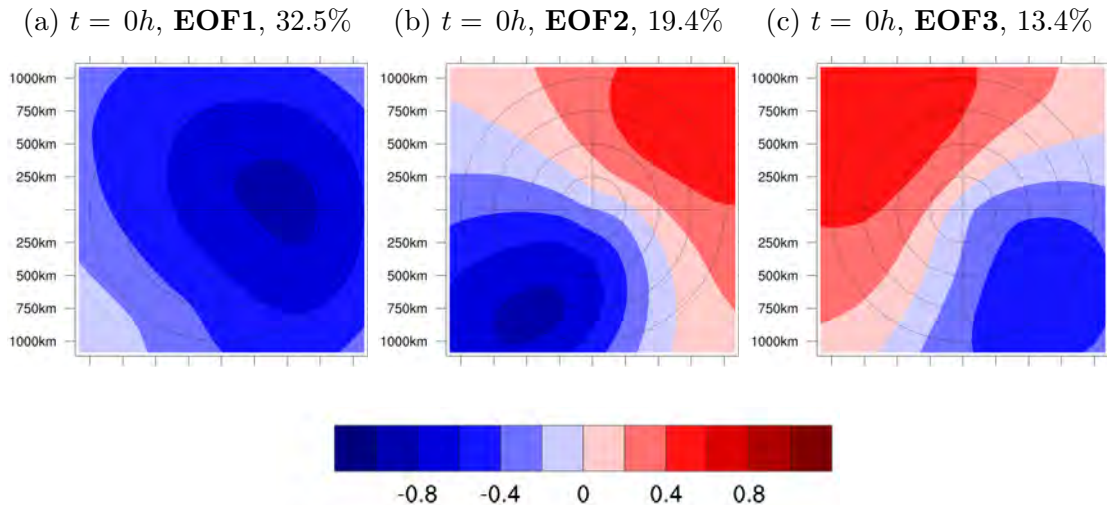


Figure 3.12: EOF loadings for equivalent potential temperature in 850hPa (Θ_E) composites in interannual standard deviation units associated with one standard deviation of the respective principle component. Shown is the time of maximum intensification of the cyclone. The part of the variance that is explained by each EOF is given in the right top corner.

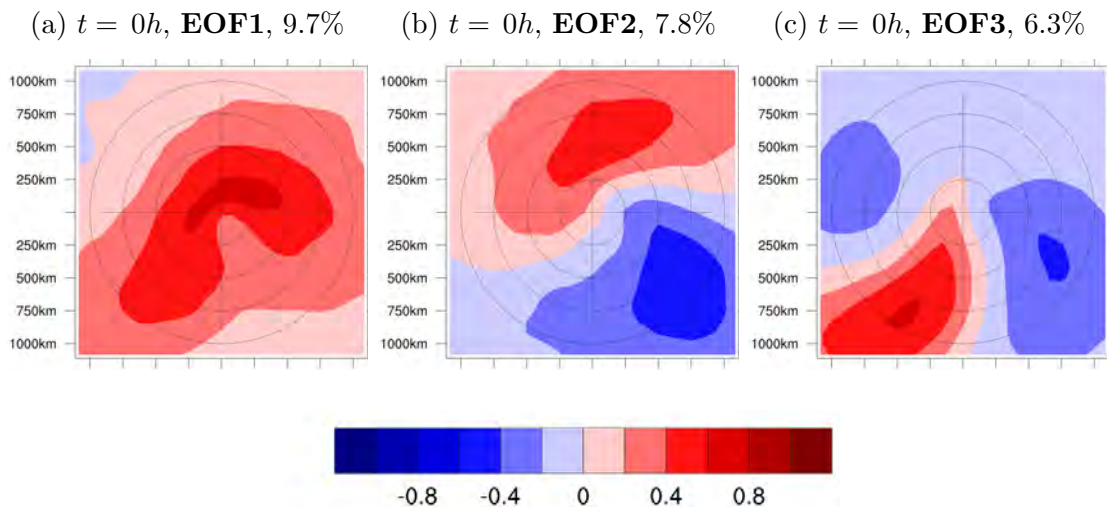


Figure 3.13: As Figure 3.12 for lower tropospheric maximum Eady growth rates (σ_{BI} , between 850 and 700hPa).

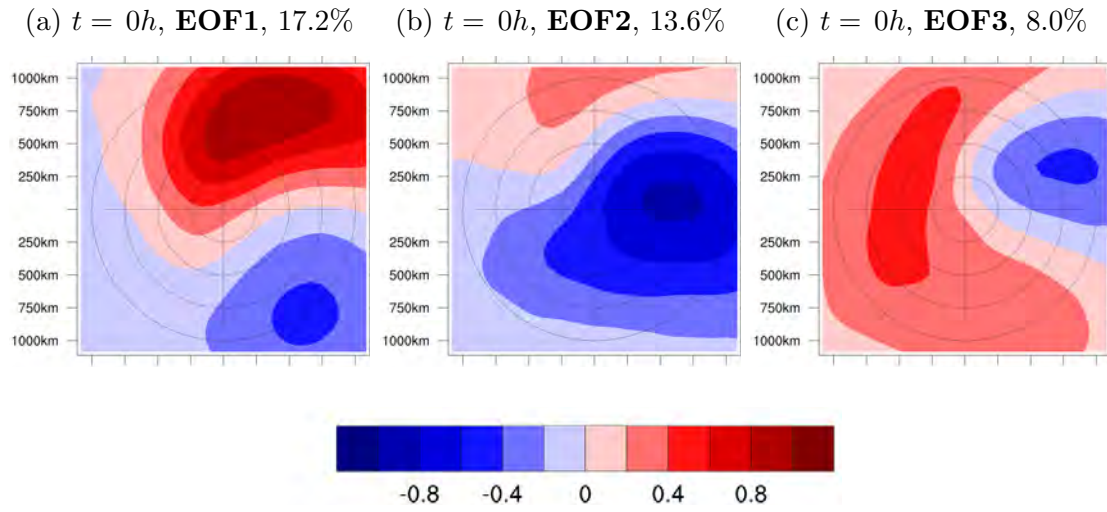


Figure 3.14: As Figure 3.12 for upper tropospheric maximum Eady growth rates (σ_{BI} , between 500 and 300hPa).

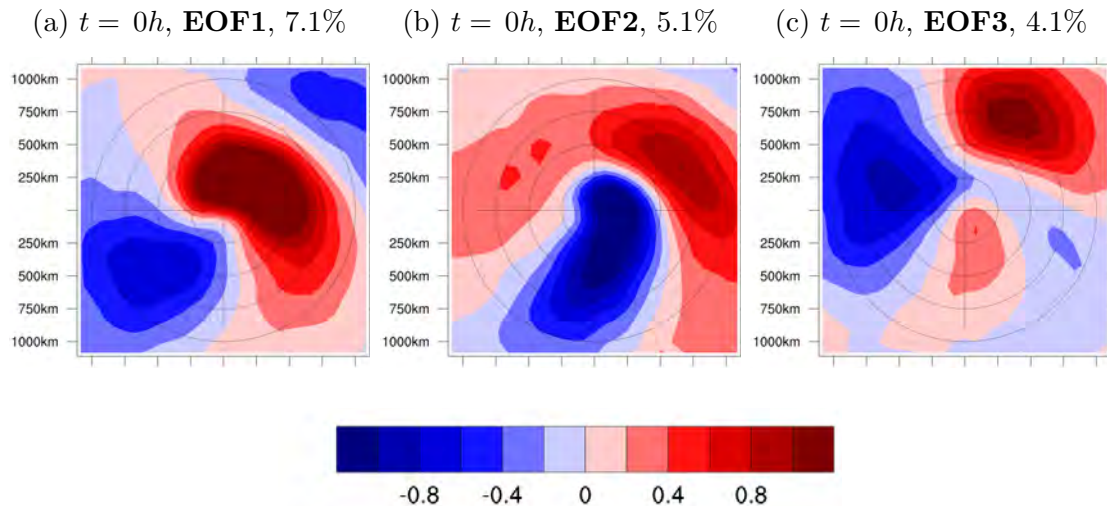


Figure 3.15: As Figure 3.12 for upper tropospheric divergence (between 500hPa and 200hPa).

3.5 Principle Component Selection

In order to reveal which of these variability pattern, i.e. EOF loadings, is more important for stronger cyclones or wind storms the distribution of principle component values for the dates with strong cyclones or wind storms are analysed. The relation between the NAO and wind storms is taken as an example to demonstrate how this new method works: Assume a PCA for monthly MSLP over the North Atlantic is carried out. The first EOF will be the NAO. All PC values are divided by their standard deviation so that and the distribution of PC values has a mean of 0 and standard deviation of 1. In a next step only PC values of months that show high wind storm frequency are selected from this distribution. These selected PC values are likely to be greater than 0 (i.e. NAO positive) as there is a positive correlation between NAO and wind storm frequency. The distribution of the selected PC values has thus a mean of greater than 0. Assume the relation between NAO and wind storm frequency is not known a priori, this method could help to identify this link by comparing the distributions of all PC values and only wind storm PC values. The newly selected set of PC values would not fulfil the synthesis equation (see Equation 2.8 in 2.2.7) but could show systematic shifts in favour of one or more EOFs.

The advantage of this way instead of a PCA for only months with strong wind storm frequency is the conservation of the order of EOFs, e.g. EOF 1 stays EOF 1. If a PCA is carried out for a smaller sample size and there is a systematic shift of variability patterns compared to the bigger sample size, the order of EOFs is likely to change.

This method is now applied to the PC values of the PCA above and the newly generated distributions of PC values for strong cyclones and wind storms are compared to the original PC distribution with a mean of 0 and standard deviation of 1. The distributions are statistically compared with a Student's t-test with the

null hypothesis that the means are the same.

Results for the newly obtained distribution of this PC selection method are shown as box-whisker plots in figure 3.16 for all growth factors. The large scale availability (or the lack thereof) for Θ_E does not seem to change in frequency for strong cyclones or wind storms as there is no significant shift in the distributions for PC 1 (Figs. 3.16a-c). EOF 2 for Θ_E , that is mainly related to the position of the cold front, shows a tendency of enhanced frequency for strong cyclones and all wind events 24 hours prior to the maximum intensification. The 2nd EOF loading is negative around the cold front, meaning that increased frequency relates to decreased Θ_E values. 24 hours after the maximum intensification the picture is reversed. For the 3rd EOF, that is associated with Θ_E in the warm air sector, shows decreased PC values for strong cyclones and wind storms. This means increase latent heat as the EOF loading is negative in this region.

The event to event variability of lower level baroclinicity is greater for stronger cyclones and wind storms than for all cyclones during maximum intensification in the region where the baroclinicity is greatest (Figs. 3.16d-f). 24 hours either side the event to event variability is reduced in this region. This means that low level baroclinicity and intensification of the cyclone are strongly linked in time around the cyclone centre.

The first EOF loadings for upper level baroclinicity and divergence show increased frequency 24 hours before and at the time of maximum intensification and decreased frequency 24 hours after (Figs. 3.16g-l). As these variability patterns are closely related to the general composites, these findings corroborate the results from section 3.3.3. At the time of maximum intensification the upper troposphere σ_{BI} PC values for the 2nd EOF show decreased frequency for strong cyclones and all wind storms, but increased frequency for strong wind storms albeit not significant. The third EOF of upper tropospheric baroclinicity, related to event to event variability of

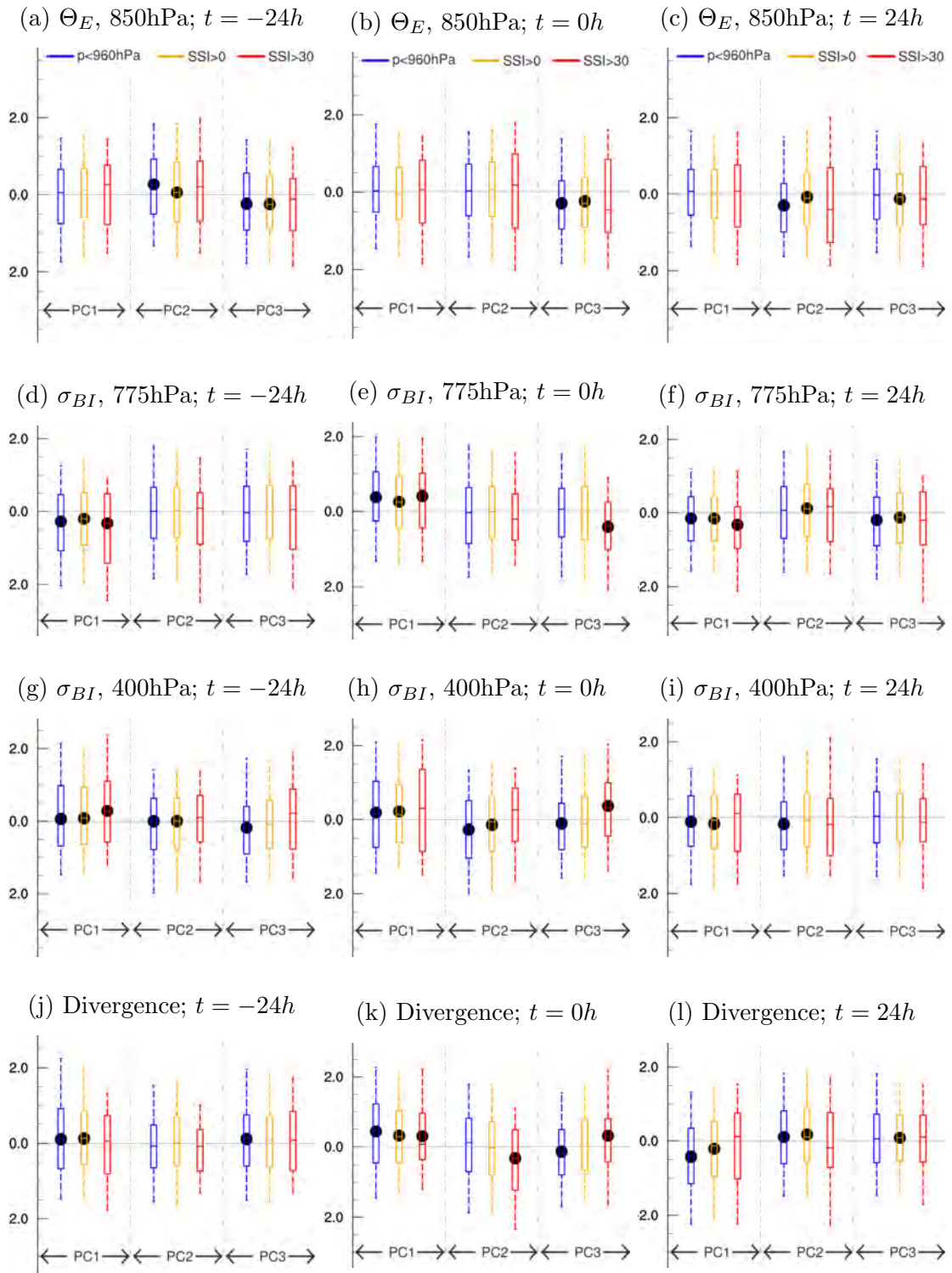


Figure 3.16: Box-whisker diagram for selected PC values of first three EOFs. PC values for each event are taken from all cyclones event set and sampled if event is also part of other event set (see colours in (a)-(c)). Central line represents median, box limits correspond to lower and upper quartile and whiskers show 5th and 95th percentile. Black dot (at mean position) indicates statistical significant difference in mean to PC value distribution of all cyclones.

baroclinicity just west of the cyclone centre, shows a statistical significant increase in importance for strong wind storms. In the composite analysis this region does not show any significant anomalies. It could be that in this region σ_{BI} is in very few cases greatly increased, e.g. in strong wind storms. The maximum Eady growth rate includes the static stability of the atmosphere (see also 2.3.2). In strong wind storms this static stability can be decreased dramatically just west of the cyclone centre when a sting jet occurs (Gray et al., 2011).

3.6 Summary and Discussion

This chapter aims to distinguish between atmospheric conditions on the **synoptic scale** that lead to mid-latitude winter wind storms and those that lead to “just” an average extra-tropical cyclone. These atmospheric conditions or cyclone growth factors analysed here are the maximum Eady growth rate σ_{BI} in the upper and lower troposphere as a measure for baroclinicity, equivalent potential temperature in 850hPa Θ_E as a measure for latent and sensible heat availability and the vertical sum of upper tropospheric divergence between 500 and 200hPa. These factors have been shown to be of crucial importance for the development and intensification of wind storms (Ulbrich et al., 2001; Pinto et al., 2009; Fink et al., 2009; Fink et al., 2012; Pirret et al., 2017; Liberato et al., 2011; Liberato, 2014).

The main result of this chapter corroborates these previous studies as strong-extra tropical cyclones and wind storm composites show higher magnitudes than all cyclones. A major new finding of this work is the similarity of the spatial structure between the different analysed samples. The climatological spatial distribution around the cyclone centre is *not* dependent on core pressure or associated wind speeds of an extra-tropical cyclone. This remains true for all investigated growth factors.

In their study about three winter storms in December 1999 Ulbrich et al., (2001)

find no major differences for σ_{BI} between the upper and lower troposphere. Pinto et al.,(2009, hereafter P09) relate σ_{BI} in the upper troposphere to deep cyclones while in other studies σ_{BI} in the lower troposphere is related to storm track activity (Hoskins and Valdes, 1990; Novak et al., 2014). There has not been a study systematically relating upper and lower level baroclinicity. This chapter shows that both are certainly linked but differ in structure and event to event variability in relation to wind storms.

The chosen method to compare all cyclones, stronger cyclones and wind storms is a composite analysis for four event sets. Results for deep cyclones (below 960hPa), which corresponds to about the strongest 5% and results for all wind storms are almost identical despite a sample size difference of a factor 2 in favour of wind storm events. There is however also a big overlap as almost all deep cyclones are also identified as a wind storm. The strongest wind storms ($SSI > 30$, 52 events) are selected with respect to the overall SSI over the lifetime of a storm (see also 2.2.3). Only 20 of these 52 events had a pressure below 960hPa. This discrepancy is either due to a mismatch between SSI and actual strength of the storm or an indication that strong wind storms are not necessarily events with the lowest pressure. The other 32 storms have likely existed relatively long, as the SSI accumulates over the life time of a storm. They might be also an example of inflated SSI values in regions with few storms or a low 98th wind speed percentile (Walz et al., 2017).

Composite analyses have been used in various previous studies about extra-tropical cyclones (Dacre et al., 2012; Catto et al., 2009; Pinto et al., 2009; Rudeva and Gulev, 2010; Bengtsson et al., 2009). The above analyses follow the composite procedure by Bengtsson et al., (2007) that was also used in some of these studies but do not include a rotation with respect to propagation direction of the cyclone. Such a rotation was also not applied in P09. Composite results for all cyclones in Θ_E and upper-tropospheric divergence are very similar to for example P09 or Dacre and Gray, (2012) if a rotational difference of about 45° is taken into account.

Although most of these studies focus on a subset of cyclones, either chosen by region or intensity, which corresponds to a much smaller number of events than in the all cyclones composite here (3610 compared to e.g. 50,200 or 567), the overall results remain qualitatively very similar.

There is however a difference for σ_{BI} in the upper troposphere in comparison to P09. The baroclinicity maximum here is located north-east of the cyclone centre at the time of maximum intensification, while in P09 the maximum is found around the cyclone centre. Their composite of *upper* tropospheric σ_{BI} for strong cyclones at the time of maximum intensification (their figure 11a) is very similar in shape to the composite of *lower* tropospheric σ_{BI} for strong cyclones 24h before the maximum intensification here. There is no obvious reason as to why such a difference is found. Potential reasons could include the different analysed data set (NCEP1 vs. ERA-Interim) and therefore also different time periods (1958-1998 vs. 1979-2013) or the different region (70°W–40°E, 30°–75°N vs 90°W–40°E 40–70°N). How the different underlying grids in the vicinity of the cyclone centres were transformed for the composites in P09 or whether a latitudinal dependency was taken into account remains unclear. P09 consider absolute exceedances of the local 95th percentile while here normalised values are used.

P09 is the only of the composite studies to also look at baroclinicity but only at the time of maximum cyclone intensification. The theoretical relation between baroclinicity and cyclones or wind storms (see 2.3.2) could be summarised as enhanced baroclinicity \rightarrow ETC \rightarrow mixing of the atmosphere \rightarrow reduced temperature gradient \rightarrow reduced baroclinicity (Hoskins and Valdes, 1990; Novak et al., 2014). The temporal evolution in the composites of baroclinicity in the upper troposphere (figure 3.6) follows this causal chain. Composites for lower level baroclinicity do however not show a substantial reduction of σ_{BI} for the analysed time period around the maximum intensification of the cyclone (figure 3.5). This could either mean that baroclinicity in the lower troposphere is generally reduced later than in the upper

troposphere during the life cycle of a cyclone or that other process such as latent heat release replenish baroclinicity in the lower troposphere fast enough that the theoretical reduction does not become obvious. This was likely the case for *Kyrill* in January 2007 when baroclinicity was still high after the passing of the storm (see figure 3.1) and could be generally the case for secondary cyclones that form in trailing cold fronts of the primary cyclone (Dacre and Gray, 2009).

Despite the differences of composite results for baroclinicity, one of the main conclusions from P09 is also found in this chapter: stronger cyclones show generally higher values of tropospheric growth factors. The composite analyses suggest, that Θ_E is increased by about half a standard deviation for strong cyclones and all wind storms and by about 1 standard deviation for strong wind storms (figure 3.8. σ_{BI} and divergence in the upper troposphere are increased by about 1 standard deviation already 24 hours before the time of maximum intensification. This is an indication that the growth factors are actually the cause for the pressure to fall (figures 3.10 and 3.11 This point is strengthened by the increased frequency of the EOF 1 (of the event to event PCA) for these two quantities that strongly relate to the general composites. The frequency of EOF 1 for σ_{BI} in the lower troposphere, which also strongly resembles the general composite, decreases before the time of maximum intensification and increases at $t = 0h$. The cause and effect relation is thus not as clear for lower level baroclinicity. From the composite analysis alone, there is no apparent difference whether upper or lower baroclinicity serves as a better precursor for strong cyclone or wind storm development.

The first event to event EOF for Θ_E with over 30% explained variability can be regarded as the large scale availability of latent heat (figure 3.12a). The position of the jet stream might thereby play an important role. Cyclones that stay longer on the southern side of the jet stream tend to be more likely driven by diabatic processes (Pirret et al., 2017).

The PC value distribution for this EOF does not change between all cyclones or

strong cyclones or cyclones with wind storms respectively (figure 3.16a-c). The relation between diabatic contributions for cyclone development due to the position of the jet does thus not change for strong cyclones or wind storms. The smaller scale relation of latent heat and cyclone structure seem to be more important especially before the time of maximum intensification (see EOF 2 3.12b and 3.16a). If latent heat is available and “accessible” in between the fronts of a cyclone, it can strongly intensify the storm. This might have been the case for winter storm *Klaus* in comparison to winter storm *Joris* (see figure 3.3) as discussed in section 3.2.

Extra-tropical cyclones have found to be more sensitive to diabatic processes in the eastern part of the North Atlantic (Dacre and Gray, 2009). Such differences are not possible to assess with the above analyses but with a pre-selection of cyclones as to where (east or west) they intensify, this composite-eof method could reveal further regional differences of the role of latent heat for cyclone development.

The PCA to investigate event to event variability generally leads to low explained variances per EOF with the exception of Θ_E . The interpretation of the EOFs for the other growth factors has to be therefore cautious. The PC-selection method as described in section 3.5 shows some interesting results as discussed above for Θ_E or the temporal shift of event-to-event variability pattern for σ_{BI} or upper tropospheric divergence. Despite a sometimes significant shift of the PC distributions, also these results have to be treated with caution. None of the box-whisker plots (figure 3.16) shows a very obvious and definite shift of the PC values to one or the other side.

The general idea of this eof-pc-selection method could proof useful for other applications in future, especially when the explained variability of the EOF loadings is higher than here. Staying with the previously introduced example of NAO and wind storm frequency: assuming a non-linear relation that wind storms only occur if the NAO has a value greater than 1 standard deviation. This method would lead to a clearly shifted distribution of PC values including the exact threshold of 1.

P09 found an influence of the NAO on the above atmospheric growth conditions.

There is therefore the remaining question in how far other variability modes, such as the East Atlantic Pattern, or further teleconnection patterns on different temporal or spatial scale could influence cyclone intensification on the synoptic scale. One potential steering mechanism for wind storm frequency on the **seasonal scale** is discussed in chapter 6.

**TROPOSPHERIC MID-LATITUDE
GEOPOTENTIAL WAVE CHARACTERISTICS
ASSOCIATED WITH STRONG WIND
EVENTS IN THE NORTH
ATLANTIC/EUROPEAN REGION**

4.1 Introduction

In recent years several studies have linked the frequency of Northern hemispheric weather extremes, mainly in temperature and precipitation, to high amplitude mid-latitude Rossby waves (Mann et al., 2017; Petoukhov et al., 2016; Kornhuber et al., 2017; Screen and Simmonds, 2014), both in summer and in winter. While the frequency of some extremes is likely to increase with global warming (IPCC, 2012; Coumou and Rahmstorf, 2012; Hoskins and Woollings, 2015) and thermodynamic effects through a change in the mean temperature are not sufficient to explain such an increase (Horton et al., 2015; Hoskins and Woollings, 2015), this has been linked to an increase in high amplitude wave activity (Francis and Vavrus, 2012; Tang et al., 2013; Petoukhov et al., 2013).

Rossby waves on a hemispheric scale have long been linked to variability modes such as the NAO (Hoskins and Karoly, 1981; Hoskins and Ambrizzi, 1993; Branstator, 2002; Scaife et al., 2017), which is strongly linked to meteorological extremes in

general and wind storm in particular (see 1.3.2). Waves with certain planetary wave numbers can be “trapped” in regions with strong jet activity and thus transport an anomaly signal over long distances (*ibid.*). The jet streams are stronger in the winter months giving such a proposed waveguide mechanism a greater likelihood. Many of the mentioned studies above analyse monthly or seasonal data (e.g. Branstator (2002), Scaife et al.,(2017), Screen and Simmonds, (2014)) and almost all of them look at hemispheric wave activity (Mann et al., 2017; Petoukhov et al., 2013; Kornhuber et al., 2017; Francis and Vavrus, 2012; Coumou and Rahmstorf, 2012; Screen and Simmonds, 2014). It has however been shown by Screen and Simmonds (2014) or Roethlisberger et al. (2016) that for some weather extremes regional differences have to be taken into account. For wind storms the synoptic scale is of crucial importance and the existence of shorter baroclinic waves (Ulbrich et al., 2001) as also seen in the previous chapter 3.

Most recent studies that linked mid-latitude planetary waves and strong wind events on the synoptic scale have focused on Rossby wave breaking especially for clustering of strong extra-tropical cyclones (Hanley and Caballero, 2012; Gómará, Rodríguez-Fonseca, Zurita-Gotor and Pinto, 2014; Pinto et al., 2014; Messori and Caballero, 2015; Priestley et al., 2017*a*; Priestley et al., 2017*b*). Rossby wave breaking has also been strongly linked to high-latitude blocking events (Woollings et al., 2008; Masato et al., 2012; Hoskins and Woollings, 2015; Michel et al., 2012), that lead to a reduction of wind storm frequency (Davini et al., 2012; Woollings et al., 2010; Woollings, 2010; Zappa et al., 2014). Blocking events show high amplitudes in mid-tropospheric planetary waves often associated with a negative phase of the NAO, they are likely to deflect the jet stream (Woollings et al., 2010), and prevent cyclones from travelling towards Europe (see also figure 3.2). Accordingly Roethlisberger et al. (2016) find a significant reduction in wind gust extremes when the jet stream shows enhanced waviness.

Such high amplitude waves over the North Atlantic can however also be related to

so-called strong and persistent ridge events (Santos et al., 2009). These events are strongly associated with anti-cyclonic Rossby wave breaking, a northward displacement of the jet stream and a positive phase of the NAO (Woollings et al., 2011). Such events *block* cyclones to reach southern Europe but could allow *more* cyclones to reach central and northern Europe. These events are in line with the studies about quasi-stationary Rossby waveguides above (e.g. Branstator, (2002)). Under the assumption that Rossby or planetary waves have to grow in amplitude first before they can break, a systematic analysis of wave amplitudes in relation to wind storms seems appropriate. This has however not been addressed systematically.

The question that this chapter will focus on are therefore:

- Do extremes of mid-latitude geopotential waves amplitudes systematically influence the likelihood of wind storm occurrence?
- Which are the most important planetary wave numbers whose amplitudes influence wind storm occurrence?
- Does the relation between wave amplitude and wind storm frequency depend on wind storm intensity?

With the exception of Roethlisberger et al. (2016) wave activity of the tropospheric flow or jet waviness respectively was assessed with two different methods: either as anomaly of geopotential height isopleths or isentropic potential vorticity contour from a zonal mean state along a certain latitude (Francis and Vavrus, 2012; Francis and Vavrus, 2015; Screen and Simmonds, 2013*b*) or as fast Fourier decomposition along certain latitudinal bands (Petoukhov et al., 2013; Coumou et al., 2014; Kornhuber et al., 2017; Screen and Simmonds, 2013*b*; Screen and Simmonds, 2014) of the meridional wind or the geopotential height. Depending on the method used results can differ substantially (Screen and Simmonds, 2013*b*). It appears that the first method can lead to wrong conclusions (Barnes and Polvani, 2013; Barnes and

Screen, 2015; Screen and Simmonds, 2013*a*), that is why Fourier decomposition will be used here as the preferred option.

This chapter is structured as follows: after this introduction, the FFT method is explained and applied on a case study in the second part. This is followed by a result section 4.3 divided into two parts. Firstly starting the analysis with wind storms and analyse the signal in the geopotential waves (4.3.1) and secondly starting with anomalies in the geopotential waves and analyse the effect on wind storm frequency (4.3.2). The chapter will conclude with a summary and discussion.

4.2 FFT for a single storm

The analysis of mid-tropospheric geopotential waves follows the study of Screen and Simmonds, (2014, hereafter SS). In SS the objective of the study was the relation of temperature and precipitation extremes to planetary and regional waves while here the focus is on the relation of such waves to strong wind events as part of a winter wind storm. The analysed data is 6-hourly ERA Interim reanalysis (see 2.1.1 from 1979 to 2011 for the winter months from October to March (Dee et al., 2011). The slightly shorter time period than in chapter 3 is chosen to provide the possibility for a subsequent comparison with long-term reanalysis, such as the NOAA 20CR data set (Compo et al., 2011).

Analogue to SS the mid-tropospheric geopotential height is decomposed into a Fourier series of periodic waves using the FFT decomposition of the meridional mean from 35° to 60°N for two regions: the entire Northern Hemisphere and the North Atlantic sector including large parts of the North American continent from 120° to 0°W.

An example of such a decomposition is shown in relation to wind storm Christian hitting Germany and Denmark in October 2013 (Von Storch et al., 2014) in figure 4.1. Note that the analysed region differs slightly for demonstration purposes (see

figure 4.2).

Using the fast Fourier transform (FFT) to compute the discrete Fourier transform (very efficiently), the longitudinal structure of a variable Z averaged over a latitudinal band can be expressed in a Fourier series as:

$$Z(x, t) = A_0(t) + \sum_{k=1}^n A_k(t) \cos(k\pi \frac{x}{180} - \varphi_k(t)) \quad (4.1)$$

with t the time, x the longitude, A_0 the zonal mean, k the wave number, n the highest wave number in the Fourier series (in figure 4.1 $n = 10$), A_k the Amplitude of wave with wave number k (hereafter only referred to as wave k) and φ_k the phase of wave k . The wave length λ of wave k is approximated at a latitude of 47.5°N (the mean of 35 and 60) as

$$\lambda = \frac{r\pi}{k} \frac{L}{180} \cos(\pi \frac{47.5}{180}) \quad (4.2)$$

with L the longitudinal sector in degrees and the Earth's radius $r = 6,371\text{km}$.

Waves with $7 < k < 13$ were described as medium scaled waves by Blackmon, (1976) and have a frequency between 2.5 and 6 days. This frequency has since become a sort of synonym for synoptic or extra-tropical storm track activity (Ulbrich et al., 2008). Zappa et al. (2013) extended that frequency range slightly to 2 to 6 days, taken into account even shorter waves as part of the storm track. These smaller planetary waves with planetary wave numbers of 12 and even shorter are therefore also of interest here, but were not considered in previous studies using FFT for geopotential height fields (Coumou et al., 2014; Kornhuber et al., 2017; Screen and Simmonds, 2014; Mann et al., 2017; Petoukhov et al., 2013). It is for this reason that the Fourier decomposition is also applied to the North Atlantic sector only in order to analyse planetary waves with high wave numbers due to geopotential anomalies in this region and not elsewhere. Fourier decomposition along a non-periodic section, such as the North Atlantic sector here, differences between the geopotential mean at

the most western and most eastern longitude (see *Original Z500* in figure 4.1) can introduce so-called red noise that influences the results of primarily longer waves. The Fourier decomposition might thus be not correct and artificial high amplitudes might occur in some waves especially with lower wave numbers. In previous studies, e.g. SS, the FFT was however applied to a non-periodic section. In order to reduce the error the geopotential meridional mean is “tapered” in the analyses prior to the FFT. This means applying a smoothing function (here a split-cosine-bell function as recommended by the NCAR Command Language, NCL, (2017) to 10% at both ends of the geopotential meridional mean for the FFT over the North Atlantic sector. The smoothing will reduce the probability of red noise and artificial high peaks and re-establish the mathematical accuracy of the FFT. Applying the FFT here along a non-periodic section can overall be regarded as a compromise between being able to analyse high planetary wave numbers over the North Atlantic domain and introducing small errors to waves with lower wave numbers over this domain.

The outcome of the FFT decomposition allows the analysis of the amplitude A_k and the phase φ_k for each wave number. The phase determines the position of the wave in a longitudinal direction. The climatology for planetary waves including their preferred positions, i.e. the distribution of φ_k , has long been addressed (Reiter and Westhoff, 1981). Here, the distribution of planetary waves with respect to wind storms is analysed.

The position of each wave in relation to a cyclone centre that is associated with a wind storm can be expressed through

$$\tilde{\varphi}(t) = 2k\pi \frac{x_0 - x_s(t)}{L} \quad \text{with } \cos(\tilde{\varphi}) = \cos(\tilde{\varphi} + 2\pi) \quad (4.3)$$

with x_0 as the western most longitude of the FFT decomposition and $\tilde{\varphi}$ as the wave position relative to x_s the location of the cyclone centre (hereafter referred to as

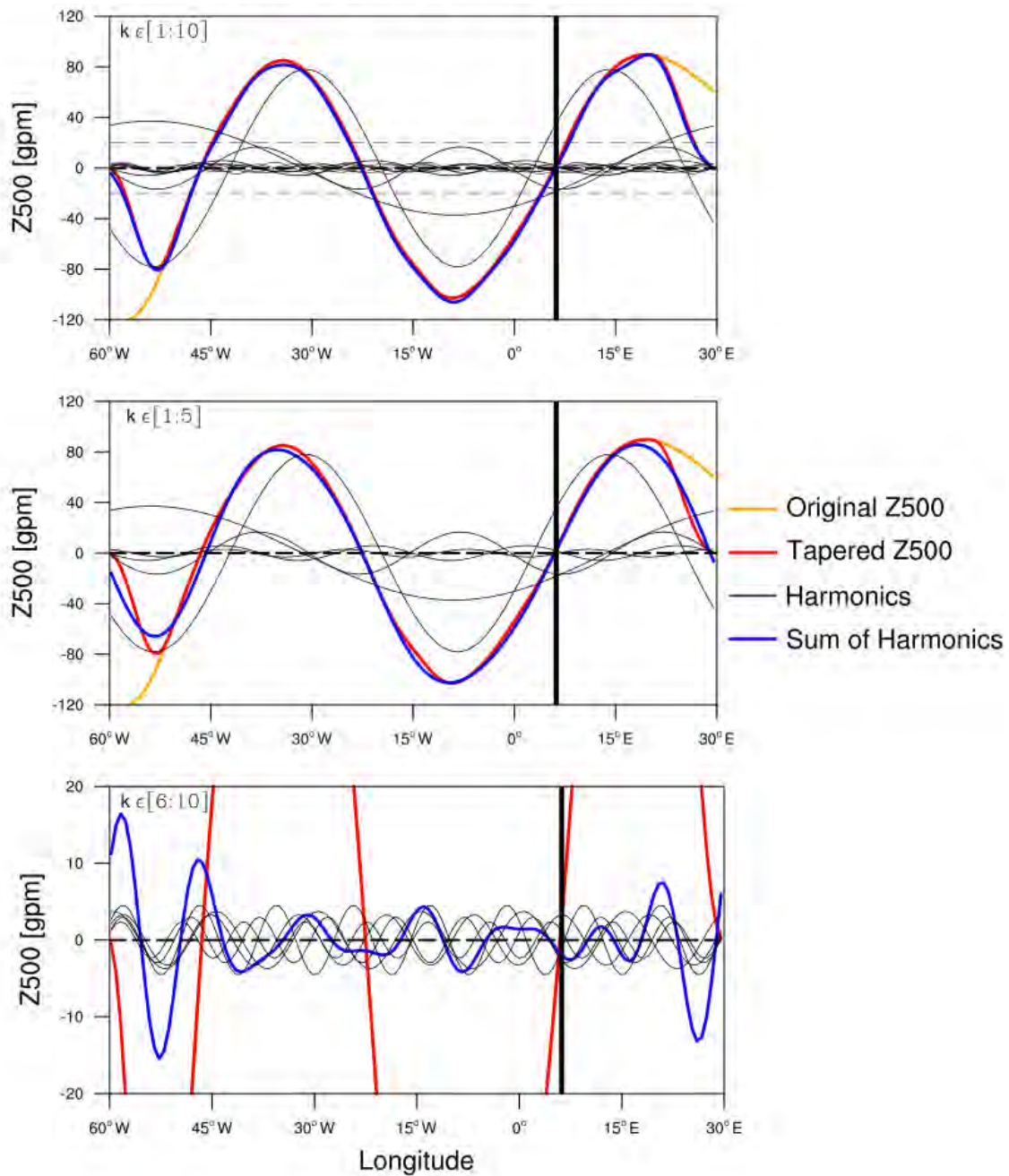


Figure 4.1: Fourier decomposition of meridional mean (35° - 60° N) of geopotential height in 500hPa for North Atlantic / European section (see red box in figure 4.2) on 13th October 2013, 12pm. First 10 harmonics in top panel, first 5 harmonics in middle panel and 6th to 10th harmonics in bottom panel. Bottom panel has different y-axis, indicated with horizontal dashed lines in top panel. Zonal mean A_0 removed. Black vertical line indicates location of cyclone centre of wind storm *Christian*. See text for details.

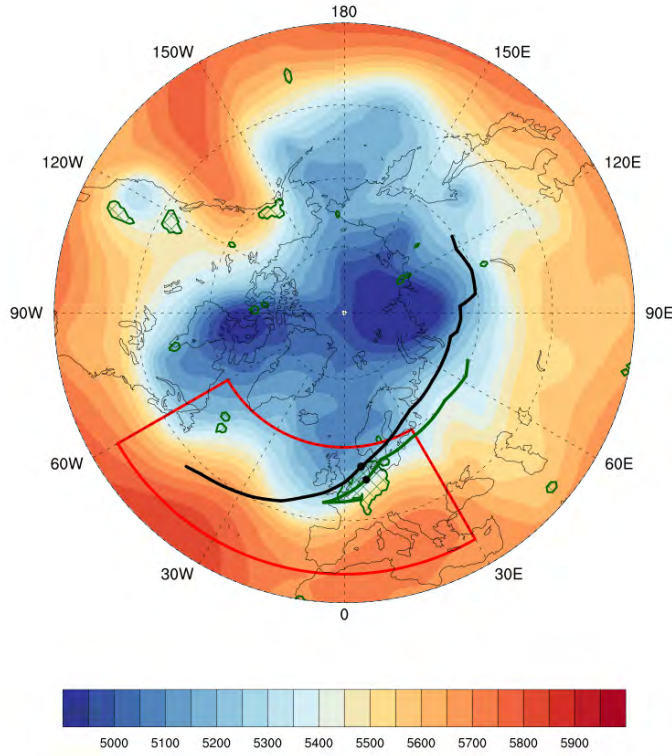


Figure 4.2:
 Geopotential Height in 500hPa on 13th October 2013, 12pm. Black line indicates cyclone track, green line indicates wind storm track of storm *Christian*. Green hatched area shows areas with exceedances 98th local percentile in 10m wind speeds. Red box shows area for Fourier decomposition in figure 4.1.

wave position). The wave with the greatest amplitude in figure 4.1 for wind storm Christian is wave 2. $\tilde{\varphi}$ for wave 2 approximately equals to $\frac{\pi}{4}$ meaning the cyclone centre is on the front side of the wave trough shortly behind the ridge. To simplify the interpretation of the following results for the wave position $\tilde{\varphi}$ will be divided into four areas:

$$\begin{aligned}
 -\frac{\pi}{4} < \tilde{\varphi} < \frac{\pi}{4} &\rightarrow \text{Ridge} \\
 \frac{\pi}{4} < \tilde{\varphi} < \frac{3\pi}{4} &\rightarrow \text{Ahead of trough} \\
 \frac{3\pi}{4} < \tilde{\varphi} < \frac{5\pi}{4} &\rightarrow \text{Trough} \\
 \frac{5\pi}{4} < \tilde{\varphi} < \frac{7\pi}{4} &\rightarrow \text{Behind the trough}
 \end{aligned}$$

The association of a wind storm to a cyclone follows the matching algorithm explained in 2.2.2.

4.3 Results

In the following result section wave amplitudes and wave positions relative to the cyclone centre of a storm are analysed. This extends most of the previously mentioned studies as they focus primarily on wave amplitudes (e.g. SS). The wave amplitudes are normalised (see 2.2.4 to make a comparison between different wave numbers possible).

How do Geopotential Waves Characteristics change during Wind Storms Occurrences?

In this first results section the analyses aim to identify differences in geopotential wave characteristics between 6h-time steps without and 6h-time steps with a wind storm that travels into the Eastern North Atlantic / European region (20°W - 40°E; 35° - 60°N, see grey box in figure 1.1a). This region is smaller than the wind storm region in chapter 3 but there are no further selection criteria to wind storms or cyclones. For this chapter a total of three subsets are analysed:

- Climatology:
All 6h time steps in ERA Interim in the winter months from October to March between 1979 and 2011
- All Wind Storms:
One time step per wind storm that crosses the Eastern North Atlantic / European region (20°W - 40°E; 35° - 60°N).
- Top 50 Storms:
One time step per strongest 50 wind storms. Strongest storms are identified using the accumulated SSI (see 2.2.3).

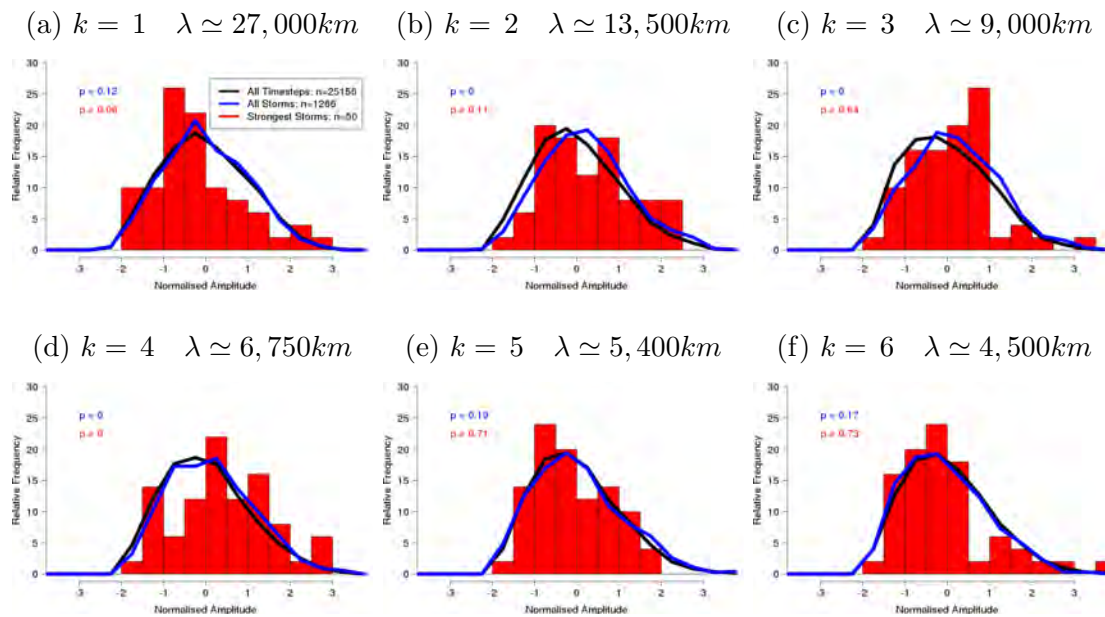


Figure 4.3: Normalised amplitude distribution for first 6 wave numbers of FFT decomposition over Northern Hemisphere and meridional mean between 35° and 60° N. Shown are all possible 6h time steps (black line), all time steps with an associated wind storm (blue line), and all time steps with a strong wind storm (red bars). P-values of a ks-test comparing the distributions of all time steps with an associated wind storm (blue) and all time steps with a strong wind storm (red) to the distribution of all possible time steps.

The selected time step for all storms and for the top 50 storms corresponds to the date and time when the storm had its strongest intensity (SSI, see 2.2.3). The strongest intensity can be outside the defined region.

The statistical significance of differences in amplitude distributions is assessed using the two-sample Kolmogorov-Smirnov test or KS-test (Wilks, 1995). It tests the null hypothesis whether two samples are drawn from the same distribution. Unlike the more common Student's t-test or the unequal variance t-test used in SS, the KS-test is a non-parametric test and allows for non-normality as it compares the cumulative distribution function of the sample distributions. This is here especially important for the case, when only the top 50 storms are selected.

Complete Northern Hemisphere

The normalised amplitudes of planetary wave 1 show no statistical significant differences between time steps with or without storm (Figure 4.3a). It appears however that there is a tendency of smaller wave amplitudes when a wind storm occurs. The amplitude of wave 2 to 4 is significantly greater during the time of a wind storm. When only the strongest 50 wind storms are considered, there is an indication of greater amplitudes in wave 2, albeit not statistically significant (Figure 4.3b). The amplitudes of wave 3 show a tendency to be greater for strong wind storms, but with an upper limit of amplitude of around one standard deviation above the mean (Figure 4.3c). The distributions between all time steps and time steps with strong storms are thus not significantly different. This different signal for all wind storms and strong wind storms is further discussed in section 4.3.2. For wave 4 the change in amplitudes between all time steps with storms and time steps with strong storms agree well (Figure 4.3d). Amplitudes of planetary waves 5, 6 (figs. 4.3e and 4.3f) bigger wave numbers (not shown) show no differences in case a wind storm occurs or not. A summary of the changes of amplitudes is given in table 4.1.

The distribution of wave positions with respect to the cyclone centres of wind storms shows generally no differences between all time steps with storms and all time steps with strong storms. The preferred position of a storm appears to be at the ridge of wave 1, ahead of the trough of wave 2 and at or behind the trough for wave 3 (Figure 4.4). The wave position is nearly equally distributed for waves with higher wave numbers. The distribution of wave positions for all time steps is not shown here as there is no obvious reference point such as the cyclone centre for these waves. The “ridge” of wave 1 one is more a shift of the geopotential height towards the North over the North Atlantic. An increase of geopotential height over the North Atlantic is usually not associated with high cyclone or wind storm activity. As the results of the wave amplitudes have shown, wave 1 tends to be not overly important

for wind storm occurrence and if at all with their amplitude should be small. If there is a storm over the North Atlantic it appears that the likelihood that wave 2 has a strong amplitude and the trough is also located over the North Atlantic is increased (see also Figure 4.7b). Planetary wave 3 is one of the slower moving Rossby waves and depending on the current zonal flow it sometimes moves even retrograd (Rhines, 1970). It is also often referred to as quasi-stationary with ridges located at high orographic regions such as the Rocky Mountains and the Himalaya and troughs in between these ridges, e.g. over the North Atlantic. Figure 4.4c is therefore very similar to the climatological mean condition for any location in the eastern North Atlantic.

It may seem surprising at first that wave amplitudes of hemispheric wave numbers shorter than 5 appear to have no connection to wind storm frequency as it is mainly medium scaled or even shorter waves that are considered to be important for storm track activity (e.g. Blackmon, 1976). These shorter waves can however not be regarded as hemispheric as they only exist over a limited longitudinal range (Simmons and Hoskins, 1978). A FFT decomposition over a smaller part of the hemisphere is thus necessary.

North Atlantic Sector, 120° to 0°W

The wave frequency analysis is also carried out for the North Atlantic. The selected sector from 120° to 0°W is almost entirely upstream of the region that storms have to pass (20°W to 40°E) to be considered in the analysis. As the analysed region spans one third of the hemisphere each North Atlantic wave number has to be multiplied by three for the corresponding planetary wave number. Wave 1 in the North Atlantic sector (hereafter NAt 1) corresponds to planetary wave 3, wave 2 in the North Atlantic sector to wave 6 and so forth. The results for the amplitudes of NAt-wave 1 and NAt-wave 2 corroborate the results for the planetary Fourier decomposition. NAt-wave 1 also shows statistical significantly greater amplitudes

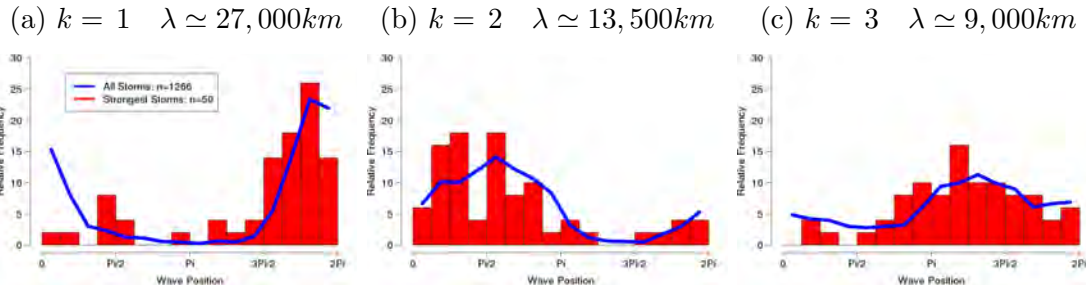


Figure 4.4: Wave position distribution for first 3 wave numbers of FFT decomposition over Northern Hemisphere and meridional mean between 35° and 60° N. Shown are all time steps with an associated wind storm and all time steps with a strong wind storm.

for wind storm time steps when compared to all time steps, but no change if only the strongest wind storms are considered. There are no differences in NAt-wave 2 and NAt-wave 3 amplitudes in comparison to the climatology. NAt-wave 4 shows clearly greater amplitudes both wind storm samples. NAt-wave 4 corresponds to planetary wave 12 and is thus just at the high frequency end of the medium scale as defined by Blackmon (1976). Amplitudes for NAt-wave 5 shows once more no differences. Mid-tropospheric geopotential waves have significantly greater amplitudes for NAt-wave 6 ($\lambda \simeq 1,500km$) and shorter waves when a wind storm occurs. Even though not always statistically significant, this remains true if only the strongest 50 storms are taken into account.

The distribution of wave positions of NAt-wave 1 corroborates again the results for planetary wave 3 (compare Figure 4.6a and 4.4a). There is slight increase in frequency for the location halfway between trough and ridge behind the trough. The position of NAt-wave 2 is quite evenly distributed for all wind storms. There is a larger part of the distribution of wave positions ahead of the trough with respect to the cyclone centre for NAt-wave 2. This is comparable to the situation for wind storm Christian as seen in figures 4.1 and 4.2. The distribution for NAt-wave 3 or shorter waves are evenly distributed.

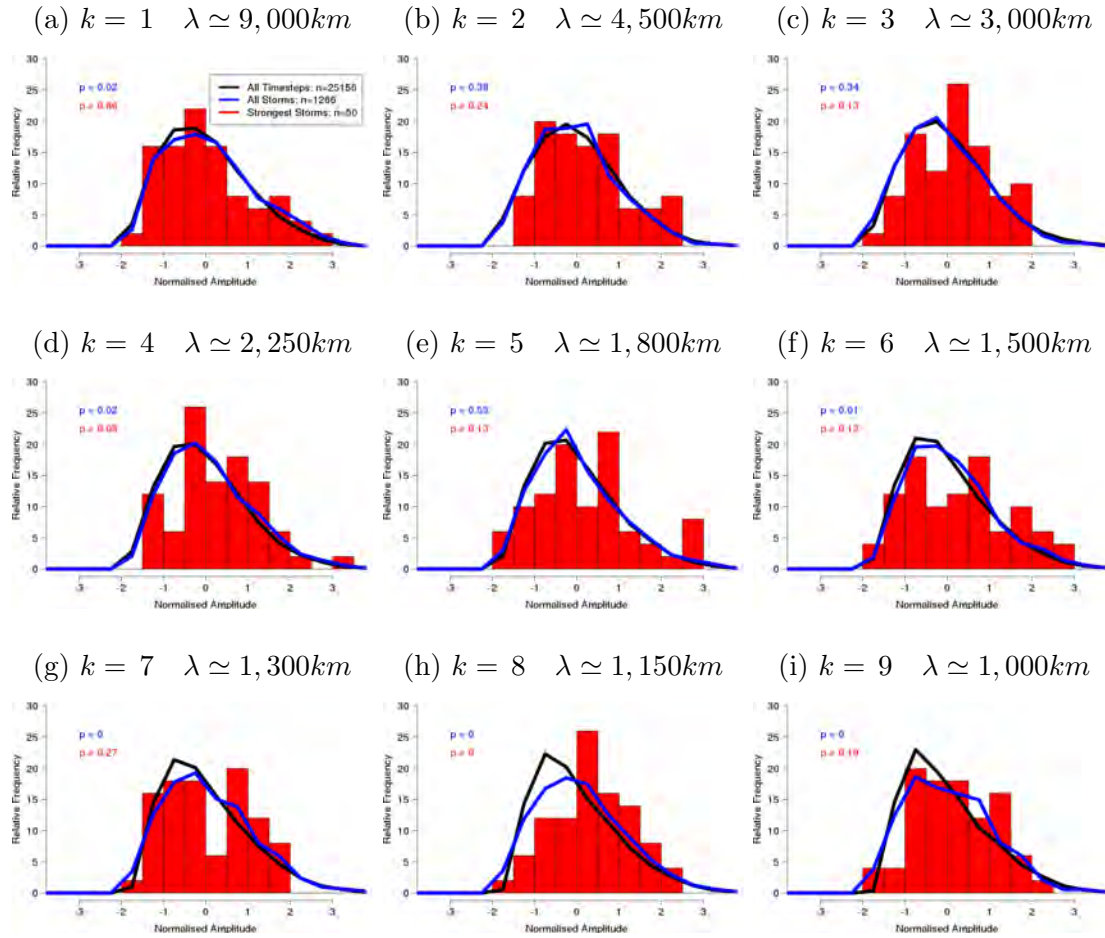


Figure 4.5: As figure 4.3 for selected wave numbers of FFT over $120^\circ - 0^\circ W$ and meridional mean between 35° and $60^\circ N$.

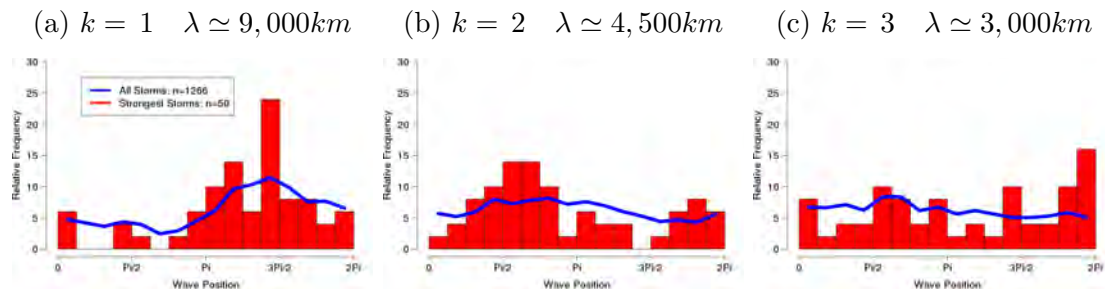


Figure 4.6: As figure 4.4 for FFT over $120^\circ - 0^\circ W$ and meridional mean between 35° and $60^\circ N$.

How does Wind Storm Frequency change for Anomalies in Geopotential Wave Characteristics?

In this result section the aim is to identify whether wind storm frequency changes if certain planetary or NAt waves have a high or low amplitude. In a first step the time steps with greatest (smallest) amplitudes of all decomposed waves are selected. The selected time steps have to be at least 48 hours apart in order not to sample one persistent high (or low) amplitude wave multiple times. It is then added up at how many of these 50 time steps a wind storm occurred. A probability is subsequently calculated whether this number of wind storm occurrence can be expected or is unlikely. Each time step is only taken into account once even if more than one storm is found.

The discrete hypergeometric distribution is used in probability theory when sampling without replacement (Berkopce, 2007). The probability of sampling k time steps with storm in 50 draws out of a sample N , representing all possible time steps is calculated. N contains a total of K time steps with storm. The probability P of selecting at least k storms is then given in equation 4.4.

$$P(k, K, N) = 1 - \sum_{k=0}^{50} \frac{\binom{K}{k} \binom{N-K}{50-k}}{\binom{N}{50}} \text{with} \quad \binom{n}{k} = \frac{n!}{k!(n-k)!} \quad (4.4)$$

For great amplitudes in planetary wave 1 there is no increased probability for wind storm occurrence. The probability of 99.5% indicates that it is very likely to find at least 4 storms at any given 50 dates. This is in agreement with the amplitude distributions in figure 4.3a where no significant difference is found for wind storm time steps in comparison to the climatology.

If the amplitude of wave 2 is exceptionally high, the probability of a wind storm occurring at the same time is strongly increased. It is extremely unlikely to draw 24 out of 50 times a time step with storm in the eastern North Atlantic / European

region (Figure 4.7b). This result also agrees with the amplitude distribution in figure 4.3b. There is no significant signal for a higher wind storm probability when other planetary waves have very high amplitudes. The 50 waves 2 with greatest amplitude have all a similar trough location in the Atlantic sector from about 70° to 10° W. Storms over the Eastern North Atlantic and Europe are then just ahead of the trough. This is coinciding with an increase for wave positions ahead of the trough for stronger storms 4.4b. The majority of the 25 identified storms when wave 2 has a high amplitude reach their maximum intensity just downstream of the average trough location (red dots in figure 4.7b). The maximum intensity of the storm occurs *after* the maximum in the wave in about two thirds of the 25 cases (not shown).

There is no significant increase in wind storm occurrence probability if any of the other planetary wave numbers high amplitudes. The only exception is wave 5 that shows a greater likelihood for wind storm occurrence with greater amplitudes, albeit statistically not significant 4.7c.

The same method for the relation of planetary wave amplitude to wind storm occurrence is applied for waves with very low amplitudes. The only statistically significant result is found for planetary wave 3 or NAt-wave 1. Wind storm occurrence is increased when planetary wave 3 4.8a of NAt-wave 1 4.8b shows a small amplitude in the Fourier series. It is coincidental that in both cases 16 storms are found. The selected days with lowest amplitudes or storms respectively are not the same. This result appears to be contradicting to the shift in amplitude distribution for these waves when wind storm occurs (see figure 4.3a and 4.5c). It could be however that the relation between wave 3 and wind storms frequency is non-linear and both high and small amplitudes of this wave have an effect on wind storm occurrence. In almost all cases the shift in wave amplitude distribution for the strongest wind storms follows the shift in amplitude for all wind storms (see table 4.1 for an overview). Planetary wave 3 seems to be the exception.

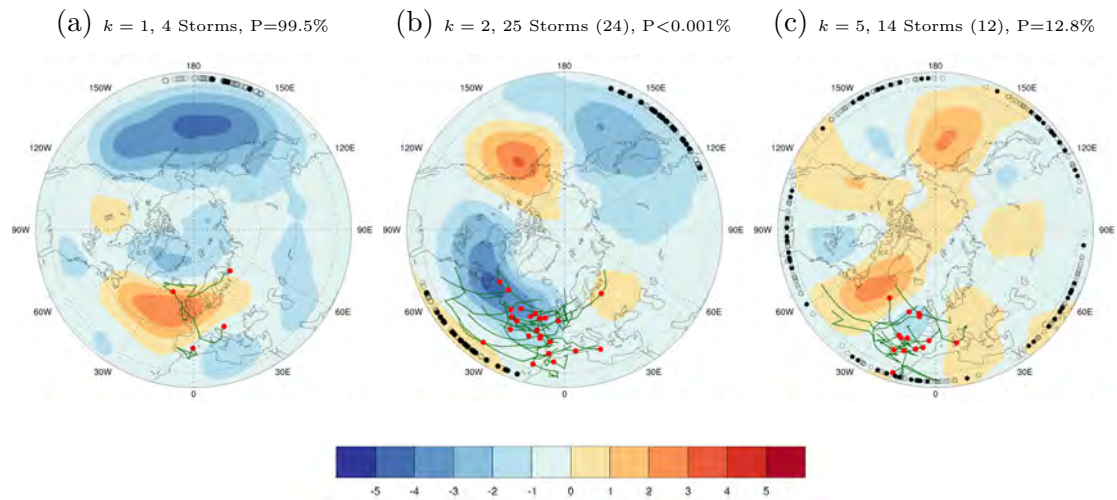


Figure 4.7: Geopotential height composites relative to climatology from 1979-2011 for planetary wave numbers 1,2 and 5. Time steps are selected for the composite when amplitude of geopotential height wave (for respective wave number) is amongst 50 greatest and a wind storm occurs. Number of storms with number of individual time steps in brackets if different. Wind storm tracks in green and point when storm reaches its maximum intensity as red dot. Probability (P) of drawing this number of storms out of a sample of 50 in top right corner. Location of trough of geopotential wave indicated with black circles. Black circles are filled when wind storm is found.

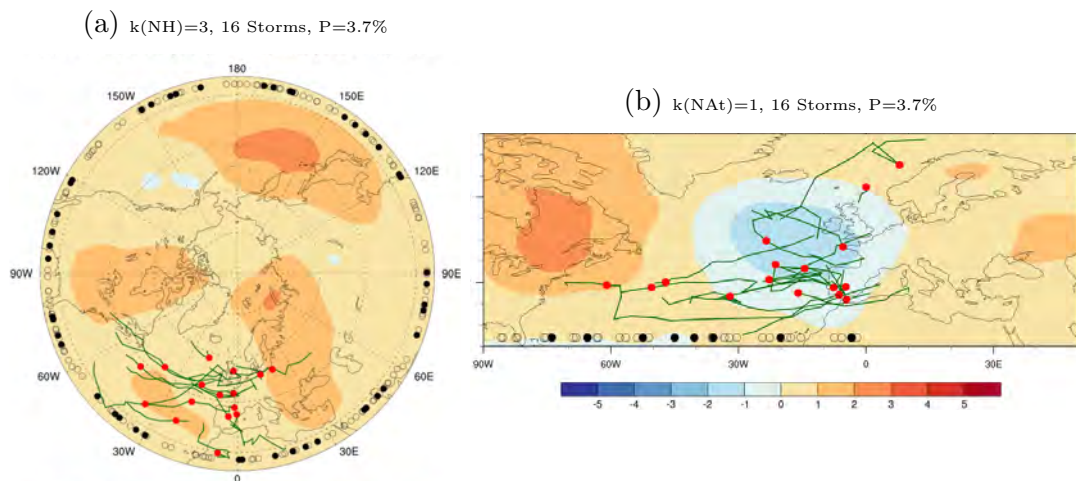


Figure 4.8: As figure 4.8 for 50 lowest amplitudes in geopotential waves. Left for FFT over Northern Hemisphere(NH); right for FFT over North Atlantic sector(NAt).

4.4 Summary and Discussion

In this chapter the relation between wave characteristics of planetary and regional scale waves and wind storm frequency is analysed. Previous studies have related planetary waves or regional waviness in the mid- and upper troposphere to meteorological extremes (Mann et al., 2017; Roethlisberger et al., 2016; Kornhuber et al., 2017; Screen and Simmonds, 2014; Coumou et al., 2014; Coumou and Rahmstorf, 2012; Francis and Vavrus, 2012; Francis and Vavrus, 2015; Petoukhov et al., 2013). With few exceptions these studies have focused on wave amplitudes and their relation to temperature and precipitation events.

There have also been numerous studies that investigate Rossby wave breaking in association with wind storm frequency and especially wind storm clustering (Hanley and Caballero, 2012; Gómara, Rodríguez-Fonseca, Zurita-Gotor and Pinto, 2014; Pinto et al., 2014; Messori and Caballero, 2015; Priestley et al., 2017*a*; Priestley et al., 2017*b*) or Rossby wave breaking in association with blocking (Woollings et al., 2008; Masato et al., 2012; Hoskins and Woollings, 2015; Michel et al., 2012), that lead to a reduction of wind storm frequency (Davini et al., 2012; Woollings et al., 2010; Woollings, 2010; Zappa et al., 2014).

The study fills the apparent gap with relating wave characteristics (i.e. amplitude and phase for different wave numbers) to North Atlantic wind storm frequency using the FFT decomposition of mid-latitude, mid-tropospheric, 6-hourly geopotential height fields.

A summary of wave amplitude distribution differences between the climatology and wind storm occurrences is given in table 4.1. Planetary wave numbers 2,3 and 4 show a systematic increase in amplitude for time steps with wind storms. This increase is also found when only the 50 time steps with the strongest wind storms are considered, with the exception of planetary wave 3. Higher wave numbers are likely to be influenced by flow anomalies in other parts than the North Atlantic.

Hemispheric Wave Number	1	2	3	4	≥ 5		
All Wind Storms	-	↑	↑	↑	-		
Strongest Wind Storms	↓*	↑*	-	↑	-		
Wave Number in NAt Sector	1	2,3	4	5	6,7	8	9
All Wind Storms	↑	-	↑	-	↑	↑	↑
Strongest Wind Storms	-	-	↑	-	↑*	↑	↑*

Table 4.1: Changes in mid-tropospheric geopotential wave amplitudes during wind storm occurrences. ↑ represents a systematic increase, ↓ represents a systematic decrease in wave amplitude. Differences are statistically significant at the 5% level unless marked with *.

Therefore a FFT decomposition is also carried out for the North Atlantic sector. NAt-wave 4, i.e. planetary wave 12, corresponding to the high-frequency end of the storm-track activity definition (Blackmon,1976), and waves with wave lengths shorter than 1,500km also show a systematic increase in wave amplitudes. There is thus a general tendency for mid-tropospheric geopotential amplitudes to be greater over the North Atlantic when a wind storm occurs over the Eastern Atlantic / European region.

NAt-wave 1 corroborates the results for planetary wave 3. On the one hand wave 3 could be related to blocking events (e.g. Woollings, 2010). When its amplitude is small the possibility of blocking is decreased and mid- and upper-tropospheric flow is more zonal. Some of the wind storms in figure 4.8a show a very direct path from west to east. The amplitude could be small due to wave breaking enhancing the jet stream and further favour conditions for strong extra-tropical cyclones.

On the other hand wave 3 could be related to the strong and persistent ridge events (Santos et al., 2009). In their composite analysis Santos et al., (2009) find these events to be around 60°in width, which corresponds exactly to one ridge of wave 3. This could provide an explanation into why wave 3 shows higher amplitudes when wind storm frequency is enhanced during as these strong ridge events have been shown to be related to a north-ward displacement of the jet axis, anti-cyclonic wave

breaking and generally NAO positive conditions (Woollings et al., 2011).

The results for this wave show in line with this apparent duality a clear non-linearity between the wave characteristics and wind storm frequency. While there is a systematic increase in amplitude for all wind storms compared to the climatology, there appears to be an upper limit of about one standard deviation above the mean for this wave when strong wind storms occur (see figure 4.3c). There is also a statistically significant probability of more wind storms when wave 3 shows very low amplitudes. Somewhat surprisingly the composite of 50 time steps with low wave 3 amplitudes looks like a wave 3 anomaly pattern albeit with small relative anomalies. This behaviour is not found for any other planetary waves. Detailed analyses of each for each of the 50 situations when wave 3 has a low amplitude reveal no final answer as to why this might be the case. The trough locations of wave 3 are fairly evenly distributed, meaning that if wave 3 has a low amplitude it appears to be not bound to one position around the hemisphere (see figure 4.8). Multiples of wave 3, such as planetary wave 6 and/or wave 9, show relatively high amplitudes in about half of the 50 situations. Their superposition could potentially resemble a wave 3 pattern. In four cases with low planetary wave 3 amplitudes, two or three of the 50 low-amplitude situations are only few days apart. One of these cases is found shortly prior to the *Great Storm of 1987* (Burt and Mansfield, 1988). Note, that the path of this storm is not included in the composite in figure 4.8a as the wave amplitude is exceptionally low 12 hours before the wind track algorithm identifies the event. As a plausibility check for the FFT method the composite for the geopotential height field for a period of around 3 days just before the *Great Storm* is shown in figure 4.9 together with the zonal wave of the two time steps when wave 3 is very low. The average amplitude of wave 3 is around 70 gpm and for the dates shown 2.0 and 3.5 gpm. The result seems plausible considering the overall spatial anomaly and the longitudinal structure of the geopotential height in 500hPa for these 2 dates.

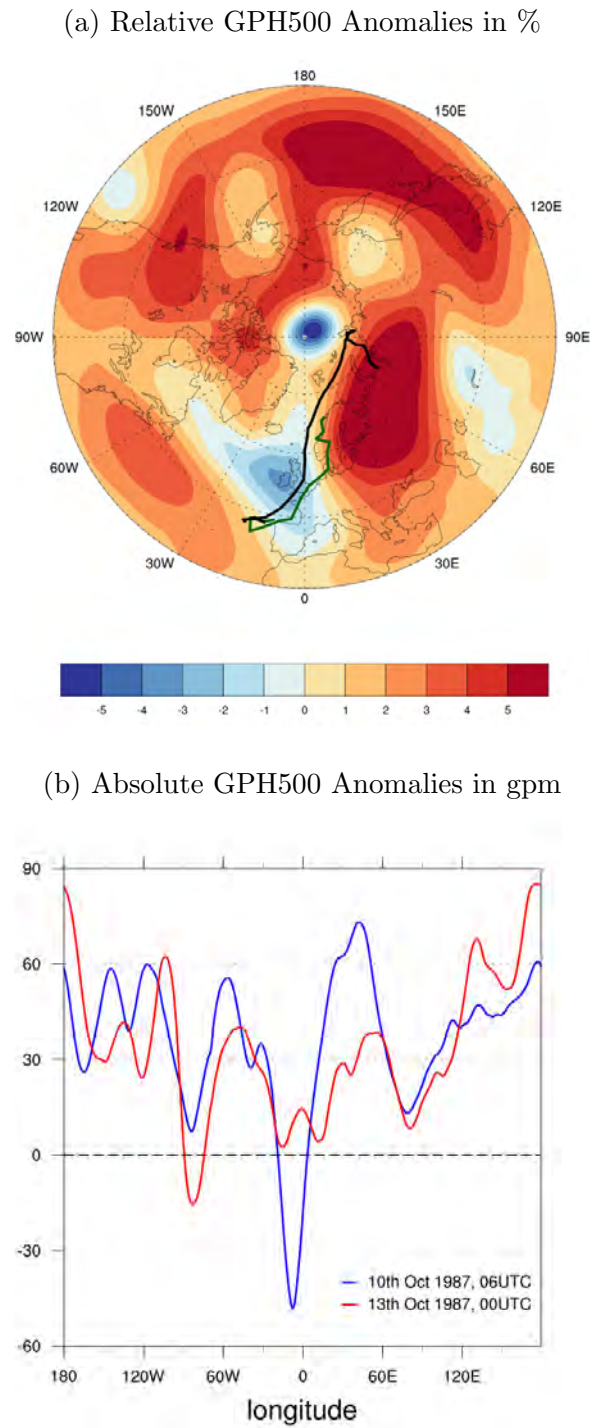


Figure 4.9: Geopotential height anomalies in 500hPa for the dates given in (b) together with the cyclone (black) and wind storm tracks (green) of the Great Storm of 1987 in (a). The cyclone starts 14th Oct, 6UTC and ends 23rd Oct, 6UTC. The wind storm starts 14th Oct, 12UTC and ends 18th Oct, 0UTC. Geopotential is averaged over from 35°-60°N in (b).

The picture is much clearer for planetary wave 2 that shows a highly statistical significant relation to wind storm frequency when its amplitude increased (see figures 4.3b and 4.7b). Wave 2 has an average amplitude with 67 gpm which is slightly smaller than the average amplitude of wave 3 and might therefore be less frequently analysed. None of the above mentioned studies consider planetary wave 2 especially but as the analyses here show, this is not a priori justified. Shorter waves with wavelengths of 1,500km or shorter show a systematic relation of their amplitude to wind storm frequency. A combined effect of planetary waves, such as for example high amplitude wave 2 together with low amplitude wave 3 and high amplitude wave 4, does not reveal any significant link to wind storm frequency.

The analysis of the wave position with respect to the location of a cyclone shows preferred positions for some wave numbers. The extent to how that is different from the climatological situation is however not fully assessed here as the phase speed of the waves is not taken into account. Various waves can be considered quasi-stationary, e.g. wave 3 through the distribution of mountain ranges in the Northern hemisphere. The climatological position for wave 3 has a trough over the western North Atlantic and a ridge eastern North Atlantic. The most likely position for this wave over the Eastern North Atlantic and Europe is therefore just behind the ridge or ahead of the trough which is the result here for cyclone centres with associated wind storm over this region. A more comprehensive study also considering the phase speed is thus required for a better understanding of the relation of planetary waves and wind storms.

Amplified planetary waves have been shown to favour meteorological extremes in the mid-latitudes. The above analyses extend this general statement which has so far only been shown systematically for temperature and precipitation extremes for winter wind storm frequency. Generally, the extremes of planetary wave amplitudes, especially the upper end of the distribution, influence systematically the occurrence of wind storms. Some wave numbers play thereby a more important role than

others as table 4.1 shows. The relation between wave amplitudes and wind storm frequency does however not change if only the most intense storms are considered. Further research is however needed about which physical mechanism(s) can explain the apparent ambiguous relation of planetary wave 3 and wind storm frequency.

SEASONAL FORECAST SKILL FOR EXTRA-TROPICAL CYCLONES AND WIND STORMS

This chapter has been submitted with the same title in almost identical form to the *Quarterly Journal of the Royal Meteorological Society* and is currently under review. The authors of the submitted manuscript are Daniel J. Befort (DJB), Simon Wild, Jeff R. Knight (JRK), Julia F. Lockwood, Hazel E. Thornton, Leon Hermanson, Philip E. Bett, Antje Weisheimer, and Gregor C. Leckebusch (GCL). A brief overview of the individual contributions of all authors can be found at the beginning of this thesis (see Author's Declaration). My contributions to the following chapter or publication respectively include the written first draft of the paper, the production of all figures as shown in this chapter, the complete analyses for figures 5.7, 5.8, and 5.9 and partially the analyses for figures 5.4 to 5.6. GCL came up with the idea and concept for the study and established the contact to the co-authors from the Met Office and ECMWF. DJB acquired and downloaded the data from these centres. He performed the tracking and the calculation of the track densities with the data. I identified the most suitable correlation method and calculated the correlations and statistical significance. I calculated the anomaly correlations. GCL, DJB, JRK, and I designed the second part of the study. I performed all the analyses for this part. After I wrote the

publication draft all authors contributed in improving the manuscript. The coordination between co-authors was mainly done by DJB.

5.1 Introduction

Extra-tropical cyclones can produce high wind speeds near the surface, damaging physical structures, causing fatalities and enormous financial losses. Insurance losses related to wind storms are second only to flood-related losses in western and central Europe (Munich RE Group, 2016). Strong mid-latitude cyclones affecting Europe form when baroclinic disturbances over the North Atlantic undergo rapid intensification, leading to a fall in surface pressure and steep pressure gradients. In conjunction with their related frontal structures, these intense cyclones can produce extremely high surface wind speeds over a large footprint region.

Across Europe, the average number of damaging cyclones and wind storms varies per season, for example, from 7-10 per season for the North of Scotland, to 2-3 over central Europe. Nevertheless, their frequency varies greatly from year to year, with many studies using climatological information to attempt to understand causative factors of such variability. The important role of large-scale atmospheric variability modes has been known for many years, although not fully understood (e.g., the steering influence of the North Atlantic Oscillation (NAO); e.g. Hurrell and Deser,(2009); Donat et al.,(2010); Renggli et al.,(2011)). Recent studies also highlight the influence of other important modes like the East Atlantic Pattern (EA) or the Scandinavian pattern over different regions of Europe (Walz, Befort, Kirchner-Bossi, Ulbrich and Leckebusch, 2018).

A skillful forecast of the severity of the coming season, in terms of wind storm occurrence, would be useful for many applications, including preparation for disaster management, mid- to short term planning of business operations, as well as military planning applications.

So far, only a few studies have directly investigated the skill of extreme event forecasts with lead times beyond a couple of weeks. The earliest one known to the authors is a study of the ENSEMBLES and DEMETER seasonal hindcast experiments (Renggli, 2011). In these early seasonal forecast systems, they found small but significant skill for extra-tropical cyclone related wind storm frequency over parts of central western Europe. One core finding was that winter seasons with enhanced or decreased frequency are better predicted than normal storm seasons, when initialised in November. More recent studies investigating the Met Office GloSea5 hindcast data set, based on the HadGEM3-GA3 model, have revealed a step-change in mid-latitude seasonal forecasting skill, demonstrating that this forecast system does now show significant, usable skill for the major climate variability mode over Europe, the NAO (Scaife et al., 2014; Scaife et al., 2016; Clark et al., 2017; Palin et al., 2016). Stationary Rossby waves, triggered by tropical convection have been proposed as a potential mechanism for this NAO skill (Trenberth and Fasullo, 2012; Trenberth et al., 2014; Scaife et al., 2017).

This study investigates the extent to which the modern seasonal forecast systems, from the European Centre for Medium-Range Weather Forecasts (ECMWF) and the Met Office Hadley Centre, are capable of forecasting the frequency of extra-tropical cyclones and wind storms over the Northern Hemisphere. We analyse the skill of forecasts starting around the beginning of November for the upcoming winter season (Dec-Feb). In addition, the skill of forecasting wind storm occurrence in the North Atlantic/European region using a prediction of the NAO and the relationship between the NAO and wind storm frequency is explored.

We describe the data used in section 2. Cyclone and wind storm tracking schemes are explained in the methods in section 3. Results are presented in section 4, with subsections assessing the models' ability to simulate the climatological distribution and interannual variability of cyclones and wind storms in the Northern Hemisphere, and whether an NAO-based forecast is beneficial. We conclude with a summary

and discussion in section 5.

5.2 Data

We use four data sets in this study: a pseudo-observational data set (ERA-Interim reanalysis, Dee et al., 2011), and three seasonal hindcast data sets: ECMWF System 3 (hereafter ECMWF-S3, Anderson et al., 2007), ECMWF System 4 (hereafter ECMWF-S4, Molteni et al., 2011) and GloSea5 (MacLachlan et al., 2015). The time period investigated, common to all datasets, comprises 20 full winters from 1992/1993 to 2011/2012. When we refer to, for example, winter 1992, we consider the three months from December 1992 to February 1993. We use 6-hourly mean sea level pressure to identify cyclones, and 12-hourly wind speeds at 925 hPa to identify wind storms (see next section). The ECMWF hindcasts are initialised on the 1st November, whereas the GloSea5 hindcasts are started on 25th October, 1st November and 9th November, with 8 realisations for each start date. All seasonal prediction systems are ensemble systems, each with a different number of individual realisations: 41 members in ECMWF-S3, 51 members in ECMWF-S4 and 24 members in GloSea5. Cyclone and wind identification and tracking is performed on each ensemble member. The skill assessment is undertaken on the ensemble mean, where each ensemble member has equal weight. The results obtained from the seasonal forecast models therefore appear smoother than the single realisation of the reanalysis.

5.3 Identification and Tracking Algorithms

In this study we identify and track cyclones using an algorithm first introduced by Murray and Simmonds (1991) with the modifications specified in Simmonds

and Murray (1999) and Simmonds et al. (1999). The analysis is based on six-hourly mean sea level pressure (MSLP) fields. Each field is interpolated onto a T159 grid, to decrease the dependency of the algorithm on grid resolution. Cyclone centres are detected by identifying maxima of the Laplacian of the MSLP field and thus a maximum of the quasi-geostrophic relative vorticity. For the cyclone tracking procedure, a subsequent position of each cyclone centre is predicted and compared to cyclone centres identified in the following time step. Cyclone tracks with a lifetime shorter than 24 hours are filtered out. Furthermore, only cyclone events which have been strong and closed at least once during their lifetime are considered, thus excluding open depressions. This tracking methodology has previously been used in numerous studies (Grieger et al., 2014; Kruschke et al., 2014; Befort et al., 2016) and is included in the Intercomparison of Mid-Latitude Storm Diagnostics Initiative (IMILAST; Neu et al.,(2013); Ulbrich et al.,(2013)).

We define extreme cyclones as those exceeding the 95th percentile of the Laplacian of the MSLP at least once in their lifetime, following Leckebusch and Ulbrich (2004). This 95th percentile is calculated based on all cyclone events over the Northern Hemisphere. The absolute number of identified extreme cyclone tracks consequently accounts for 5% of all cyclone tracks on the integrated, hemispheric scale, but shows significant spatial variations on regional scales.

For wind storm events we follow the identification and tracking scheme developed by Leckebusch et al. (2008). A more recent and extensive description of this algorithm can be found in Kruschke (2015). Originally established for wind speeds at a height of 10 metres and 6 hourly data, we here apply the algorithm to wind speeds at 925 hPa and 12 hourly data due to data availability from the GloSea5/ECMWF hindcasts. The scheme identifies regions where the wind speed exceeds the local (grid point level) 98th percentile of climatology. The region must exceed 150,000km² to be considered a wind storm. The 98th percentile is calculated from the wind

speed distribution for the winter months December to February from 1992 to 2012 as this period is available for all data sets. The wind storm tracking procedure follows a nearest neighbour approach. Wind storm tracks with a lifetime shorter than 24 hours, i.e. 2 time steps are filtered out. This algorithm has also been applied previously (Renggli, 2011; Nissen et al., 2014; Nissen et al., 2013; Befort et al., 2015; Kruschke et al., 2014; Wild et al., 2015; Befort et al., 2016). Note that, due to using 12 hourly 925hPa wind speeds rather than 6 hourly 10m wind speeds, a reduction in the number of wind storm events is seen.

We apply both algorithms to the core winter months. Spatial track densities are calculated following Befort et al. (2016) with a search radius of 700km. In GloSea5, wind speeds are set to zero if the 925hPa pressure level is below the surface, making it impossible to track wind fields over these areas. To minimise this effect we exclude all grid cells for where this occurs in more than 5% of all time steps. This mask is then applied to all the datasets we use. Temporal correlations are based on Kendall's τ_b rank correlation coefficient. This coefficient takes into account ties, i.e. the same absolute number of events, in the ranks of the time series, which is necessary in our case of absolute cyclone/wind storm counts. Statistical significance is obtained under the null hypothesis of no association, and as our data contains ties, a normal approximation with continuity correction is applied when the correlation coefficient is calculated (Kendall and Dickinson, 1990). Comparisons to other more common correlation methods (i.e. Pearson and Spearman) and other statistical significance tests (i.e. Student's t-test and r-test) show only minimal differences.

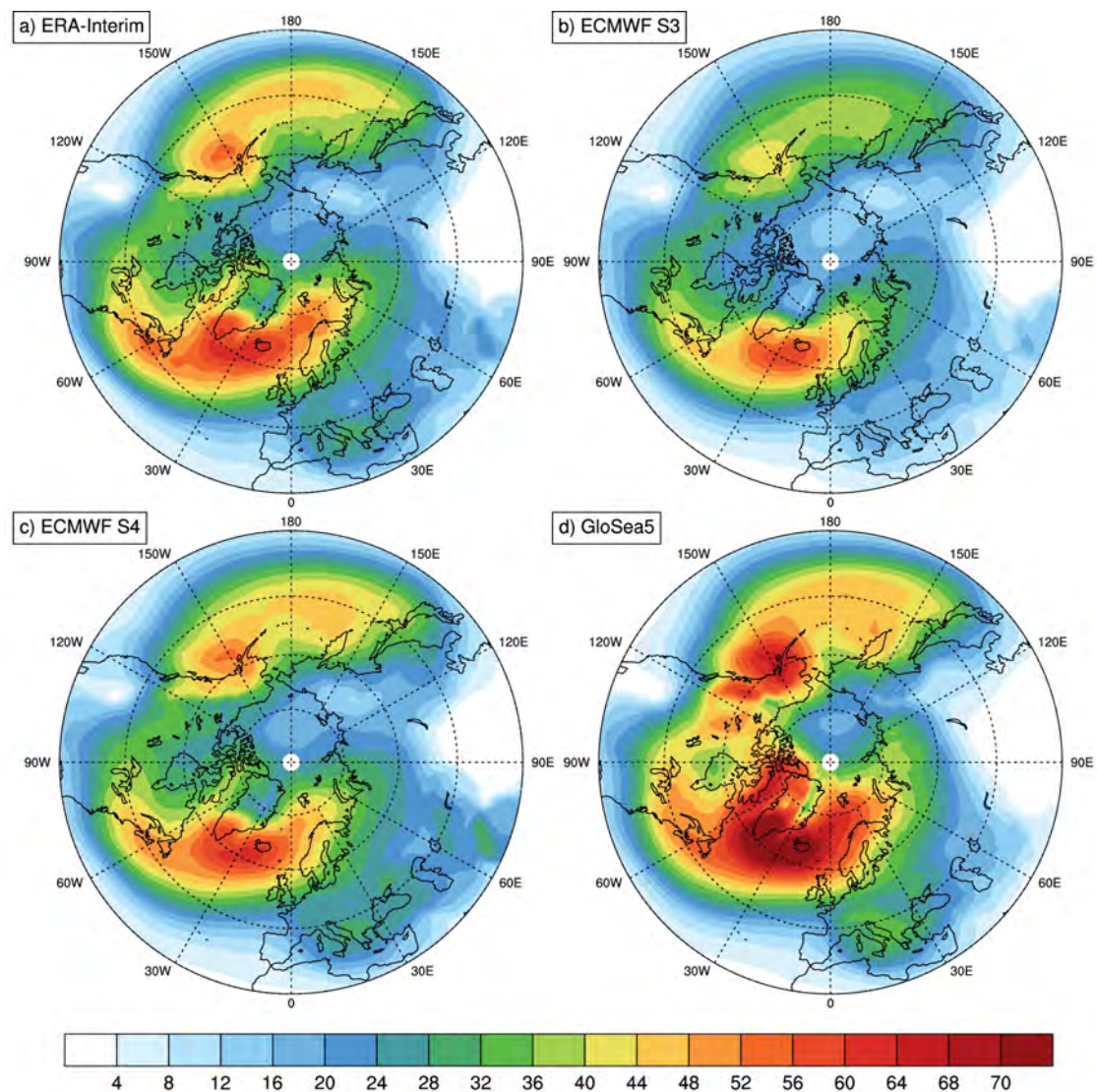


Figure 5.1: Track density of **all cyclone events** per winter season (1992-2011)

5.4 Climatological Representation of Cyclones and Wind Storms in the Northern Hemisphere

The observed climatological spatial track density of all extra-tropical cyclones shows the two well-known centres of activity over the North Pacific and the North Atlantic (Figure 5.1). The highest number of cyclones occurs at the respective jet exit region with around 60 cyclones per winter. There is also a secondary maximum with up to

30 cyclones per winter over the Mediterranean region. All seasonal forecast systems generally capture this spatial distribution, but show slight discrepancies with the reanalysis regarding the absolute number of cyclones in some regions. ECMWF-S3 underestimates the number of cyclones over the whole Northern Hemisphere and has no secondary maximum over the Mediterranean. The ECMWF-S4 extratropical cyclone track density compares very well to the reanalysis. GloSea5 generally overestimates the number of cyclone events over the Northern Hemisphere with around 20% more cyclones in the North Atlantic storm track region. These climatological results change little if we consider only the 5% strongest cyclones for the same time period (Figure 5.2). The observed spatial distribution of the wind storm event track density also shows two climatological centres of activity over the North Pacific and the North Atlantic (Figure 5.3). Similar to cyclone track densities, both centres of activity are orientated southwest-northeast. The two main differences to the spatial distribution of cyclones are fewer wind storm events and an equatorward shift of around 1000km of the regions with most wind storms. The smaller number of wind storms compared to cyclones is due to the fact that for wind storms only events exceeding a specific intensity and size are taken into account (clustered extreme wind speeds above the 98th percentile). The southward shift of the maximum reflects that the highest wind speeds associated with northern hemispheric cyclones are typically located to the south of the pressure centre, along frontal zones. The spatial wind storm distribution is well-captured by all seasonal forecast models, with smaller biases (absolute and relative) for all models compared to cyclones and extreme cyclones.

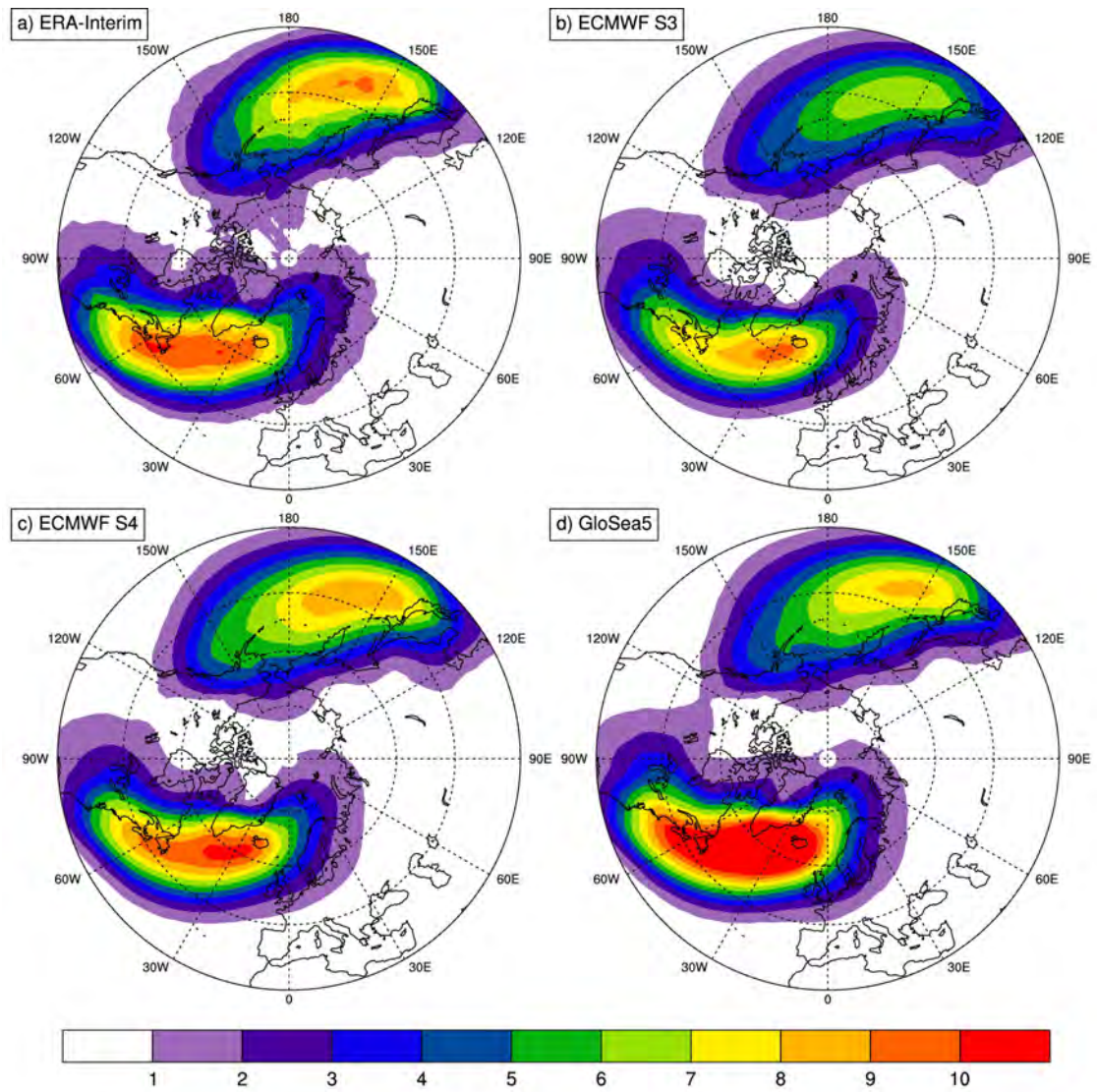


Figure 5.2: Track density of **extreme cyclone** events (> 95th percentile) per winter season (1992-2011)

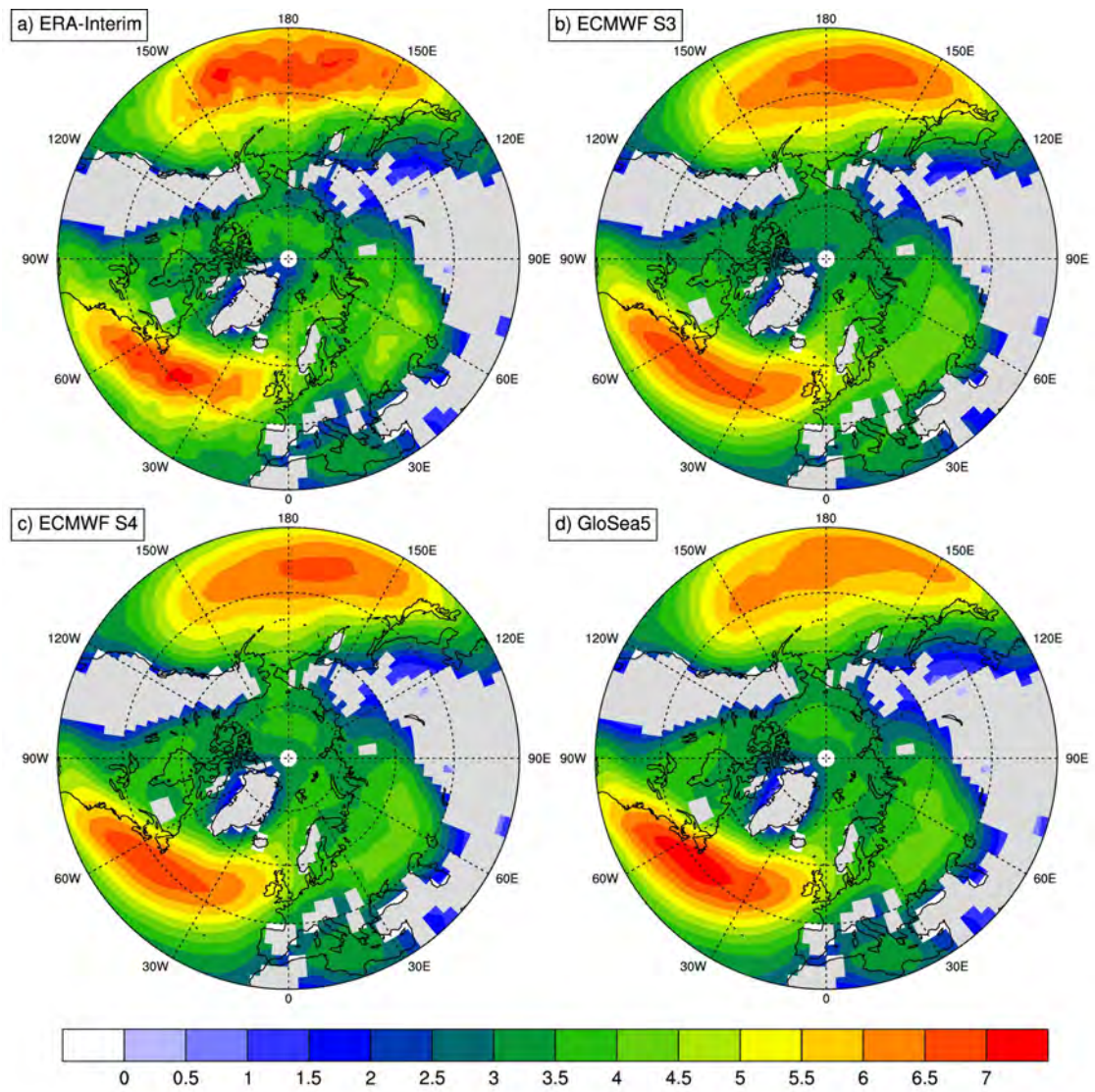


Figure 5.3: Track density of **wind storm** events per winter season (1992-2011)

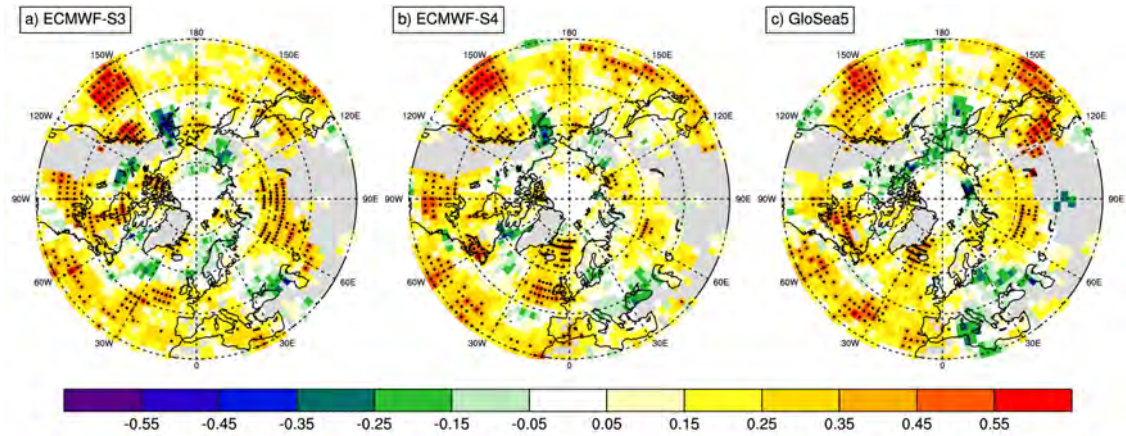


Figure 5.4: Kendall's τ_b rank correlation coefficient of annual track density of **all cyclones**, between ERA-Interim and: the hindcast data set labelled (1992- 2011). Stippling indicates the correlation is significantly non-zero at the 5% level

5.5 Forecasted Interannual Variability of Cyclones and Wind Storms in the Northern Hemisphere (direct method)

Temporal Variability

We assess the skill of forecasting the interannual cyclone and wind storm variability by correlating the number of events per winter with the reanalysis, at each grid point and for each model. We call this approach the direct method. The picture that emerges for all cyclones reveals several regions with high correlations across all models: in the eastern and western Pacific, in the majority of the stormtrack region in the Atlantic including parts of north-western Europe especially for ECMWF-S4 and in northern parts of the Atlantic especially in ECMWF-S4 and GloSea5 (Figure 5.4). The forecast skill for extreme cyclones is generally lower than that of all cyclones for most parts of the Northern Hemisphere (Figure 5.5). Significant correlations are found over the Bering Sea for all models, and small regions such as Eastern Scandinavia for ECMWF-S4, or a few grid points south-west of the British

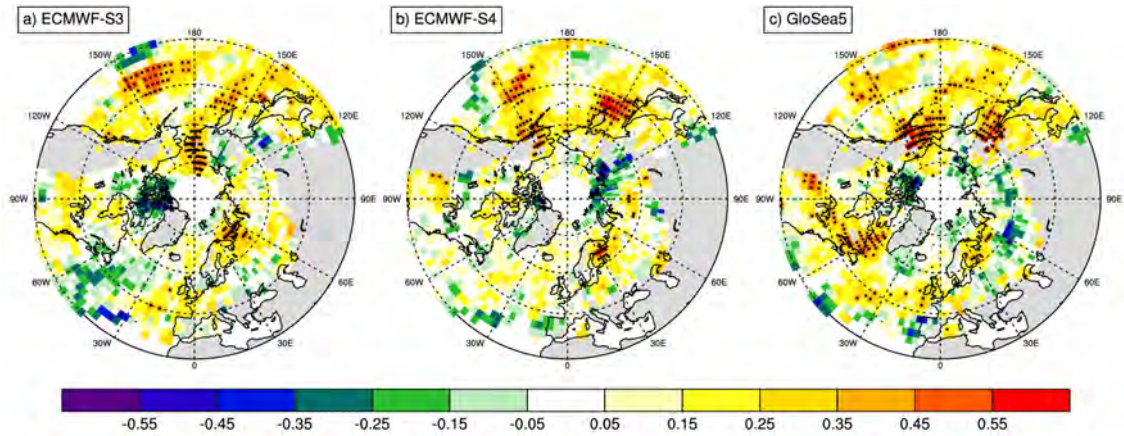


Figure 5.5: As figure 5.4 but for **extreme cyclones** (cyclones with a maximum Laplacian of the MSLP exceeding the northern hemispheric 95th percentile)

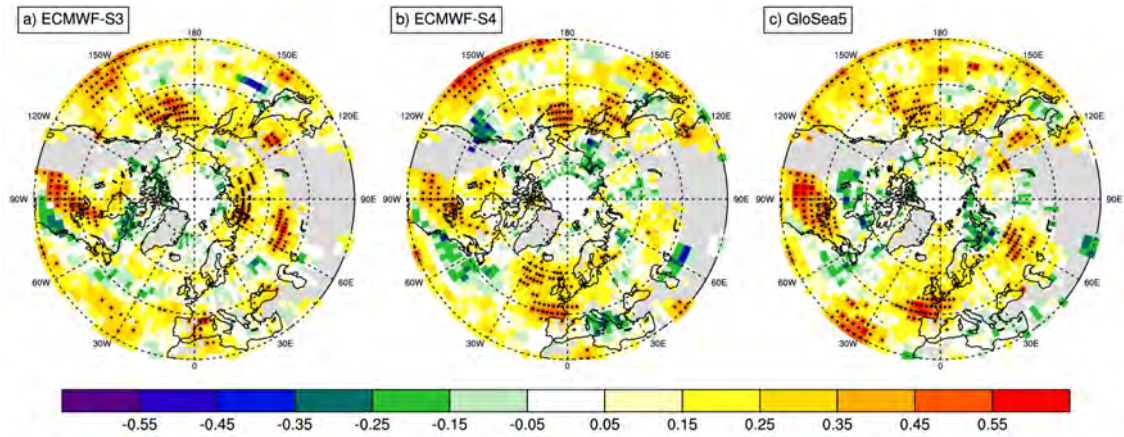


Figure 5.6: As figure 5.4 but for **wind storms** (defined as spatially organised clusters exceeding the 98th percentile in local wind speeds exceeding a minimum area and duration)

Isles and over the central/eastern Atlantic for GloSea5.

When comparing the skill of the models in forecasting the winter frequency of wind storms across the Northern Hemisphere, some common features are seen (Figure 5.6). ECMWF-S4 and GloSea5 show high and mostly significant correlations over the eastern North Atlantic and central Europe, which is particularly useful given the high damage potential in these areas. In addition, there are high correlations over parts of the northern Pacific and northern America, but slightly negative correlations over the western North Atlantic for all forecast systems.

Spatial Variability

To assess the models' ability to capture the inter-annual variability of the spatial track density patterns, the centred anomaly correlation coefficient (ACC; Wilks,(1995)) for the Atlantic sector (90°W-10°E, 20°-70°N) is calculated. For all cyclones it is found that the agreement of the models' ensemble mean spatial distribution of events per winter with ERA-Interim is strongly dependant on the year under consideration (Figure 5.7a). Overall, ECMWF-S4 shows the highest mean ACC over the time period analysed. In some years the value of the ACC exceeds 0.4 in ECMWF-S4 and GloSea5, while in other years the models fail to capture the reanalysis' cyclone spatial distribution. ACC time series for extreme cyclones show higher year-to-year fluctuations than for all cyclones, indicating that the forecast skill in predicting the spatial pattern is more variable (compare Figure 5.7a & Figure 5.7b).

Regarding wind storm events, we find years with both high and low agreement when comparing to reanalysis (Figure 5.7c). The overall temporal mean of ACC values is similar to the one found for all cyclones and higher than for extreme cyclones, with GloSea5 a slightly higher mean ACC than the other two models.

To compare the models more directly we used one of the models as reference instead of ERA-Interim as done previously. Here, we made the arbitrary choice of the ECMWF-S4 ensemble mean (GloSea5 or ECMWF-S3 could equally have been used). The analysis reveals that for all cyclones there is a slightly higher agreement between the models than the models show with the reanalysis (compare Figure 5.7a & Figure 5.7d). Interestingly, ACC values are notably higher in the last analysed decade compared to the first decade for GloSea5. For extreme cyclones, we also find temporal means of the ACC values being increased if ECMWF-S4 replaces ERA-Interim, again suggesting higher agreement amongst the models (Figure 5.7d & Figure 5.7e). The apparent opposing values in the first 10 years or so between

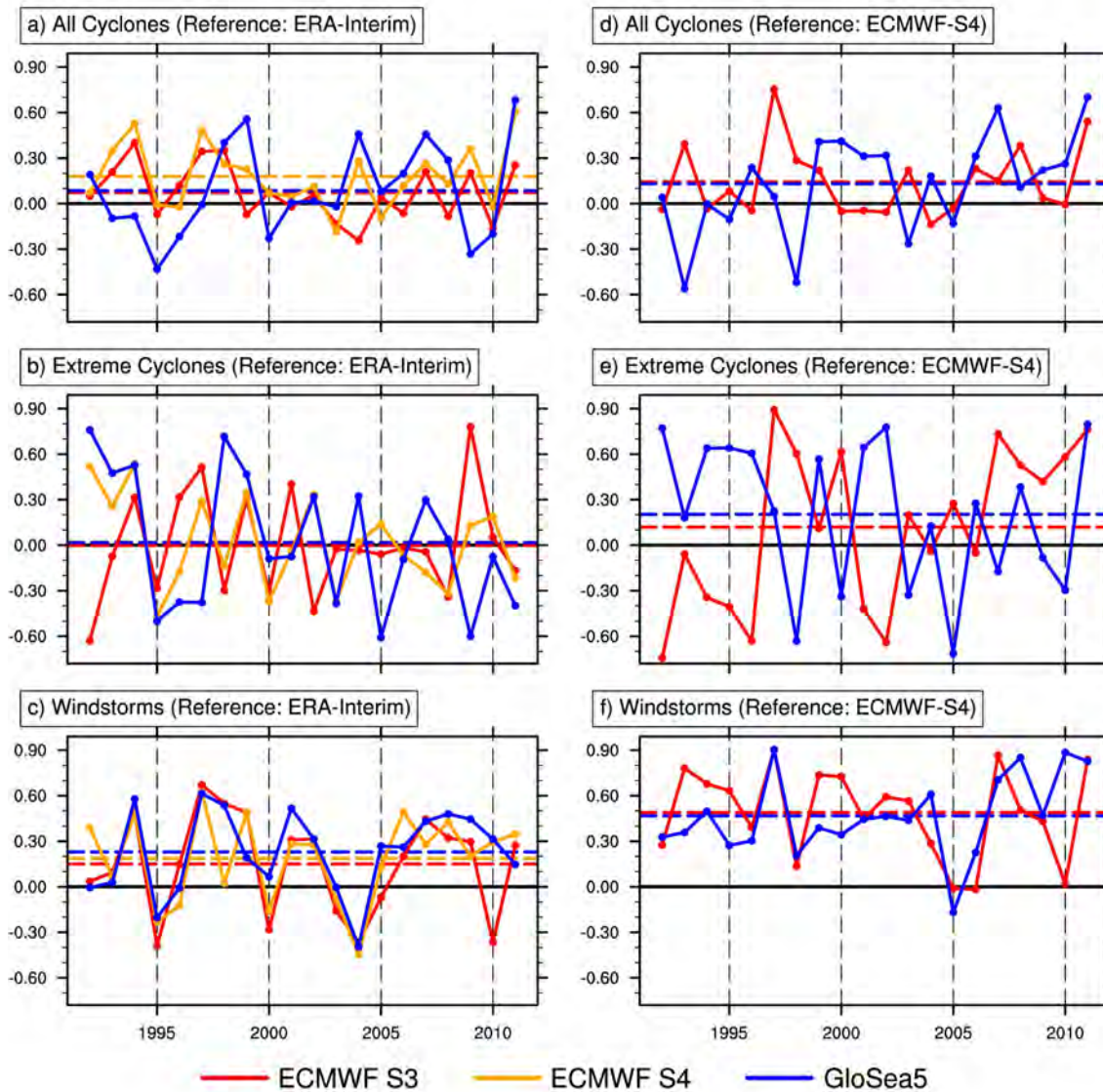


Figure 5.7: Centred anomaly correlation coefficients of track density over 90°W - 10°E , 20° - 70°N , for all cyclones (a and d), extreme cyclones (b and e) and wind storms (c and f). Spatial correlations are calculated as anomalies from long-term averages of the respective reference data set (left column: ERA Interim; right column: ECMWF System4). Mean correlations for the period 1992-2011 are indicated with dashed lines.

the ACC values of ECMWF-S3 and GloSea5 in Figure 5.7e are due to opposing trends of extreme cyclones over the North Atlantic (not shown). The number of extreme cyclones in ECMWF-S3 is primarily increasing from 1992 to 2011 over the North Atlantic, especially around the southern tip of Greenland with values greater than one cyclone per decade or about 10 to 20%. Extreme cyclones show however largely a negative trend in ECMWF-S4 and GloSea5 with a trend maximum in the area of maximum storm track activity in both data sets. The trends are smaller in magnitude in ECMWF-S4 and GloSea5 than in ECMWF-S3, especially in relative terms to the model mean. Anomalies of ECMWF-S3 can therefore have a different sign to anomalies of ECMWF-S4 or GloSea5. We follow here the ACC calculation of Wilks (1995) without a removal of the long-term trend leading to opposing ACC values in such a case.

The impact of using ECMWF-S4 as reference in contrast to ERA-Interim is largest for wind storm events. The temporal average of the ACC value is about 0.2 if using ERA-Interim as reference, and this increases to about 0.5 if using ECMWF-S4 (compare Figure 5.7c & Figure 5.7f).

5.6 Forecasted Interannual Variability of Wind Storms derived using the NAO for the North Atlantic/European Region (indirect method)

The North Atlantic Oscillation (NAO) is the most prominent variability pattern in the North Atlantic/European region, with a substantial influence on winter wind storms on various time scales (Hurrell and Deser, 2009; Pinto et al., 2009; Donat, Leckebusch, Pinto and Ulbrich, 2010; Renggli, 2011). UK Met Office seasonal hindcasts of the winter mean NAO have recently shown promising results (Scaife et al., 2014; Scaife et al., 2016). Consequently, in this section we forecast the

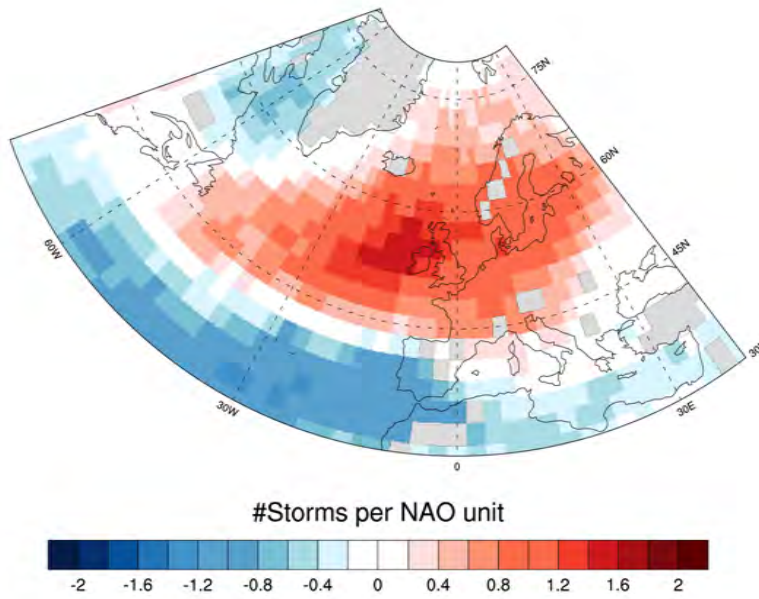


Figure 5.8: Regression slope of wind storm track density regressed onto station-based winter mean NAO derived from ERA-Interim

variation in winter wind storm frequency using the models' forecast of the NAO and the observed relationship between the NAO and wind storm frequency (derived from ERA-Interim). We call this statistical approach using the NAO as the predictor, the indirect method.

The NAO index is calculated according to the station-based definition used by Hurrell (1995) based on the geographical locations of Ponte Delgada, Portugal (22.7°W, 37.8°N) and Keflavik, Iceland (22.6°W, 64.0°N). We firstly calculate the ensemble mean MSLP for each winter and then bi-linearly interpolate to the above coordinates. Next, each time series at the two points is normalised by their local mean and standard deviation, prior to calculating the difference of both. The highest correlation between forecasted and observed NAO (derived from ERA-Interim) is found for GloSea5 (correlation coefficient of 0.62), followed by much smaller correlations for ECMWF-S3 (0.27) and ECMWF-S4 (0.24).

The regression map of wind storm track densities onto the interannual NAO calculated from ERA-Interim reveals a dipole structure, with a nodal line around 45°N (Figure 5.8). The positive wind storm response shows a maximum west of

Ireland of around 2 more storms per winter for each NAO unit, and affects most of northern and parts of central Europe. The negative response is primarily located over the southern parts of the North Atlantic (south of 40°N), and affects to a lesser extent the Mediterranean region [U+2500] predominantly its western part. The NAO has no effect on interannual wind storm variability in between these two nodes.

The correlation maps of ERA-Interim track densities and NAO-predicted track densities from the three seasonal forecasts (indirect approach) show principally similar patterns, with positive skill over large parts of the North Atlantic and western Europe in ECMWF-S4 and GloSea5 (Figure 5.1e-f). The skill in ECMWF-S3 is lower in comparison to both these models in the entire north Atlantic region (Figure 5.1d). Regarding the spatial skill pattern, we find overall good agreement between the direct and indirect approach in predicting wind storms in the north Atlantic sector. There are, however, regional quantitative differences of skill, as shown by the correlation coefficient differences (Figure 5.9g-i). The direct method performs better along a latitudinal band from around 40° to 50°N over the eastern north Atlantic and central western Europe. This can be mainly explained by the small impact of NAO variability onto wind storm variability over this region (see Figure 5.8), leading to a less skillful prediction compared to directly detecting wind storms (direct approach).

In the cyclogenesis region east of the North American continent, the indirect approach shows higher (but mostly not significant) skill for all hindcasts. Furthermore, the indirect method also adds a small amount of skill over the North Sea in ECMWF-S4 and GloSea5, and west of the British Isles in GloSea5. In summary, in all forecast systems, the direct method typically shows higher (significant) skill in forecasting winter storm frequency in central-western Europe, whilst the NAO approach slightly improves skill over north-western Europe.

Interestingly, the indirect approach performs only slightly better in GloSea5

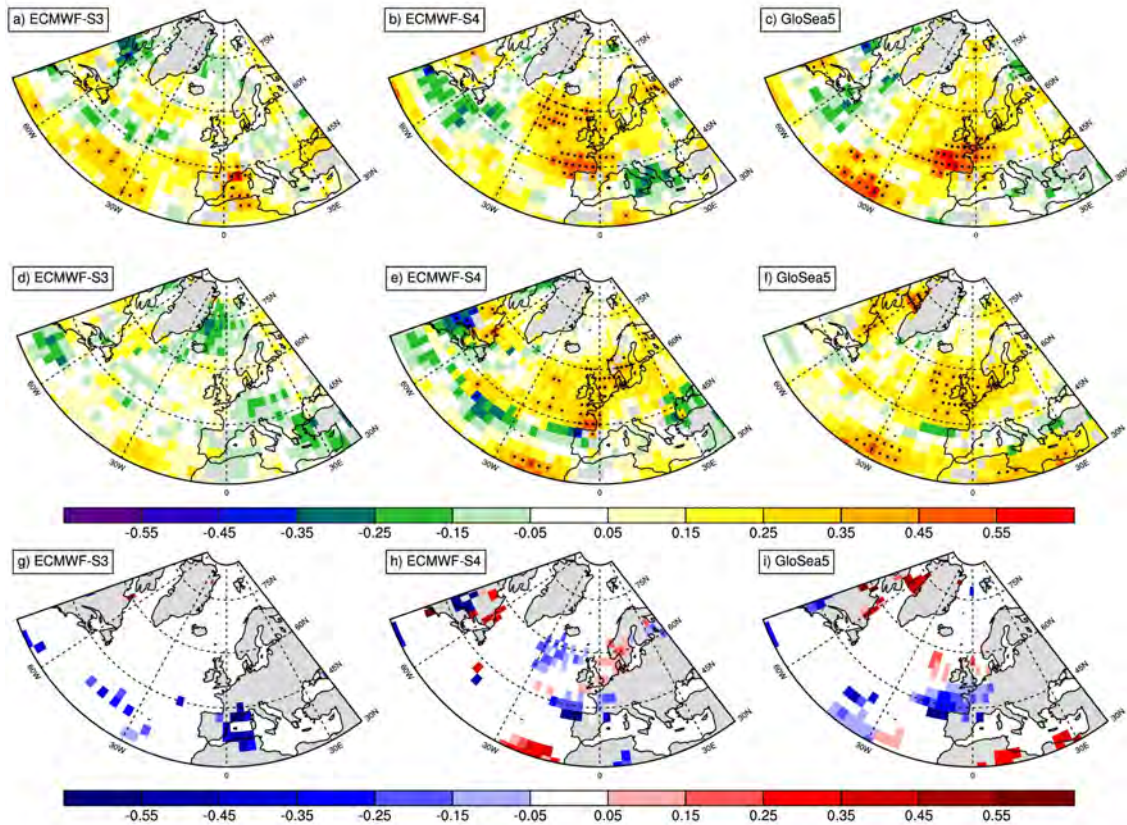


Figure 5.9: Kendall's τ_b rank correlation coefficients of wind storm frequency between ERA-Interim and seasonal forecast models. First row (a-c): Wind storm frequency using the direct method (as in Fig.5.3). Second row (d-f): Wind storm frequency in seasonal models predicted from NAO regression (indirect method). (g-i): Difference of correlation values (Second minus first row; only grid boxes where either method has significant skill). Blue/red: direct/indirect method respectively has higher skill.

compared to ECMWF-S4 even though the forecast skill of the NAO index is much higher in GloSea5 than it is in ECMWF-S4. This could reflect the importance of other large-scale variability modes in driving wind storm activity over Europe (see discussion), but also be related to the small NAO signals in GloSea5 predictions (low signal-to-noise ratio, Scaife et al.,(2014)).

5.7 Summary and Discussion

In this study, we have analysed the climatological representation and seasonal prediction skill of wintertime extra-tropical cyclones and wind storms in a three ensemble-based seasonal prediction systems. In addition to investigating the skill of predicting the winter frequency of extra-tropical cyclones, this is the first study to explicitly investigate the capability of such models to forecast wind storm impact – through assessing near-surface, damage-relevant winds.

The main features of the long-term mean spatial distribution of both extra-tropical cyclones and wind storms are well represented in each of the models, across the Northern Hemisphere, although some regional biases are seen. Wind storms often result from strong and deep cyclones. Our results show differences in the regions where cyclone and wind storm frequency is skillfully predicted, which highlights the benefit of analysing both measures independently; otherwise, skillful winter predictions might be underestimated or vice versa. In the direct approach (by detecting cyclones and wind storms), the seasonal prediction systems all generally show small to moderate positive (and often significant) skill for all analysed quantities in many parts of the Northern Hemisphere. Skill values are generally higher for all cyclones and wind storm events than for extreme cyclones, supporting the approach of detecting wind storms directly to derive information on extreme events and damage. For wind storms the regions of positive and negative skill are at similar locations between the three model suites. In addition to these spatial

similarities in skill between the models, we also find temporal similarity across the models in the pattern correlation of the storm frequency with the observations over the Atlantic basin. These temporal similarities are especially pronounced for wind storms.

The temporal similarities between the models may indicate that the predictability of wind storm activity is higher for some seasons compared to others and that this season-dependant predictability is model independent. Higher predictability could further reflect physical processes linked to wind storm frequency, which are especially pronounced in specific seasons. In this case, our results suggest that these relevant physical processes are represented similarly in the three different model suites.

Scaife et al. (2014) have recently shown that the GloSea5 seasonal prediction system can generate skillful NAO forecasts with a correlation skill higher than 0.6. Consequently, we also examine whether an NAO based regression model can be used for the seasonal forecast of wind storms in the North Atlantic region, making use of the observed relationship between the NAO and wind storm frequency in reanalysis data. For most regions with significant skill in either method, the direct outperforms the indirect approach. The indirect statistical approach can improve upon the direct method in some regions, e.g. around the North Sea. However, as expected, the results show lower skill along the nodal line of the NAO including most central western European countries when compared to the direct approach (where actual wind events are directly identified from wind speeds). We thus conclude that the NAO is a useful predictor of interannual variability of European wind storms north of its nodal line in current seasonal forecast models. As the indirect and direct method reveal different areas with positive significant skill, a combination of both approaches would optimise the forecast skill for wind storms over Europe. However, if the NAO is used as the sole predictor for European wind storms forecast

skill would be lost in regions along its nodal line (from around 40° to 50°N) including regions with large damage potential due to storminess. Further investigations into which processes other than the NAO, affect wind storm frequency on seasonal timescales in Western Europe are necessary. In particular, the East Atlantic (EA) pattern may play an important role: Woollings et al. (2010) showed that the EA has a large effect on the latitude of the North Atlantic jet stream position, which can steer cyclones and wind storms. Mailier et al. (2006) also found that the EA was more important than the NAO in explaining monthly variability in winter cyclone counts on the southern flank of the North Atlantic storm track, over an area coincident with the nodal line of the NAO. This is also supported by findings from Walz et al. (2018), who showed that the EA pattern strongly influences wind storm activity between nodes of the NAO. Currently, further analysis is carried out to clarify in how far the EA pattern is responsible for the skill in central western Europe found in ECMWF-S4 and GloSea5. It should be further mentioned, that the skill measure is based on correlation coefficients only, however, the amplitude of the prediction is also important to judge its usefulness.

Our results appear promising overall and corroborate the emerging evidence of predictability on seasonal time scales regarding extra-tropical cyclones and wind storms (Renggli, 2011; Riddle et al., 2013; Scaife et al., 2014; Smith et al., 2016). Our analyses extend these recent studies by considering different seasonal prediction systems. Using identification and tracking algorithms, we are further able to assess the frequency of extreme extra-tropical cyclones and wind storms directly rather than deriving these quantities by distribution quantiles. Our results suggest that ECMWF-S4 has a more realistic representation of the climatological frequency of extra-tropical cyclones and wind storms compared to the other models. However, with respect to forecast performance over the Eastern Atlantic/Western Europe, both: GloSea5 and ECMWF-S4 reveal significant skill in forecasting wind storm events on seasonal time-scales, with higher values as found for extreme extra-tropical

cyclones.

While the forecast skill of the three systems is similar both for all cyclones and for extreme cyclones, the performance of both ECMWF-S4 and GloSea5 is superior to ECMWF-S3 for wind storms, especially over the Eastern Atlantic/Western Europe. One reason might be the configuration of the multi-member ensembles, e.g. the number of members, or how they are initialised. As we do not explicitly address the influence of the ensemble size on the results in this study we cannot definitively quantify the benefit of more members. The higher skill for ECMWF-S4 compared to ECMWF-S3 might also reflect improvements caused by model development (S4 uses a newer model version than S3) and the higher horizontal resolution of ECMWF-S4 compared to ECMWF-S3. Better representation of relevant processes linked to extra-tropical cyclone and wind storm frequency may be a further reason for quantitative differences in skill.

It is important to note that the time period used in this study is limited to 20 years (1992/93-2011/12) due to the fact that GloSea5 hindcasts were produced for these years only. Both ECMWF-S4 and ECMWF-S3 are available for longer time periods, e.g. from 1982 onward in case of ECMWF-S4. Our results show that the skill for wind storms in ECMWF-S4 decreases if using the years 1982 to 2011 compared to using 1992 to 2011, whereas the general skill pattern remains similar. Further analyses are needed to explain the reason for this decrease in skill for ECMWF-S4 when using the longer hindcast period.

The striking similarities in the anomaly correlation coefficients for North Atlantic/European wind storms between the different model suites once more raises the question of which processes are responsible for seasonal variability and the extent to which these are captured by the models. Potential drivers of winter storm variability include a horseshoe-like sea surface temperature anomaly pattern in the north Atlantic a few months ahead of the winter season (Renggli, 2011) and an

increased meridional surface temperature gradient in the west Atlantic cyclogenesis region (Wild et al., 2015). Besides these oceanic drivers, further analysis is needed to quantify the role of atmospheric large-scale variability modes in steering wind storm variability in current seasonal forecast suites (as done by Walz et al., 2018b for the European continent).

Further research to improve our understanding of such drivers of seasonal variability will be essential and ultimately pave the way to successfully predicting whether a calm or severe storm season lies ahead.

VARIABILITY OF WIND STORM
FREQUENCY IN RELATION TO SEA
SURFACE TEMPERATURES UP TO SEVEN
MONTHS AHEAD

6.1 Potential Predictability on Seasonal Scale

In the previous chapter 5 the question emerged where the predictive skill for wind storm frequency in the seasonal models originates. Which process or mechanism(s) are responsible for turning the predictability of the real world into predictive skill in the models? In short: what do the models get right? This in turn raises the question about the seasonal predictability of the real world. In short: what is there to get right? In the case of extra-tropical cyclones and wind storms there remains lots to be investigated about both of these questions.

The existence of relatively slow and predictable variations of boundary conditions on land such as snow cover and soil moisture (Shukla and Kinter, 2006; Doblas-Reyes et al., 2013)), on and in the ocean including sea-ice (ibid.) and stratospheric variability (Scaife et al., 2016; Hansen et al., 2017) are a necessity for successful seasonal predictions. The seasonal time scale can be further considered externally forced by even lower frequencies of climate variables, primarily temperature, due

to human-induced influence on aerosol and greenhouse gas concentrations as well as land use changes and natural variations in e.g. volcanic aerosol or solar activity (Doblas-Reyes et al., 2013).

Besides the interaction through air-sea heat and momentum fluxes, the coupling between oceans and the atmosphere is on the ocean side strongly dependent on the SST which is in turn influenced by heat transport through ocean currents, vertical mixing and boundary layer depth. On the atmospheric side numerous variables play an important part in the coupling such as wind speed, temperature, and humidity (Deser et al., 2010). The oceans, i.e. H_2O , has a greater heat capacity than atmospheric gases and therefore a longer memory than the atmosphere. This memory can also include an atmospheric signal. In the tropics the ocean dominates the coupling and has generally a stronger influence on the atmosphere than vice versa (Smith et al., 2016). The most pronounced signal of climate variability stemming from the ocean is the ENSO phenomenon (Anderson, 2008). To what extent ENSO or Pacific SST variability in general influences the atmospheric conditions in the North Atlantic region has been discussed in literature for some time (Scaife et al., 2017; van Oldenborgh et al., 2015; Frías et al., 2010). See also the next chapter 7 for the influence of Pacific SST on winter wind storm climate over the North Atlantic and Europe. In the extra-tropics convection above the ocean is much shallower and releases less energy than in the tropics. It is therefore more the atmosphere that imprints a signal on the ocean or SST in the mid-latitudes (Kushnir et al., 2002). Atmosphere-induced SST anomalies are primarily generated by turbulent heat exchanges (Gastineau and Frankignoul, 2014; Deser et al., 2010) at least in the North Atlantic region. The NAO as the most dominant atmospheric mode over the North Atlantic in its positive phase is followed by positive SST anomalies in the western subtropical North Atlantic. A negative NAO is followed by negative SST anomalies in the northern North Atlantic and off the western coast of West Africa. This SST anomaly pattern is also referred to as the North Atlantic

Tripole (Gastineau and Frankignoul, 2014; Czaja and Frankignoul, 1999) or NAT in short. The highest covariance is found when the atmosphere leads the SST by about two to three weeks up to (Deser and Timlin, 1997), around one month (García-Serrano et al., 2008) or around two months (Gastineau and Frankignoul, 2014).

There is however observational evidence of oceanic influence on the atmosphere on spatial scales of around 100km (Chelton et al., 2004) not only limited to the boundary layer but reaching up to tropopause-level (Minobe et al., 2008; Czaja and Blunt, 2011). There is further evidence in observations that a weak but significant covariability exists in early winter over the North Atlantic when the SST leads by about 4 to 5 months (Czaja and Frankignoul, 1999; Czaja and Frankignoul, 2002; García-Serrano et al., 2008; Rodwell and Folland, 2002; Gastineau and Frankignoul, 2014). These findings are corroborated by modelling studies (Peng et al., 2002; Cassou et al., 2004; Deser et al., 2007).

SST anomalies resembling a horseshoe or crescent shape pattern in late summer and early autumn (see also figure 6.1) can be related to geopotential height anomalies in the subsequent winter (Czaja and Frankignoul, 2002). The pattern is often referred to as the North Atlantic Horseshoe or NAH. The proposed causal chain e.g. by (Gastineau and Frankignoul, 2014) can be summarised as follows: NAH \rightarrow NAO \rightarrow NAT. While this potential causal chain could be even extended further back (García-Serrano et al., 2008) the focus of this chapter is on the NAH as a potential source of predictability in the North Atlantic region for winter wind storm frequency.

In line with the two short questions raised at the beginning of this introduction the main objectives of this chapter are:

- What is the explained variability of winter wind storm frequency through the North Atlantic Horseshoe (NAH) pattern?
- What are the physical mechanism linking the SST and wind storms?

A complete answer of the second question might be somewhat overambitious, but this chapter aims to identify at least some plausible physical link between SST and wind storm.

The approach followed in this chapter is to analyse the influence of the Horseshoe pattern on atmospheric growth conditions for extra-tropical cyclones as in chapter 3 in ERA-Interim Reanalysis in the section 6.2 and in AMIP-type sensitivity experiments using the AGCM ECHAM5 in the section 6.3. Each section has its own summary. The chapter ends with an overall discussion.

6.2 North Atlantic Horseshoe Pattern and Wind Storm Frequency in ERA-I

Definition of the Horseshoe-Index

Following the analyses of Renggli (2011) the Horseshoe pattern can be described with the so-called *Horseshoe Index (HSI)*. It is based on three centres of high interannual correlation of the SST from August to October and the number of wind storms in the Northeastern North Atlantic and European region in the core winter months December until February (figure 6.2). The number of wind storms is the sum of events crossing the region from 45°W to 20°E and 45° to 70°N, while every event is only taken into account once. There is no weighting with respect to

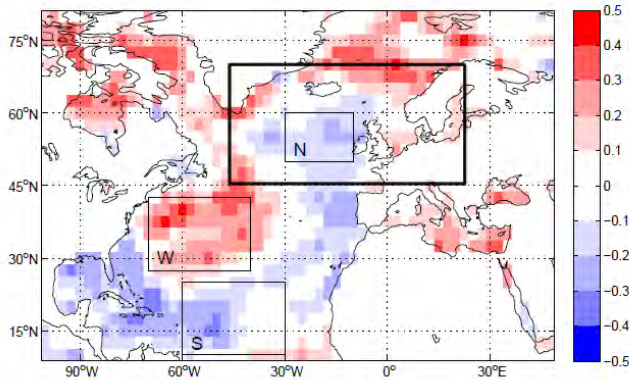


Figure 6.1: Figure 4.1a from Renggli (2011): Spearman correlation coefficient between SST in ASO and wind storm frequency in subsequent DJF in ERA-40 from 1959-2001. Black box added retrospectively

the affected area and the duration of an event in the box or the intensity of the storm. The HSI is calculated as given in equation 6.1:

$$HSI = \overline{SST}_W - \frac{1}{2}(\overline{SST}_N + \overline{SST}_S) \quad (6.1)$$

with \overline{SST}_X as the area weighted field mean of three regions (SST_W : 70° - 40°W, 27.5° - 42.5°N; SST_N : 30° - 10°W, 50° - 60°N; SST_S : 60° - 30°W, 10° - 25°N; figure 6.2).

The correlation pattern resembles a horseshoe - hence the name - with positive correlations in the western North Atlantic with a maximum around 60°W and 35°N surrounded by negative correlations stretching from the Caribbean Sea eastwards to the coast of West Africa and then northwards until about 60°N just off the coast of the British Isles. The location of the boxes for the HSI follows the definition of Renggli (2011) based on analyses with ERA-40. The boxes are centred in areas of strongest correlations (anticorrelations) in the ERA-40 data set but their size and exact borders remain arbitrary.

The correlation between SST in ASO and the number of wind storms in the following DJF in ERA-Interim also resembles a horseshoe, albeit with differences to the correlation pattern in ERA-40. The correlation patterns between ERA-40 and ERA-Interim match well over most parts of the North Atlantic when considering the years from 1979 to 1999. The main difference are negative correlations which

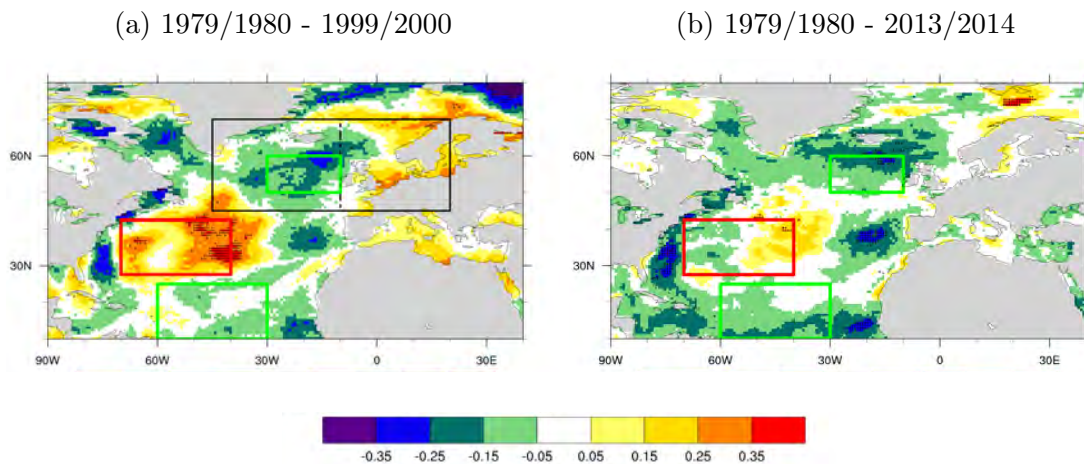


Figure 6.2: Kendall's τ_b correlation coefficient between SST averaged over ASO and accumulated number of wind storms over $45^\circ\text{W} - 20^\circ\text{E}$ and $45^\circ - 70^\circ\text{N}$ (black box) summed up over DJF for two different time periods. Dots show significance at 5% level. Red and blue boxes indicate areas for the calculation of the HSI.

appear along the Eastern North American coast in ERA-Interim and are not present in ERA-40. The correlation patterns match less well when also the years until 2013 are taken into account. The positive correlations in the Western North Atlantic are reduced and shifted eastwards and are partly replaced by negative correlations. The negative correlations as part of the horseshoe remain similar (figure 6.2b).

Lead lag Correlations between the HSI and Wind Storm Frequency in ERA-I

The accumulated number of wind storms in the region $10^\circ\text{W} - 20^\circ\text{E}$ and $45^\circ - 70^\circ\text{N}$ (eastern part of the black box in figure 6.2a) in DJF and the HSI correlate strongest and significantly when the HSI leads by three to four months when only the years from 1979 to 1999 are considered (figure 6.3 blue line). Starting at one year lag between the HSI and the number of wind storms, correlation values gradually increase when the lead time of the HSI is decreased until a significant maximum of 0.55 is reached for a lead time of three months. Shorter lead times up to concurrent

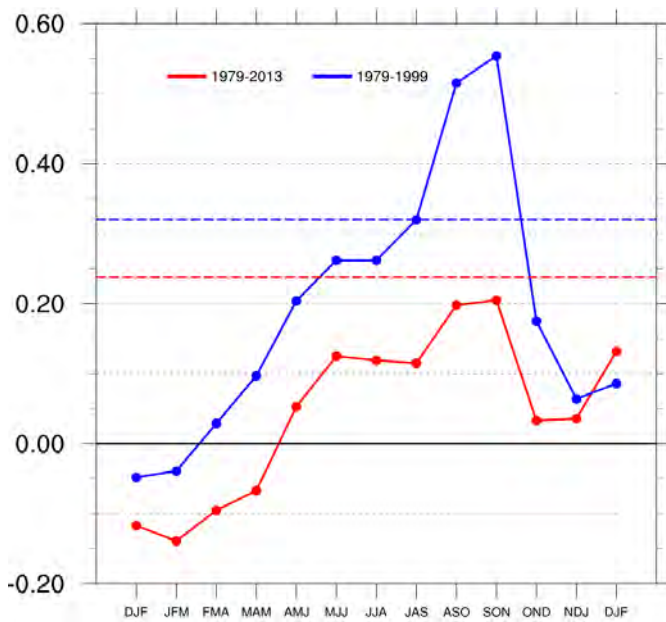


Figure 6.3: Lead lag Kendall's τ_b correlation between HSI and accumulated number of storms in $10^{\circ}\text{W} - 20^{\circ}\text{E}$ and $45^{\circ} - 70^{\circ}\text{N}$ for two different time periods in ERA-Interim. Lead time of HSI ranges from 12 months at the furthest left to 0 months at the furthest right. Stippled horizontal lines indicate 5% significance level.

correlations reveal a sharp reduction in correlation to non-significant values. These results corroborate Renggli (2011) with two small differences: i) the concurrent correlation between HSI and wind storm numbers is stronger and significant in the ERA-40 data set from 1958 to 2001 and ii) the maximum correlation is reached for lead times of four months instead of the three months here. The wind storm region is smaller compared to Renggli (2011) and can be considered more impact orientated. The difference in size of the region affects the results only marginally. When the years from 1979 to 2013 are considered the correlation values between the HSI and the number of wind storms are reduced for all lead times except for the concurrent correlation (figure 6.3 red curve). The shape of the curve remains similar with strongest correlations for lead times of three to four months but none of the correlations are significant. Longer lead times for the HSI also result in lower correlation values.

This dependency on the correlation time period is also apparent when the relation between HSI and NAO is analysed. While the HSI in late summer and autumn strongly and significantly correlates with the NAO in the subsequent winter in the

years 1979-1999, this relation completely disappears when only the years from 2000 to 2014 are considered (figure 6.4). Such a dependency on the time period has not been found for the correlation between HSI and wind storm frequency or NAO respectively in Renggli (2011) nor has it been shown for the Horseshoe pattern (NAH) in general in other previous studies.

It is worth mentioning that the point in time when the correlation between HSI and wind storm frequency or NAO declines or vanishes, happens to be around the time when the ERA-40 data set ends. Besides a physical reason in the atmosphere-ocean system, the possibility of a statistical artefact needs to be considered. The definition of the HSI is entirely based on the work by Renggli (2011) and based on ERA-40. A possible explanation for the time-dependent relation between HSI and wind storm frequency and HSI and NAO breakdown could be an overfitting to the ERA-40 data. Overfitting occurs when a function is too closely fit to a limited set of data points. In the case here, this would mean that the choice of the HSI is not general enough and too specific to the ERA-40 data set or its covered time period. The additional years from 2001 to 2014 from ERA-Interim which are not used for the fitting of the function do not show the previously identified relation and thus show a common symptom of overfitting: a correlation in the *fitting* period but no correlation in the *testing* period.

Influence of the HSI on atmospheric growth factors for the intensification of ETCs in ERA-I

The previous section 6.2.1 shows the relation of the HSI and wind storm frequency over Europe and the NAO respectively which is significant at least for the end of the 20th century. In this section the influence of the SST and in particular the HSI on factors for the intensification of ETCs is investigated. This refers to the second

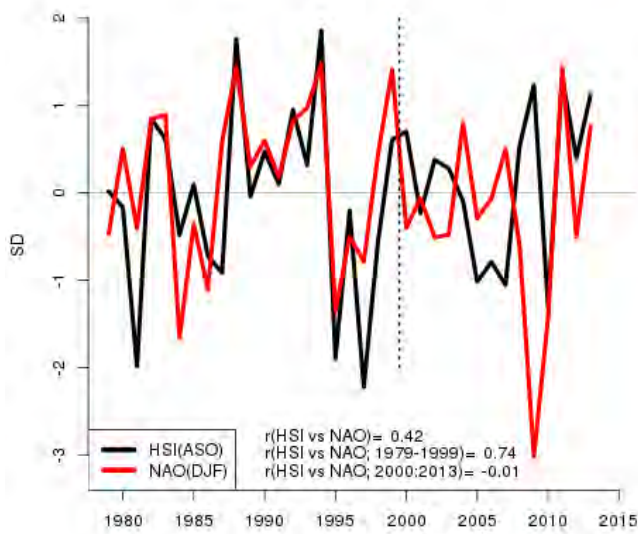


Figure 6.4: Normalised time series of the HSI averaged over ASO from 1979-2013 in ERA-Interim (black curve) and NAO averaged over DJF from 1979/1980 to 2013/2014 as taken from NOAA CPC (red curve). Kendall's τ_b correlation values between the two indices are given for the whole time period and two parts of the time series divided by the vertical dashed line.

objective of this chapter. The analysed variables and quantities correspond to the growth factors in chapter 3, described in 2.3. Composite differences as explained in 2.2.6 are used to quantify the influence of the HSI on the different growth factors. Only years with HSI anomalies greater than one standard deviation are taken into account, corresponding to about one third of all years of the overall time period from 1979 to 2014. The years for strong positive HSI are 1988, 1994, 2009, 2011, and 2013 and years with strong negative HSI are 1981, 1995, 1997, 2005, 2007, and 2010. Note, that these years are either side of 1999/2000 the point in time when the relation between HSI and wind storm frequency is strongly reduced. Composite differences for the jet in 200hPa, equivalent potential temperature in 850hPa, and Maximum Eady Growth Rates in the upper and lower troposphere are shown in Figures 6.5 to 6.7. Their results are summarised in the tables 6.1 to 6.3.

The Maximum Eady Growth Rate is a quantity to measure the potential of baroclinic waves to grow (Hoskins and Valdes, 1990). Wave amplitudes of baroclinic waves with wavelength on the synoptic scale or below can therefore be expected to be greater when the Maximum Eady Growth Rate shows positive anomalies. Considering only years with strong positive HSI anomalies the FFT decomposition

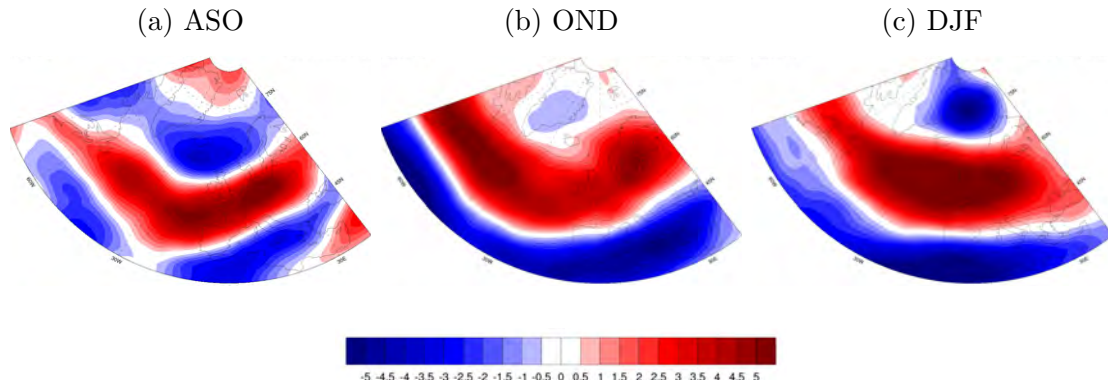


Figure 6.5: Composite differences for zonal wind in 200hPa in ms^{-1} . Average of strong positive HSI minus average of negative HSI years for three three-months averages.

ASO	OND	DJF
<ul style="list-style-type: none"> • Enhanced over North Atlantic in a latitudinal band between $40^{\circ}N$ and $60^{\circ}N$ • Negative anomaly around Iceland 	<ul style="list-style-type: none"> • Enhanced over North Atlantic in a latitudinal band between $40^{\circ}N$ and $60^{\circ}N$ • Anomalies stronger than in ASO • Maximum over Newfoundland and Scandinavia 	<ul style="list-style-type: none"> • Enhanced over North Atlantic in a latitudinal band between $40^{\circ}N$ and $60^{\circ}N$ • Anomalies stronger than in ASO and OND and more zonal • Maximum from 30° - $0^{\circ}W$ along $50^{\circ}N$

Table 6.1: Horseshoe composite differences for zonal wind in 200hPa

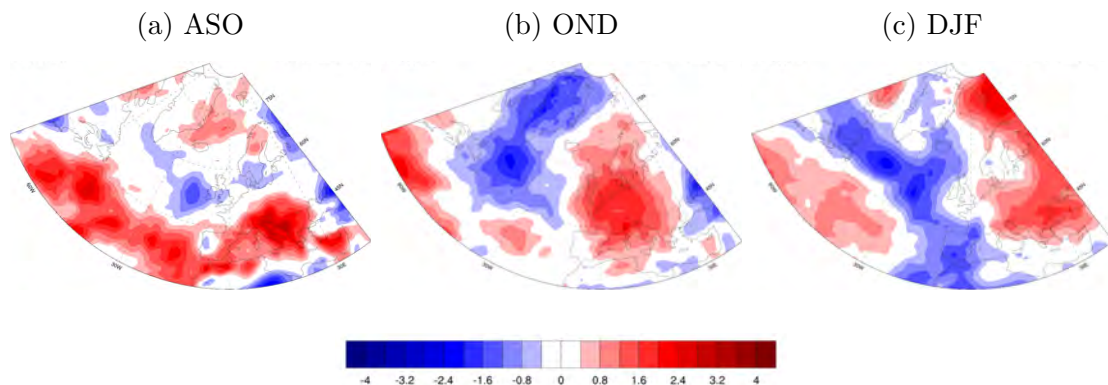


Figure 6.6: Composite differences for equivalent potential temperature in 850hPa in Kelvin. Average of strong positive HSI minus average of negative HSI years for three three-months averages.

ASO	OND	DJF
<ul style="list-style-type: none"> • Positive anomalies in a zonal band south of 45°N from North America to Europe • Maximum over Adriatic Sea • Slight negative anomalies west of British Isles in region of Northern HSI box and over Greenland 	<ul style="list-style-type: none"> • Strong East – West divide of anomalies with meridional nodal line around 20°W • Strong positive anomalies over all of Europe with maximum over North Sea • Strong negative anomalies reaching until about 45°N with maximum over Greenland 	<ul style="list-style-type: none"> • East-West divide shifted eastward with slight NW-SE tilt in axis • Negative anomalies from Greenland towards Spain and North Africa • Slight positive anomalies over Western North Atlantic south of 45°N

Table 6.2: Horseshoe composite differences for equivalent potential temperature in 850hPa

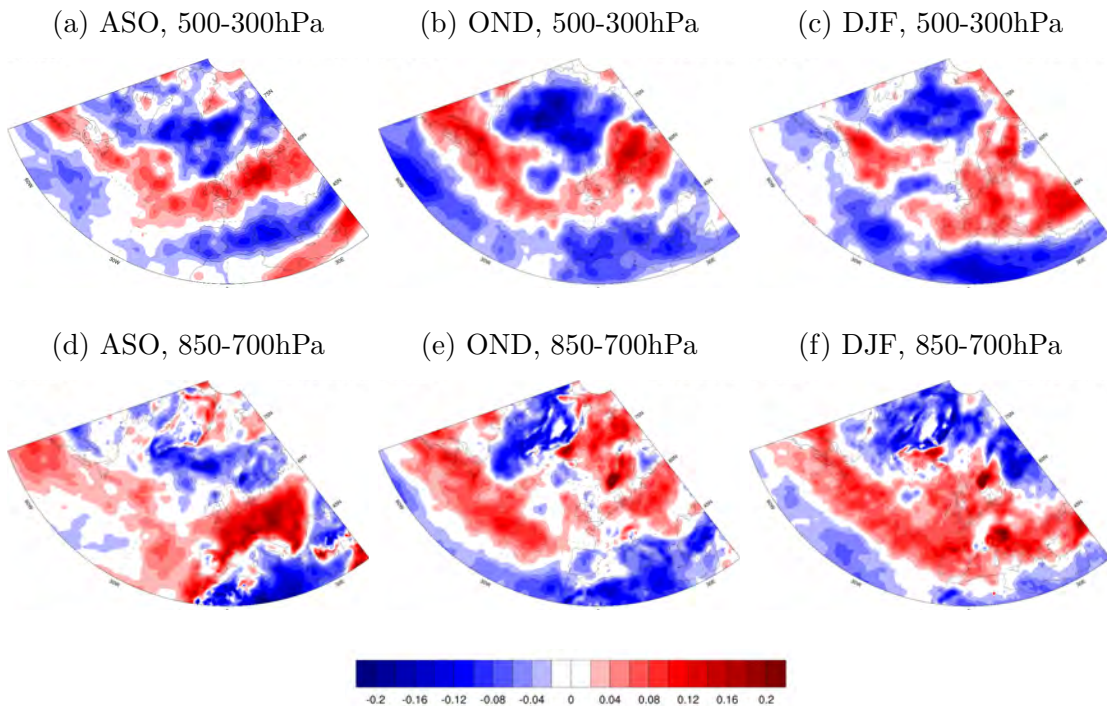


Figure 6.7: Composite differences for Maximum Eady Growth Rates in upper (between 500 and 300hPa) and lower (between 850 and 700hPa) troposphere in days^{-1} . Average of strong positive HSI minus average of negative HSI years for three three-months averages

ASO	OND	DJF
<ul style="list-style-type: none"> • Strong positive anomaly over European land areas • Slight positive anomaly over central North Atlantic • Negative anomaly from southern tip of Greenland towards Scandinavia 	<ul style="list-style-type: none"> • Positive anomalies over central North Atlantic • Stronger and more zonal (from 35° to 50°N) than in ASO • Positive anomalies extend eastward to 15°W • No strong anomalies over Europe • Negative anomalies south of 35°N over the North Atlantic and Mediterranean 	<ul style="list-style-type: none"> • Anomalies shifted eastward compared to OND with positive anomalies over Central North Atlantic and Western Europe • Positive Anomalies in zonal band from 35° to 50°N • Maximum west of Portugal and in Bay of Biscay

Table 6.3: Horseshoe composite differences for Maximum Eady Growth Rates in upper (between 500 and 300hPa) and lower (between 850 and 700hPa) troposphere

as in chapter 4 for the North Atlantic sector (120° - 0°W, 35° - 60°N) reveals a systematic change in wave amplitude 6.8 of meridional averaged mid-tropospheric geopotential waves. Wave amplitudes are generally increased for shorter waves ($\lambda \leq 3,000km$ or wave number 3 respectively) in years with positive HSI in the months from November to January. In the same years these waves show a below than average amplitude in February and March.

In years with strong negative HSI anomalies the signal in wave amplitudes is analogue with opposite sign from November to January with slightly smaller anomalies than for years with strong positive HSI. There is no clear signal in February and March for negative HSI anomalies. The longest resolved wave in the FFT over the North Atlantic sector ($\lambda \simeq 9,000km$) shows greater amplitudes in October and November in these years. This is in agreement with the analysis in chapter 4 where a smaller amplitude of planetary wave number 3 can lead to a higher probability of wind storms (figure 4.8a).

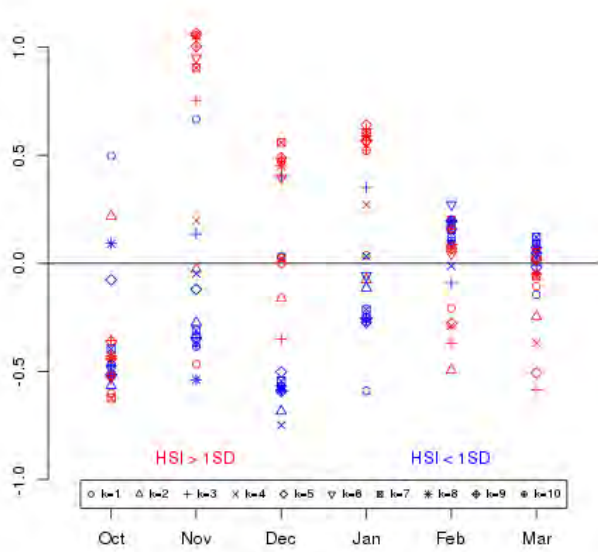


Figure 6.8: Wave amplitude anomalies in geopotential height in 500hPa for first 10 wave numbers. Wave frequency analysis between 120° and 0° W for the meridional average between 35° and 60° N for extended winter season from October to March. Symbols indicate different wave numbers for years with strong positive HSI in red and years with strong negative HSI in blue. Amplitudes are normalised with respect to ERA-Interim climatology from 1979 to 2014.

Summary of HSI results in ERA-I

The above analyses can be seen as a continuation of Renggli (2011). While the above results corroborate this study in general, they also reveal new insights into a possible variability of the relation NAH or HSI and NAO or wind storms respectively. The correlation results between the number of wind storms in DJF and SST, respectively the HSI, in ASO confirm the results from Renggli (2011) for the overlapping time period of ERA-40 and ERA-Interim. However, after the year 2000 it appears that the relation between NAH or HSI and the NAO breaks down or at least changes (see figure 6.2 and 6.3). Especially the correlation area between the number of wind storms and SST in the western North Atlantic shifts to a more central position in the North Atlantic. This dependency on the considered time period could stem from either a decadal modulation of the relation HSI and NAO (or wind storm frequency) or from statistical overfitting to the ERA-40 data.

Independent of the time varying relation between HSI and NAO, the composite analyses show enhanced growth conditions for wind storms in years with positive HSI and reduced or shifted conditions resembling a more negative NAO situation

in years with negative HSI. The composite differences show generally a pattern for wind storm growth factors similar to positive NAO conditions. Growth conditions are generally enhanced already in ASO when correlations of HSI and wind storm frequency are strongest. The conditions remain enhanced throughout the autumn and even intensify in the core winter months DJF. The anomalies in the zonal wind speeds in the upper troposphere, i.e. the jet stream, can be classified as the “northern jet” in Woollings et al., (2010) corresponding to a positive NAO and negative EA pattern (Mahlstein et al., 2012).

The composites for the latent heat availability show positive (negative) anomalies in autumn in years with positive (negative) HSI giving extra-tropical cyclones a higher probability to deepen and turn into a wind storm. Higher SST lead to an enhanced moisture availability in (at least) the lower atmosphere and increase the equivalent potential temperature. The further north the jet, the higher the probability the extra-tropical cyclone can “make use” of the available energy stored as latent heat (Pirret et al., 2017). The greater number of storms in years with positive HSI lead therefore to the conclusion that the latent heat is actually used to turn extra-tropical cyclones into wind storms in these years. The composite pattern for equivalent potential temperature changes from a more north-south divide into a definite west-east divide within two to three months in years with strong HSI. While in the late summer and early autumn months the signal in equivalent potential temperature in the lower troposphere can be seen as a source of potential cyclone growth, the signal in late autumn and winter is likely an effect of the existence of more (and stronger) cyclones. Extra-tropical cyclones, either wind storms or not, transport heat and moisture in a north-easterly direction, and letting cold and dry air from further north flow behind the cyclone in a more southerly direction. Figure 6.6b resembles figure 3.8h from chapter 3 on a larger scale. The direction of travel of the cyclones appear to be primarily on a south-north pathway along the 10° W meridian in these months. It could thus be hypothesised that through additional

availability of latent heat the pathway of extra-tropical cyclones and their associated wind storms is systematically influenced.

The composite differences for the Maximum Eady Growth Rate shows an enhanced baroclinicity over the North Atlantic in years with strong HSI. Strongly influenced by meridional temperature gradients, baroclinicity is enhanced in both cases when the HSI is either strongly positive or strongly negative. The main difference is the region where this enhancement takes place. While in years with positive HSI baroclinicity is increased along a latitudinal band around 50° N and reduced elsewhere, in years with negative HSI baroclinicity is increased further south around 30° N (see figure 6.7). The wave frequency analysis clearly shows greater amplitudes in years with positive HSI especially from November to January. In these years wave amplitudes are smaller than the climatological mean in February and March, suggesting less baroclinic activity and fewer wind storms towards the end of the season. Years with negative HSI show reduced amplitudes in the wave frequency analysis also especially in the months from November to January. The wave frequency analysis is applied to the geopotential height in 500hPa on the meridional mean of a latitudinal band from 35° to 60° N. The enhanced baroclinicity in years with negative HSI is however somewhat further south than 35° N, while further north baroclinicity might well be reduced in these years (see composite differences in figure 6.7).

6.3 North Atlantic Horseshoe Pattern and Wind Storm Frequency in AMIP-type GCM Simulations

The previous sections show that the NAH or HSI respectively may have an influence on wind storm frequency albeit possible time-varying. SST anomalies in late summer and early autumn show a clear influence on atmospheric growth conditions for extra-tropical cyclones from a climatological perspective. To further analyse the this SST influence on wind storms three AMIP-type sensitivity experiments are performed. With these experiments the following questions can be further investigated.

- Do positive HSI and negative HSI patterns have the same effect with only opposite signs?
- Are both NAH/HSI and wind storm frequency steered by a previous driver?
- What part of the signal transported in the atmosphere?

Set-Up of AMIP-type sensitivity experiments with ECHAM5

The AGCM ECHAM5 (Roeckner et al., 2006) is used for three sensitivity AMIP-type experiments (Gates et al., 1999). The model has 31 vertical levels and a horizontal spectral resolution is T63 corresponding to 2.5° by 2.5° or about 200km x 275km in the mid-latitudes. The procedure to create the boundary conditions follow Hurrell et al. (2008) and are provided by the Max-Planck-Institute of Meteorology, Hamburg, Germany. SST are monthly mean values for the mid of each month averaged over the period from 1970 to 2000. Other boundary conditions are also climatological values, such as sea-ice or aerosols. Greenhouse gases are set to

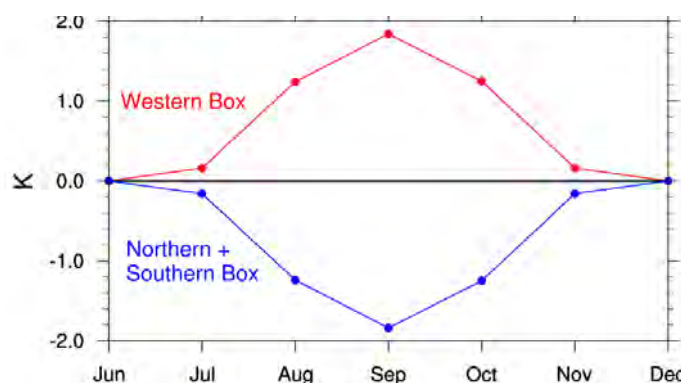


Figure 6.9: Yearly prescribed SST anomalies in HSI boxes +2K ECHAM5 sensitivity experiment. Line colours correspond to box colours in figure 6.10a. Anomalies are reversed for -2K experiment.

pre-industrial conditions and there is no additional forcing through volcanic aerosol. Each of the simulations lasts 30 years with the same yearly SST cycle. The first experiment has no additional anomalies applied to the model and is referred to as the climatological simulation or CLIM in the following. For the other two experiments, additional SST anomalies are added (or subtracted) from the SST CLIM conditions in the three boxes used for the HSI calculation over the North Atlantic (see figure 6.9). The additional anomalies are very small in July and November, slightly more than 1° C in August and October and about 1.8° C in September to provide some transition between the months and not to create a “shock” experiment. The anomalies are positive in the western HSI box and negative in the northern and southern box in the +2K experiment. The same anomalies with opposite sign for the respective boxes are added in the -2K experiment. The overall anomaly in September corresponds to about three standard deviations of the HSI. There is an additional spacial transition of two grid cells at the edges of the HSI boxes. The transition weights for these cells at the edges of the box are the same as the temporal weights for the months shown in figure 6.9.

Influence of the HSI on atmospheric growth factors for the intensification of ETCs in ECHAM5

The track density (see 2.2.1) for CLIM (figure 6.10a) matches the track density of ERA-Interim (figure 1.1a) both in shape and in number of storms very well. The +2K experiment (figure 6.10c) shows a higher number of wind storms than CLIM over almost the entire European continent reaching from the Mediterranean to central Scandinavia, including also the eastern subtropical North Atlantic between the Azores and Portugal. There is a reduction of wind storms in the storm track region with a south-west to north-east tilt starting at the western HSI box reaching to about 20°W.

In the -2K experiment (figure 6.10d) the number of wind storms is also increased over the Iberian Peninsula but to a lesser extent than in the +2K experiment. Starting around the British Channel and further north including the North Sea and Scandinavia there is a reduction of the number of wind storms compared to CLIM. This North-South divide with a slight south-west to north-east tilt continues over the North Atlantic with a positive and significant anomaly maximum in the central subtropical North Atlantic and a negative and significant anomaly maximum around 40°W and 50°N. In general the -2K experiment resembles a NAO negative situation.

The previous section suggested that the HSI influences cyclone growth conditions eventually leading to higher wind storm frequency. The same growth factors are therefore analysed here again for the +2K and -2K experiment and shown in composite differences (Figs. 6.11-6.13). The main results of this composite analysis are summarised in tables 6.4 to 6.6.

The wave activity of mid-latitude geopotential waves is analysed analogue to ERA-

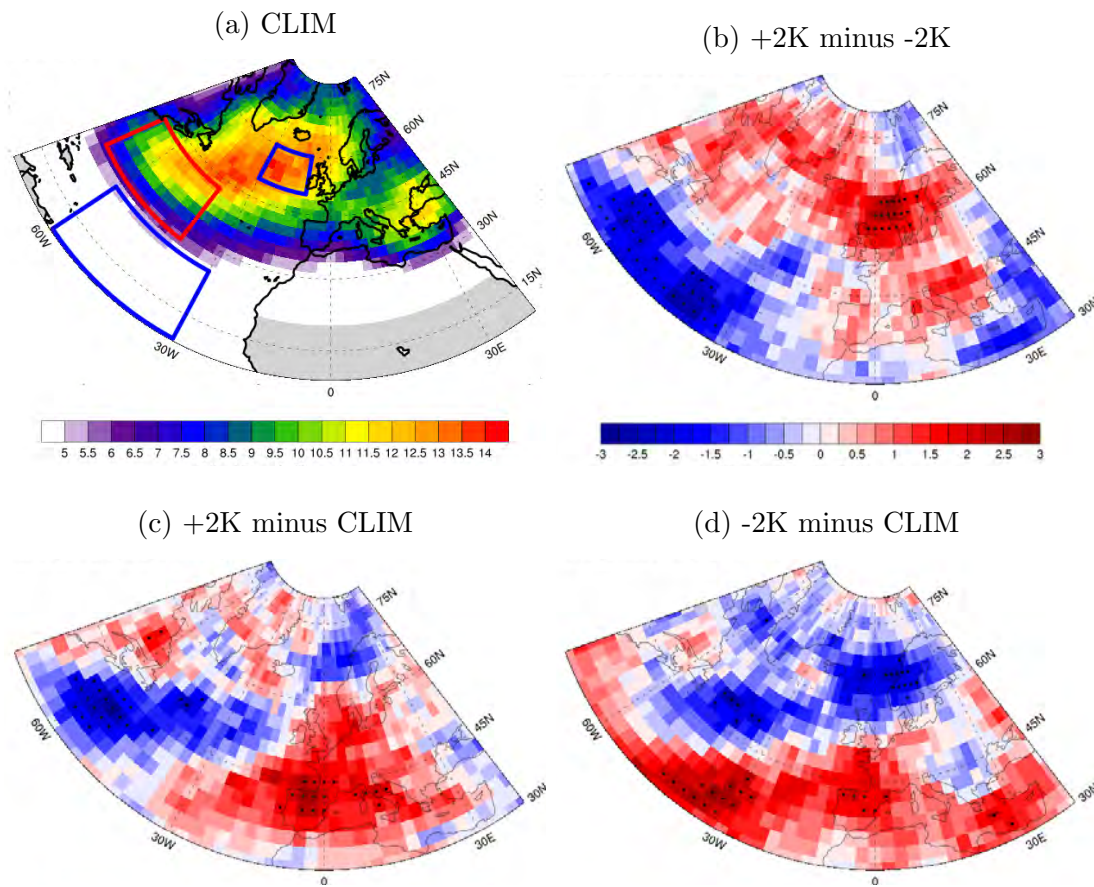


Figure 6.10: Wind storm track density (differences) in ECHAM5 sensitivity experiments in average number of storms per winter from October until March in 30 simulation years with search radius of 700km. Shadings in (c) and (d) are the same as in (b). Boxes in (a) show HSI regions. Dots in (b), (c), and (d) show statistical significance between the two sample sizes at the 5% level.

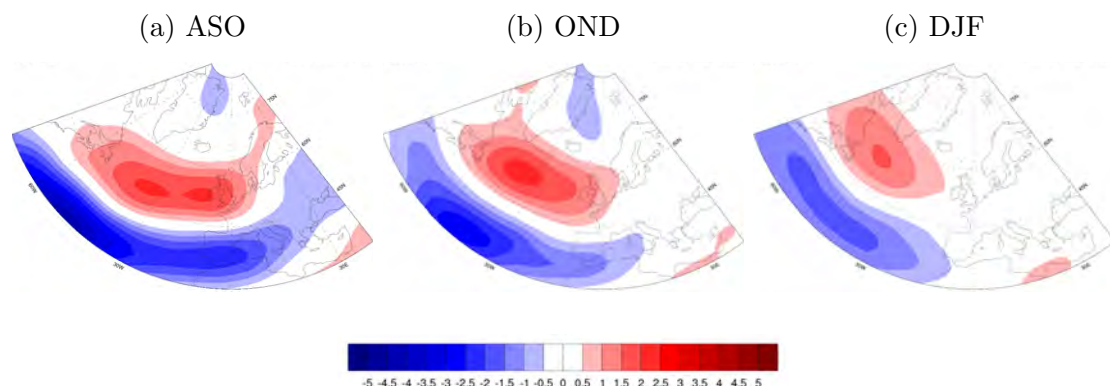


Figure 6.11: Composite differences of +2K minus -2K experiment for zonal wind in 200hPa in $m.s^{-1}$. Shown are three-months averages.

ASO	OND	DJF
<ul style="list-style-type: none"> • Enhanced over North Atlantic along a latitudinal band between 50° and 60° N • Strongly reduced along a latitudinal band between 25° and 45° N • Maximum of negative anomalies around western HSI box 	<ul style="list-style-type: none"> • Enhanced over North Atlantic along a latitudinal band between 50° and 60° N • Reduced along a latitudinal band between 25° and 45° N • Anomalies in same regions but smaller than in ASO 	<ul style="list-style-type: none"> • Positive anomalies over the north-western North Atlantic with maximum in Labrador Sea region • Reduced along a latitudinal band between 30° and 45° N • Anomalies further reduced compared to ASO or OND • Anomalies “stop” around 10° W

Table 6.4: HSI composite differences for zonal wind in 200hPa in ECHAM5

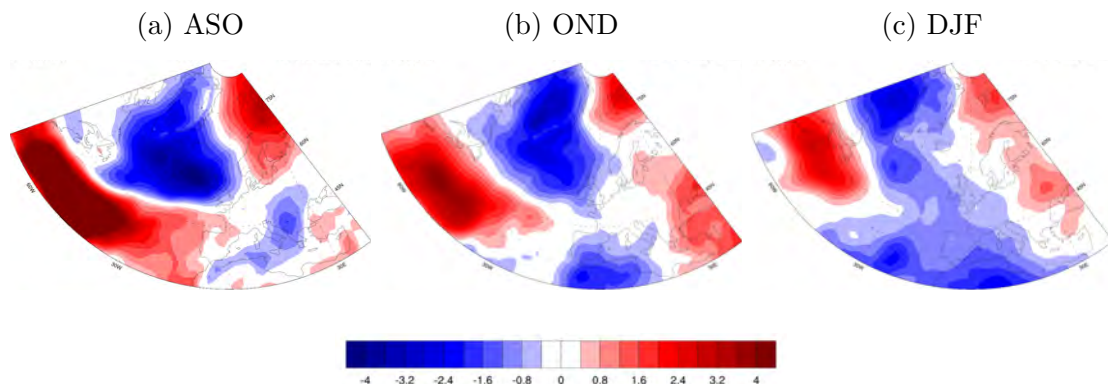


Figure 6.12: Composite differences of +2K minus -2K experiment for equivalent potential temperature in 850hPa in Kelvin. Shown are three-months averages.

ASO	OND	DJF
<ul style="list-style-type: none"> • Positive anomaly in western North Atlantic with maximum in above western HSI box • Negative anomaly in northern North Atlantic and Greenland with maximum around northern HSI box 	<ul style="list-style-type: none"> • Similar positive anomalies than in ASO but smaller in amplitude and extent • Negative anomalies similar with shift of maximum towards Greenland • Small negative anomaly over northern Africa and southern Spain 	<ul style="list-style-type: none"> • Positive anomalies only marginal in cyclogenesis region • Negative anomalies reaching from Greenland towards northern Africa but small in amplitude

Table 6.5: Horseshoe composite differences for equivalent potential temperature in 850hPa in ECHAM5

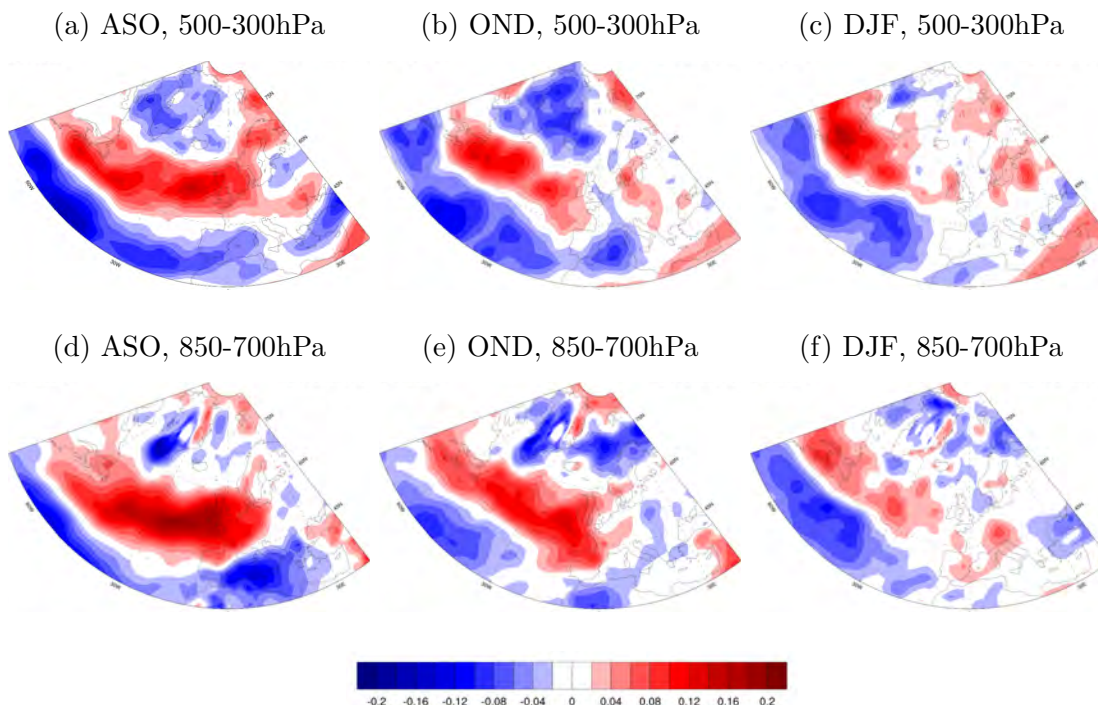


Figure 6.13: Composite differences of +2K minus -2K experiment for Maximum Eady Growth Rates in upper (between 500 and 300hPa) and lower (between 850 and 700hPa) troposphere in days^{-1} . Shown are three-months averages.

ASO	OND	DJF
<ul style="list-style-type: none"> • Enhanced baroclinicity along a latitudinal band between 45° and 55° N reaching from the cyclogenesis region to central Europe • Reduced baroclinicity in the western subtropical North Atlantic between the western and southern HSI box • Signal qualitative very similar in upper and lower troposphere but stronger in magnitude in lower troposphere 	<ul style="list-style-type: none"> • Signal qualitative very similar but smaller in magnitude compared to ASO • Difference between upper and lower troposphere remains 	<ul style="list-style-type: none"> • Enhanced baroclinicity signal over central North Atlantic basically vanished • Negative anomaly in subtropical North Atlantic comparable to OND but smaller in magnitude than ASO

Table 6.6: Horseshoe composite differences for Maximum Eady Growth Rates in upper (between 500 and 300hPa) and lower (between 850 and 700hPa) troposphere in ECHAM5

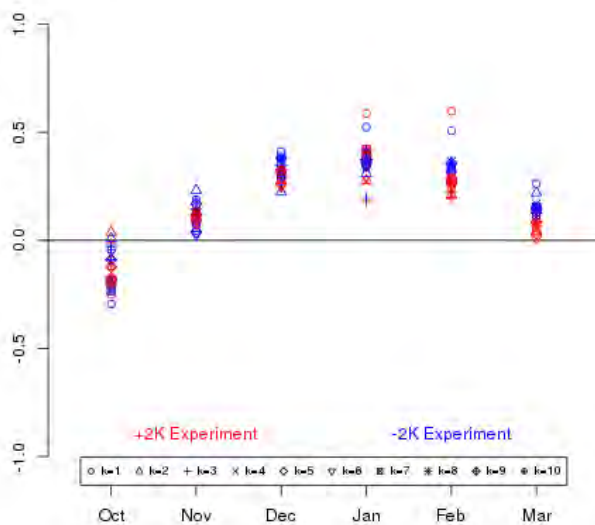


Figure 6.14: Average wave amplitude anomalies in geopotential height in 500hPa for first 10 wave numbers in +2K and -2K ECHAM5 experiments. Amplitudes are normalised with respect to CLIM. Wave frequency analysis between 120° and 0°W for the meridional average between 35° and 60°N for extended winter season from October to March. Symbols indicate different wave numbers for years with strong positive HSI in red and years with strong negative HSI in blue.

Interim with the FFT decomposition of chapter 4. The differences to CLIM of wave activity as obtained by the wave frequency analysis in both the +2K and -2K experiment are very similar. There is a slightly negative anomaly in wave amplitudes for both experiments in October, changing into slightly positive anomalies in November and increasing further until December. For DJF the anomalies remain very similar generally half a standard deviation above CLIM. In March wave amplitude anomalies are only slightly above zero. It is worth mentioning that the longest resolved wave ($\lambda \simeq 9,000km$) has the greatest amplitude anomaly in January and February in both experiments.

Summary of HSI experiment results in ECHAM5 compared to ERA-I

The performed experiments with prescribed boundary conditions reveal further insight into the relation between the NAH or HSI and wind storm frequency. In general the ECHAM5 model reproduces the number of winter storm very well compared to ERA-Interim. The coupled AOGCM has been used previously to assess factors contributing to the development of strong cyclones (Pinto et al., 2009) and can therefore be assumed to be suitable for such a study. Both +2K and -2K experiments show differences to CLIM in wind storm frequency and growth conditions for extra-tropical cyclones. There is therefore a genuine influence of the HSI onto wind storm frequency.

The absolute composite differences for the analysed atmospheric quantities are generally greater in the ECHAM5 experiments than in ERA-Interim. If relative differences are considered this statement reverses and composite difference in ERA-Interim show the greater signal (not shown). The greater magnitude in the ECHAM5 experiments can be related to the larger prescribed SST anomaly compared to ERA-Interim. The atmospheric signal as a consequence of HSI

anomaly forcing clearly dampens from ASO to eventually DJF in the +2K and -2K experiments. This damping appears to be smaller if at all present in ERA-Interim.

The experiments show that the influence of positive HSI on growth conditions of extra-tropical cyclones and ultimately wind storms is not opposite to the influence from negative HSI conditions. In some regions the effect of a positive or negative HSI compared to the climatology is very similar, e.g. for the wind storm frequency over south-western Europe. The -2K experiment resembles a NAO negative situation while the +2K experiment is only partly similar to a NAO positive situation. The wave amplitudes for the +2K and -2K experiment are almost identical when compared to CLIM. In the later winter months this is in accordance with the Maximum Eady Growth Rate which is also very similar for both experiments. In the early winter months however this is an effect of meridional averaging. The Maximum Eady Growth Rate signal is shifted in north-south direction between the +2K and -2K experiment but due to the meridional average for the wave frequency analysis this difference disappears in the slightly coarser resolution of ECHAM5 compared to ERA-Interim.

6.4 Discussion

This study confirms a relation between SST in late summer / early autumn over the North Atlantic and atmospheric conditions over Europe in the subsequent winter. (Czaja and Frankignoul, 1999; Czaja and Frankignoul, 2002; García-Serrano et al., 2008; Rodwell and Folland, 2002; Gastineau and Frankignoul, 2014; Peng et al., 2002; Cassou et al., 2004; Deser et al., 2007). The lead-lag correlation between the HSI and wind storm frequency exceeds 0.5 when the SST leads by about three months if only the period until 2000 are considered. The correlation decreases to about 0.2 if the whole ERA-Interim period is taken into account. SST anomalies

can have an influence on cyclone growth factors, such as jet strength and position or latent heat availability. This influence from SST to atmosphere is confirmed with AMIP-type sensitivity experiments. The mean prescribed SST anomalies in the sensitivity experiments are about three times greater than the one standard deviation that is considered in the reanalysis. The signal in the atmospheric growth conditions is found also to be greater in the sensitivity experiments, but does not scale by a factor of 3. The less persistent signal in the AGCM experiments suggest however that either some of the signal is transported via deeper ocean layers and re-emerges at a later stage or that the NAO acts as a positive feedback mechanism and influences the SST closer to the European continent that in turn could influence wind storm activity.

The shift of the relation in the reanalysis around the year 2000 show that the relation is either time-varying, meaning a process on the decadal time scale could act modulating, or that the HSI definition of Renggli (2011) is an overfitting to the ERA-40 dataset.

The performed composite analyses with ERA-Interim corroborate however the study from Renggli (2011) **but for the entire ERA-Interim period**. This could mean that the NAH or HSI relation to the NAO changes after the year 2000 but the influence on the number of wind storms remains, albeit to a smaller amount (see figure 6.4). Since around the year 2000, NAO values follow a declining trend (Dawkins et al., 2016) while the number of wind storms does not (see figure 1.1b). In fact the winter 2013/14 has seen the most storms in large regions over the North Atlantic for the whole ERA-Interim period (see also next chapter 7). In the composite analysis above only wind storm frequency is taken into account. Extending the analysis to wind storm frequency combined with intensity could provide a solution to this apparent discrepancy. The relation between NAO and

intensity of storms remains true also after the year 2000 (Dawkins et al., 2016). In summary this could mean that there is a constant relation between the number of storms and the NAH **independent** of the exact shape of the NAH and location of SST anomalies but the intensity of storms and the NAO respectively **is dependent** on the position of the NAH.

This clearly shows high potential for further investigations also in the light of decadal variability, e.g. as to what extent the AMOC might steer the positioning of the NAH as it also seems to undergo a declining trend since the early 2000s (Smeed et al., 2014).

The relation HSI \rightarrow wind storms can also be seen as a source of potential predictability for wind storm frequency on the seasonal time scale due to its three to four months lag. Regarding the previous chapter 5 about seasonal prediction skill, the obvious question now arises whether the analysed seasonal models can reproduce this mechanism. Either way an analyses of seasonal prediction models appears to be useful: if the mechanism *is not* found in the models these results provide a great opportunity to further increase forecast skill for wind storms, and if the mechanism *is* found, the seasonal models provide an excellent opportunity to further analyse this break down between HSI and NAO. First results using the ECMWF System 4 August initialisations show indications that SST patterns in the crucial HSI regions show almost no persistence. The effect of HSI anomalies on wind storm frequency can therefore be expected to be relatively small in this model.

**WAS THE EXTREME STORM SEASON OVER
THE NORTH ATLANTIC AND THE UK IN
WINTER 2013/14 TRIGGERED BY CHANGES
IN THE WEST PACIFIC WARM POOL?**

This chapter has been published with the same title in almost identical form in the Special Supplement to the *Bulletin of the American Meteorological Society* “Explaining Extremes of 2014 from a Climate Perspective” in 2015. The authors of the publication are Simon Wild, Daniel J. Befort, and Gregor C. Leckebusch. The individual contributions of all authors can be found at the beginning of this thesis (see Author’s Declaration)

7.1 Introduction

In winter 2013/14, the United Kingdom experienced exceptionally stormy and rainy weather conditions. The period from December 2013 to February 2014 was the stormiest for at least 20 years according to the Met Office. Two further studies also revealed this season to have been the stormiest in the United Kingdom since 1871. Matthews et al. (2014) found the highest value of a combined index of cyclone counts and intensity in the winter 2013/14, while a study by the Climate Research Unit at the University of East Anglia derived an unprecedented number of severe

gale days with a circulation weather type analysis from mean sea level pressure fields. While the United Kingdom was hit by several high-intensity storms, surface temperatures over large parts of central North America fell to near record minimum values (National Climatic Data Center, 2014; Environment Canada, 2014). These low temperatures have been connected to warm sea surface temperatures in the North Pacific (Hartmann, 2015; Lee et al., 2015). A potential driver for positive sea surface temperature anomalies in the North Pacific and cold conditions in central North America further downstream is warm surface waters in the tropical west Pacific (Palmer, 2014; Hartmann, 2015). It has been suggested that increasing sea surface temperatures in the tropical west Pacific could also be the cause for extreme weather over the British Isles (Huntingford et al., 2014; Slingo et al., 2014; Kendon and McCarthy, 2015). In line with this hypothesis, we first quantify the interannual variability of winter windstorm frequency over the North Atlantic/European region, which can be related to very low temperatures over North America. Secondly, we test whether a mechanism originating in the tropical Pacific continues beyond the North American continent affecting storminess over the North Atlantic and Europe.

7.2 Data and Methods

All our analyses cover the core winter months, December–February, from 1979/80 to 2013/14. In our analyses we make use of the following data sets: 6-hourly ERA Interim reanalysis (Dee et al., 2011) in its original T255 spatial resolution is used for wind speeds, 2m temperature and mean sea level pressure (MSLP). Absolute wind speeds are calculated from the zonal and meridional components. Two-meter temperature data is normalised by its standard deviation with respect to the long-term climatology mean of each 6-hourly time step to remove daily and seasonal cycles. The seasonal anomaly mean is calculated from these normalised values.

Additionally, we use MSLP data to identify cyclones in the North Pacific. For the analysis of convective activity over the tropical Pacific, NOAA/NCAR gridded monthly outgoing longwave radiation (OLR) data is used (Liebmann and Smith, 1996). Sea surface temperatures are taken from the 4th version of the ERSST data (Huang et al., 2014). The seasonal cycle is removed from both these data sets. We further use the winter mean of the monthly Pacific–North America pattern index (PNA) provided by NOAA Climate Prediction Center (Barnston and Livezey, 1987). Strong wind events associated with extra-tropical cyclones are identified with an objective algorithm developed by Leckebusch et al. (2008) using exceedances of the local 98th percentile of the 10m wind speeds. Events with a lifetime shorter than 18 hours are neglected to focus on wind fields caused by synoptic-scale extra-tropical cyclones. Cyclones over the North Pacific are determined by a cyclone identification and tracking algorithm (Murray and Simmonds, 1991) that locates a minimum of MSLP in the vicinity of a maximum in the Laplacian of the MSLP. Local system track density for both types of tracks (windstorms and cyclones) are calculated in agreement with settings used in Neu et al. (2012) with a search radius of 500 km around the centre of each box in a $2^\circ \times 2^\circ$ grid.

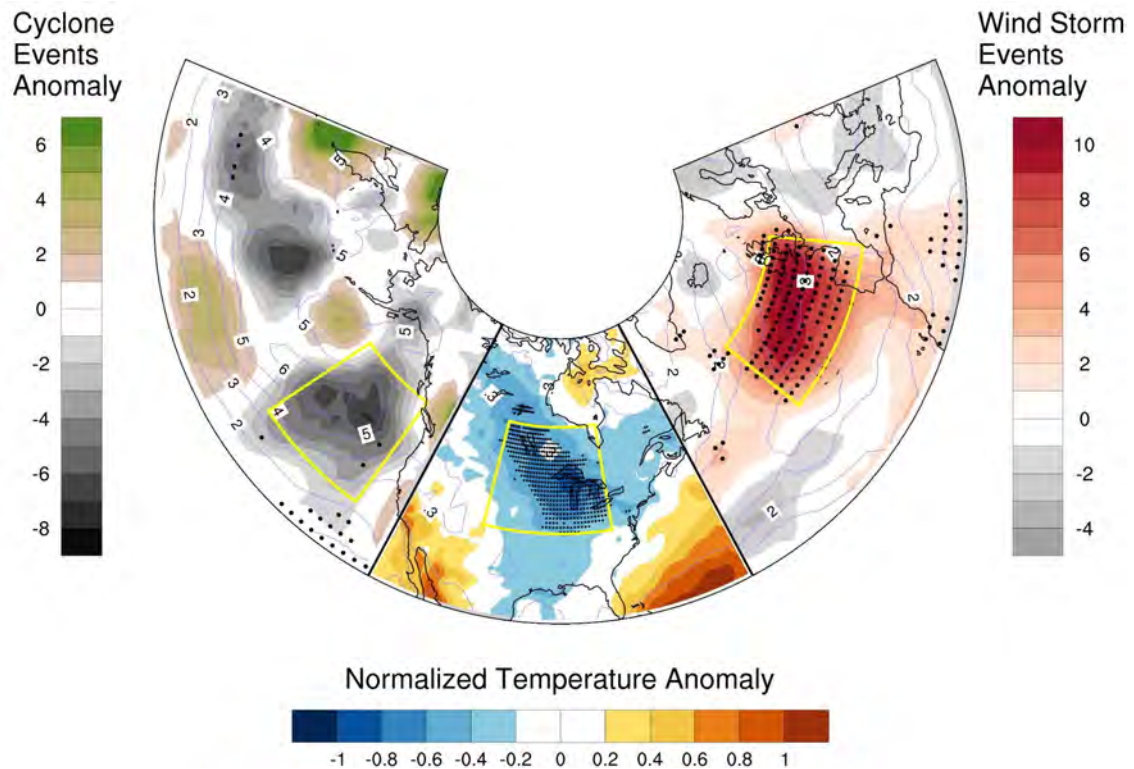


Figure 7.1: Anomalies (ERA Interim) for Dec 2013–Feb 2014 compared to long-term climatology (1979–2014) in shadings; interannual standard deviation in contours. (right) 60° W– 30° E, 25° – 70° N; absolute windstorm events anomaly; black dots indicate a maximum in winter 2013/14. (centre) 120° – 60° W, 25° – 70° N; 2m temperature seasonal normalised anomaly mean; black dots indicate a minimum in winter 2013/14. (left) 150° E – 120° W, 25° – 70° N; absolute cyclone events anomaly; black dots indicate a minimum in winter 2013/14. Yellow boxes mark regions used for the calculation of correlation coefficients for Table 7.1

7.3 Results

The winter 2013/14 over the British Isles and upstream conditions

Compared to the long-term seasonal mean, we find an increase of up to 200% in the number of identified windstorm events in the eastern North Atlantic for the winter season 2013/14. This corresponds to an increase of about 10 systems per winter or to more than three times the interannual standard deviation. Considering the period from 1979 to 2014, the winter 2013/14 showed the highest storm frequency on record (Fig. 7.1, right panel). The main area of this positive windstorm anomaly extends from about 35° W to the Greenwich meridian along a latitudinal belt from about 40° N to 55° N, and it includes large parts of the British Isles. These results about pure wind storms corroborate findings of previous studies about cyclone counts or gale days derived from pressure data (Matthews et al., 2014; CRU - Climate Research Unit - University of East Anglia, 2014). Concurrently, further upstream over the central North American continent, 2m temperatures dropped extremely below normal conditions. The interannual standard deviation (one value per season) of the normalised temperatures (one value every six hours) shows values between 0.3 and 1.0 below the long-term seasonal mean setting the overall temperature minimum for large parts of the U.S. Midwest, the southern part of the Canadian prairies, and southwestern Ontario for the whole investigated period (Fig. 7.1, central panel). The North American extreme cold temperatures are strongly linked to an equatorward shift of the circumpolar vortex (Ballinger et al., 2014). The circumpolar vortex accompanied by the upper tropospheric jet was deflected to the north over the eastern North Pacific (Slingo et al., 2014) allowing polar air masses to flow over North America on the trough upstream side. Associated with large amplitude Rossby waves in the mid and upper troposphere with a ridge over the North Pacific, anomalously high mean sea level pressure can decrease the number

of cyclone systems and increase temperatures in the region of the climatological Aleutian Low (Lau, 1988; Honda et al., 2001). In the winter 2013/14, the number of cyclones was indeed strongly reduced compared to the long-term climatology with a reduction of about 30% to 60% equivalent to about 5-10 fewer cyclones per grid point over the eastern North Pacific (Fig. 7.1, left panel). The Pacific–North American Pattern (PNA) can be regarded as one mode of variability that links the tropical and extra-tropical Pacific on a monthly to seasonal scale and is known to be strongly related to the surface temperature over North America (Leathers et al., 1991; Ning and Bradley, 2014). In the winter 2013/14, the PNA was weakly positive in January and strongly negative in December and February. Sea surface temperatures in the tropical west Pacific were exceptionally high in winter 2013/14 (Lee et al., 2015) causing enhanced convective activity, indicated by negative outgoing longwave radiation (OLR) anomalies, in this region (Fig.7.2).

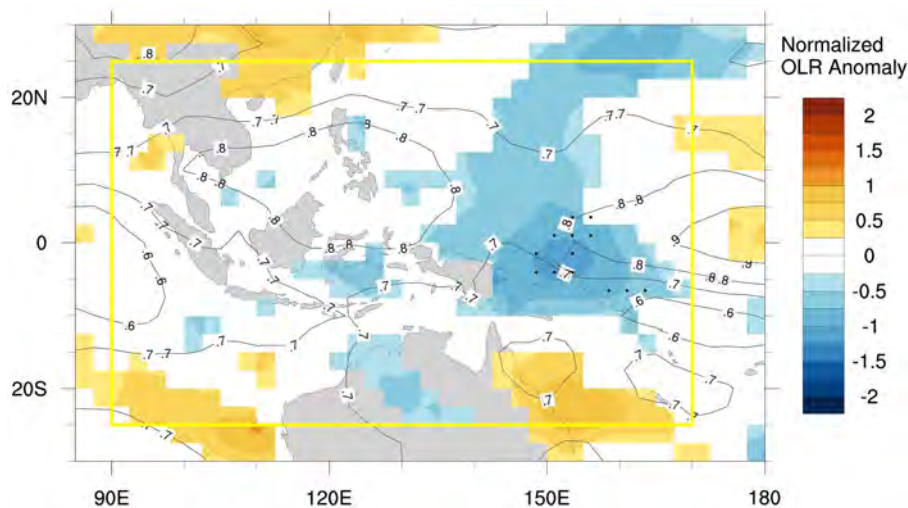


Figure 7.2: Seasonal normalised anomaly mean of OLR for December 2013 to February 2014 compared to long-term climatology (1979–2014) in shadings; interannual standard deviation in contours; black dots indicate a minimum in winter 2013/14. Negative OLR values indicate high convective activity. Yellow box marks regions used for the calculation of correlation coefficients in Table 7.1

	OLR, WP	PNA	Cyclone Events NEP	Temperature NA	SST WA
Wind Storms, NAt	-0.05	-0.22	-0.21	-0.38	0.29
Temperature, NA	-0.41	0.46	0.37		0.03
Cyclone Events, NEP	0.17	-0.41			0.02
PNA	0.36				0.32
OLR, WP					0.18

Table 7.1: Spearman rank correlation coefficient between area-averaged detrended time series from 1979/80 to 2013/14. NAt: Northeast Atlantic/British Isles (40°-55°N, 35°W-0°); NA: North America (38°-55°N, 105°-80°W); NEP: Northeast Pacific (33°-52°N, 150°-128°W); SST NP: Sea surface temperature, North Pacific (35°-60°N, 160°E-45°W); WP: tropical west Pacific. (25S°-25°N, 90°-170°E); WA: West Atlantic(85°-50°W, 35°-60°N). For regions, see also yellow boxes in Fig. 7.1-7.3 and green box in Fig.7.5. Statistically significant values in bold ($p < 0.05$)

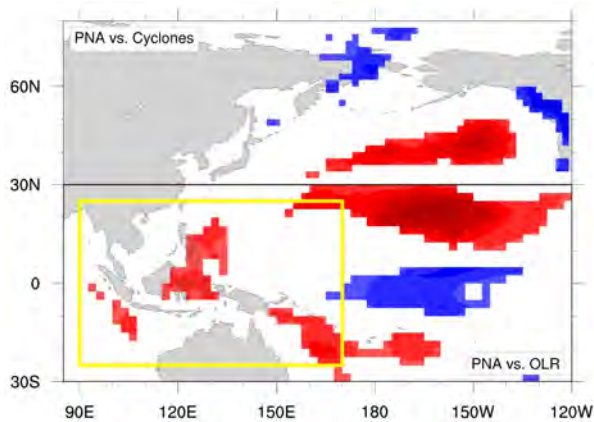


Figure 7.3: Interannual correlation coefficient (Pearson) of seasonal mean (December–February) values from 1979/80 to 2013/14: (top, north of 30° N) PNA index and cyclone events; (bottom, south of 30° N) PNA index and OLR. Correlations below the 95% significance level are omitted.

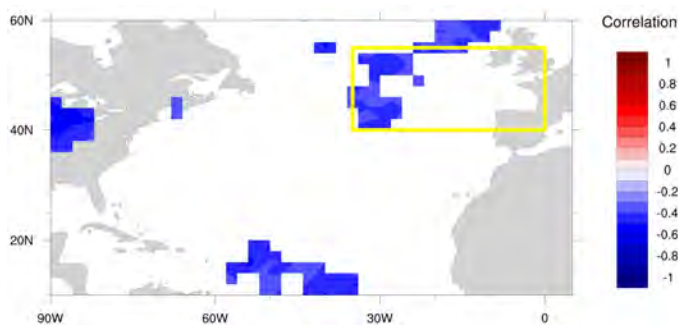


Figure 7.4: same as Figure 7.3 for PNA and wind storms.

The Role of the PNA

The PNA correlates positively with the cyclone track density in the central and eastern North Pacific around 40° N (Fig 7.3, top panel). The maximum correlation of about 0.75 is located in the region of the climatological Aleutian low, which is slightly shifted to the west, compared to the location of the 2013–14 most negative cyclone track density anomaly (Fig. 7.1, left panel). The correlation between PNA and OLR shows an El Niño–Southern Oscillation-like pattern with highest values at the northern edge of the tropical Pacific (Fig 7.3, bottom panel). The PNA is significantly linked to the OLR and thus convective activity over about half of the west Pacific warm pool. However, the PNA and North Pacific sea surface temperatures show only weak and no significant correlation to wind storms in most parts of the considered North Atlantic region (Table 7.1; Fig. 7.4).

7.4 Discussion and Attribution to Climate Change

This study tests and quantifies a proposed mechanism linking convective activity over the tropical west Pacific and storminess over Europe. If such a link exists, the record number of storms over the British Isles in winter 2013/14 could be seen as an enhanced response of the climate system triggered by increased sea surface temperatures in the tropical west Pacific, which themselves stem from anthropogenic influences (Palmer, 2014; Chan and Wu, 2015). Thus, anthropogenic influences would act via a natural link leading to anomalously high storm frequency over Europe. We diagnose that the year-to-year variability of storm frequency over the northeast Atlantic and the British Isles is significantly anti-correlated to surface temperatures in central North America (Table 7.1, regions outlined as yellow boxes in Fig. 7.1). We further confirm the link between the interannual variability of surface temperatures over North America and the PNA. The PNA is

in turn significantly linked to cyclone activity in the northeast Pacific, sea surface temperatures in the North Pacific, and convective activity (OLR) over about half of the west Pacific warm pool (Table 7.1 and Fig. 7.3). The direct relation between wind storm frequency anomalies over Europe and sea surface temperatures in the west Pacific warm pool, respectively OLR anomalies, is however weak and not significant (Table 7.1). Thus, we find that parts of the proposed mechanism in previous studies (Huntingford et al., 2014; Slingo et al., 2014; Kendon and McCarthy, 2015) linking the tropical west Pacific and European storminess show significant covariability, but we cannot find evidence for a direct relation from the beginning to the end of such a mechanism.

In addition, the correlation between North American temperatures and wind storm anomalies drops to insignificant values when the winter 2013/14 is excluded from the analysis. We thus conclude that the conditions in the Pacific and its induced anomalies over the North American continent are generally not sufficient to explain the extraordinary high winter wind storm frequency over the northeast Atlantic and the British Isles. The induced conditions were favourable to increase the number of storms in winter 2013/14, but the explained variability is too small to attribute this particular extreme mainly to conditions in the tropical Pacific and its imprinted anthropogenic signal.

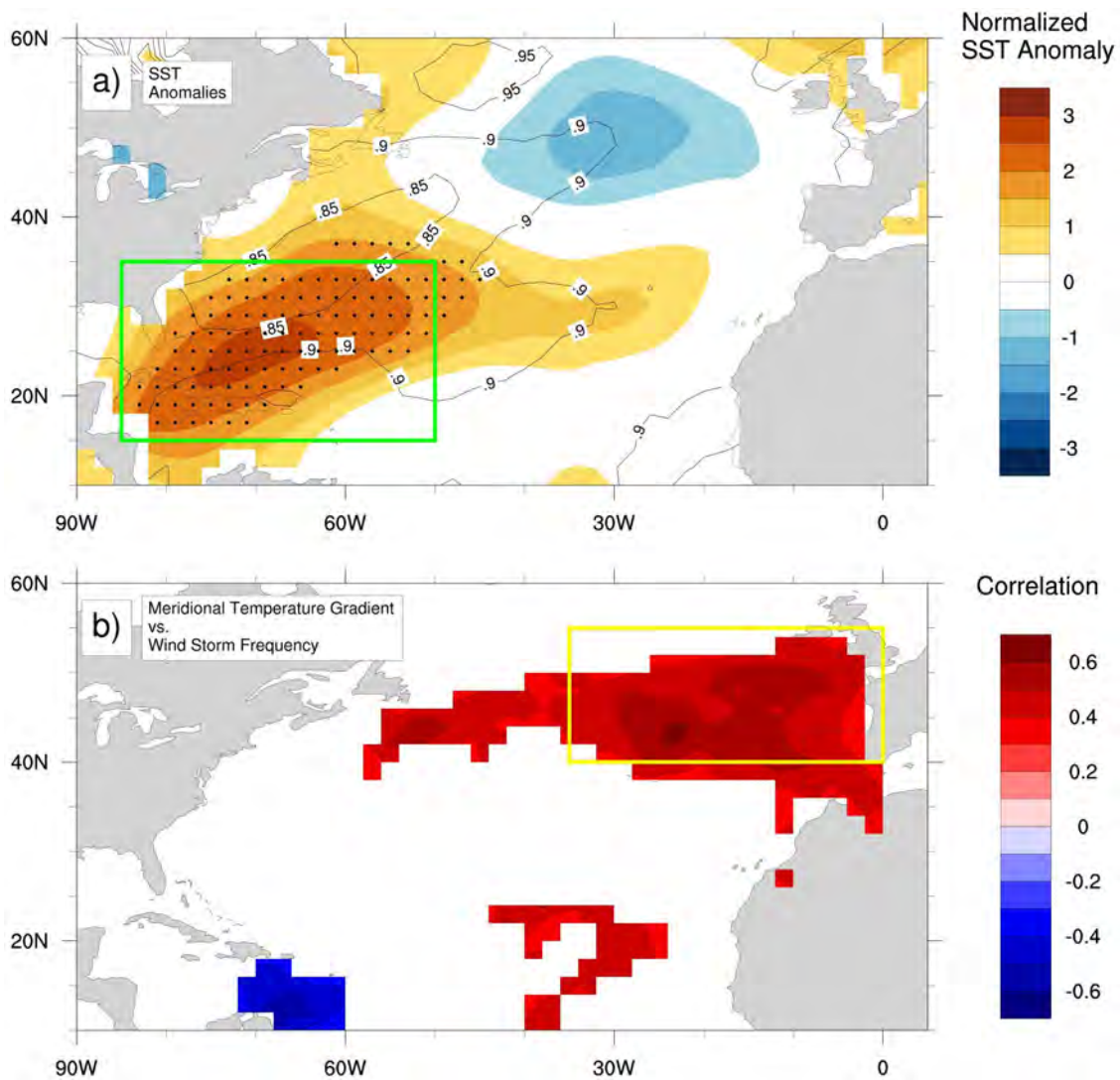


Figure 7.5: (a) Normalised sea surface temperature (SST) anomalies (ERSSTv4) for Dec 2013–Feb 2014 compared to long-term climatology (1979–2014) in shadings; interannual standard deviation in contours. Black dots indicate a maximum in winter 2013/14 for the considered time period from 1979 to 2014. (b) Interannual correlation coefficient (Pearson) between winter wind storm frequency and meridional temperature gradient index from 1979/80 to 2013/14. The meridional temperature index is calculated by subtracting the area-averaged sea surface temperature value for the west Atlantic (15° - 35° N, 85° - 50° W; green box in Fig. 7.5a) minus the area-averaged 2m temperature value for central North America (38° - 55° N, 105° - 80° W; yellow box in centre panel of Fig.7.1). Correlations below the 95% significance level are omitted. (For clarity: Yellow box in Fig. 7.5b corresponds to yellow box in right panel in Fig.7.1)

One alternative potential driver partly explaining the anomalously high storm frequency in 2013/14 could have been the unprecedented anomalies of sea surface temperatures in the west Atlantic (Fig.7.5a). High sea surface temperatures in the subtropical west Atlantic (green box, Fig. 7.5a) and low temperatures over North America (yellow box, centre panel Fig. 7.1 are unrelated (the correlation equals 0.03), but when occurring concurrently, they substantially increase the meridional temperature gradient over the core genesis region of extra-tropical cyclones. This meridional temperature gradient is positively related to wind storm frequency over the North Atlantic and Europe (Fig. 7.5b). Baroclinic instability in this region can be positively influenced through a strong temperature gradient, leading to enhanced cyclogenesis and potentially strong deepening of cyclones responsible for high wind speeds.

SYNTHESIS

8.1 Summary and Discussion

This thesis' main aim is to increase the understanding of reasons for increased wind storm frequency and to some extent wind storm intensity on different time scales. Successful prediction of extra-tropical cyclones and especially high impact wind storms, Europe's natural hazard with the highest loss potential for society and economy, is crucial for risk management practices. The underestimation of the *Great Storm of 1987* is an example of inaccurate assumptions about atmospheric conditions on the **synoptic scale** (Houghton, 1988; Burt and Mansfield, 1988). Differences on this time and spatial scale between average extra-tropical cyclone conditions and those leading to (strong) wind storms are shown in the **chapters 3 and 4** with a composite analysis of atmospheric growth factors of extra-tropical cyclones and a wave frequency analysis of mid-latitude mid-tropospheric geopotential height.

In **Chapter 3 synoptic scale differences of tropospheric growth factors between average extra-tropical cyclones and wind storms** are analysed. The applied composite analysis consists of a larger event set than 58 storms as in Pirret et al. (2017). The analysed growth factors are the maximum Eady growth rate σ_{BI} in the upper and lower troposphere as a measure for baroclinicity, equivalent potential temperature in 850hPa Θ_E as a measure for latent and sensible heat availability and the vertical sum of upper tropospheric divergence between 500 and

200hPa. All growth factors show generally higher values for events with either lower pressure or stronger winds corroborating previous studies (Pinto et al., 2009; Ulbrich et al., 2001; Liberato, 2014). Different composite sets allow here additionally for a quantification and the analysis whether there are differences between extreme extra-tropical cyclone (defined by mean sea level pressure) and wind storms (defined by surface wind speeds). The magnitude of growth factors increases by about 50% (Θ_E) and often up to 100% (other quantities) for strong extra-tropical cyclones and wind storms. For strong wind storms this increase can even be greater. All wind storm events ($SSI > 0$) and strong cyclone events ($p < 960hPa$) do not show any major differences. The increase of growth factor magnitude can even be greater for strong wind storm events ($SSI > 30$) which are however in about 60% *not* part of the strong cyclone event set. This highlights the necessity for a separate investigation of wind storms instead of “only” strong extra-tropical cyclone events. It is worth mentioning again at this point that the months October to March are used in this study. A reduction of the investigated period to the months December to February could influence the results as mean values for growth factors such as baroclinicity would likely increase.

Different wind storm events have been found to be strong due to different reasons (Ulbrich et al., 2001; Fink et al., 2012). Therefore, the wind storm event to event variability for growth factors from a Lagrangian perspective is also analysed in chapter 3 using a newly developed method using an event space PCA. Due to small values in explained variability the results have to be generally interpreted with caution. From a composite analysis alone upper and lower baroclinicity seem to behave similarly, however with the PCA results show that the variability between events is greater in the upper troposphere. The PCA reveals that if latent heat is available it also has to be “accessible” in between the fronts to intensify an extra-tropical cyclone.

In Chapter 4 mid-latitude, mid-tropospheric geopotential wave char-

acteristic during wind storm occurrence are analysed. Geopotential wave amplitudes are generally increased during wind storm events. This is in agreement with greater rates for potential wave growth as identified in chapter 3. For the synoptic scale waves (wave number 7-12) this ought to be expected given the stormtrack definition by Blackmon (1976). There is no wave number or wave number combination of these synoptic scale waves that could be described as dominant when wind storms occur. There is however an increased likelihood of wind storm occurrence when planetary wave number 2 shows greater amplitudes. The relation of amplitudes of planetary wave 3 to wind storm frequency is found to be non-linear. Very *low* amplitudes seem to favour more strong wind events, while amplitudes are on average *greater* during wind storm occurrence (see next section for potential future research). The relation of wave amplitudes and wave breaking is not analysed in chapter 4 but the assumption that waves have to increase in amplitude first before they can break and then influence extra-tropical cyclones and/or wind storms appears to be true. Rossby wave breaking usually occurs few days before a strong wind event reaches the European continent. The analyses in chapter 4 do however not take into account a potential time lag between amplitude and wind storm event. Results from ECHAM5 in chapter 6 show that the choice for the latitudinal band from 35° to 60° N might be not ideal if wind storms are the target quantity. The analysis and the northern and southern boundary of the wave frequency analysis closely followed the procedure of (Screen and Simmonds, 2014). In this and other similar studies (e.g. Kornhuber et al., 2017) the variable of interest is primarily temperature, which is largely driven by longer planetary waves. Chapter 6 shows that for wind storms, strongly depend on shorter, baroclinic waves, a distinction between wave activity further north and south might be necessary to not mix up seasons with more wind storms in either northern or southern Europe, or a positive NAO and a negative NAO situation respectively.

Seasonal forecasts for the extra-tropics are not as broadly communicated to the

general public as for example weather forecasts. The reason is simply a limited reliability in the extra-tropics (Weisheimer and Palmer, 2014) and in the case of the Met Office potentially bad experience with a “barbecue summer” in the past (Eden, 2011). Seasonal forecasts are however increasingly used across a wider-getting range of applications (Dessai and Bruno Soares, 2013). Recent studies have shown an increased skill in forecasting the NAO with seasonal prediction models (Scaife et al., 2014; Hansen et al., 2017) raising the question whether small seasonal skill previously found for wind storm frequency in older models has also increased in state-of-the art seasonal forecast suites. **The prediction skill for extra-tropical cyclone and wind storm frequency is therefore assessed in chapter 5.**

The November initialised forecasts for three model suites namely the ECMWF-System 3, ECMWF-System 4 and GloSea 5 are compared to reanalysis. All models show small to moderate but significant skill for some parts of western Europe, with ECMWF-System 4 and GloSea 5 outperforming ECMWF-System 3. Using the NAO as indirect wind storm predictor leads to a reduction in skill suggesting 1) that analysing the NAO is not sufficient for the assessment of European storminess and 2) that the models appear to predict successfully at least to some extent other drivers for interannual wind storm frequency, otherwise the skill in the direct method would not be higher.

The temporal variability of the seasonal prediction skill assessed with the ACC over the North Atlantic is remarkably similar across the models. This suggests that some years have a higher potential seasonal predictability than others, a result also proposed by Renggli (2011).

A potential source of predictability on the seasonal scale is analysed in **chapter 6: the influence of North Atlantic sea surface temperatures on European wind storm frequency.** North Atlantic SST have been shown to provide a source of predictability for the NAO on the seasonal time scale (Gastineau and Frankignoul, 2014; García-Serrano et al., 2008). An anomaly SST pattern named

the North Atlantic Horseshoe (NAH) shows thereby the highest correlations to the NAO when leading by about five months. Renggli (2011) defined the Horseshoe Index (HSI) to quantify the NAH. The HSI is found to significantly correlate with the NAO and wind storm frequency with similar lead times. The link HSI-NAO seems however to undergo some decadal variability, as correlations drop to non-significant values after around the year 2000. Following on from Renggli (2011) the composite analyses show an influence for the HSI and tropospheric growth factors as in chapter 3 and wave amplitudes as in chapter 4. Despite the possible decadal variability between HSI and NAO the influence of the HSI onto growth factors is found before and after the decoupling. The influence from the North Atlantic SST to atmospheric conditions is also found in AMIP-type sensitivity experiments using ECHAM5. The signal in the AGCM simulations in growth factors is however smaller and less persistent suggesting that either some of the signal is transported via deeper ocean layers and re-emerges at a later stage or that the NAO acts as a positive feedback mechanism and influences the SST closer to the European continent that in turn could influence wind storm activity. Because of the prescribed SST such a feedback mechanism would not be present in the experiments.

Another possible mechanism for the interannual variability of European storminess is analysed in **chapter 7: whether a link between SST in the Western Pacific Warm Pool and wind storm frequency over the Eastern Atlantic / north western Europe exists and whether this link made the extreme storm season 2013/14 more likely**. The causal chain - convective activity over tropical western Pacific → triggered Rossby waves / PNA anomaly → temperature anomaly over North America → greater extra-tropical cyclone frequency over North Atlantic - as suggested by Huntingford et al. (2014) could however not be confirmed.

The results of chapter 7 have since its publication been confirmed by a study of van Oldenborgh et al. (2015) and somewhat challenged by Messori et al. (2016). The latter study suggests that a link from the Western Pacific Warm Pool to Europe is

not steered by the PNA but by the Western Pacific Pattern. Watson et al. (2016) find evidence for a connection between low latitudes over the Pacific and the extra-tropics over the North Atlantic but argue that the link is not strong enough to explain the conditions for the winter in question.

Western subtropical Atlantic SST showed a very strong positive anomaly in the winter 2013/14, largely independent of SST in the Western Pacific Warm Pool. Together with very cold conditions over the North American continent, that were driven by the tropical Pacific, baroclinicity was increased and provided the conditions for more extra-tropical cyclones (and wind storms) to be generated.

Long-term trends and decadal variability of European storminess have been discussed extensively in the recent literature as different studies come to different conclusions (Donat et al., 2011; Krueger et al., 2013; Wang et al., 2014; Krueger et al., 2014). The newly available **ERA20C reanalysis is therefore compared to the NOAA 20th Century reanalysis (see appendix)**. The results show major differences for low frequencies of extra-tropical cyclone and wind storm events on both hemispheres especially before the year 1950. The data sets do however agree well when their individual long-term trends and low frequencies are removed.

8.2 Outlook

This thesis provides numerous starting points for future research:

The newly developed EOF-PC-selection method in chapter 3 could prove to be a powerful tool for non-linear mechanisms as the example at the end of the chapter briefly demonstrates. The influence of large scale teleconnection patterns on the results of tropospheric growth factors in chapter 3 remains a further area to be investigated. Pinto et al. (2009) has shown an influence of the NAO while chapter 6 shows an influence of North Atlantic SST on synoptic scale growth factors on an interannual time scale. Other teleconnection patterns such as the East Atlantic or Scandinavian Pattern have been found to be more influential than the NAO for wind storms in some European regions and it can thus be expected to find a relation between these patterns and atmospheric growth conditions.

The wave frequency analysis in chapter 4 revealed a non-linear relation between planetary wave 3 and wind storm frequency. Due to the distribution of continents and mountain ranges this wave plays an important role in northern hemispheric mid-latitude weather and climate. Further understanding in how this wave and wind storm frequency are linked could therefore be beneficial for short- to long-term predictions and projections. Zappa et al. (2014) linked storm track biases to blocking frequency in CMIP5 climate models. As discussed in chapter 4 the non-linearity could stem from the link of wave 3 to blocking events and strong and persistent ridge events (as defined by Santos et al. (2009)) but this has to be investigated systematically.

The relation of wave amplitudes and wave breaking could further be investigated as to whether a critical amplitude for an individual wave exists, when it is likely to break. Priestly et al. (2017) found that the winter 2013/14 (as investigated in chapter 7) showed more than average Rossby wave breaking, Pinto et al. (2014) come to the same conclusion for January 2007. This raises further the question

whether Rossby wave amplitudes also show different interannual behaviour. On the one hand it is shown in chapter 5 that seasonal forecast models have prediction skill for North Atlantic winter wind storms. On the other hand some sources of predictability on seasonal time scales are shown in the chapters 6 and 7. Ongoing work shows some correlation of the west Atlantic SST region identified to be important for the winter 2013/14 with the East Atlantic Pattern. This is in line with a recent study of Ossó et al. (2017) who show some predictability of the summer East Atlantic Pattern through Atlantic SST using a similar method than in this thesis with the HSI and wind storm frequency or NAO respectively. The next logical step is thus to investigate whether current seasonal prediction models are able of capturing these mechanisms.

ERA Interim reanalysis are used in the majority of the analysis in this thesis. The shortly available ERA 5 reanalysis will have higher spatial and temporal resolution and is thus more likely to resolve wind storm features, such as sting jets, not adequately resolved in ERA Interim (Hewson and Neu, 2015). A change of reference data set can sometimes change results as is shown in chapter 6. It will therefore certainly be interesting to see whether how wind storm frequency and intensity and their drivers on different time scales are represented in ERA 5.

Bibliography

- Anderson, D. L. T. (2008), Overview of Seasonal Forecasting, *in* A. Troccoli, M. Harrison, D. L. T. Anderson and S. J. Mason, eds, ‘Seasonal Climate: Forecasting and Managing Risk’, Springer Netherlands, Dordrecht, pp. 45–65.
- Anderson, D., Stockdale, T., Balmaseda, M., Ferranti, L., Vitart, F., Molteni, F., Doblas-Reyes, F., Mogensen, K. and Vidard, A. (2007), ‘Development of the ECMWF seasonal forecast System 3’, *ECMWF Tech. Memo.* **503**, 1–58.
- Athanasiadis, P. J., Bellucci, A., Scaife, A. A., Hermanson, L., Materia, S., Sanna, A., Borrelli, A., MacLachlan, C. and Gualdi, S. (2017), ‘A Multisystem View of Wintertime NAO Seasonal Predictions’, *Journal of Climate* **30**(4), 1461–1475.
URL: <http://dx.doi.org/10.1175/JCLI-D-16-0153.1>
- Ballinger, T. J., Allen, M. J. and Rohli, R. V. (2014), ‘Spatiotemporal analysis of the January Northern Hemisphere circumpolar vortex over the contiguous United States’, *Geophysical Research Letters* **41**(10), 3602–3608.
URL: <http://dx.doi.org/10.1002/2014GL060285>
- Barnes, E. A. and Polvani, L. (2013), ‘Response of the Midlatitude Jets, and of Their Variability, to Increased Greenhouse Gases in the CMIP5 Models’, *Journal of Climate* **26**(18), 7117–7135.
URL: <http://dx.doi.org/10.1175/JCLI-D-12-00536.1>
- Barnes, E. A. and Screen, J. A. (2015), ‘The impact of Arctic warming on the midlatitude jet-stream: Can it? Has it? Will it?’, *Wiley Interdisciplinary Reviews: Climate Change* **6**(3), 277–286.
URL: <http://dx.doi.org/10.1002/wcc.337>
- Barnston, A. and Livezey, R. (1987), ‘Classification, Seasonality and Persistence of low-frequency Atmospheric Circulation Patterns’, *Monthly Weather Review* **115**(6), 1083–1126.
- Beare, R., Thorpe, A. and White, A. (2003), ‘The predictability of extratropical cyclones: Nonlinear sensitivity to localized potential vorticity perturbations’, *Quarterly Journal of the Royal Meteorological Society* **129**(587), 219–237.
URL: <https://rmets.onlinelibrary.wiley.com/doi/abs/10.1256/qj.02.15>
- Befort, D. J., Fischer, M., Leckebusch, G. C., Ulbrich, U., Ganske, A., Rosenhagen, G. and Heinrich, H. (2015), ‘Identification of storm surge events over the German Bight

- from atmospheric reanalysis and climate model data’, *Natural Hazards and Earth System Sciences* **15**(6), 1437–1447.
URL: <https://www.nat-hazards-earth-syst-sci.net/15/1437/2015/>
- Befort, D. J., Wild, S., Kruschke, T., Ulbrich, U. and Leckebusch, G. C. (2016), ‘Different long-term trends of extra-tropical cyclones and windstorms in ERA-20C and NOAA-20CR reanalyses’, *Atmospheric Science Letters* **17**(11), 586–595.
URL: <http://dx.doi.org/10.1002/asl.694>
- Bell, C. J., Gray, L. J., Charlton-Perez, A. J., Joshi, M. M. and Scaife, A. A. (2009), ‘Stratospheric Communication of El Niño Teleconnections to European Winter’, *Journal of Climate* **22**(15), 4083–4096.
URL: <https://doi.org/10.1175/2009JCLI2717.1>
- Bengtsson, L., Hodges, K. I., Esch, M., Keenlyside, N., Kornblueh, L., Luo, J.-J. and Yamagata, T. (2007), ‘How may tropical cyclones change in a warmer climate?’, *Tellus A: Dynamic Meteorology and Oceanography* **59**(4), 539–561.
URL: <https://doi.org/10.1111/j.1600-0870.2007.00251.x>
- Bengtsson, L., Hodges, K. I. and Keenlyside, N. (2009), ‘Will Extratropical Storms Intensify in a Warmer Climate?’, *Journal of Climate* **22**(9), 2276–2301.
URL: <https://doi.org/10.1175/2008JCLI2678.1>
- Berkopec, A. (2007), ‘HyperQuick algorithm for discrete hypergeometric distribution’, *Journal of Discrete Algorithms* **5**(2), 341 – 347. 2004 Symposium on String Processing and Information Retrieval.
URL: <http://www.sciencedirect.com/science/article/pii/S1570866706000499>
- Binder, H., Boettcher, M., Joos, H. and Wernli, H. (2016), ‘The Role of Warm Conveyor Belts for the Intensification of Extratropical Cyclones in Northern Hemisphere Winter’, *Journal of the Atmospheric Sciences* **73**(10), 3997–4020.
URL: <http://dx.doi.org/10.1175/JAS-D-15-0302.1>
- Bjerknes, J. and Solberg, H. (1922), ‘Life cycle of cyclones and the polar front theory of atmospheric circulation’, *Geophys. Publ.* **3**, 1–18.
- Blackmon, M. L. (1976), ‘A Climatological Spectral Study of the 500 mb Geopotential Height of the Northern Hemisphere’, *Journal of the Atmospheric Sciences* **33**(8), 1607–1623.
URL: [https://doi.org/10.1175/1520-0469\(1976\)033<1607:ACSSOT>2.0.CO;2](https://doi.org/10.1175/1520-0469(1976)033<1607:ACSSOT>2.0.CO;2)
- Blackmon, M. L., Wallace, J. M., Lau, N.-C. and Mullen, S. L. (1977), ‘An Observational Study of the Northern Hemisphere Wintertime Circulation’, *Journal of the Atmospheric Sciences* **34**(7), 1040–1053.
URL: [https://doi.org/10.1175/1520-0469\(1977\)034<1040:AOSOTN>2.0.CO;2](https://doi.org/10.1175/1520-0469(1977)034<1040:AOSOTN>2.0.CO;2)

- Bolton, D. (1980), ‘The Computation of Equivalent Potential Temperature’, *Monthly Weather Review* **108**(7), 1046–1053.
- Branstator, G. (2002), ‘Circumglobal Teleconnections, the Jet Stream Waveguide, and the North Atlantic Oscillation’, *Journal of Climate* **15**(14), 1893–1910.
URL: [https://doi.org/10.1175/1520-0442\(2002\)015<1893:CTTJSW>2.0.CO;2](https://doi.org/10.1175/1520-0442(2002)015<1893:CTTJSW>2.0.CO;2)
- Broennimann, S., Martius, O., von Waldow, H., Welker, C., Luterbacher, J., Compo, G. P., Sardeshmukh, P. D. and Usbeck, T. (2012), ‘Extreme winds at northern mid-latitudes since 1871’, *Meteorologische Zeitschrift* **21**(1), 13–27.
- Burningham, H. and French, J. (2013), ‘Is the NAO winter index a reliable proxy for wind climate and storminess in northwest Europe?’, *International Journal of Climatology* **33**(8), 2036–2049.
URL: <https://rmets.onlinelibrary.wiley.com/doi/abs/10.1002/joc.3571>
- Burt, S. D. and Mansfield, D. A. (1988), ‘The Great Storm of 15–16 October 1987’, *Weather* **43**(3), 90–110.
URL: <http://dx.doi.org/10.1002/j.1477-8696.1988.tb03885.x>
- Cassou, C., Deser, C., Terray, L., Hurrell, J. W. and Drevillon, M. (2004), ‘Summer sea surface temperature conditions in the North Atlantic and their impact upon the atmospheric circulation in early winter’, *Journal of Climate* **17**(17), 3349–3363.
- Catto, J. L. (2016), ‘Extratropical cyclone classification and its use in climate studies’, *Reviews of Geophysics* **54**(2), 486–520.
URL: <http://dx.doi.org/10.1002/2016RG000519>
- Catto, J. L., Madonna, E., Joos, H., Rudeva, I. and Simmonds, I. (2015), ‘Global Relationship between Fronts and Warm Conveyor Belts and the Impact on Extreme Precipitation’, *Journal of Climate* **28**(21), 8411–8429.
URL: <https://doi.org/10.1175/JCLI-D-15-0171.1>
- Catto, J. L., Shaffrey, L. C. and Hodges, K. I. (2009), ‘Can Climate Models Capture the Structure of Extratropical Cyclones?’, *Journal of Climate* **23**(7), 1621–1635.
URL: <http://dx.doi.org/10.1175/2009JCLI3318.1>
- Chan, D. and Wu, Q. (2015), ‘Attributing Observed SST Trends and Subcontinental Land Warming to Anthropogenic Forcing during 1979–2005’, *Journal of Climate* **28**(8), 3152–3170.
URL: <http://dx.doi.org/10.1175/JCLI-D-14-00253.1>
- Charney, J. G. (1947), ‘THE DYNAMICS OF LONG WAVES IN A BAROCLINIC WESTERLY CURRENT’, *Journal of Meteorology* **4**(5), 136–162.
URL: [https://doi.org/10.1175/1520-0469\(1947\)004<0136:TDOLWI>2.0.CO;2](https://doi.org/10.1175/1520-0469(1947)004<0136:TDOLWI>2.0.CO;2)

- Chelton, D. B., Schlax, M. G., Freilich, M. H. and Milliff, R. F. (2004), ‘Satellite Measurements Reveal Persistent Small-Scale Features in Ocean Winds’, *Science*.
URL: <http://science.sciencemag.org/content/early/2004/01/15/science.1091901>
- Clark, R. T., Bett, P. E., Thornton, H. E. and Scaife, A. A. (2017), ‘Skilful seasonal predictions for the European energy industry’, *Environmental Research Letters* **12**(2), 024002.
URL: <http://stacks.iop.org/1748-9326/12/i=2/a=024002>
- Cohen, J. and Entekhabi, D. (1999), ‘Eurasian snow cover variability and northern hemisphere climate predictability’, *Geophysical Research Letters* **26**(3), 345–348.
URL: <https://agupubs.onlinelibrary.wiley.com/doi/abs/10.1029/1998GL900321>
- Cohen, J., Screen, J. A., Furtado, J. C., Barlow, M., Whittleston, D., Coumou, D., Francis, J., Dethloff, K., Entekhabi, D., Overland, J. and Jones, J. (2014), ‘Recent Arctic amplification and extreme mid-latitude weather’, *Nature Geoscience* **7**(9), 627–637.
- Compo, G. P., Whitaker, J. S., Sardeshmukh, P. D., Matsui, N., Allan, R. J., Yin, X., Gleason, B. E., Vose, R. S., Rutledge, G., Bessemoulin, P., Brönnimann, S., Brunet, M., Crouthamel, R. I., Grant, A. N., Groisman, P. Y., Jones, P. D., Kruk, M. C., Kruger, A. C., Marshall, G. J., Maugeri, M., Mok, H. Y., Nordli, O., Ross, T. F., Trigo, R. M., Wang, X. L., Woodruff, S. D. and Worley, S. J. (2011), ‘The Twentieth Century Reanalysis Project’, *Quarterly Journal of the Royal Meteorological Society* **137**(654), 1–28.
URL: <http://dx.doi.org/10.1002/qj.776>
- Coumou, D., Petoukhov, V., Rahmstorf, S., Petri, S. and Schellnhuber, H. J. (2014), ‘Quasi-resonant circulation regimes and hemispheric synchronization of extreme weather in boreal summer’, *Proceedings of the National Academy of Sciences of the United States of America* **111**(34), 12331–12336.
URL: <http://www.ncbi.nlm.nih.gov/pmc/articles/PMC4151761/>
- Coumou, D. and Rahmstorf, S. (2012), ‘A decade of weather extremes’, *Nature Climate Change* **2**(7), 491–496.
- CRU - Climate Research Unit - University of East Anglia (2014), ‘Lamb Weather Types - UK Jenkinson Gale Index’,
URL: http://www.cru.uea.ac.uk/cru/data/lwt/webdocs/NDJFMA_G_thresh_counts_UK.pdf
- Cusack, S. (2013), ‘A 101 year record of windstorms in the Netherlands’, *Climatic Change* **116**(3-4), 693–704.

- Czaja, A. and Blunt, N. (2011), ‘A new mechanism for ocean–atmosphere coupling in midlatitudes’, *Quarterly Journal of the Royal Meteorological Society* **137**(657), 1095–1101.
URL: <http://dx.doi.org/10.1002/qj.814>
- Czaja, A. and Frankignoul, C. (1999), ‘Influence of the North Atlantic SST on the atmospheric circulation’, *Geophysical Research Letters* **26**(19), 2969–2972.
- Czaja, A. and Frankignoul, C. (2002), ‘Observed Impact of Atlantic SST Anomalies on the North Atlantic Oscillation’, *Journal of Climate* **15**(6), 606–623.
URL: [http://dx.doi.org/10.1175/1520-0442\(2002\)015<0606:OIOASA>2.0.CO;2](http://dx.doi.org/10.1175/1520-0442(2002)015<0606:OIOASA>2.0.CO;2)
- Dacre, H. F. and Gray, S. L. (2009), ‘The Spatial Distribution and Evolution Characteristics of North Atlantic Cyclones’, *Monthly Weather Review* **137**(1), 99–115.
URL: <http://dx.doi.org/10.1175/2008MWR2491.1>
- Dacre, H. F., Hawcroft, M. K., Stringer, M. A. and Hodges, K. I. (2012), ‘An Extratropical Cyclone Atlas: A Tool for Illustrating Cyclone Structure and Evolution Characteristics’, *Bulletin of the American Meteorological Society* **93**(10), 1497–1502.
URL: <http://dx.doi.org/10.1175/BAMS-D-11-00164.1>
- Davini, P., Cagnazzo, C., Neale, R. and Tribbia, J. (2012), ‘Coupling between Greenland blocking and the North Atlantic Oscillation pattern’, *Geophysical Research Letters* **39**(14), L14701.
URL: <http://dx.doi.org/10.1029/2012GL052315>
- Dawkins, L. C., Stephenson, D. B., Lockwood, J. F. and Maisey, P. E. (2016), ‘The 21st century decline in damaging European windstorms’, *Natural Hazards and Earth System Sciences* **16**(8), 1999–2007.
URL: <http://www.nat-hazards-earth-syst-sci.net/16/1999/2016/>
- Dee, D. P., Uppala, S. M., Simmons, A. J., Berrisford, P., Poli, P., Kobayashi, S., Andrae, U., Balmaseda, M. A., Balsamo, G., Bauer, P., Bechtold, P., Beljaars, A. C. M., van de Berg, L., Bidlot, J., Bormann, N., Delsol, C., Dragani, R., Fuentes, M., Geer, A. J., Haimberger, L., Healy, S. B., Hersbach, H., Holm, E. V., Isaksen, L., Kallberg, P., Koehler, M., Matricardi, M., McNally, A. P., Monge-Sanz, B. M., Morcrette, J. J., Park, B. K., Peubey, C., de Rosnay, P., Tavolato, C., Thepaut, J. N. and Vitart, F. (2011), ‘The ERA-Interim reanalysis: configuration and performance of the data assimilation system’, *Quarterly Journal of the Royal Meteorological Society* **137**(656, A), 553–597.
- Della-Marta, P. M., Liniger, M. A., Appenzeller, C., Bresch, D. N., Köllner-Heck, P. and Muccione, V. (2010), ‘Improved Estimates of the European Winter Windstorm

- Climate and the Risk of Reinsurance Loss Using Climate Model Data', *Journal of Applied Meteorology and Climatology* **49**(10), 2092–2120.
URL: <https://doi.org/10.1175/2010JAMC2133.1>
- Deser, C., Alexander, M. A., Xie, S.-P. and Phillips, A. S. (2010), 'Sea Surface Temperature Variability: Patterns and Mechanisms', *Annual Review of Marine Sciences* **2**, 115–143.
- Deser, C. and Timlin, M. S. (1997), 'Atmosphere–Ocean Interaction on Weekly Timescales in the North Atlantic and Pacific', *Journal of Climate* **10**(3), 393–408.
URL: [https://doi.org/10.1175/1520-0442\(1997\)010<0393:AOIOWT>2.0.CO;2](https://doi.org/10.1175/1520-0442(1997)010<0393:AOIOWT>2.0.CO;2)
- Deser, C., Tomas, R. A. and Peng, S. (2007), 'The transient atmospheric circulation response to North Atlantic SST and sea ice anomalies', *Journal of Climate* **20**(18), 4751–4767.
- Dessai, S. and Bruno Soares, M. (2013), 'Systematic literature review on the use of seasonal to decadal climate and climate impacts predictions across European sectors', *University of Leeds, European Provision Of Regional Impact Assessment on a Seasonal-to-decadal timescale, Deliverable Report D 12*.
- Doblas-Reyes, F. J., García-Serrano, J., Lienert, F., Biescas, A. P. and Rodrigues, L. R. L. (2013), 'Seasonal climate predictability and forecasting: status and prospects', *Wiley Interdisciplinary Reviews: Climate Change* **4**(4), 245–268.
URL: <http://dx.doi.org/10.1002/wcc.217>
- Donat, M. G., Leckebusch, G. C., Pinto, J. G. and Ulbrich, U. (2010), 'Examination of wind storms over Central Europe with respect to circulation weather types and NAO phases', *International Journal of Climatology* **30**(9), 1289–1300.
- Donat, M. G., Leckebusch, G. C., Wild, S. and Ulbrich, U. (2010), 'Benefits and limitations of regional multi-model ensembles for storm loss estimations', *Climate Research* **44**(2/3), 211–225.
URL: <http://www.jstor.org/stable/24870390>
- Donat, M. G., Renggli, D., Wild, S., Alexander, L. V., Leckebusch, G. C. and Ulbrich, U. (2011), 'Reanalysis suggests long-term upward trends in European storminess since 1871', *Geophysical Research Letters* **38**(14). L14703.
URL: <http://dx.doi.org/10.1029/2011GL047995>
- Douville, H. (2010), 'Relative contribution of soil moisture and snow mass to seasonal climate predictability: a pilot study', *Climate Dynamics* **34**(6), 797–818.
URL: <https://doi.org/10.1007/s00382-008-0508-1>

- Duchon, C. E. (1979), ‘Lanczos Filtering in One and Two Dimensions’, *Journal of Applied Meteorology* **18**(8), 1016–1022.
URL: [https://doi.org/10.1175/1520-0450\(1979\)018<1016:LFIOAT>2.0.CO;2](https://doi.org/10.1175/1520-0450(1979)018<1016:LFIOAT>2.0.CO;2)
- Eady, E. (1949), ‘Long Waves and Cyclone Waves’, *Tellus* **1**(3), 33–52.
- Economou, T., Stephenson, D. B., Pinto, J. G., Shaffrey, L. C. and Zappa, G. (2014), ‘Serial clustering of extratropical cyclones in a multi[U+2010]model ensemble of historical and future simulations’, *Quarterly Journal of the Royal Meteorological Society* **141**(693), 3076–3087.
URL: <https://rmets.onlinelibrary.wiley.com/doi/abs/10.1002/qj.2591>
- Eden, P. (2011), ‘From Observations to Forecasts – Part 14: Communicating forecasts’, *Weather* **66**(12), 325–327.
URL: <https://rmets.onlinelibrary.wiley.com/doi/abs/10.1002/wea.872>
- Environment Canada (2014), ‘Climate Trends and Variations Bulletin – Winter 2013-2014.’,
URL: https://www.ec.gc.ca/adsc-cmda/383F5EFA-508D-45E8-89AD-4B14B53B429E/CTVB_Winter20132014_E.pdf.
- Fink, A. H., Bruecher, T., Ermert, V., Krueger, A. and Pinto, J. G. (2009), ‘The European storm Kyrill in January 2007: synoptic evolution, meteorological impacts and some considerations with respect to climate change’, *Natural Hazards and Earth System Science* **9**(2), 405–423.
- Fink, A. H., Pohle, S., Pinto, J. G. and Knippertz, P. (2012), ‘Diagnosing the influence of diabatic processes on the explosive deepening of extratropical cyclones’, *Geophysical Research Letters* **39**(7), L07803.
URL: <http://dx.doi.org/10.1029/2012GL051025>
- Francis, J. A. and Vavrus, S. J. (2012), ‘Evidence linking Arctic amplification to extreme weather in mid-latitudes’, *Geophysical Research Letters* **39**.
- Francis, J. A. and Vavrus, S. J. (2015), ‘Evidence for a wavier jet stream in response to rapid Arctic warming’, *Environmental Research Letters* **10**(1), 014005.
URL: <http://stacks.iop.org/1748-9326/10/i=1/a=014005>
- Franzke, C. and Woollings, T. (2011), ‘On the Persistence and Predictability Properties of North Atlantic Climate Variability’, *Journal of Climate* **24**(2), 466–472.
- Frías, M. D., Herrera, S., Cofiño, A. S. and Gutiérrez, J. M. (2010), ‘Assessing the Skill of Precipitation and Temperature Seasonal Forecasts in Spain: Windows of Opportunity Related to ENSO Events’, *Journal of Climate* **23**(2), 209–220.
URL: <https://doi.org/10.1175/2009JCLI2824.1>

- García-Serrano, J., Losada, T., Rodríguez-Fonseca, B. and Polo, I. (2008), ‘Tropical Atlantic Variability Modes (1979–2002). Part II: Time-Evolving Atmospheric Circulation Related to SST-Forced Tropical Convection’, *Journal of Climate* **21**(24), 6476–6497.
URL: <https://doi.org/10.1175/2008JCLI2191.1>
- Gastineau, G. and Frankignoul, C. (2014), ‘Influence of the North Atlantic SST Variability on the Atmospheric Circulation during the Twentieth Century’, *Journal of Climate* **28**(4), 1396–1416.
URL: <http://dx.doi.org/10.1175/JCLI-D-14-00424.1>
- Gates, W. L., Boyle, J. S., Covey, C., Dease, C. G., Doutriaux, C. M., Drach, R. S., Fiorino, M., Gleckler, P. J., Hnilo, J. J., Marlais, S. M., Phillips, T. J., Potter, G. L., Santer, B. D., Sperber, K. R., Taylor, K. E. and Williams, D. N. (1999), ‘An Overview of the Results of the Atmospheric Model Intercomparison Project (AMIP I)’, *Bulletin of the American Meteorological Society* **80**(1), 29–55.
URL: [https://doi.org/10.1175/1520-0477\(1999\)080<0029:AOOTRO>2.0.CO;2](https://doi.org/10.1175/1520-0477(1999)080<0029:AOOTRO>2.0.CO;2)
- Grams, C. M., Wernli, H., Böttcher, M., Čampa, J., Corsmeier, U., Jones, S. C., Keller, J. H., Lenz, C.-J. and Wiegand, L. (2011), ‘The key role of diabatic processes in modifying the upper-tropospheric wave guide: a North Atlantic case-study’, *Quarterly Journal of the Royal Meteorological Society* **137**(661), 2174–2193.
URL: <http://dx.doi.org/10.1002/qj.891>
- Gray, S. L., Martínez-Alvarado, O., Baker, L. H. and Clark, P. A. (2011), ‘Conditional symmetric instability in sting-jet storms’, *Quarterly Journal of the Royal Meteorological Society* **137**(659), 1482–1500.
URL: <http://dx.doi.org/10.1002/qj.859>
- Greatbatch, R. J. and Jung, T. (2007), ‘Local versus Tropical Diabatic Heating and the Winter North Atlantic Oscillation’, *Journal of Climate* **20**(10), 2058–2075.
URL: <https://doi.org/10.1175/JCLI4125.1>
- Grieger, J., Leckebusch, G., Donat, M., Schuster, M. and Ulbrich, U. (2014), ‘Southern Hemisphere winter cyclone activity under recent and future climate conditions in multi-model AOGCM simulations’, *International Journal of Climatology* **34**(12), 3400–3416.
URL: <http://dx.doi.org/10.1002/joc.3917>
- Gómara, I., Pinto, J. G., Woollings, T., Masato, G., Zurita-Gotor, P. and Rodríguez-Fonseca, B. (2014), ‘Rossby wave-breaking analysis of explosive cyclones in the Euro-Atlantic sector’, *Quarterly Journal of the Royal Meteorological Society*

140(680), 738–753.

URL: <http://dx.doi.org/10.1002/qj.2190>

Gómara, I., Rodríguez-Fonseca, B., Zurita-Gotor, P. and Pinto, J. G. (2014), ‘On the relation between explosive cyclones affecting Europe and the North Atlantic Oscillation’, *Geophysical Research Letters* **41**(6), 2182–2190.

URL: <http://dx.doi.org/10.1002/2014GL059647>

Haeseler, S., Lefebvre, C., Bissolli, P., Dassler, J. and Mamtimin, B. (2018), ‘Orkantief FRIEDERIKE wütet am 18. Januar 2018 über Europa’, *German Weather Service - Deutscher Wetterdienst*.

URL: https://www.dwd.de/DE/leistungen/besondereereignisse/stuerme/20180123-friederike-europa.pdf?__blob=publicationFile&v=4

Hanley, J. and Caballero, R. (2012), ‘The role of large-scale atmospheric flow and Rossby wave breaking in the evolution of extreme windstorms over Europe’, *Geophysical Research Letters* **39**(21), L21708.

URL: <http://dx.doi.org/10.1029/2012GL053408>

Hanna, E., Jones, J. M., Cappelen, J., Mernild, S. H., Wood, L., Steffen, K. and Huybrechts, P. (2008), ‘The influence of North Atlantic atmospheric and oceanic forcing effects on 1900–2010 Greenland summer climate and ice melt/runoff’, *International Journal of Climatology* **33**(4), 862–880.

URL: <https://rmets.onlinelibrary.wiley.com/doi/abs/10.1002/joc.3475>

Hansen, F., Greatbatch, R. J., Gollan, G., Jung, T. and Weisheimer, A. (2017), ‘Remote control of North Atlantic Oscillation predictability via the stratosphere’, *Quarterly Journal of the Royal Meteorological Society* **143**(703), 706–719.

URL: <http://dx.doi.org/10.1002/qj.2958>

Hartmann, D. L. (2015), ‘Pacific sea surface temperature and the winter of 2014’, *Geophysical Research Letters* **42**(6), 1894–1902. 2015GL063083.

URL: <http://dx.doi.org/10.1002/2015GL063083>

Harvey, B. J., Shaffrey, L. C. and Woollings, T. J. (2014), ‘Equator-to-pole temperature differences and the extra-tropical storm track responses of the CMIP5 climate models’, *Climate Dynamics* **43**(5-6), 1171–1182.

Harvey, B. J., Shaffrey, L. C., Woollings, T. J., Zappa, G. and Hodges, K. I. (2012), ‘How large are projected 21st century storm track changes?’, *Geophysical Research Letters* **39**.

Hawcroft, M., Dacre, H., Forbes, R., Hodges, K., Shaffrey, L. and Stein, T. (2017), ‘Using satellite and reanalysis data to evaluate the representation of latent heating

- in extratropical cyclones in a climate model', *Climate Dynamics* **48**(7), 2255–2278.
URL: <https://doi.org/10.1007/s00382-016-3204-6>
- Held, I. M. (1978), 'The Vertical Scale of an Unstable Baroclinic Wave and Its Importance for Eddy Heat Flux Parameterizations', *Journal of the Atmospheric Sciences* **35**(4), 572–576.
URL: [https://doi.org/10.1175/1520-0469\(1978\)035<0572:TVSOAU>2.0.CO;2](https://doi.org/10.1175/1520-0469(1978)035<0572:TVSOAU>2.0.CO;2)
- Hersbach, H. and Dee, D. (2016), 'ERA5 reanalysis is in production', *ECMWF Newsletter* **147**.
- Hewson, T. D. and Neu, U. (2015), 'Cyclones, windstorms and the IMILAST project', *Tellus A: Dynamic Meteorology and Oceanography* **67**(1), 27128.
URL: <https://doi.org/10.3402/tellusa.v67.27128>
- Hewson, Tim D. and Tittley, Helen A. (2010), 'Objective identification, typing and tracking of the complete life-cycles of cyclonic features at high spatial resolution', *Meteorological Applications* **17**(3), 355–381.
URL: <http://dx.doi.org/10.1002/met.204>
- Hodges, K. I., Lee, R. W. and Bengtsson, L. (2011), 'A Comparison of Extratropical Cyclones in Recent Reanalyses ERA-Interim, NASA MERRA, NCEP CFSR, and JRA-25', *Journal of Climate* **24**(18), 4888–4906.
URL: <http://dx.doi.org/10.1175/2011JCLI4097.1>
- Hoffmann, G. (1999), 'Die Bedeutung der diabatischen Heizung fuer die synoptische Stoerungsaktivitaet der Nordhemisphaere im heutigen und zukuenftigen Klima', *Mitteilungen aus dem Institut fuer Geophysik und Meteorologie der Universitaet zu Koeln Heft* **126**.
- Honda, M., Nakamura, H., Ukita, J., Kousaka, I. and Takeuchi, K. (2001), 'Interannual Seesaw between the Aleutian and Icelandic Lows. Part I: Seasonal Dependence and Life Cycle', *Journal of Climate* **14**(6), 1029–1042.
URL: [http://dx.doi.org/10.1175/1520-0442\(2001\)014<1029:ISBTAA>2.0.CO;2](http://dx.doi.org/10.1175/1520-0442(2001)014<1029:ISBTAA>2.0.CO;2)
- Horton, D. E., Johnson, N. C., Singh, D., Swain, D. L., Rajaratnam, B. and Diffenbaugh, N. S. (2015), 'Contribution of changes in atmospheric circulation patterns to extreme temperature trends', *Nature* **522**, 465–.
URL: <http://dx.doi.org/10.1038/nature14550>
- Hoskins, B. J. and Ambrizzi, T. (1993), 'Rossby Wave Propagation on a Realistic Longitudinally Varying Flow', *Journal of the Atmospheric Sciences* **50**(12), 1661–1671.
URL: [https://doi.org/10.1175/1520-0469\(1993\)050<1661:RWPOAR>2.0.CO;2](https://doi.org/10.1175/1520-0469(1993)050<1661:RWPOAR>2.0.CO;2)

- Hoskins, B. J. and Karoly, D. J. (1981), 'The Steady Linear Response of a Spherical Atmosphere to Thermal and Orographic Forcing', *Journal of the Atmospheric Sciences* **38**(6), 1179–1196.
URL: [https://doi.org/10.1175/1520-0469\(1981\)038<1179:TSLROA>2.0.CO;2](https://doi.org/10.1175/1520-0469(1981)038<1179:TSLROA>2.0.CO;2)
- Hoskins, B. J., McIntyre, M. E. and Robertson, A. W. (1985), 'On the use and significance of isentropic potential vorticity maps', *Quarterly Journal of the Royal Meteorological Society* **111**(470), 877–946.
URL: <http://dx.doi.org/10.1002/qj.49711147002>
- Hoskins, B. J. and Valdes, P. J. (1990), 'On the Existence of Storm-Tracks', *Journal of the Atmospheric Sciences* **47**(15), 1854–1864.
URL: [http://dx.doi.org/10.1175/1520-0469\(1990\)047<1854:OTEOST>2.0.CO;2](http://dx.doi.org/10.1175/1520-0469(1990)047<1854:OTEOST>2.0.CO;2)
- Hoskins, B. J. and Woollings, T. (2015), 'Persistent Extratropical Regimes and Climate Extremes', *Current Climate Change Reports* **1**(3), 115–124.
URL: <https://doi.org/10.1007/s40641-015-0020-8>
- Houghton, J. T. (1988), 'The Storm, the Media and the Enquiry', *Weather* **43**(3), 67–70.
URL: <https://rmets.onlinelibrary.wiley.com/doi/abs/10.1002/j.1477-8696.1988.tb03883.x>
- Huang, B., Banzon, V. F., Freeman, E., Lawrimore, J., Liu, W., Peterson, T. C., Smith, T. M., Thorne, P. W., Woodruff, S. D. and Zhang, H.-M. (2014), 'Extended Reconstructed Sea Surface Temperature Version 4 (ERSST.v4). Part I: Upgrades and Intercomparisons', *Journal of Climate* **28**(3), 911–930.
URL: <http://dx.doi.org/10.1175/JCLI-D-14-00006.1>
- Huntingford, C., Marsh, T., Scaife, A. A., Kendon, E. J., Hannaford, J., Kay, A. L., Lockwood, M., Prudhomme, C., Reynard, N. S., Parry, S., Lowe, J. A., Screen, J. A., Ward, H. C., Roberts, M., Stott, P. A., Bell, V. A., Bailey, M., Jenkins, A., Legg, T., Otto, F. E. L., Massey, N., Schaller, N., Slingo, J. and Allen, M. R. (2014), 'Potential influences on the United Kingdom's floods of winter 2013/14', *Nature Climate Change* **4**(9), 769–777.
URL: <http://dx.doi.org/10.1038/nclimate2314>
- Hurrell, J. and VanLoon, H. (1997), 'Decadal variations in climate associated with the north Atlantic oscillation', *Climatic Change* **36**(3-4), 301–326.
- Hurrell, J. W. (1995), 'Decadal Trends in the North Atlantic Oscillation: Regional Temperatures and Precipitation', *Science* **269**(5224), 676–679.
URL: <http://science.sciencemag.org/content/269/5224/676>

- Hurrell, J. W. (1996), 'Influence of variations in extratropical wintertime teleconnections on northern hemisphere temperature', *Geophysical Research Letters* **23**(6), 665–668.
URL: <https://agupubs.onlinelibrary.wiley.com/doi/abs/10.1029/96GL00459>
- Hurrell, J. W. and Deser, C. (2009), 'North Atlantic climate variability: The role of the North Atlantic Oscillation', *Journal of Marine Systems* **78**(1), 28 – 41.
URL: <http://www.sciencedirect.com/science/article/pii/S0924796309000815>
- Hurrell, J. W., Hack, J. J., Shea, D., Caron, J. M. and Rosinski, J. (2008), 'A New Sea Surface Temperature and Sea Ice Boundary Dataset for the Community Atmosphere Model', *Journal of Climate* **21**(19), 5145–5153.
URL: <https://doi.org/10.1175/2008JCLI2292.1>
- Hurrell, J. W., Kushnir, Y., Ottersen, G. and Visbeck, M. (2003), *An Overview of the North Atlantic Oscillation*, American Geophysical Union (AGU), pp. 1–35.
URL: <https://agupubs.onlinelibrary.wiley.com/doi/abs/10.1029/134GM01>
- Ineson, S. and Scaife, A. A. (2008), 'The role of the stratosphere in the European climate response to El Niño', *Nature Geoscience* **2**, 32–.
URL: <http://dx.doi.org/10.1038/ngeo381>
- IPCC (2012), *Managing the Risks of Extreme Events and Disasters to Advance Climate Change Adaptation. A Special Report of Working Groups I and II of the Intergovernmental Panel on Climate Change.*, Cambridge University Press.
- Kendall, M. G. and Dickinson, J. G. (1990), *Rank Correlation Methods (Charles Griffin Book Series)*, A Charles Griffin Book, 5th edn, E. Arnold.
- Kendon, M. and McCarthy, M. (2015), 'The UK's wet and stormy winter of 2013/2014', *Weather* **70**(2, SI), 40–47.
- Klawa, M. and Ulbrich, U. (2003), 'A model for the estimation of storm losses and the identification of severe winter storms in Germany', *Natural Hazards and Earth System Science* **3**(6), 725–732.
URL: <http://www.nat-hazards-earth-syst-sci.net/3/725/2003/>
- Kornhuber, K., Petoukhov, V., Petri, S., Rahmstorf, S. and Coumou, D. (2017), 'Evidence for wave resonance as a key mechanism for generating high-amplitude quasi-stationary waves in boreal summer', *Climate Dynamics* **49**(5), 1961–1979.
URL: <https://doi.org/10.1007/s00382-016-3399-6>
- Kotlarski, S., Keuler, K., Christensen, O. B., Colette, A., Déqué, M., Gobiet, A., Goergen, K., Jacob, D., Lüthi, D., van Meijgaard, E., Nikulin, G., Schär, C., Teichmann, C., Vautard, R., Warrach-Sagi, K. and Wulfmeyer, V. (2014), 'Regional climate

modeling on European scales: a joint standard evaluation of the EURO-CORDEX RCM ensemble’, *Geoscientific Model Development* **7**(4), 1297–1333.

URL: <https://www.geosci-model-dev.net/7/1297/2014/>

Krueger, O., Feser, F., Bärring, L., Kaas, E., Schmith, T., Tuomenvirta, H. and von Storch, H. (2014), ‘Comment on “Trends and low frequency variability of extra-tropical cyclone activity in the ensemble of twentieth century reanalysis” by Xiaolan L. Wang, Y. Feng, G. P. Compo, V. R. Swail, F. W. Zwiers, R. J. Allan, and P. D. Sardeshmukh, *Climate Dynamics*, 2012’, *Climate Dynamics* **42**(3), 1127–1128.

URL: <https://doi.org/10.1007/s00382-013-1814-9>

Krueger, O., Schenk, F., Feser, F. and Weisse, R. (2013), ‘Inconsistencies between Long-Term Trends in Storminess Derived from the 20CR Reanalysis and Observations’, *Journal of Climate* **26**(3), 868–874.

URL: <http://dx.doi.org/10.1175/JCLI-D-12-00309.1>

Kruschke, T. (2015), Winter wind storms: Identification, verification of decadal predictions, and regionalization, PhD thesis, Institut für Meteorologie, Freie Universität Berlin.

Kruschke, T., Rust, H. W., Kadow, C., Leckebusch, G. C. and Ulbrich, U. (2014), ‘Evaluating decadal predictions of northern hemispheric cyclone frequencies’, *Tellus A: Dynamic Meteorology and Oceanography* **66**.

Kurz, M. (1990), *Synoptische Meteorologie*, Selbstverlag des Deutschen Wetterdienstes.

Kushnir, Y., Robinson, W. A., Bladé, I., Hall, N. M. J., Peng, S. and Sutton, R. (2002), ‘Atmospheric GCM Response to Extratropical SST Anomalies: Synthesis and Evaluation’, *Journal of Climate* **15**(16), 2233–2256.

URL: [https://doi.org/10.1175/1520-0442\(2002\)015<2233:AGRTES>2.0.CO;2](https://doi.org/10.1175/1520-0442(2002)015<2233:AGRTES>2.0.CO;2)

Lambert, S. J. and Fyfe, J. C. (2006), ‘Changes in winter cyclone frequencies and strengths simulated in enhanced greenhouse warming experiments: results from the models participating in the IPCC diagnostic exercise’, *Climate Dynamics* **26**(7), 713–728.

URL: <https://doi.org/10.1007/s00382-006-0110-3>

Lau, N.-C. (1988), ‘Variability of the Observed Midlatitude Storm Tracks in Relation to Low-Frequency Changes in the Circulation Pattern’, *Journal of the Atmospheric Sciences* **45**(19), 2718–2743.

URL: [http://dx.doi.org/10.1175/1520-0469\(1988\)045<2718:VOTOMS>2.0.CO;2](http://dx.doi.org/10.1175/1520-0469(1988)045<2718:VOTOMS>2.0.CO;2)

Leathers, D., Yarnal, B. and Palecki, M. (1991), ‘The Pacific North-American Teleconnection Pattern and United-States Climate.1. Regional Temperature and Precipitation Associations’, *Journal of Climate* **4**(5), 517–528.

- Leckebusch, G. C., Koffi, B., Ulbrich, U., Pinto, J. G., Spanghel, T. and Zacharias, S. (2006), 'Analysis of frequency and intensity of European winter storm events from a multi-model perspective, at synoptic and regional scales', *Climate Research* **31**(1), 59–74.
URL: <http://www.int-res.com/abstracts/cr/v31/n1/p59-74/>
- Leckebusch, G. C., Renggli, D. and Ulbrich, U. (2008), 'Development and application of an objective storm severity measure for the Northeast Atlantic region', *Meteorologische Zeitschrift* **17**(5, SI), 575–587.
- Leckebusch, G. and Ulbrich, U. (2004), 'On the relationship between cyclones and extreme windstorm events over Europe under climate change', *Global and Planetary Change* **44**(1-4), 181–193.
- Lee, M.-Y., Hong, C.-C. and Hsu, H.-H. (2015), 'Compounding effects of warm sea surface temperature and reduced sea ice on the extreme circulation over the extratropical North Pacific and North America during the 2013-2014 boreal winter', *Geophysical Research Letters* **42**(5), 1612–1618.
URL: <http://dx.doi.org/10.1002/2014GL062956>
- Lehmann, J., Coumou, D., Frieler, K., Eliseev, A. V. and Levermann, A. (2014), 'Future changes in extratropical storm tracks and baroclinicity under climate change', *Environmental Research Letters* **9**(8), 084002.
URL: <http://stacks.iop.org/1748-9326/9/i=8/a=084002>
- Liberato, M. L. (2014), 'The 19 January 2013 windstorm over the North Atlantic: large-scale dynamics and impacts on Iberia', *Weather and Climate Extremes* **5-6**, 16 – 28.
URL: <http://www.sciencedirect.com/science/article/pii/S2212094714000620>
- Liberato, M. L. R., Pinto, J. G., Trigo, I. F. and Trigo, R. M. (2011), 'Klaus – an exceptional winter storm over northern Iberia and southern France', *Weather* **66**(12), 330–334.
URL: <http://dx.doi.org/10.1002/wea.755>
- Liebmann, B. and Smith, C. (1996), 'Description of a Complete (Interpolated) Outgoing Longwave Radiation Dataset', *Bulletin of the American Meteorological Society* **77**, 1275–1277.
- Lim, E.-P. and Simmonds, I. (2002), 'Explosive Cyclone Development in the Southern Hemisphere and a Comparison with Northern Hemisphere Events', *Monthly Weather Review* **130**(9), 2188–2209.
URL: [https://doi.org/10.1175/1520-0493\(2002\)130<2188:ECDITS>2.0.CO;2](https://doi.org/10.1175/1520-0493(2002)130<2188:ECDITS>2.0.CO;2)

- Lindzen, R. S. and Farrell, B. (1980), ‘A Simple Approximate Result for the Maximum Growth Rate of Baroclinic Instabilities’, *Journal of the Atmospheric Sciences* **37**(7), 1648–1654.
URL: [https://doi.org/10.1175/1520-0469\(1980\)037<1648:ASARFT>2.0.CO;2](https://doi.org/10.1175/1520-0469(1980)037<1648:ASARFT>2.0.CO;2)
- Ludwig, P., Pinto, J. G., Hoeppe, S. A., Fink, A. H. and Gray, S. L. (2014), ‘Secondary Cyclogenesis along an Occluded Front Leading to Damaging Wind Gusts: Windstorm Kyrill, January 2007’, *Monthly Weather Review* **143**(4), 1417–1437.
URL: <http://dx.doi.org/10.1175/MWR-D-14-00304.1>
- Luo, D., Yao, Y. and Dai, A. (2014), ‘Decadal Relationship between European Blocking and the North Atlantic Oscillation during 1978–2011. Part I: Atlantic Conditions’, *Journal of the Atmospheric Sciences* **72**(3), 1152–1173.
URL: <http://dx.doi.org/10.1175/JAS-D-14-0039.1>
- MacLachlan, C., Arribas, A., Peterson, K. A., Maidens, A., Fereday, D., Scaife, A. A., Gordon, M., Vellinga, M., Williams, A., Comer, R. E., Camp, J., Xavier, P. and Madec, G. (2015), ‘Global Seasonal forecast system version 5 (GloSea5): a high-resolution seasonal forecast system’, *Quarterly Journal of the Royal Meteorological Society* **141**(689), 1072–1084.
URL: <http://dx.doi.org/10.1002/qj.2396>
- Mahlstein, I., Martius, O., Chevalier, C. and Ginsbourger, D. (2012), ‘Changes in the odds of extreme events in the Atlantic basin depending on the position of the extratropical jet’, *Geophysical Research Letters* **39**.
- Mailier, P. J., Stephenson, D. B., Ferro, C. A. T. and Hodges, K. I. (2006), ‘Serial Clustering of Extratropical Cyclones’, *Monthly Weather Review* **134**(8), 2224–2240.
URL: <http://dx.doi.org/10.1175/MWR3160.1>
- Mann, M. E., Rahmstorf, S., Kornhuber, K., Steinman, B. A., Miller, S. K. and Coumou, D. (2017), ‘Influence of Anthropogenic Climate Change on Planetary Wave Resonance and Extreme Weather Events’, *Scientific Reports* **7**, 45242–.
URL: <http://dx.doi.org/10.1038/srep45242>
- Masato, G., Hoskins, B. J. and Woollings, T. (2013), ‘Wave-Breaking Characteristics of Northern Hemisphere Winter Blocking: A Two-Dimensional Approach’, *Journal of Climate* **26**(13), 4535–4549.
URL: <https://doi.org/10.1175/JCLI-D-12-00240.1>
- Masato, G., Hoskins, B. J. and Woollings, T. J. (2012), ‘Wave-breaking characteristics of midlatitude blocking’, *Quarterly Journal of the Royal Meteorological Society* **138**(666), 1285–1296.
URL: <http://dx.doi.org/10.1002/qj.990>

- Matthews, T., Murphy, C., Wilby, R. L. and Harrigan, S. (2014), ‘Stormiest winter on record for Ireland and UK’, *Nature Climate Change* **4**(9), 738–740.
URL: <http://dx.doi.org/10.1038/nclimate2336>
- Matulla, C., Schöner, W., Alexandersson, H., von Storch, H. and Wang, X. L. (2008), ‘European storminess: late nineteenth century to present’, *Climate Dynamics* **31**(2), 125–130.
URL: <https://doi.org/10.1007/s00382-007-0333-y>
- McCallum, E. and Norris, W. J. T. (1990), ‘The storms of January and February 1990’, *Meteorological Magazine* .
- McIntyre, M. E. and Palmer, T. N. (1983), ‘Breaking planetary waves in the stratosphere’, *Nature* **305**, 593–.
URL: <http://dx.doi.org/10.1038/305593a0>
- Messori, G. and Caballero, R. (2015), ‘On double Rossby wave breaking in the North Atlantic’, *Journal of Geophysical Research: Atmospheres* **120**(21), 11,129–11,150. 2015JD023854.
URL: <http://dx.doi.org/10.1002/2015JD023854>
- Met Office (2014), ‘Winter 2013/14.’,
URL: <http://www.metoffice.gov.uk/climate/uk/summaries/2014/winter>.
- Michel, C., Rivière, G., Terray, L. and Joly, B. (2012), ‘The dynamical link between surface cyclones, upper-tropospheric Rossby wave breaking and the life cycle of the Scandinavian blocking’, *Geophysical Research Letters* **39**(10), L10806.
URL: <http://dx.doi.org/10.1029/2012GL051682>
- Minobe, S., Kuwano-Yoshida, A., Komori, N., Xie, S. P. and Small, R. J. (2008), ‘Influence of the Gulf Stream on the troposphere’, *Nature* **452**(7184), 206–U51.
- Molteni, F., Stockdale, T., Balmaseda, M., Balsamo, G., Buizza, R., Ferranti, L., Magnusson, L., Mogensen, K., Palmer, T. and Vitart, F. (2011), ‘The new ECMWF seasonal forecast system (System 4)’, *ECMWF Tech. Memo.* **656**, 1–51.
- Müller, W. A., Appenzeller, C. and Latif, M. (2008), ‘NAO und Vorhersagbarkeit’, *Promet* **34**, 130–137.
- Müller, W. A., Appenzeller, C. and Schär, C. (2005), ‘Probabilistic seasonal prediction of the winter North Atlantic Oscillation and its impact on near surface temperature’, *Climate Dynamics* **24**(2-3), 213–226.
- Munich RE Group (2016), ‘NatCatSERVICE Schadenereignisse weltweit 1980-2015’,
URL: https://www.munichre.com/site/touch-naturalhazards/get/documents_

E123793997/mr/assetpool.shared/Documents/5_Touch/_NatCatService/
Focus_analyses/Schadenereignisse_weltweit_1980-2015.pdf.

Murray, R. and Simmonds, I. (1991), ‘A numerical scheme for tracking cyclone centres from digital data. I. Development and operation of the scheme’, *Australian Meteorological Magazine* **39**(3), 155–166.

Nakamura, H. (1992), ‘Midwinter suppression of baroclinic wave activity in the pacific’, *Journal of the Atmospheric Sciences* **49**(17), 1629–1642.

URL: [https://doi.org/10.1175/1520-0469\(1992\)049<1629:MSOBWA>2.0.CO;2](https://doi.org/10.1175/1520-0469(1992)049<1629:MSOBWA>2.0.CO;2)

Nakamura, M. and Plumb, R. A. (1994), ‘The Effects of Flow Asymmetry on the Direction of Rossby Wave Breaking’, *Journal of the Atmospheric Sciences* **51**(14), 2031–2045.

URL: [https://doi.org/10.1175/1520-0469\(1994\)051<2031:TEOFAO>2.0.CO;2](https://doi.org/10.1175/1520-0469(1994)051<2031:TEOFAO>2.0.CO;2)

National Climatic Data Center (2014), ‘Nov 2013 - Jan 2014 Divisional Ranks Temperature.’,

URL: <http://www.ncdc.noaa.gov/sotc/service/national/divisionaltavgrank/201311-201401.gif>.

Neu, U., Akperov, M. G., Bellenbaum, N., Benestad, R., Blender, R., Caballero, R., Coccozza, A., Dacre, H. F., Feng, Y., Fraedrich, K., Grieger, J., Gulev, S., Hanley, J., Hewson, T., Inatsu, M., Keay, K., Kew, S. F., Kindem, I., Leckebusch, G. C., Liberato, M. L. R., Lionello, P., Mokhov, I. I., Pinto, J. G., Raible, C. C., Reale, M., Rudeva, I., Schuster, M., Simmonds, I., Sinclair, M., Sprenger, M., Tilinina, N. D., Trigo, I. F., Ulbrich, S., Ulbrich, U., Wang, X. L. and Wernli, H. (2012), ‘IMILAST: A Community Effort to Intercompare Extratropical Cyclone Detection and Tracking Algorithms’, *Bulletin of the American Meteorological Society* **94**(4), 529–547.

URL: <http://dx.doi.org/10.1175/BAMS-D-11-00154.1>

Ning, L. and Bradley, R. S. (2014), ‘Winter Climate Extremes over the Northeastern United States and Southeastern Canada and Teleconnections with Large-Scale Modes of Climate Variability’, *Journal of Climate* **28**(6), 2475–2493.

URL: <http://dx.doi.org/10.1175/JCLI-D-13-00750.1>

Nissen, K., Leckebusch, G., Pinto, J. and Ulbrich, U. (2013), ‘Mediterranean cyclones and windstorms in a changing climate’, *Regional Environmental Change* .

URL: <http://dx.doi.org/10.1007/s10113-012-0400-8>

Nissen, K., Ulbrich, U., Leckebusch, G. and Kuhnel, I. (2014), ‘Decadal windstorm activity in the North Atlantic-European sector and its relationship to the meridional overturning circulation in an ensemble of simulations with a coupled climate model’, *Climate Dynamics* **43**(5-6), 1545–1555.

URL: <http://dx.doi.org/10.1007/s00382-013-1975-6>

- North, G. R., Bell, T. L., Cahalan, R. F. and Moeng, F. J. (1982), ‘Sampling Errors in the Estimation of Empirical Orthogonal Functions’, *Monthly Weather Review* **110**(7), 699–706.
URL: [https://doi.org/10.1175/1520-0493\(1982\)110<0699:SEITEO>2.0.CO;2](https://doi.org/10.1175/1520-0493(1982)110<0699:SEITEO>2.0.CO;2)
- Novak, L., Ambaum, M. H. P. and Tailleux, R. (2014), ‘The Life Cycle of the North Atlantic Storm Track’, *Journal of the Atmospheric Sciences* **72**(2), 821–833.
URL: <http://dx.doi.org/10.1175/JAS-D-14-0082.1>
- Palin, E. J., Scaife, A. A., Wallace, E., Pope, E. C. D., Arribas, A. and Brookshaw, A. (2016), ‘Skillful Seasonal Forecasts of Winter Disruption to the U.K. Transport System’, *Journal of Applied Meteorology and Climatology* **55**(2), 325–344.
URL: <https://doi.org/10.1175/JAMC-D-15-0102.1>
- Palmer, T. (2014), ‘Record-breaking winters and global climate change’, *Science* **344**(6186), 803–804.
URL: <http://www.sciencemag.org/content/344/6186/803.short>
- Palutikof, J. P. and Skellern, A. R. (1991), ‘Storm Severity over Britain, A Report to Commercial Union General Insurance’, *Climatic Research Unit, School of Environmental Sciences, University of East Anglia, Norwich (UK)* .
- Pearson, K. (1901), ‘LIII. On lines and planes of closest fit to systems of points in space’, *The London, Edinburgh, and Dublin Philosophical Magazine and Journal of Science* **2**(11), 559–572.
URL: <https://doi.org/10.1080/14786440109462720>
- Peng, S., Robinson, W. A. and Li, S. (2002), ‘North Atlantic SST forcing of the NAO and relationships with intrinsic hemispheric variability’, *Geophysical Research Letters* **29**(8), 1276.
- Petoukhov, V., Petri, S., Rahmstorf, S., Coumou, D., Kornhuber, K. and Schellnhuber, H. J. (2016), ‘Role of quasiresonant planetary wave dynamics in recent boreal spring-to-autumn extreme events’, *Proceedings of the National Academy of Sciences* **113**(25), 6862–6867.
URL: <http://www.pnas.org/content/113/25/6862>
- Petoukhov, V., Rahmstorf, S., Petri, S. and Schellnhuber, H. J. (2013), ‘Quasiresonant amplification of planetary waves and recent Northern Hemisphere weather extremes’, *Proceedings of the National Academy of Sciences* **110**(14), 5336–5341.
URL: <http://www.pnas.org/content/110/14/5336>
- Phillips, N. A. (1951), ‘A simple three-dimensional model for the study of large-scale extratropical flow patterns’, *Journal of Meteorology* **8**(6), 381–394.
URL: [https://doi.org/10.1175/1520-0469\(1951\)008<0381:ASTDMF>2.0.CO;2](https://doi.org/10.1175/1520-0469(1951)008<0381:ASTDMF>2.0.CO;2)

- Pinto, J. G., Gómara, I., Masato, G., Dacre, H. F., Woollings, T. and Caballero, R. (2014), ‘Large-scale dynamics associated with clustering of extra-tropical cyclones affecting Western Europe’, *Journal of Geophysical Research: Atmospheres* pp. 13704–13719.
URL: <http://dx.doi.org/10.1002/2014JD022305>
- Pinto, J. G., Karremann, M. K., Born, K., Della-Marta, P. M. and Klawe, M. (2012), ‘Loss potentials associated with European windstorms under future climate conditions’, *Climate Research* **54**(1), 1–20.
URL: <http://www.jstor.org/stable/24895220>
- Pinto, J. G. and Raible, C. C. (2012), ‘Past and recent changes in the North Atlantic oscillation’, *Wiley Interdisciplinary Reviews: Climate Change* **3**(1), 79–90.
- Pinto, J. G., Reyers, M. and Ulbrich, U. (2011), ‘The variable link between PNA and NAO in observations and in multi-century CGCM simulations’, *Climate Dynamics* **36**(1), 337–354.
URL: <https://doi.org/10.1007/s00382-010-0770-x>
- Pinto, J. G., Zacharias, S., Fink, A. H., Leckebusch, G. C. and Ulbrich, U. (2009), ‘Factors contributing to the development of extreme North Atlantic cyclones and their relationship with the NAO’, *Climate Dynamics* **32**(5), 711–737.
- Pinto, J., Spanghel, T., Ulbrich, U. and Speth, P. (2005), ‘Sensitivities of a cyclone detection and tracking algorithm: individual tracks and climatology’, *Meteorologische Zeitschrift* **14**(6), 823–838.
- Pirret, J. S. R., Knippertz, P. and Trzeciak, T. M. (2017), ‘Drivers for the deepening of severe European windstorms and their impacts on forecast quality’, *Quarterly Journal of the Royal Meteorological Society* **143**(702), 309–320.
URL: <http://dx.doi.org/10.1002/qj.2923>
- Poli, P. & National Center for Atmospheric Research Staff (Eds). (2016), ‘The Climate Data Guide: ERA-20C: ECMWF’s atmospheric reanalysis of the 20th century (and comparisons with NOAA’s 20CR).’,
URL: <https://climatedataguide.ucar.edu/climate-data/era-20c-ecmwf-atmospheric-reanalysis-20th-century-and-comparisons-noaas-20cr>.
- Poli, P., Hersbach, H., Dee, D. P., Berrisford, P., Simmons, A. J., Vitart, F., Laloyaux, P., Tan, D. G. H., Peubey, C., Thépaut, J.-N., Trémolet, Y., Hólm, E. V., Bonavita, M., Isaksen, I. and Fisher, M. (2016), ‘ERA-20C: An Atmospheric Reanalysis of the Twentieth Century’, *Journal of Climate* **29**(11), 4083–4097.
URL: <http://dx.doi.org/10.1175/JCLI-D-15-0556.1>

- Priestley, M. D. K., Pinto, J. G., Dacre, H. F. and Shaffrey, L. C. (2017*a*), ‘Rossby wave breaking, the upper level jet, and serial clustering of extratropical cyclones in western Europe’, *Geophysical Research Letters* **44**(1), 514–521. 2016GL071277.
URL: <http://dx.doi.org/10.1002/2016GL071277>
- Priestley, M. D. K., Pinto, J. G., Dacre, H. F. and Shaffrey, L. C. (2017*b*), ‘The role of cyclone clustering during the stormy winter of 2013/2014’, *Weather* **72**(7), 187–192.
URL: <http://dx.doi.org/10.1002/wea.3025>
- Rayner, N. A., Parker, D. E., Horton, E. B., Folland, C. K., Alexander, L. V., Rowell, D. P., Kent, E. C. and Kaplan, A. (2003), ‘Global analyses of sea surface temperature, sea ice, and night marine air temperature since the late nineteenth century’, *Journal of Geophysical Research: Atmospheres* **108**(D14). 4407.
URL: <http://dx.doi.org/10.1029/2002JD002670>
- Reiter, E. R. and Westhoff, D. (1981), ‘A Planetary-Wave Climatology’, *Journal of the Atmospheric Sciences* **38**(4), 732–750.
URL: [https://doi.org/10.1175/1520-0469\(1981\)038<0732:APWC>2.0.CO;2](https://doi.org/10.1175/1520-0469(1981)038<0732:APWC>2.0.CO;2)
- Renggli, D. (2011), ‘Seasonal predictability of wintertime windstorm climate over the North Atlantic and Europe’, PhD thesis, Institut für Meteorologie, Freie Universität Berlin.
- Renggli, D., Leckebusch, G. C., Ulbrich, U., Gleixner, S. N. and Faust, E. (2011), ‘The Skill of Seasonal Ensemble Prediction Systems to Forecast Wintertime Windstorm Frequency over the North Atlantic and Europe’, *Monthly Weather Review* **139**(9), 3052–3068.
URL: <http://dx.doi.org/10.1175/2011MWR3518.1>
- Revell, C. G. (2015), ‘A note on a Southern Ocean storm’, *Weather* **70**(1), 25–26.
URL: <http://dx.doi.org/10.1002/wea.2337>
- Rhines, P. (1970), ‘Edge-, bottom-, and Rossby waves in a rotating stratified fluid’, *Geophysical Fluid Dynamics* **1**(3-4), 273–302.
URL: <https://doi.org/10.1080/03091927009365776>
- Riddle, E. E., Butler, A. H., Furtado, J. C., Cohen, J. L. and Kumar, A. (2013), ‘CFSv2 ensemble prediction of the wintertime Arctic Oscillation’, *Climate Dynamics* **41**(3), 1099–1116.
URL: <http://dx.doi.org/10.1007/s00382-013-1850-5>
- Rodwell, M. J. and Folland, C. K. (2002), ‘Atlantic air-sea interaction and seasonal predictability’, *Quarterly Journal of the Royal Meteorological Society* **128**(583), 1413–1443.
URL: <http://dx.doi.org/10.1002/qj.200212858302>

- Rodwell, M., Rowell, D. and Folland, C. (1999), ‘Oceanic forcing of the wintertime North Atlantic Oscillation and European climate’, *Nature* **398**(6725), 320–323.
- Roeckner, E., Brokopf, R., Esch, M., Giorgetta, M., Hagemann, S., Kornbluh, L., Manzini, E., Schlese, U. and Schulzweida, U. (2006), ‘Sensitivity of Simulated Climate to Horizontal and Vertical Resolution in the ECHAM5 Atmosphere Model’, *Journal of Climate* **19**(16), 3771–3791.
URL: <https://doi.org/10.1175/JCLI3824.1>
- Roethlisberger, M., Pfahl, S. and Martius, O. (2016), ‘Regional-scale jet waviness modulates the occurrence of midlatitude weather extremes’, *Geophysical Research Letters* **43**(20), 10,989–10,997. 2016GL070944.
URL: <http://dx.doi.org/10.1002/2016GL070944>
- Rudeva, I. and Gulev, S. K. (2010), ‘Composite Analysis of North Atlantic Extratropical Cyclones in NCEP-NCAR Reanalysis Data’, *Monthly Weather Review* **139**(5), 1419–1446.
URL: <http://dx.doi.org/10.1175/2010MWR3294.1>
- Santos, J. A., Pinto, J. G. and Ulbrich, U. (2009), ‘On the development of strong ridge episodes over the eastern North Atlantic’, *Geophysical Research Letters* **36**(17). L17804.
URL: <http://dx.doi.org/10.1029/2009GL039086>
- Scaife, A. A., Arribas, A., Blockley, E., Brookshaw, A., Clark, R. T., Dunstone, N., Eade, R., Fereday, D., Folland, C. K., Gordon, M., Hermanson, L., Knight, J. R., Lea, D. J., MacLachlan, C., Maidens, A., Martin, M., Peterson, A. K., Smith, D., Vellinga, M., Wallace, E., Waters, J. and Williams, A. (2014), ‘Skillful long-range prediction of European and North American winters’, *Geophysical Research Letters* **41**(7), 2514–2519.
URL: <http://dx.doi.org/10.1002/2014GL059637>
- Scaife, A. A., Comer, R. E., Dunstone, N. J., Knight, J. R., Smith, D. M., MacLachlan, C., Martin, N., Peterson, K. A., Rowlands, D., Carroll, E. B., Belcher, S. and Slingo, J. (2017), ‘Tropical rainfall, Rossby waves and regional winter climate predictions’, *Quarterly Journal of the Royal Meteorological Society* **143**(702), 1–11.
URL: <http://dx.doi.org/10.1002/qj.2910>
- Scaife, A. A., Karpechko, A. Y., Baldwin, M. P., Brookshaw, A., Butler, A. H., Eade, R., Gordon, M., MacLachlan, C., Martin, N., Dunstone, N. and Smith, D. (2016), ‘Seasonal winter forecasts and the stratosphere’, *Atmospheric Science Letters* **17**(1), 51–56.
URL: <http://dx.doi.org/10.1002/asl.598>

- Screen, J. A. and Simmonds, I. (2013a), ‘Caution needed when linking weather extremes to amplified planetary waves’, *Proceedings of the National Academy of Sciences of the United States of America* **110**(26), E2327.
- Screen, J. A. and Simmonds, I. (2013b), ‘Exploring links between Arctic amplification and mid-latitude weather’, *Geophysical Research Letters* **40**(5), 959–964.
- Screen, J. A. and Simmonds, I. (2014), ‘Amplified mid-latitude planetary waves favour particular regional weather extremes’, *Nature Climate Change* **4**(8), 704–709.
- Seiler, C. and Zwiers, F. W. (2015a), ‘How well do CMIP5 climate models reproduce explosive cyclones in the extratropics of the Northern Hemisphere?’, *Climate Dynamics* **46**(3), 1241–1256.
URL: <http://dx.doi.org/10.1007/s00382-015-2642-x>
- Seiler, C. and Zwiers, F. W. (2015b), ‘How will climate change affect explosive cyclones in the extratropics of the Northern Hemisphere?’, *Climate Dynamics* pp. 1–12.
URL: <http://dx.doi.org/10.1007/s00382-015-2791-y>
- Shapiro, M. and Keyser, D. (1990), Fronts, jet streams, and the tropopause, *in* M. Shapiro and D. Keyser, eds, ‘Extratropical Cyclones, The Erik Palmén Memorial Volume’, American Meteorological Society, p. 167–191.
- Shukla, J. and Kinter, J. (2006), Predictability of seasonal climate variations a pedagogical review, *in* P. T and H. R, eds, ‘Predictability of Weather and Climate.’, Cambridge University Press.
- Simmonds, I., Murray, R. and Leighton, R. (1999), ‘A refinement of cyclone tracking methods with data from FROST’, *Australian Meteorological Magazine* (SI), 35–49.
- Simmons, A. J. and Hoskins, B. J. (1978), ‘The Life Cycles of Some Nonlinear Baroclinic Waves’, *Journal of the Atmospheric Sciences* **35**(3), 414–432.
URL: [https://doi.org/10.1175/1520-0469\(1978\)035<0414:TLCOSN>2.0.CO;2](https://doi.org/10.1175/1520-0469(1978)035<0414:TLCOSN>2.0.CO;2)
- Slingo, J. et al. (Met Office and Centre for Ecology and Hydrology). (2014), ‘The recent storms and floods in the UK’,
URL: http://www.metoffice.gov.uk/media/pdf/n/i/Recent_Storms_Briefing_Final-07023.pdf. Last accessed in June 2015.
- Smeed, D. A., McCarthy, G. D., Cunningham, S. A., Frajka-Williams, E., Rayner, D., Johns, W. E., Meinen, C. S., Baringer, M. O., Moat, B. I., Duchez, A. and Bryden, H. L. (2014), ‘Observed decline of the Atlantic meridional overturning circulation 2004 - 2012’, *Ocean Science* **10**(1), 29–38.
URL: <https://www.ocean-sci.net/10/29/2014/>

- Smith, D. M., Scaife, A. A., Eade, R. and Knight, J. R. (2016), ‘Seasonal to decadal prediction of the winter North Atlantic Oscillation: emerging capability and future prospects’, *Quarterly Journal of the Royal Meteorological Society* **142**(695), 611–617.
URL: <http://dx.doi.org/10.1002/qj.2479>
- Sogalla, M. (1996), ‘Die Rolle der Baroklinitaet fuer die synoptische Stoerungsaktivitaet im nordhemisphaerischen Winter’, *Mitteilungen aus dem Institut fuer Geophysik und Meteorologie der Universitaet zu Koeln* **Heft 111**.
- Solomon, A., Goddard, L., Kumar, A., Carton, J., Deser, C., Fukumori, I., Greene, A. M., Hegerl, G., Kirtman, B., Kushnir, Y., Newman, M., Smith, D., Vimont, D., Delworth, T., Meehl, G. A. and Stockdale, T. (2011), ‘Distinguishing the Roles of Natural and Anthropogenically Forced Decadal Climate Variability’, *Bulletin of the American Meteorological Society* **92**(2), 141–156.
URL: <https://doi.org/10.1175/2010BAMS2962.1>
- Spearman, C. (1904), ‘The Proof and Measurement of Association between Two Things’, *The American Journal of Psychology* **15**(1), 72–101.
URL: <http://www.jstor.org/stable/1412159>
- Swiss Re (2011), ‘Sigma, No 1’,
URL: http://media.swissre.com/documents/40_costly_losses_1970_2010.pdf.
- Tang, Q., Zhang, X. and Francis, J. A. (2013), ‘Extreme summer weather in northern mid-latitudes linked to a vanishing cryosphere’, *Nature Climate Change* **4**, 45–.
URL: <http://dx.doi.org/10.1038/nclimate2065>
- Titchner, H. A. and Rayner, N. A. (2014), ‘The Met Office Hadley Centre sea ice and sea surface temperature data set, version 2: 1. Sea ice concentrations’, *Journal of Geophysical Research: Atmospheres* **119**(6), 2864–2889. 2013JD020316.
URL: <http://dx.doi.org/10.1002/2013JD020316>
- Trenberth, K. E. and Fasullo, J. T. (2012), ‘Climate extremes and climate change: The Russian heat wave and other climate extremes of 2010’, *Journal of Geophysical Research* **117**(D17). D17103.
URL: <http://dx.doi.org/10.1029/2012JD018020>
- Trenberth, K. E., Fasullo, J. T., Branstator, G. and Phillips, A. S. (2014), ‘Seasonal aspects of the recent pause in surface warming’, *Nature Climate Change* **4**(10), 911–916.
URL: <http://dx.doi.org/10.1038/nclimate2341>
- Uccellini, L. W., Petersen, R. A., Kocin, P. J., Brill, K. F. and Tuccillo, J. J. (1987), ‘Synergistic Interactions between an Upper-Level Jet Streak and Diabatic Processes

that Influence the Development of a Low-Level Jet and a Secondary Coastal Cyclone’, *Monthly Weather Review* **115**(10), 2227–2261.

URL: [https://doi.org/10.1175/1520-0493\(1987\)115<2227:SIBAUL>2.0.CO;2](https://doi.org/10.1175/1520-0493(1987)115<2227:SIBAUL>2.0.CO;2)

Ulbrich, U. and Christoph, M. (1999), ‘A shift of the NAO and increasing storm track activity over Europe due to anthropogenic greenhouse gas forcing’, *Climate Dynamics* **15**(7), 551–559.

Ulbrich, U., Fink, A. H., Klawka, M. and Pinto, J. G. (2001), ‘Three extreme storms over Europe in December 1999’, *Weather* **56**(3), 70–80.

URL: <http://dx.doi.org/10.1002/j.1477-8696.2001.tb06540.x>

Ulbrich, U., Leckebusch, G. C., Grieger, J., Schuster, M., Akperov, M., Bardin, M. Y., Feng, Y., Gulev, S., Inatsu, M., Keay, K., Kew, S. F., Liberato, M. L., Lionello, P., Mokhov, I. I., Neu, U., Pinto, J. G., Raible, C. C., Reale, M., Rudeva, I., Simmonds, I., Tilinina, N. D., Trigo, I. F., Ulbrich, S., Wang, X. L. and Wernli, H. (2013), ‘Are Greenhouse Gas Signals of Northern Hemisphere winter extra-tropical cyclone activity dependent on the identification and tracking algorithm?’, *Meteorologische Zeitschrift* **22**(1), 61–68.

Ulbrich, U., Pinto, J. G., Kupfer, H., Leckebusch, G. C., Spanghel, T. and Reyers, M. (2008), ‘Changing Northern Hemisphere Storm Tracks in an Ensemble of IPCC Climate Change Simulations’, *Journal of Climate* **21**(8), 1669–1679.

URL: <https://doi.org/10.1175/2007JCLI1992.1>

Uppala, S. M., Kallberg, P. W., Simmons, A. J., Andrae, U., Bechtold, V. D., Fiorino, M., Gibson, J. K., Haseler, J., Hernandez, A., Kelly, G. A., Li, X., Onogi, K., Saarinen, S., Sokka, N., Allan, R. P., Andersson, E., Arpe, K., Balmaseda, M. A., Beljaars, A. C. M., Van De Berg, L., Bidlot, J., Bormann, N., Caires, S., Chevallier, F., Dethof, A., Dragosavac, M., Fisher, M., Fuentes, M., Hagemann, S., Holm, E., Hoskins, B. J., Isaksen, L., Janssen, P. A. E. M., Jenne, R., McNally, A. P., Mahfouf, J. F., Morcrette, J. J., Rayner, N. A., Saunders, R. W., Simon, P., Sterl, A., Trenberth, K. E., Untch, A., Vasiljevic, D., Viterbo, P. and Woollen, J. (2005), ‘The ERA-40 re-analysis’, *Quarterly Journal of the Royal Meteorological Society* **131**(612), 2961–3012.

van Oldenborgh, G. J., Stephenson, D. B., Sterl, A., Vautard, R., Yiou, P., Drijfhout, S. S., von Storch, H. and van den Dool, H. (2015), ‘Drivers of the 2013/14 winter floods in the UK’, *Nature Climate Change* **5**, 490–491.

URL: <http://dx.doi.org/10.1038/nclimate2612>

Von Storch, H., Feser, F., Haeseler, S., Lefebvre, C. and Stendel, M. (2014), ‘A violent midlatitude storm in Northern Germany and Denmark, 28 October 2013’, *Bulletin of the American Meteorological Society* **95**, S76–S78.

- Walz, M. A., Kruschke, T., Rust, H. W., Ulbrich, U. and Leckebusch, G. C. (2017), ‘Quantifying the extremity of windstorms for regions featuring infrequent events’, *Atmospheric Science Letters* **18**(7), 315–322.
URL: <http://dx.doi.org/10.1002/asl.758>
- Walz, M., Befort, D. J., Kirchner-Bossi, N., Ulbrich, U. and Leckebusch, G. (2018), ‘Large scale drivers and serial clustering of European winter windstorms (under review)’, *International Journal of Climatology* .
- Walz, M., Donat, M. and Leckebusch, G. (2018), ‘Drivers and seasonal predictability of extreme wind speed in Europe in the ECMWF System 4 and a statistical model (under review)’, *Journal of Geophysical Research: Atmospheres* .
- Wang, X. L., Feng, Y., Compo, G. P., Swail, V. R., Zwiers, F. W., Allan, R. J. and Sardeshmukh, P. D. (2013), ‘Trends and low frequency variability of extra-tropical cyclone activity in the ensemble of twentieth century reanalysis’, *Climate Dynamics* **40**(11-12), 2775–2800.
- Wang, X. L., Feng, Y., Compo, G. P., Zwiers, F. W., Allan, R. J., Swail, V. R. and Sardeshmukh, P. D. (2014), ‘Is the storminess in the Twentieth Century Reanalysis really inconsistent with observations? A reply to the comment by Krueger et al. (2013b)’, *Climate Dynamics* **42**(3), 1113–1125.
URL: <https://doi.org/10.1007/s00382-013-1828-3>
- Wang, X. L., Wan, H., Zwiers, F. W., Swail, V. R., Compo, G. P., Allan, R. J., Vose, R. S., Jourdain, S. and Yin, X. (2011), ‘Trends and low-frequency variability of storminess over western Europe, 1878-2007’, *Climate Dynamics* **37**(11-12), 2355–2371.
- Wang, X. L., Zwiers, F. W., Swail, V. R. and Feng, Y. (2009), ‘Trends and variability of storminess in the Northeast Atlantic region, 1874-2007’, *Climate Dynamics* **33**(7-8), 1179–1195.
- Wanner, H., Brönnimann, S., Casty, C., Gyalistras, D., Luterbacher, J., Schmutz, C., Stephenson, D. B. and Xoplaki, E. (2001), ‘North Atlantic Oscillation – Concepts And Studies’, *Surveys in Geophysics* **22**(4), 321–381.
URL: <https://doi.org/10.1023/A:1014217317898>
- Weisheimer, A. and Palmer, T. N. (2014), ‘On the reliability of seasonal climate forecasts’, *Journal of The Royal Society Interface* **11**(96).
URL: <http://rsif.royalsocietypublishing.org/content/11/96/20131162>
- Welker, C. and Martius, O. (2014), ‘Decadal-scale variability in hazardous winds in northern Switzerland since end of the 19th century’, *Atmospheric Science Letters* **15**(2), 86–91.
URL: <http://dx.doi.org/10.1002/asl2.467>

- Wernli, H., Dirren, S., Liniger, M. A. and Zillig, M. (2002), ‘Dynamical aspects of the life cycle of the winter storm ‘Lothar’ (24–26 December 1999)’, *Quarterly Journal of the Royal Meteorological Society* **128**(580), 405–429.
URL: <http://dx.doi.org/10.1256/003590002321042036>
- Wild, S., Befort, D. J. and Leckebusch, G. C. (2015), ‘Was the Extreme Storm Season in Winter 2013/14 Over the North Atlantic and the United Kingdom Triggered by Changes in the West Pacific Warm Pool? [in “Explaining Extremes of 2014 from a Climate Perspective”]’, *Bulletin of the American Meteorological Society* **96**(12), S29–S34.
URL: <http://dx.doi.org/10.1175/BAMS-D-15-00118.1>
- Wilks, D. S. (1995), *Statistical Methods in the Atmospheric Sciences*, International Geophysics Series, 2 edn, Academic Press.
- Woollings, T. (2010), ‘Dynamical influences on European climate: an uncertain future’, *Philosophical Transactions of the Royal Society of London A: Mathematical, Physical and Engineering Sciences* **368**(1924), 3733–3756.
URL: <http://rsta.royalsocietypublishing.org/content/368/1924/3733>
- Woollings, T., Hannachi, A. and Hoskins, B. (2010), ‘Variability of the North Atlantic eddy-driven jet stream’, *Quarterly Journal of the Royal Meteorological Society* **136**(649, Part b), 856–868.
- Woollings, T., Hoskins, B., Blackburn, M. and Berrisford, P. (2008), ‘A new Rossby wave-breaking interpretation of the North Atlantic Oscillation’, *Journal of the Atmospheric Sciences* **65**(2), 609–626.
- Woollings, T., Pinto, J. G. and Santos, J. A. (2011), ‘Dynamical Evolution of North Atlantic Ridges and Poleward Jet Stream Displacements’, *Journal of the Atmospheric Sciences* **68**(5), 954–963.
- Wu, Q. and Zhang, X. (2010), ‘Observed forcing feedback processes between Northern Hemisphere atmospheric circulation and Arctic sea ice coverage’, *Journal of Geophysical Research: Atmospheres* **115**(D14).
URL: <https://agupubs.onlinelibrary.wiley.com/doi/abs/10.1029/2009JD013574>
- Yu, L. and Weller, R. A. (2007), ‘Objectively Analyzed Air–Sea Heat Fluxes for the Global Ice-Free Oceans (1981–2005)’, *Bulletin of the American Meteorological Society* **88**(4), 527–539.
URL: <https://doi.org/10.1175/BAMS-88-4-527>
- Zappa, G., Masato, G., Shaffrey, L., Woollings, T. and Hodges, K. (2014), ‘Linking Northern Hemisphere blocking and storm track biases in the CMIP5 climate models’,

Geophysical Research Letters **41**(1), 135–139.

URL: <http://dx.doi.org/10.1002/2013GL058480>

Zappa, G., Shaffrey, L. C. and Hodges, K. I. (2013), ‘The Ability of CMIP5 Models to Simulate North Atlantic Extratropical Cyclones’, *Journal of Climate* **26**(15), 5379–5396.

URL: <http://dx.doi.org/10.1175/JCLI-D-12-00501.1>

Zappa, G., Shaffrey, L. C., Hodges, K. I., Sansom, P. G. and Stephenson, D. B. (2013), ‘A Multimodel Assessment of Future Projections of North Atlantic and European Extratropical Cyclones in the CMIP5 Climate Models’, *Journal of Climate* **26**(16), 5846–5862.

URL: <http://dx.doi.org/10.1175/JCLI-D-12-00573.1>

APPENDIX

DIFFERENT LONG-TERM TRENDS OF EXTRA-TROPICAL CYCLONES AND WINDSTORMS IN ERA-20C AND NOAA-20CR REANALYSES

This chapter has been published with the same title in almost identical form in *Atmospheric Science Letters* in 2016. The authors of the publication are Daniel J. Befort, Simon Wild, Tim Kruschke, and Gregor C. Leckebusch. A brief overview of the individual contributions of all authors can be found at the beginning of this thesis (see Author's Declaration). My contributions of the following chapter or publication respectively included parts of the overall analyses (I performed some of the tracking) and editing of the manuscript.

9.1 Introduction

Wind storms caused by extra-tropical cyclones are one of the major natural hazards in the mid-latitudes of both hemispheres. They can kill people, disrupt critical infrastructure, damage buildings and industry installations and generate large economic losses. One example of a particularly stormy winter was 2013/2014 over the UK (Kendon and McCarthy, 2015), which was classed as the most active season regarding wind storm frequency for at least the last 35 years (Wild et al., 2015) and the most active season regarding cyclone frequency for over a century in the UK (Matthews et al., 2014). For the Southern Hemisphere land extent is less in the latitudes of interest, meaning less direct

impacts on losses, though severe wind storms are generally an even more pronounced feature over the ocean here than in the Northern Hemisphere (hence the terms ‘roaring forties’ and ‘furious fifties’). These can have severe consequences for shipping in the southern ocean (Lim and Simmonds, 2002; Revell, 2015).

While our understanding of synoptic scale processes involved in the generation of (severe) extra-tropical cyclones is generally well developed, scientific research has not fully understood the governing physical processes steering the variability of storm frequencies on time scales from inter-annual to multi-decadal (see for inter-annual variability, e.g. Wild et al. 2015; Huntingford et al., 2014). For Europe, the influence of ocean heat content anomalies over the North Atlantic has recently been highlighted by Nissen et al. (2014), using coupled climate model simulations. As climate model responses to such anomalies are often model specific (Yu and Weller, 2007), it is important to assess observed variability. Physically consistent, global gridded three-dimensional datasets for the past have been produced by different re-analysis projects. The NOAA-20CR data set (Compo et al., 2011) was used by Donat et al. (2011), suggesting long-term trends in extreme storms in the NOAA-20CR ensemble for the European region. This finding triggered a scientific discussion about the reliability of historic trends derived from reanalyses and estimates from station observations in specific regions (Broennimann et al., 2012; Krueger et al., 2013; Krueger et al., 2014; Wang et al., 2013; Wang et al., 2014). With the release of the ECMWF 20th century reanalysis (ERA-20C; Poli et al., 2016) a new data set is now available to investigate the multi-decadal variability of extreme mid-latitude cyclone and wind storm events. In addition to mean-sea level pressure (MSLP) observations (as used by NOAA-20CR), surface wind observations over the oceans are also assimilated. Our present study compares trends in these two reanalysis datasets, considering both extra-tropical cyclones and strong, potentially damaging wind events over both hemispheres. We address the question of different trends in the two datasets, their time dependency and separate between multi-decadal and high-frequency spectral components.

9.2 Data and Methods

In this study the ECMWF 20th century reanalysis (ERA-20C) data set with a horizontal resolution of T159 (1.125°) and 91 vertical levels for the period 1901 until 2008 is used. Atmospheric pressure observations as well as near-surface wind observations over the oceans are assimilated employing a 4D-Var-scheme (Poli et al., 2016). Sea-surface temperature and sea ice conditions are provided by the HadISST2.1.0.0 (Titchner and Rayner, 2014) data set. Additionally, the NOAA 20th century reanalysis datasets (NOAA-20CR (v2), Compo et al., 2011) with a horizontal resolution of 2° for the period from 1871 until 2009 is analysed. In this case, sea-surface temperature and sea ice conditions are taken from the HadISST1.1 data set (Rayner et al., 2003), whereas only atmospheric pressure observations are assimilated, employing an Ensemble Kalman Filter, producing a reanalysis ensemble with 56 members.

Cyclones are identified in the Northern and Southern Hemisphere extra-tropics (excluding the tropical belt within 20° N–20° S). Cyclones are identified and tracked using the algorithm developed by Murray and Simmonds (1991) . This algorithm has been used by several studies investigating extra-tropical cyclones under recent and future climate conditions (Leckebusch and Ulbrich, 2004; Pinto et al., 2005; Leckebusch et al., 2006; Kruschke et al., 2014) and is included in the intercomparison of mid-latitude storm diagnostics initiative (Ulbrich et al., 2013; Neu et al., 2012). Six hourly MSLP fields are used as input, which are available for both datasets: ERA-20C and NOAA-20CR. Analyses are carried out for all cyclones and for the most extreme events. Extreme cyclones are defined as those events with a minimum core pressure below 970 hPa over the Northern and below 960 hPa over the Southern Hemisphere, in accordance with Lambert and Fyfe (2006) .

The representation of extreme wind storms in reanalysis products is not perfect. Like model simulations of comparable resolution they underestimate maximum gusts in terms

of absolute measures (Hewson and Neu, 2015). For this reason an algorithm introduced by Leckebusch et al. (2008) which identifies wind storms based on instantaneous near-surface wind speeds relative to the climatology of the respective data set is applied. The method identifies areas in which wind speeds exceed the local 98th percentile. A minimum affected area of $150\,000\text{ km}^2$ is required for assigning the ‘wind storm’ attribute to a weather situation. Tracking of wind storm fields is primarily based on a nearest-neighbour approach. Wind storm tracks lasting less than 18 hours are excluded from the statistics. A comprehensive description of the scheme is given by Kruschke (2015). This algorithm has been proven useful in several studies to identify extra-tropical wind storm events in gridded climate data (Renggli et al., 2011; Nissen et al., 2013; Nissen et al., 2014; Befort et al., 2015; Kruschke et al., 2014; Wild et al., 2015). In general, these studies used 10-m level wind speeds for their analyses. This parameter is only available for ERA-20C, but not for NOAA-20CR. Therefore the 0.995 sigma level ($\sim 1008\text{ hPa}/44\text{ m}$ using a surface pressure of 1013 hPa) for NOAA-20CR is used instead. Sensitivity tests using ERA-20C confirmed that this difference in base height yields no large impact on the temporal variability of wind storms nor the absolute number of events identified. The 98th percentile of each data set (NOAA-20CR, ERA-20C) is calculated for the years from 1961 until 2000.

Wind storm as well as cyclone events are identified over both hemispheres for the extended winter season (NH: October to March; SH: April to September). In case of NOAA-20CR, events are identified for all 56 ensemble member separately. Spatial track densities are calculated similar to Kruschke et al. (2014), but using a ‘search’ radius of 700 km. To analyse in how far differences between both datasets change in time, analyses are carried out for the periods 1901–1930, 1931–1960 and 1961–1990. Additionally, the number of cyclones/wind storms within three northern hemispheric regions (Northern Europe, North Atlantic, Polar Region, see Figure 1(a)) and three southern hemispheric regions (Atlantic Ocean, Indian Ocean, Pacific Ocean, see Figure 4(a)) is analysed. A Lanczos low-pass filter (Duchon, 1979) with a cut-off frequency of $1/31\text{ years}^{-1}$ using 31

weights is applied to investigate the lower-frequency variability. The high-pass filtered time series are obtained by calculating the residuum between the original and the low-pass filtered time series. Eventually, a linear regression model is fitted to the original time series (the ensemble mean for NOAA-20CR) for each period. The similarity of low-frequency variability (LFV) between both datasets is assessed by calculating the difference of the relative linear regression slope for each period using a common reference period (1961–1990). A Mann–Kendall test is applied to test the significance of the long-term trends. The similarity of the high-frequency variability (HFV) is assessed by correlation coefficients between both high-pass filtered time series, which is only possible for the second and third period as no low-pass filtered information is available for the complete first period.

9.3 Results

Northern Hemisphere

All cyclone events

The cyclone track density pattern (Fig.9.1(a), for the 1961–1990 period) is characterised by the two well-known centres of activity over the North Atlantic and North Pacific. It is assumed that the quality of both reanalyses is best for this most recent period. Consequently, the highest agreement between both datasets is expected for the last period. However, more cyclone tracks for ERA-20C than in NOAA-20CR are found (about 29% between 1961 and 1990 over the Northern Hemisphere using ERA-20C as reference), which is partly related to the finer resolution of ERA-20C (Pinto et al., 2005). Consistently, about 11% fewer cyclones over the Northern Hemisphere are identified when interpolating the ERA-20C data to the coarser NOAA-20CR grid compared to the original ERA-20C data. Note that interpolating to a coarser resolution will not lead to the same results as running the model on a coarser resolution, because more processes are resolved in

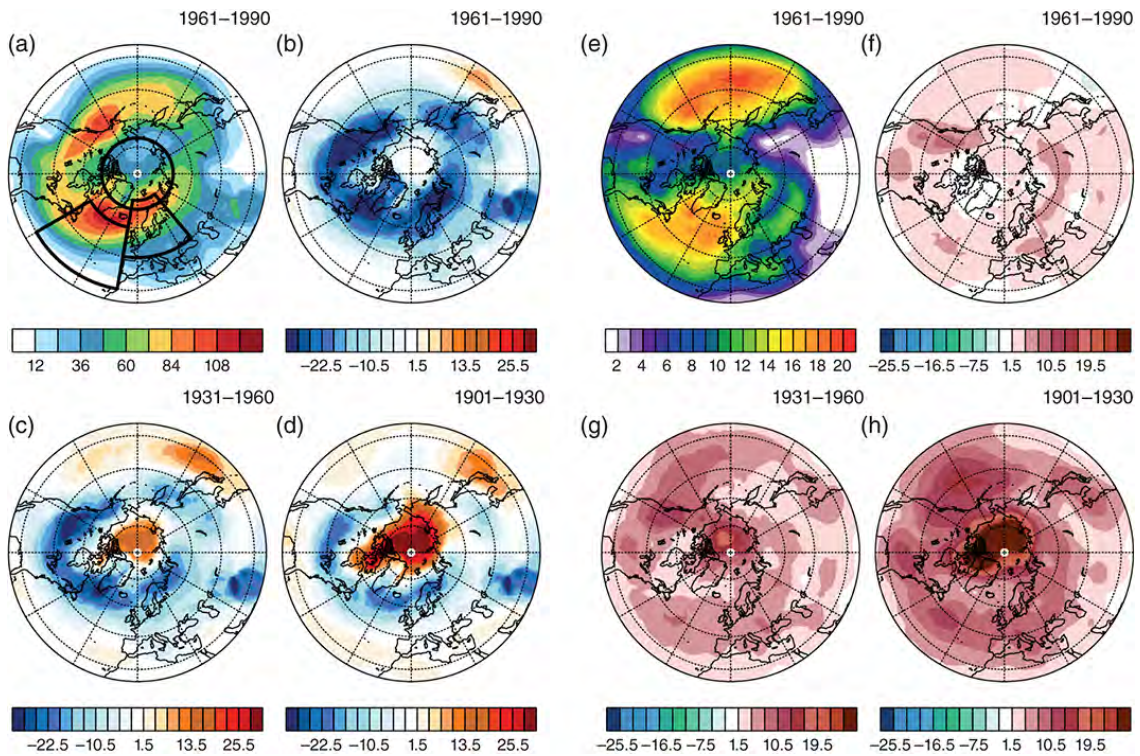


Figure 9.1: Track densities for cyclones (a–d) and wind storms (e–h) over the Northern Hemisphere in number of events per season. Cyclones: (a) ERA-20C (1961–1990), (b) NOAA-20CR minus ERA-20C (1961–1990), (c) NOAA-20CR minus ERA-20C (1931–1960) and (d) NOAA-20CR minus ERA-20C (1901–1930). Wind storms: (e) ERA-20C (1961–1990), (f) NOAA-20CR minus ERA-20C (1961–1990), (g) NOAA-20CR minus ERA-20C (1931–1960) and (h) NOAA-20CR minus ERA-20C (1901–1930). Northern Hemispheric regions used for time series analyses (North Atlantic, Northern Europe, Polar Region) are shown (a).

simulations with higher resolution.

Trends of cyclone track numbers over the NH differ drastically between the two datasets for the first (1901–1930) and second (1931–1960) period (9.2(a)). For the first period an increasing trend of cyclones is found for both datasets, which is smaller in ERA-20C compared to those in NOAA-20CR. For the second period the long-term trend reverses in NOAA-20CR, yet the increasing trend is still found for ERA-20C. The disagreement in the first and second period is due to a distinct increase of events over the Polar Region and (to a lower degree) over the North Atlantic with its maximum around the year 1920 in the NOAA-20CR dataset, which is not present in the ERA-20C (Figure 2(a), (c) and (d)). The NOAA-20CR maximum is followed by a decreasing trend until the end of the

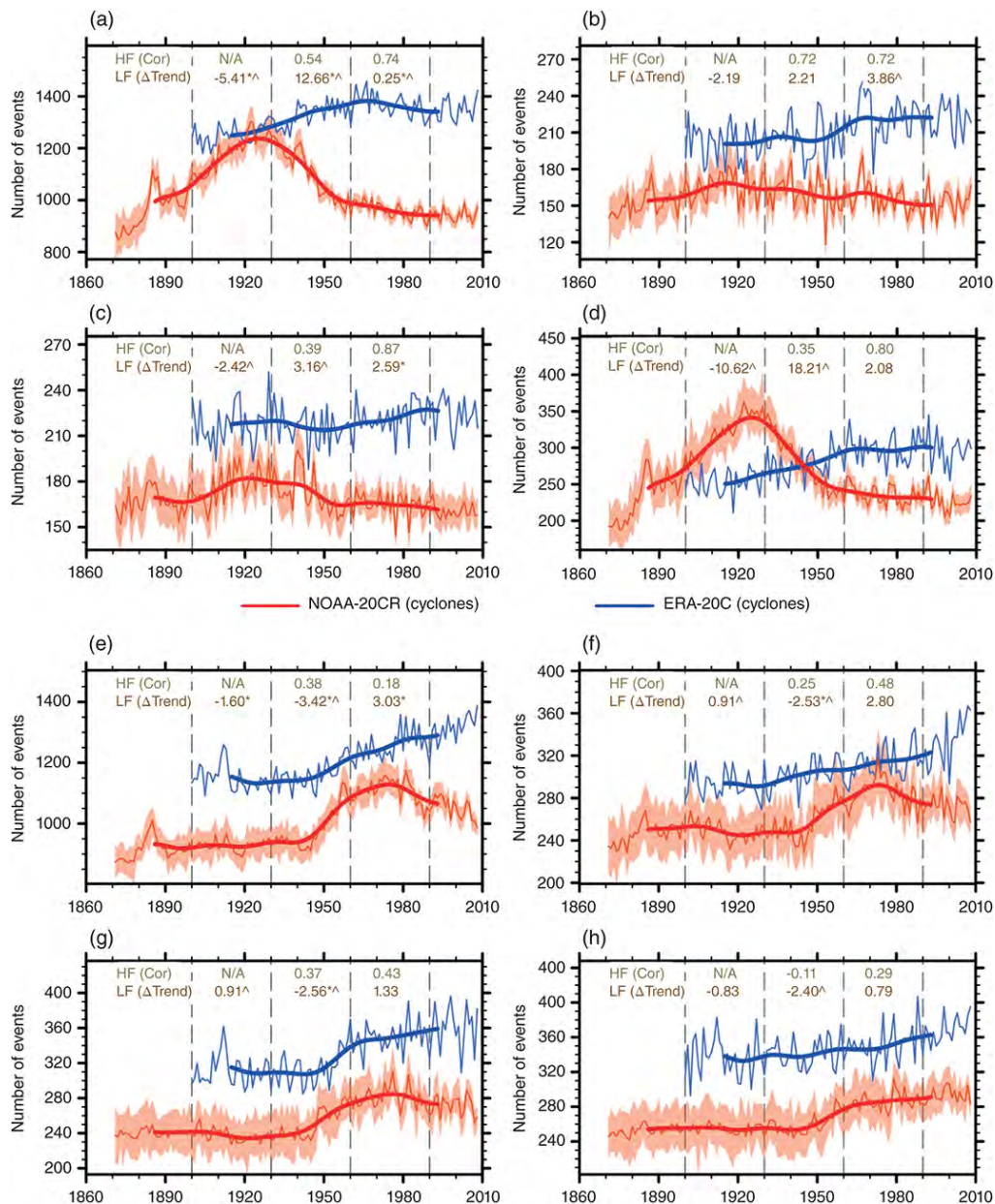


Figure 9.2: Time series of cyclone events for three selected regions over the Northern Hemisphere (a–d) and Southern Hemisphere (e–h). Northern Hemisphere: (a) extra-tropical NH, (b) Northern Europe, (c) North Atlantic and (d) Polar Region (see Fig.9.1(a) for NH regions). Southern Hemisphere: (e) extra-tropical SH, (f) Atlantic Ocean, (g) Indian Ocean and (h) Pacific Ocean. (see Fig.9.4(a) for SH regions). The bold lines indicate the low-pass filtered time series (with a cut-off frequency of 1 per 31years). NOAA-20CR ensemble mean is shown as the red thin line, whereas the ensemble spread is indicated as shaded area. The similarity of the high frequency (HF) is given as correlation coefficients (green values, top of each Figure). Relative differences (ERA-20C–NOAA-20CR) of linear regression coefficients are given in % events per decade using a common reference period from 1961 to 1990. The coefficients are bold if trends differ in sign. Superscripts * and \wedge indicate trends significantly different from zero (ERA-20C (*)) and/or NOAA-20CR(\wedge)).

century, again mainly influenced by the Polar Region, while ERA-20C shows a positive trend from 1900 until 1960 both over the entire hemisphere and over the pole. A good agreement between ERA-20C and NOAA-20CR is found for the last period.

Long-term trends between ERA-20C and NOAA-20CR differ in their sign and magnitude for most selected northern hemispheric regions for the first and second period, while a better agreement is found during the third period. It should be noted that even though the sign of the linear trends differ partly, the individual trends in each dataset are often not significant.

Assessing similarity of the HFV, generally positive correlations are found for all periods and regions, with highest coefficients (above 0.7) for the third period.

Extreme Cyclone Events

The analysis of the extreme cyclones (core pressure below 970 hPa) shows a reduced maximum of cyclone events around 1920 in NOAA-20CR (Fig.9.3(a) compared to all cyclones (Fig.9.2(a)). This suggests that the increased number of all cyclone events around 1920 is mainly due to weaker events. An increased number of events around 1990 is found in both datasets and in all regions. In general, LFV of extreme cyclones is in better agreement between ERA-20C and NOAA-20CR compared to all cyclones. Long-term trends show the same sign in all regions and all periods except for the second period over the Northern Hemisphere (Fig.9.3(a)–(d)). However, only ERA-20C shows a trend significantly different from zero for the second period over the Northern Hemisphere (Fig.9.3(a)). Despite the same sign of trends for most periods and regions, large differences in their magnitudes are found, e.g. of about 4% per decade during the third period over Northern Europe (Fig. 9.3(b)). In general, HFV of both datasets is in better agreement for intense cyclones than those for all cyclones (except for very similar correlations of 0.87 and 0.83, respectively, during the third period over the North Atlantic).

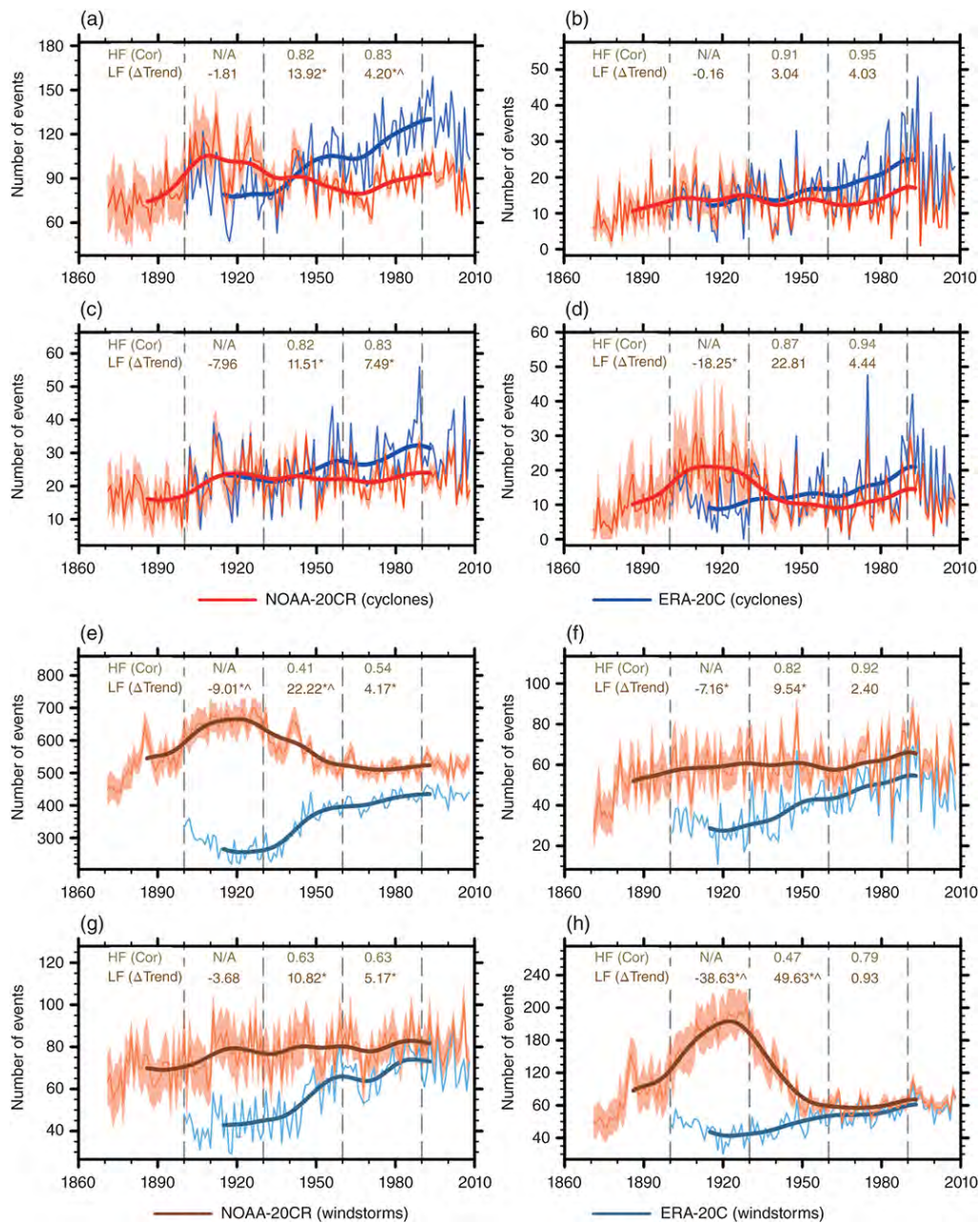


Figure 9.3: Time series of extreme cyclone events (minimum core pressure below 970 hPa) (a–d) and wind storm events (e–h) for three selected regions over the Northern Hemisphere. Cyclones: (a) extra-tropical NH, (b) Northern Europe, (c) North Atlantic and (d) Polar Region (see Fig.9.1 for NH regions). Wind storms: (e) extra-tropical NH, (f) Northern Europe, (g) North Atlantic and (h) Polar Region (see Fig.9.1 for NH regions). Time series, correlations and trend characteristics analogue to Fig.9.2.

Wind Storm Events

The two main centres of wind storm activity over the Pacific and Atlantic oceans (cf. e.g. Leckebusch et al., 2008; Kruschke et al., 2015) are well represented by ERA-20C during the period from 1961 until 1990 (Fig.9.1(e)). For this period differences between both datasets are comparatively small and partly related to the different height level used to identify wind storm events. As expected, absolute differences between both datasets decrease from the beginning to the end of the 20th century (Fig.9.1(f)–(h)). For the period from 1901 until 1930 (Fig.9.1(h)) more wind storm events in NOAA-20CR compared to ERA-20C are found mostly over the Polar Region in line with the enhanced cyclone activity for the same region and period in NOAA-20CR (Fig.9.1(d)).

Regional trends of wind storms are similar to extreme cyclone events (Fig.9.3). Large differences are found during the first and second period over the Northern Hemisphere/Polar Region, which is caused by the large number of wind storms in NOAA-20CR around 1920 (Figure 3(h)). In contrast, ERA-20C shows an increasing trend in wind storms during the 20th century in all regions. Similar to results obtained for cyclones, a good agreement with respect to the long-term trends is found for the last period. The HFV of wind storms is in good agreement, with positive correlations for all periods and generally higher correlations for the last period. This is similar to the results obtained for all cyclone and extreme cyclone events.

Southern Hemisphere

All Cyclone Events

More cyclones over most parts of the SH are found in ERA-20C compared to those in NOAA-20CR (Fig.9.4(b)–(d)), again related to differences in the horizontal resolution. The overall mean difference is about 12% (1961–1990), whereas there are on average around 10% fewer cyclones when interpolating ERA-20C to the coarser NOAA-20CR grid

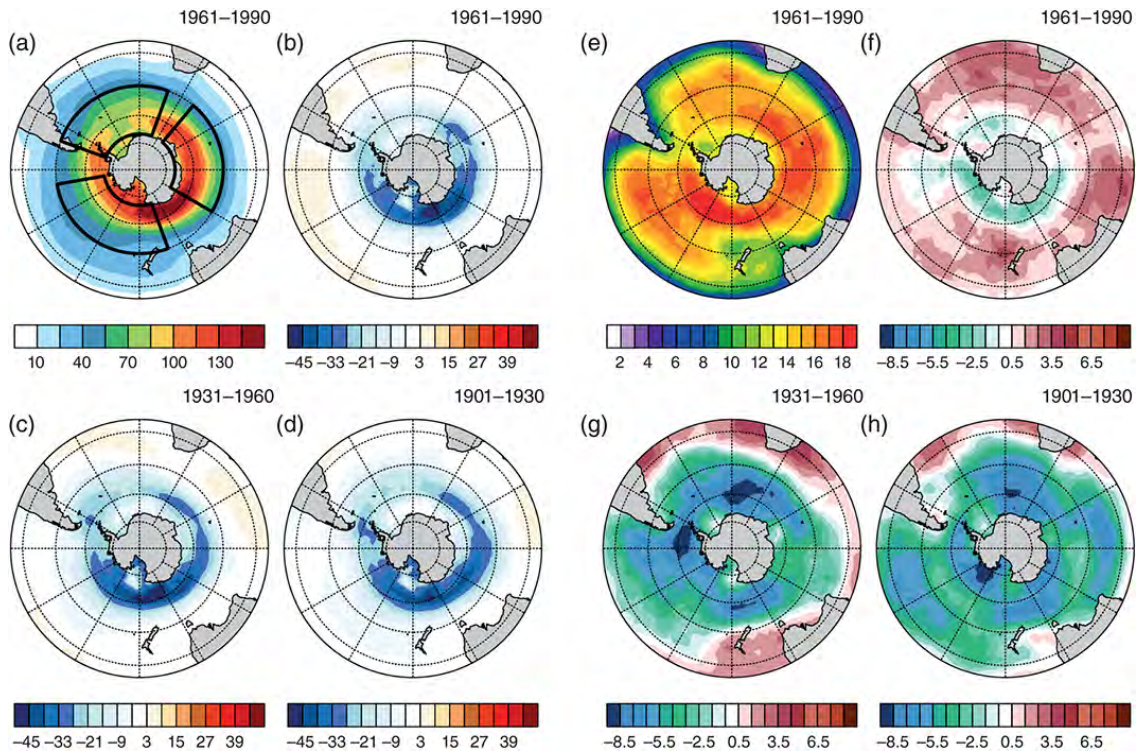


Figure 9.4: Track densities for cyclones (a–d) and wind storms (e–h) over the Southern Hemisphere in number of events per season. Cyclones: (a) ERA-20C (1961–1990), (b) NOAA-20CR minus ERA-20C (1961–1990), (c) NOAA-20CR minus ERA-20C (1931–1960) and (d) NOAA-20CR minus ERA-20C (1901–1930). Wind storms: (e) ERA-20C (1961–1990), (f) NOAA-20CR minus ERA-20C (1961–1990), (g) NOAA-20CR minus ERA-20C (1931–1960) and (h) NOAA-20CR minus ERA-20C (1901–1930). Southern Hemispheric regions used for time series analyses (Atlantic Ocean, Indian Ocean, Pacific Ocean) are shown in (a).

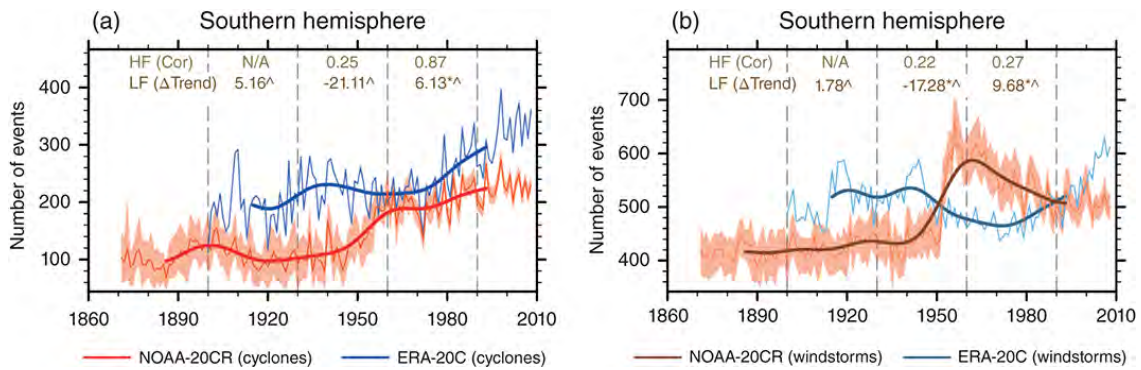


Figure 9.5: Time series of extreme cyclone events (minimum core pressure below 960 hPa) (a) and wind storm events (b) over the extra-tropical Southern Hemisphere. Time series, correlations and trend characteristics analogue to Fig.9.2.

compared to the original ERA-20C data. These absolute differences tend to get smaller over time, with the highest deviations at the beginning of the 20th century (Fig.9.4(d)). In NOAA-20CR, an increased cyclone activity around 1970 is found in all regions except the Pacific Ocean (Fig.9.2(e)–(h)), followed by a negative trend. In contrast, ERA-20C shows an increasing trend of cyclone events over the entire 20th century. LFV is in good agreement during the second period with long-term trends having the same sign. For the third period different signs of the regression coefficients in all regions except the Pacific Ocean are present, but most of these trends are not statistically significant. However, large deviations between both datasets regarding the magnitudes of relative trends at the end of the century are found, especially over the Atlantic Ocean (2.8% per decade) for which both time series are diverging at the end of the century. Correlations coefficients of high-pass filtered time series are mostly positive, except for the Pacific during the second period. However, the agreement of both datasets is smaller compared to results carried out for the Northern Hemisphere.

Extreme Cyclone Events

For extreme cyclone events (core pressure below 960 hPa) a positive trend from 1920 until 2000 is present in NOAA-20CR (Fig.9.5(a)). ERA-20C shows a local maximum around 1940 and a local minimum at the beginning of the 20th century and around 1960. Best agreements regarding LFV is found for the first and third periods, whereas different signs

of the regression coefficients are found for the second period with both linear trends being significantly different from zero. Similarly, HFV shows highest agreement for the last period with a correlation coefficient of about 0.85, whereas it is only about 0.25 for the second period.

Wind Storm Events

The spatial distribution of wind storms in ERA-20C over the Southern Hemisphere for the period 1971–2000 indicates high wind storm activity over the Pacific and Indian Ocean and to a lesser extent over the Atlantic Ocean (9.4(e)). The largest differences are found for the first period (9.4(h)) characterised by a higher number of events in ERA-20C compared to those in NOAA-20CR. These differences decrease during the 20th century (Fig.9.4(g) and (h)).

Over the entire SH, NOAA-20CR shows a maximum of wind storms around 1960 (Figure 5(b)), similar to the results for all cyclones (Fig.9.2(e)). ERA-20C shows fewer events around 1970, followed by a positive trend until the end of the century. Trends show the same sign in the first period, but differ in the second and third period. Additionally, the magnitudes of the trends show high deviations of up to 17% per decade for the second period. HFV is in better agreement than LFV, with positive but small correlations for both periods of about 0.2.

9.4 Discussion and Conclusion

In this study, cyclones and wind storms in the NOAA-20CR and ERA-20C 20th century reanalyses are analysed regarding their spatial distribution and temporal evolution over the Northern and Southern Hemispheres. Differences in long-term trends are assessed by comparing the linear regression coefficients derived from both datasets and three periods: 1901–1930, 1931–1960 and 1961–1990. The similarity of the HFV is obtained by calculating correlation coefficients between both high-passed filtered time series.

Substantial differences regarding the long-term trend of both, cyclones and wind storms between NOAA-20CR and ERA-20C are found over both hemispheres. This is partly expressed by different signs of the linear regression coefficients as well as by large differences regarding their magnitudes. Deviations tend to be largest for the beginning of the last century with better agreement for the second part of the 20th century in most cases.

Over the Northern Hemisphere, different signs of long-term trends are partly related to an enhanced cyclone and wind storm activity around 1920 followed by a decreasing trend of events in NOAA-20CR (also found by Wang et al., 2013). In contrast, ERA-20C shows increasing numbers of cyclone/wind storm events over the Polar Region between 1910 and 1960. For all cyclones, the magnitudes of the trends differ drastically especially during the second period (1931–1960) over the Northern Hemisphere and Polar Region, but large deviations of the trend magnitudes over Northern Europe and the North Atlantic are also found at the end of the 20th century. The agreement of long-term trends is higher for extreme cyclones compared to all cyclones with the same sign in linear trends for both datasets in most periods. However, large differences regarding their magnitudes are present. Large deviations of long-term trends are also found for wind storm events over the NH, with largest differences around 1920, possibly related to the large differences in cyclone frequency during this time. Similar to extreme cyclones, both datasets show similar long-term trends in terms of their signs for wind storms over Northern Europe and the North Atlantic. In general, there is a better agreement of HFV compared to LFV with mostly positive correlations even if long-term trends differ substantially in sign and/or magnitude.

Over the Southern Hemisphere, different long-term trends for all cyclones, extreme cyclones and wind storms are also present. For all cyclones over the Atlantic Ocean differences are most striking at the end of the 20th century, where time series of track

numbers diverge. Similarly to the NH, the agreement of HFV in both datasets is higher than for LFV with mostly positive correlations. However, results for the SH indicate less agreement for both LFV and HFV compared to the NH.

As pointed out by Wang et al. (2013) inhomogeneities in cyclone counts in NOAA-20CR are related to the changing number of observational counts during the 20th century and this might also be the case for ERA-20C. Differences might partly arise from the assimilation of near-surface winds over the oceans in ERA-20C, which was not done in NOAA-20CR. Furthermore, differences in the assimilation schemes themselves might lead to differences how observations are used to generate the respective reanalysis product, e.g. it is found that in most of the tropical cyclones bogus observations are rejected by ERA-20C (Poli et al., 2016). Please refer to Poli and National Center for Atmospheric Research Staff (2016a) for a brief overview about similarities and differences between ERA-20C and NOAA-20CR.

In summary, our results show that analyses of long-term trends of cyclone and wind storm events using both datasets should be interpreted carefully. In our opinion, it seems to be difficult to extend cyclone and wind storm event time series backwards to before around 1950 using NOAA-20CR and ERA-20C. However, as HFV is generally in better agreement than LFV, we conclude that investigations on shorter timescales can be useful if dataset-specific long-term trends are taken into account and properly removed.